NASA/TP–2007-213475

Synthesis from Design Requirements of a Hybrid System for Transport Aircraft Longitudinal Control

Volume II

Charles S. Hynes and Gordon H. Hardy
Ames Research Center, Moffett Field, California

Lance Sherry
Honeywell International Inc., Phoenix, Arizona

December 2007

The NASA STI Program Office . . . in Profile

Since its founding, NASA has been dedicated to the advancement of aeronautics and space science. The NASA Scientific and Technical Information (STI) Program Office plays a key part in helping NASA maintain this important role.

The NASA STI Program Office is operated by Langley Research Center, the Lead Center for NASA's scientific and technical information. The NASA STI Program Office provides access to the NASA STI Database, the largest collection of aeronautical and space science STI in the world. The Program Office is also NASA's institutional mechanism for disseminating the results of its research and development activities. These results are published by NASA in the NASA STI Report Series, which includes the following report types:

- TECHNICAL PUBLICATION. Reports of completed research or a major significant phase of research that present the results of NASA programs and include extensive data or theoretical analysis. Includes compilations of significant scientific and technical data and information deemed to be of continuing reference value. NASA's counterpart of peer-reviewed formal professional papers but has less stringent limitations on manuscript length and extent of graphic presentations.

- TECHNICAL MEMORANDUM. Scientific and technical findings that are preliminary or of specialized interest, e.g., quick release reports, working papers, and bibliographies that contain minimal annotation. Does not contain extensive analysis.

- CONTRACTOR REPORT. Scientific and technical findings by NASA-sponsored contractors and grantees.

- CONFERENCE PUBLICATION. Collected papers from scientific and technical conferences, symposia, seminars, or other meetings sponsored or cosponsored by NASA.

- SPECIAL PUBLICATION. Scientific, technical, or historical information from NASA programs, projects, and missions, often concerned with subjects having substantial public interest.

- TECHNICAL TRANSLATION. English-language translations of foreign scientific and technical material pertinent to NASA's mission.

Specialized services that complement the STI Program Office's diverse offerings include creating custom thesauri, building customized databases, organizing and publishing research results . . . even providing videos.

For more information about the NASA STI Program Office, see the following:

- Access the NASA STI Program Home Page at *http://www.sti.nasa.gov*

- E-mail your question via the Internet to help@sti.nasa.gov

- Fax your question to the NASA Access Help Desk at (301) 621-0134

- Telephone the NASA Access Help Desk at (301) 621-0390

- Write to:
  NASA Access Help Desk
  NASA Center for AeroSpace Information
  7115 Standard Drive
  Hanover, MD 21076-1320

NASA/TP–2007-213475

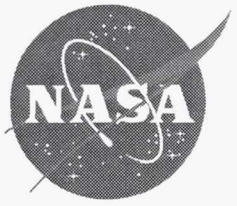

Synthesis from Design Requirements of a Hybrid System for Transport Aircraft Longitudinal Control

Volume II

Charles S. Hynes and Gordon H. Hardy
Ames Research Center, Moffett Field, California

Lance Sherry
Honeywell International Inc., Phoenix, Arizona

National Aeronautics and
Space Administration

Ames Research Center
Moffett Field, California 94035-1000

December 2007

Acknowledgments

We thank Michael Heymann for suggesting the investigation of validity regions in state space, and for many discussions. Charles E. Billings, William Bjorkman, James Franklin, Charles W. (Bill) Harper, Feng Lin, George Meyer, and Everett Palmer reviewed the report and provided useful comments on both content and presentation. We are grateful to them all.

Available from:

NASA Center for AeroSpace Information
7115 Standard Drive
Hanover, MD 21076-1320
(301) 621-0390

National Technical Information Service
5285 Port Royal Road
Springfield, VA 22161
(703) 487-4650

TABLE OF CONTENTS

VOLUME II

APPENDIX A
THE STANDARD ATMOSPHERE

APPENDIX B
ELEMENTS OF TRANSPORT AIRCRAFT DESIGN AND OPERATION

APPENDIX B
ELEMENTS OF TRANSPORT AIRCRAFT DESIGN AND OPERATION (continued)

LIST OF FIGURES

LIST OF TABLES

APPENDIX C
SYMMETRIC (COORDINATED) TURNING FLIGHT

LIST OF FIGURES

APPENDIX D
ELEMENTS OF PROPOSITIONAL LOGIC

APPENDIX D
ELEMENTS OF PROPOSITIONAL LOGIC (continued)

LIST OF TABLES

APPENDIX E
STATECHART SEMANTICS

LIST OF FIGURES

APPENDIX E
STATECHART SEMANTICS (continued)

LIST OF TABLES

APPENDIX F
THEOREMS ON SYSTEM BEHAVIORAL PROPERTIES

APPENDIX F
THEOREMS ON SYSTEM BEHAVIORAL PROPERTIES (continued)

LIST OF FIGURES

LIST OF TABLES

APPENDIX G
SELECTED TRANSPORT AIRCRAFT ACCIDENTS AND INCIDENTS

LIST OF ACRONYMS

AFS	Autoflight system
ATC	Air traffic control
CDU	Control display unit
EAS	Equivalent airspeed
EGT	Exhaust gas temperature
EPR	Exhaust pressure ratio
FAA	Federal Aviation Administration
FMS	Flight management system
ILS	Instrument landing system
MCP	Mode control panel
QSRA	Quiet short-haul research aircraft
TAS	True airspeed
VNAV	vertical navigation

LIST OF SYMBOLS

English Symbols

a	=	a (H)	Sonic velocity, ft/sec
a_{NLIM}			Normal acceleration limit, 3 ft/sec^2
AR	≡	b^2/S	Wing aspect ratio, dimensionless
b			Wing span, ft
C_L			Lift coefficient, dimensionless
C_{DP}	=	C_{DP} (M)	Parasite drag coefficient, dimensionless
dH/dt			Rate of change of height H, ft/sec
$(dH/dt)_0$			Threshold rate of change of height H, 250 ft/min
dV/dt			Rate of change of airspeed V, ft/sec^2
$d\gamma/dt$			Rate of change of flightpath angle γ, rad/sec
D			Drag, lb
e	=	e (M)	Span efficiency, dimensionless
g			Acceleration of gravity, ft/sec^2
H			Height in Standard Atmosphere, ft
H_0			Altitude deviation threshold, ft
ΔH			Altitude error, ft
I_Y			Pitch moment of inertia, slug/ft^2

LIST OF SYMBOLS (continued)

English Symbols (continued)

K_V			Longitudinal acceleration limiter parameter, dimensionless
L			Lift, lb
M	=	V/a	Mach number, dimensionless
M_Y			Pitching moment, ft-lb
N			Engine rpm (revolutions per minute), percent
P_0			Standard sea-level barometric pressure, 2116.22 lb/ft^2
q			Rate of change of pitch angle θ, rad/sec
S			Aircraft wing area, ft^2
T			Thrust, lb
T/δ	=	f (N, M)	Corrected thrust, lb
V			Airspeed, ft/sec
V_E	=	$V\sqrt{\sigma}$	Equivalent airspeed, ft/sec
W			Aircraft weight, lb
W/S			Aircraft wing loading, lb/ft^2

Greek Symbols

α	Angle of attack, rad
γ	Flightpath angle, rad
$\Delta\gamma$	Flightpath angle increment, 3 deg
γ_{POT}	Trim (equilibrium) flightpath angle, rad
γ_{SPEED}	Flightpath angle for airspeed control, rad
$\delta \equiv p/p_0 \equiv \delta$ (H)	Ambient pressure ratio, dimensionless
δ_{ELEV}	Elevator deflection, rad
δ_T	Throttle position, rad
θ	Pitch angle, rad
ρ_0	Standard sea-level density, 0.00237691 sl/ft^3
$\sigma \equiv \rho/\rho_0 \equiv \sigma$ (H)	Ambient density ratio, dimensionless
ϕ	Bank angle, rad

LIST OF SYMBOLS (continued)

Subscripts

CMD	Commanded
EXP	Exponential law
LIM	Limited
MAX	Maximum
MIN	Minimum
MC	Minimum control airspeed
PAR	Parabolic law
POT	Potential (equilibrium or trim) conditions
REF	Reference
SAFE	Safety envelope limit
TGT	Target

Logical Symbols

Equivalence	$\equiv$	Negation	$\neg$	Implication	$\Rightarrow$
Logical OR	$\cup$	Logical AND omitted			

LIST OF SYMBOLS (continued)

Logical Conditions

$VT1 \equiv (V_{TGT} < V_{MIN})$ $\qquad$ $VT2 \equiv (V_{TGT} > V_{MAX})$

$VT3 \equiv (V_{TGT} \leq V_{MIN\ DRAG})$

$V1 \equiv (V \leq V_{MIN\ DRAG})$ $\qquad$ $V2 \equiv (V < V_{TGT})$

$V3 \equiv (V = V_{TGT})$ $\qquad$ $V4 \equiv (V > V_{TGT})$

$G1 \equiv (\gamma = 0)$

$GT1 \equiv (\gamma_{TGT} < \gamma_{SAFE})$ $\qquad$ $GT2 \equiv (\gamma_{TGT} < \gamma_{POT\ TGT})$

$GT3 \equiv (\gamma_{TGT} = \gamma_{POT\ TGT})$ $\qquad$ $GT4 \equiv (\gamma_{TGT} > \gamma_{POT\ TGT})$

$GT5 \equiv (\gamma_{TGT} \leq \gamma_{POT\ MIN})$ $\qquad$ $GT6 \equiv (\gamma_{TGT} \geq \gamma_{POT\ MAX})$

$Q \equiv (\gamma_{TGT} \leq \gamma_{SPEED\ MIN})$ $\qquad$ $P \equiv (\gamma_{TGT} \geq \gamma_{SPEED\ MAX})$

$DC1 \equiv (\gamma_{POT\ MIN} < 0)$ $\qquad$ $PF1 \equiv (\gamma_{POT\ MAX} = \gamma_{POT\ MIN})$

$TC1 \equiv (\gamma_{POT\ MAX} < 0)$ $\qquad$ $TC2 \equiv (\gamma_{POT\ MAX} = 0)$

$TS1 \equiv (\gamma \leq \gamma_{SPEED\ MIN})$ $\qquad$ $TS2 \equiv (\gamma \geq \gamma_{SPEED\ MAX})$

$TT1 \equiv (\gamma_{POT\ TGT} = \gamma_{POT\ MIN})$ $\qquad$ $TT2 \equiv (\gamma_{POT\ TGT} = \gamma_{POT\ MAX})$

$TT3 \equiv (\gamma_{POT\ TGT} < \gamma_{POT\ MIN})$ $\qquad$ $TT4 \equiv (\gamma_{POT\ TGT} > \gamma_{POT\ MAX})$

$\neg PP \equiv (PRIORITY \equiv SPEED)$ $\qquad$ $PP \equiv (PRIORITY \equiv PATH)$

$PE\ (V) \equiv \neg\ [P\ TT1] \neg\ [Q\ TT2]$ $\qquad$ $PE\ (\gamma) \equiv \neg\ (GT6\ V1\ TS2)$

$H1 \equiv (H_{TGT} < H_{SAFE})$ $\qquad$ $H2 \equiv (H_{TGT} > H_{MAX})$

$NE1 \equiv \neg\ [(GT2 \cup GT3)\ V4] \neg\ [GT2\ V3]$

$NE2 \equiv \neg\ [(GT32 \cup GT4)\ V2] \neg\ [GT4\ V3]$

APPENDIX A
THE STANDARD ATMOSPHERE

The aerodynamic and propulsive forces acting on an aircraft depend on the local pressure, temperature, density, and sonic velocity that prevail within the atmosphere in the region where the aircraft operates. It is the purpose of the standard atmosphere to define representative values of these properties as functions of altitude. It is assumed that the atmosphere is static, and rotates with the Earth. For current subsonic transport aircraft, the range of interest extends from the surface to about 45,000 ft, while supersonic transport aircraft may operate at altitudes up to 70,000 ft.

BASIC EQUATIONS

The standard atmosphere (Anonymous, 1962) is defined by three basic equations. The hydrostatic equation

$$dp = -\rho\, g\, dH \tag{A-1}$$

relates, in differential form, the pressure p and the density ρ to the height H, where g is the gravitational acceleration. The equation of state for air as a perfect gas

$$p = \rho\, R\, T \tag{A-2}$$

relates the pressure p and the density ρ to the temperature T, where R is the gas constant for air. The third equation specifies the temperature variation with height, separating the atmosphere into two regions within the altitude range of interest.

Troposphere

The lower region, which is termed the troposphere, extends from the surface to an upper limit termed the tropopause at 11 km, or 36,089 ft above the Earth's surface. Within the troposphere, the temperature decreases linearly with height according to the equation

$$T_T = T_0 + L\, H \qquad 0 \le H \le H_T \tag{A-3a}$$

where the parameter $L \equiv dT/dH$ is termed the temperature lapse rate, T_0 is the standard sea-level temperature, and H_T is the tropopause height of 11 km.

Stratosphere

Above the troposphere lies an isothermal layer termed the stratosphere, within which the temperature remains constant at the tropopause value

$$T_S = T_0 + L\, H_T \qquad H > H_T \tag{A-3b}$$

The sonic velocity a is related to temperature by the thermodynamic equation

$$a = \sqrt{(\gamma R T)} \qquad \text{(A-4)}$$

where γ is the ratio of specific heats for air. Therefore, the sonic velocity is constant throughout the stratosphere.

DEFINING PROPERTIES AND CONSTANTS

Primary Constants

The following parameters are taken as primary constants (Anonymous, 1962), with the values in metric (SI) units regarded as the defining values:

- g — Gravitational acceleration at the Earth's surface at 45-deg latitude, 9.80665 m/sec^2 = 32.17405 ft/sec^2
- R — Gas constant for air, 287.053 joules/kg-deg K = 1716.551 ft-lb/sl-deg R
- γ — Ratio of specific heats for air, 1.40 (dimensionless)

Defining Properties

The following parameters are taken as defining properties for the standard atmosphere:

- H_T — Height of tropopause, 11 km = 36,089.2 ft
- L — Temperature lapse rate dT/dH, –6.5 deg K per km = –0.00356616 deg R per ft
- Pp_0 — Standard sea-level pressure, 101325 n/m^2 = 2116.22 lb/ft^2 (76 cm Hg = 29.9213 in Hg at temperature T_0 = 14.6960 lb/in^2)
- T_0 — Standard sea-level temperature, 288.15 deg K = 518.67 deg R (15 deg C = 59 deg F)

Derived Quantities

The following parameters are derived from equations (A-2) and (A-4):

- a_0 — Standard sea-level sonic velocity, 340.294 m/sec = 1116.45 ft/sec
- ρ_0 — Standard sea-level density, 1.22500 kg/m^3 = 0.00237691 sl/ft^3

DEFINING EQUATIONS FOR THE TROPOSPHERE

It will be convenient to normalize the temperature within the troposphere by dividing equation (A-3a) by the standard sea-level temperature T_0, defining the dimensionless ratio θ:

$$\theta \equiv T/T_0 = 1 + L\,H/T_0 \qquad 0 \le H \le H_T \tag{A-5}$$

Eliminating ρ from equation (A-l) with the help of equation (A-2), and eliminating T with the help of equation (A- 3a), the hydrostatic equation (A-1) can be put in the form

$$\frac{dp}{p} = -\frac{g}{R}\frac{dH}{T_0 + L\,H}$$

which (neglecting the slight decrease of gravitational acceleration with height) can be integrated upward from the surface to obtain

$$\text{In}\,\frac{p}{p_0} = -\frac{g}{LR}\,\text{In}\left(1 + \frac{H}{T_0/L}\right) \qquad 0 \le H \le H_T \tag{A-6}$$

Defining the normalized pressure by $\delta \equiv p/p_0$ and taking anti-logarithms, equation (A-6) becomes

$$\delta \equiv \frac{p}{p_0} = \left(1 + \frac{H}{T_0/L}\right)^{-g/LR} \qquad 0 \le H \le H_T \tag{A-6a}$$

Similarly defining the normalized density by $\sigma \equiv \rho/\rho_0$, the equation of state (A-2) takes the normalized form $\delta = \sigma\,\theta$, so that, making use of equation (A-6a), the normalized density is found to be

$$\sigma \equiv \frac{\delta}{\theta} = \theta^{-(1+g/LR)} = \left(1 + \frac{H}{T_0/L}\right)^{-(1+g/LR)} \qquad 0 \le H \le H_T \tag{A-7}$$

The normalized sonic velocity $\mu \equiv a/a_0$ is found from equation (A-4):

$$\mu \equiv \frac{a}{a_0} = \sqrt{\theta} = \sqrt{(1 + LH/T_0)} \qquad 0 \le H \le H_T \tag{A-8}$$

DEFINING EQUATIONS FOR THE STRATOSPHERE

Eliminating ρ with the help of equation (A-2), the hydrostatic equation (A-1) can be put in the form

$$\frac{dp}{p} = -\frac{g}{RT_S}\,dH$$

which, since the temperature T_S is constant in the stratosphere (equation (A-3b)), can be integrated upward from the tropopause to obtain

$$\ln\frac{p}{P_T} = -\frac{H - H_T}{RT_S/g} \qquad H > H_T \tag{A-9}$$

In the normalized form, equation (A-9) becomes

$$\delta = \delta_T \exp\left(-\frac{H - H_T}{RT_S/g}\right) \qquad H > H_T \tag{A-9a}$$

where δ_T denotes the normalized pressure at the tropopause. The normalized temperature, density, and sonic velocity in the stratosphere are given by the equations

$$\theta_S = \frac{T_S}{T_0} = 1 + \frac{H_T}{T_0/L} \qquad H > H_T \tag{A-10}$$

$$\sigma = \frac{\delta}{\theta} = \frac{\delta_T}{\theta_S}\exp\left(-\frac{H - H_T}{RT_S/g}\right) \qquad H > H_T \tag{A-11}$$

$$\mu_S = \sqrt{\theta_S} \qquad H > H_T \tag{A-12}$$

STANDARD ATMOSPHERE TABLE

Numerical Constants

Numerical evaluation of the constants in equations (A-1) to (A-12) results in the following values for English units:

$$\frac{T_0}{L} = \frac{518.67 \text{ deg R}}{-0.00356616 \text{ deg R/ft}} = -145{,}442 \text{ ft}$$

$$-\frac{g}{LR} = -\frac{32.17405 \text{ ft/sec}^2}{(-0.00356616 \text{ deg R/ft})(1716.551 \text{ ft-lb/sl-deg R})}$$
$$= 5.255913 \text{ (dimensionless)}$$

$$T_S = 518.67 \text{ deg R} + (-0.00356616 \text{ deg R/ft})(36{,}089.2 \text{ ft})$$
$$= 389.97 \text{ deg R}$$

$$\delta_T = \left(1 - \frac{36{,}089.2 \text{ ft}}{145{,}442 \text{ ft}}\right)^{5.255\,913} = 0.223\,359 \text{ (dimensionless)}$$

$$\frac{R\,T_S}{g} = \frac{(1716.551 \text{ ft-lb/sl-deg R})(389.97 \text{ deg R})}{32.17405 \text{ ft/sec/sec}} = 20{,}805.7 \text{ ft}$$

Numerical Equations

With these numerical values, the equations for the normalized quantities become

$$\theta = 1 - \frac{H_{ft}}{145{,}442} \qquad 0 \le H \le H_T \qquad \text{(A-5)}$$

$$\theta = \theta_S = \frac{T_S}{T_0} = 0.751865 \qquad H > H_T \qquad \text{(A-10)}$$

$$\delta = \left(1 - \frac{H_{ft}}{145{,}442}\right)^{5.255\,913} \qquad 0 \le H \le H_T \qquad \text{(A-6a)}$$

$$\delta = 0.223\,359 \exp\left(-\frac{H_{ft} - 36{,}089.2}{20{,}805.7}\right) \qquad H > H_T \qquad \text{(A-9a)}$$

$$\sigma = \left(1 - \frac{H_{ft}}{145{,}442}\right)^{4.255\,913} \qquad 0 \le H \le H_T \qquad \text{(A-7)}$$

$$\sigma = 0.297\,073 \exp\left(-\frac{H_{ft} - 36{,}089.2}{20{,}805.7}\right) \qquad H > H_T \qquad \text{(A-11)}$$

$$\mu = \sqrt{(1 - H_{ft}/145{,}422)} \qquad 0 \le H \le H_T \qquad \text{(A-8)}$$

$$\mu_S = \sqrt{\theta_S} = 0.867\,107 \qquad H > H_T \qquad \text{(A-12)}$$

Tabulated Values

Evaluation of these equations for several selected altitudes between the surface and 45,000 ft results in the following tabulated values. Comparison with the reference document (Anonymous, 1962) shows agreement within 5 units in the last place.

STANDARD ATMOSPHERE TABLE FOR SIX SELECTED ALTITUDES

Sea-Level Properties				
H, ft	**T_0, deg R**	**p_0, lb/ft^2**	**ρ_0, sl/ft^3**	**a_0, ft/sec**
0	518.67	2116.22	0.00237 691	1116.45
Dimensionless Ratios				
	$\theta \equiv T/T_0$	**$\delta \equiv p/p_0$**	**$\sigma \equiv \rho/\rho_0$**	**$\mu \equiv a/a_0$**
5,000	0.965 622	0.832 047	0.861 669	0.982 661
10,000	0.931 244	0.687 702	0.738 447	0.965 010
15,000	0.896 866	0.564 339	0.629 235	0.947 030
25,000	0.828 110	0.371 089	0.448 116	0.910 006
35,000	0.759 354	0.235 302	0.309 872	0.871 409
45,000	0.751 865	0.145 546	0.193 580	0.867 101

REFERENCES

Anonymous: U. S. Standard Atmosphere, 1962. National Aeronautics and Space Administration, United States Air Force, and United States Weather Bureau. U.S. Government Printing Office, Washington, D.C., Dec. 1962.

APPENDIX B
ELEMENTS OF TRANSPORT AIRCRAFT DESIGN AND OPERATION

INTRODUCTION

The purpose of this appendix is to present a concise, tutorial overview of transport aircraft design and operation for readers without this background. In particular, the review of aircraft dynamic response presented in the final section of this appendix supports the discussion of dynamical system properties in the main report. The treatment is at the level of an introductory course, starting from elementary principles and using simplifying assumptions commonly used within the aircraft industry during preliminary design. Readers desiring more detail can consult the references provided.

Only the longitudinal motions of the aircraft within its plane of symmetry are treated by this appendix, but these motions provide the basis for discussing aircraft performance and other reference material needed for the main report. A nonelementary generalization of the longitudinal equations for coordinated turning flight is presented in appendix C.

The plan of presentation for this appendix is as follows. After discussing simplified models for the Earth, the atmospheric environment, and the aircraft structure, the three longitudinal equations of motion for flight in still air are derived from Newton's second law. A brief discussion then shows how those equations can be generalized to include the effects of wind and wind shear. The motion of the aircraft is subject to aerodynamic and propulsive forces, which are analyzed next.

For simplicity, aerodynamic forces are discussed entirely from the experimental viewpoint, avoiding the complexities of aerodynamic theory. Dimensional analysis is used to simplify experimental results by identifying the nondimensional combinations of parameters that constitute Reynolds number, Mach number, and the aerodynamic force coefficients. Dynamic similarity based on these nondimensional parameters enables the aerodynamic forces acting on full-scale aircraft to be predicted from the results of model tests. Aircraft lift and drag characteristics are presented, and a generic aerodynamic model representative of large transport aircraft is developed.

Propulsive thrust is treated from an experimental viewpoint similar to that for aerodynamic forces. Dimensional analysis provides the basis for correlating engine manufacturers' data gathered under various altitude and temperature conditions, and a generic engine model is developed based on NASA simulation models that is representative of the high-bypass-ratio turbofan engines installed on current transport aircraft. The dynamic response of the engine to throttle control is specified in block-diagram form.

The steady-state solution of the longitudinal equations of motion is then used to define the performance envelope of the aircraft. The selection of operating points within this envelope that optimize performance is discussed. The Breguet range equation is derived, and a representative payload-vs-range diagram is constructed to show primary economic influences on design. Brief comments on airport performance show the influence of wing loading and thrust loading as design parameters.

The selection of operating points for climb and descent is described, and the performance discussion concludes with some comments on trajectory optimization for complete mission profiles.

In the final section, the dynamic response of the generic airplane to control is treated in some detail, and simulation models are developed at three levels of dynamical fidelity. Simulation equations and block diagrams are provided, and numerical simulation techniques are illustrated by using a widely available spread-sheet package, enabling interested readers to perform their own dynamic response calculations. In addition to providing results needed for the main report, it is hoped that such simulations may aid readers, especially those with flying experience, to gain an improved grasp of transport aircraft dynamic response characteristics without requiring a detailed mathematical understanding of the nonlinear differential equations on which those response characteristics depend.

LONGITUDINAL EQUATIONS OF MOTION

The equations of motion for transport aircraft are obtained by application of Newton's second law to a rigid aircraft subject to aerodynamic, propulsion, and gravitational forces. Six ordinary differential equations result, three scalar force equations and three scalar moment equations. Because transport aircraft are bilaterally symmetric and operate in symmetric (coordinated) flight with near-zero sideslip angles, the six equations of motion are decoupled to form a longitudinal set describing motions in the plane of symmetry, and a lateral-directional set describing asymmetric motions. This appendix treats only the longitudinal motions.

Earth Model

The Earth is represented as flat and nonrotating, with uniform gravity independent of latitude and height (local tangent plane approximation). This simplified Earth model neglects the very small contributions from Coriolis force encountered in great-circle flight over a rotating Earth, and from centrifugal "weightlessness" force encountered in flight over a spherical Earth at high speeds approaching orbital velocity, neither of which is of interest for control of subsonic transport aircraft.

Atmospheric Environment

For flight in still air, the atmospheric environment is completely specified by the properties of the standard atmosphere, which describes the variations with altitude of ambient pressure, temperature, density, and sonic velocity (app. A). After discussing the equations of motion for flight in still air, it is shown how these equations can be generalized to include the effects of steady wind and those of wind shear. The effects of atmospheric turbulence, which are usually studied by simulation employing suitably filtered random noise, are not treated here.

Aircraft Structural Model

Transport aircraft are not structurally rigid, but the natural frequencies of their structural modes usually lie far above the frequencies of concern for control, justifying the approximation that elastic structural deformations can be considered to take place instantaneously. This quasi-static approximation enables the airflow to be represented as acting on the deformed aircraft. The gyroscopic effects of rotating engine machinery are omitted, and the control surfaces of the aircraft are assumed to be actuated irreversibly, so that they involve no additional degrees of freedom.

Reference Frames

The frame of reference in which the aircraft motions are described could be taken as fixed in the Earth, which under our assumptions is an inertial (unaccelerated) frame in which the Newtonian equations are directly valid. Alternatively, the motion of the aircraft with respect to the Earth can be described in a reference frame fixed in the aircraft itself (the body frame), with its origin located at the aircraft center of mass and its three orthogonal axes aligned with the aircraft fuselage and wing structure (fig. B-l(a)). It is essential to describe the aircraft rotational motions in the body frame to avoid the appearance of the moments and products of inertia in the equations of motion as time-varying parameters.

For the translational motions of the aircraft, this report uses the path frame, which by definition is fixed in the aircraft with its origin at the aircraft center of mass like that of the body frame, but with one of its three orthogonal axes aligned with the aircraft velocity vector, and the other two normal to it, as illustrated by figure B-1(b). Both the body-frame and path-frame descriptions include acceleration cross-product terms that account for rotation of the reference frame with respect to the Earth.

For wings-level flight, the orientation of the body frame relative to the Earth is specified by the pitch angle θ (fig. B-1(a)), and the orientation of the path frame relative to the Earth is specified by the flightpath angle γ (fig. B-1(b)). In still air, the angle of the body-frame longitudinal axis relative to the airstream, which is termed the fuselage angle of attack (fig. B-1(b)), is given by the equation

$$\alpha = \theta - \gamma \tag{B-1}$$

where the notation is

α Fuselage angle of attack, rad

θ Pitch angle, rad

γ Flightpath angle, rad

Choice of the path frame for the translational motions is convenient from two viewpoints. First, the force description is simplified because, by definition, the aerodynamic streamwise (drag) force and the normal (lift) force are aligned with the axes of the path frame (fig. B-1(c)). Furthermore, normal forces contributed by the propulsion system (that is, powered lift owing to thrust inclination) are small in conventional transport aircraft and can be neglected, together with forces resulting from interaction of engine efflux with aerodynamic flow. Therefore, both the aerodynamic forces and the thrust are aligned with the path-frame axes, so that only the gravitational force requires trigonometric transformation.

Second, from the human-factors perspective, the pilot's primary control task can be regarded as the moment-to-moment control of the aircraft velocity vector in such a way as to realize the mission objectives summarized by the flight plan. During manual control, the pilot's task is facilitated by providing separate control of each of the three components of the velocity vector (that is the directional track angle, the flightpath angle, and the airspeed), and by eliminating dynamical coupling between these elements. The parameterization resulting from choice of the path frame contributes to these design objectives.

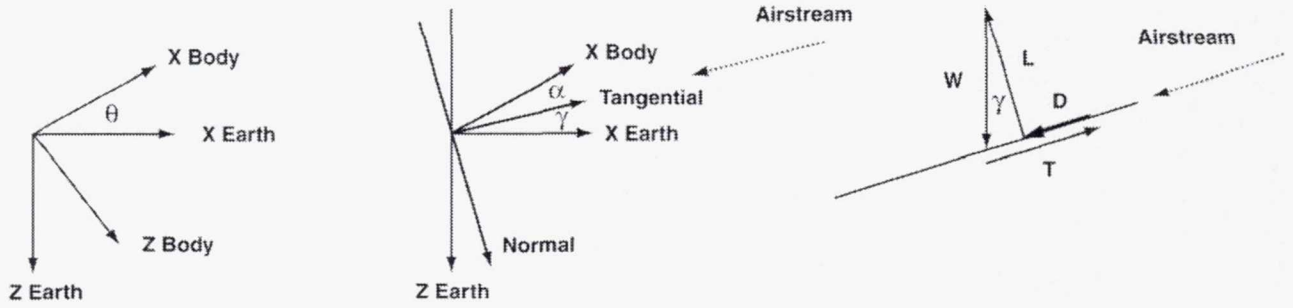

a) Earth frame and body frame.

b) Path frame aligned with velocity vector.

c) Force equilibrium.

Figure B-1. Reference frames.

Equations of Motion

Under the assumptions just discussed, the longitudinal motions of the aircraft can be described by the following three scalar equations (fig. B-1(c)), which result directly from application of Newton's second law to a rigid aircraft subject to aerodynamic, propulsive, and gravitational forces, and are valid during straight (nonturning) flight in still air:

Longitudinal force equation: $$m\,a_T = T - D - W \sin \gamma_{IN} \tag{B-1a}$$

Normal force equation: $$m\,a_N = L - W \cos \gamma_{IN} \tag{B-1b}$$

Pitching moment equation: $$I_Y \frac{dq}{dt} = M_Y \tag{B-1c}$$

where the notation is as follows:

English symbols

a_T	Tangential acceleration, ft/sec^2	m	Aircraft mass, slug
a_N	Normal acceleration, ft/sec^2	M_Y	Pitching moment, ft-lb
D	Drag, lb	q	Pitch rate, rad/sec
g	Gravitational acceleration, 32.1741 ft/sec^2	T	Thrust, lb
I_Y	Pitching moment of inertia, slug-ft^2	V_{IN}	Tangential acceleration, ft/sec
L	Lift, lb	W	Aircraft weight, lb

Greek symbols

γ_{IN} Inertial flightpath angle, rad

The kinematic acceleration a_T in the direction of the velocity vector is equal to dV_{IN}/dt, and the normal (centripetal) acceleration a_N toward the instantaneous center of rotation is given by the cross-product $V_{IN}\,(d\gamma_{IN}/dt)$. Furthermore, the aircraft mass m is equal to W/g. Making these substitutions,

and dividing the two force equations by the weight W, the longitudinal equations can be put in the form

$$\frac{1}{g}\frac{dV_{IN}}{dt} = \frac{T - D}{W} - \sin\gamma_{IN} \tag{B-2a}$$

$$\frac{V_{IN}}{g}\frac{d\gamma_{IN}}{dt} = \frac{L}{W} - \cos\gamma_{IN} \tag{B-2b}$$

$$I_Y \frac{dq}{dt} = M_Y \tag{B-2c}$$

A formal derivation of these equations using vector methods is presented in appendix C, which generalizes the equations for coordinated turning flight. It should be noted that, in still air, the airspeed V coincides with the inertial velocity V_{IN}, and the flightpath angle γ relative to the airmass coincides with the inertial flightpath angle γ_{IN}.

Wind and Wind Shear

For a steady tailwind acting in the streamwise direction along the velocity vector, the airmass moves uniformly with respect to the Earth, so that the airspeed V is related to the inertial velocity V_{IN} by the Galilean transformation

$$V_{IN} = V + w \tag{B-3a}$$

where the notation is as follows:

V Airspeed, ft/sec w Tailwind component of wind velocity, ft/sec

Because the tailwind is assumed to act in the streamwise direction, the flightpath angle γ relative to the airmass continues to coincide with the inertial flightpath angle γ_{IN}. It can be seen that the substitution of equation (B-3a) into equation (B-2a) does not produce additional terms, since the time derivative of the tailwind w vanishes for a steady wind.

If the airmass accelerates instead of moving uniformly, or if the wind field varies with altitude so that the aircraft encounters changing winds during climb or descent, then substitution of equation (B-3a) into equation (B-2a) causes an additional term involving the wind shear dw/dt to appear in the longitudinal (streamwise) force equation:

$$\frac{1}{g}\frac{dV}{dt} = \frac{T - D}{W} - \sin\gamma_{IN} - \frac{1}{g}\frac{dw}{dt} \tag{B-3b}$$

In an increasing tailwind, the wind shear term (l/g) dw/dt on the right side of equation (B-2a) acts to reduce airspeed in the same way as a drag increase or a thrust reduction. Since the lift L in equation (B-2b) is proportional to the square of airspeed, the loss of lift owing to reduced airspeed results in

downward acceleration, causing the aircraft to settle below its still-air path. Aircraft performance can be severely degraded. Steady downdrafts have a similar performance-degrading effect on the aircraft even though the airmass moves uniformly, because level flight relative to the Earth requires climbing flight relative to the airmass.

In general, for flight in steady horizontal wind and steady vertical draft, the longitudinal equations of motion remain unchanged in form, provided that the speed and flightpath angle are measured relative to the airmass. The aerodynamic lift and drag forces and the thrust force are, of course, referred to the airmass by their definitions. These forces will be examined in detail in the following sections.

AERODYNAMIC FORCES

Similarity in Fluid Mechanics

The fluid forces acting on a submerged body such as an aircraft are related to the size and shape of the body, its motion relative to the fluid, and to the physical properties of the fluid by a general functional relation of the form

$$\mathbf{f}\,(\text{force, size, shape, motion, fluid properties}) = 0$$

Size and Shape

Body size can be represented by a characteristic length such as the wing span of an aircraft or its fuselage diameter. Its shape can be represented by dimensionless ratios such as the thickness/chord ratio that characterizes an airfoil section. In addition to the geometric shape factors that remain fixed for a given body, shape also involves the angle of attack of the body relative to the fluid flow, which is defined by the angle between the velocity vector and a longitudinal reference axis fixed in the body, such as the fuselage floor of an aircraft (fig. B-1).

Motion

In general, the motion of the body involves both its velocity and its acceleration relative to the fluid. In steady motion the acceleration vanishes, and the forces depend only on the velocity of the body relative to the fluid. If an aircraft maneuvers, the necessary force is generated by changes in the aerodynamic pressures acting on its surfaces. In subsonic flight, these pressure changes are propagated throughout the flow field near the aircraft, and produce changes in the flow pattern that modify the forces acting on the aircraft. Therefore, the total force depends in general (that is, in unsteady flow) on the acceleration of the fluid as well as on its relative velocity.

However, if the aircraft maneuvers slowly enough, the resulting flow-pattern changes can be regarded as taking place instantaneously relative to the velocity changes of the aircraft, so that the aerodynamic forces depend only on the relative velocity of the fluid, and not on its acceleration. This approximation, termed quasi-steady flow, is justified for transport aircraft by their limited maneuvering capability.

Fluid Properties

The fundamental properties of a fluid that influence the forces acting on a submerged body are its density, which influences inertia force, its viscosity, which influences fluid friction (shear) force, and its compressibility, which influences elastic force. The compressibility of a fluid can be specified by giving the value of sonic velocity. Gravity is not involved, because the buoyancy force resulting from gravity acts on a submerged body independently of its motion.

Functional Relation

Accounting for size, shape, motion, and fluid properties, the aerodynamic forces acting on transport aircraft can be expressed symbolically by the following functional equation:

$$\mathbf{f}\,(F, l, V, \rho, \upsilon, a, \alpha, \text{body shape}) = 0 \qquad \text{(B-4)}$$

where the notation is as follows:

F	force, lb	ρ	density, slug/ft^3
l	characteristic length, ft	υ	viscosity, slug/ft-sec
V	relative velocity, ft/sec	a	sonic speed, ft/sec

α angle of attack, rad

The nature of this functional relationship can be clarified by dimensional analysis, which enables the functional dependence of the aerodynamic force to be expressed in nondimensional form.

Dimensional Analysis

The Buckingham π theorem asserts that any function of **r** dimensional variables involving **s** fundamental quantities can be reduced to a function of (**r – s**) dimensionless groups (Bridgman, 1970; Taylor, 1974). Since there are six unknown dimensional variables involving the three fundamental quantities mass, length, and time in equation (B-4), it follows from the theorem that the functional relation can be expressed in terms of three unknown dimensionless groups in the following way:

$$\mathbf{f}\,(\pi_1, \pi_2, \pi_3, \alpha, \text{body shape}) = 0 \qquad \text{(B-4a)}$$

where each of the three dimensionless groups π_1, π_2, π_3 consists of a product of the dimensional variables with unknown exponents.

In general, each group involves all except one of the dimensional variables. The choice of the variables in each group is arbitrary, but can be guided by heuristic knowledge. Since it is desired to find the functional variation of the force F, it is included only in the first group π_1 to permit its later isolation. Since the force is known experimentally to depend weakly on the viscosity, the latter is omitted from the first group in order to separate it from the force.

Thus the variables chosen for the first group π_1 are F, V, ρ, l, and a. Denoting their unknown exponents by the symbols i, j, k, and n, dimensional homogeneity requires that the dimension of the product ($F\, V^i\, \rho^j\, l^k\, a^n$) must vanish. In terms of the fundamental physical quantities mass M, length L, and time T, the dimensions of the quantities appearing in this product are as follows:

$$\text{Dim } F = \frac{ML}{T^2} \qquad \text{Dim } V^i = \frac{L^i}{T^i} \qquad \text{Dim } \rho^j = \frac{M^j}{L^{3j}} \qquad \text{Dim } a = \frac{L^n}{T^n}$$

By substituting these dimensions into the first product, the following dimensional equation is obtained:

$$\frac{ML}{T^2}\ \frac{L^i}{T^i}\ \frac{M^j}{L^{3j}}\ L^k\ \frac{L^n}{T^n} = M^0\ L^0\ T^0 \tag{B-4b}$$

Collecting terms and equating exponents in equation (B-4b) results in the following system of linear equations in the unknown exponents:

$$1 + j = 0 \qquad 1 + i + k + n - 3j = 0 \qquad 2 + i + n = 0 \tag{B-4c}$$

There are three equations in the four unknown exponents i, j, k, and n. Solving for i, j, and k in terms of n results in the solution

$$i = -2 - n \qquad j = -1 \qquad k = -2$$

With these exponents, the π_1 product becomes

$$(F\ V^{-2-n}\ \rho^{-1}\ l^{-2}\ a^n) = \frac{F}{\rho V^2 l^2}\left(\frac{a}{V}\right)^n \tag{B-4d}$$

Since both the factors $F/\rho V^2\ l^2$ and a/V are nondimensional, they correspond to the π_1 and π_2 groups.

Removing both of the variables F and a from the third dimensionless product π_3, it becomes $(V^i\ \rho^j\ l^k\ \upsilon^m)$. The dimensions of the quantities appearing in this product are

$$\text{Dim } V^i = \frac{L^i}{T^i} \qquad \text{Dim } \rho^j = \frac{M^j}{L^{3j}} \qquad \text{Dim } l^k = L^k \qquad \text{Dim } \upsilon^m = \frac{M^m}{L^m T^m} \tag{B-4e}$$

Solving the dimensional equation in the manner just illustrated to obtain the exponents i, j, and k in terms of m, the π_3 product is found to be

$$(V^{-m}\ \rho^{-m}\ l^{-m}\ \upsilon^m) = \left(\frac{\upsilon}{\rho V l}\right)^m \tag{B-4f}$$

Defining the dimensionless quantities π_1, π_2, and π_3 to be

$$C_F \equiv 2\ F\ /\ \rho\ V^2\ l^2 \qquad M \equiv V\ /\ a \qquad Re \equiv \rho\ V\ l/\upsilon \tag{B-5}$$

the functional relation (B-4a) becomes

$$\mathbf{f}\,(C_F,\ \alpha,\ M,\ Re,\ \text{body shape}) = 0 \qquad \text{(B-6a)}$$

Equation (B-6a) can be solved for C_F to obtain the nondimensional force equation

$$C_F = \mathbf{g}\,(\alpha,\ M,\ Re,\ \text{body shape}) \qquad \text{(B-6b)}$$

in which the form of the function **g** is entirely unrestricted by the dimensional analysis.

Force Coefficient

The nondimensional quantity $C_F \equiv 2\ F/\rho\ V^2\ l^2$ is termed the coefficient of the aerodynamic force F. The quantity l^2 represents a characteristic area that is taken as the frontal area for bodies such as fuselages and as the wing planform area S for wings and for complete airplanes. The important quantity $\rho\ V^2/2$, which is termed the dynamic pressure, corresponds to the kinetic energy of a unit volume of air moving at velocity V. The factor of 2 is introduced for convenience without changing the nondimensional nature of the force coefficient.

Mach Number

The quantity $M \equiv V/a$ is termed the Mach number. It represents the ratio of the inertia force acting on a fluid element to the elastic force resulting from the compressibility of the fluid. For flight at Mach numbers less than about 0.3, air can be considered "incompressible"; that is, its density is nearly constant in fluid flow. At such low Mach numbers, elastic forces are unimportant, so that the Mach number can be dropped from the functional relation B-6(b).

Reynolds Number

The quantity $Re \equiv \rho V l/\upsilon$ is termed the Reynolds number. It represents the ratio of the inertia force acting on a fluid element to the viscous force. At sufficiently large Reynolds numbers, it is found experimentally that the force coefficient depends weakly on Reynolds number, which can therefore be dropped from the functional relation. It is not that viscous effects are unimportant at high Reynolds number, but that they become insensitive to changes in Reynolds number at the large values characterizing flight of transport aircraft.

Force Equation

For a given aircraft of known wing, tail, and fuselage shape, the aircraft shape factor is constant and can also be dropped. By combining the definition of force coefficient with the functional relation (B-6b) and dropping the Reynolds number and body shape factors as just discussed, the force equation is finally obtained in the form

$$F = \left(\frac{\rho\ V^2}{2}\right) S\ C_F\ (\alpha,\ M) \qquad \text{(B-6c)}$$

The primary airplane force coefficients used in this report are the lift coefficient C_L and the drag coefficient C_D, which are defined by specializing equation (B-6c):

$$L = (\frac{\rho V^2}{2})S C_L(\alpha, M) \qquad D = (\frac{\rho V^2}{2})S C_D(\alpha, M) \tag{B-6d}$$

Moment Equation

Aerodynamic moments acting on an aircraft result from the distribution of aerodynamic forces over the aircraft surface. By carrying out a similar dimensional analysis with the pitch rate q included as a separate motion variable, it can be shown that the pitching moment M_Y (equation (B-2c)) can be expressed in the nondimensional form

$$M_Y = (\frac{\rho V^2}{2})S c C_M(\alpha, qL_T / V, M, \delta_E, \delta_{STAB}) \tag{B-6e}$$

where c is the wing chord and C_M is termed the pitching moment coefficient. The elevator deflection δ_E provides pitch control, and the stabilizer deflection δ_{STAB} provides the pitching moment required for pitch equilibrium (trim) with the elevator faired ($\delta_E = 0$). The pitch rate has been expressed nondimensionally by multiplying it by the tail arm L_T and dividing by the airspeed V. This nondimensional pitch rate corresponds to the change in angle of attack at the horizontal tailplane, which contributes most of the damping in pitch. For simplicity, pitching moment contributions owing to thrust are omitted from equation (B-6e).

Dynamic Pressure

An alternate form of the dynamic pressure $\rho V^2/2$ can be obtained as follows. Substitute the relation $\rho = p/RT$ from the equation of state, where p denotes the ambient pressure, T the ambient temperature, and R the gas constant (app. A). Then substitute $V = M a$ from equation (B-5) to obtain the relation

$$(\frac{\rho V^2}{2}) = (\frac{p}{RT})\frac{M^2}{2}a^2$$

In a compressible fluid, the sonic speed a is given by the relation $a^2 = \gamma_S RT$ (app. A), where γ_S denotes the specific heat ratio ($\gamma_S = 1.40$ for air). With this, the dynamic pressure becomes

$$(\frac{\rho V^2}{2}) = \frac{\gamma_s}{2} p M^2 \tag{B-6f}$$

This result could have been obtained directly from the dimensional analysis by choosing pressure and temperature as fluid properties instead of density and sonic velocity.

Dynamic Similarity

Because the Mach number and Reynolds number together determine the force ratios acting on each fluid element, they determine the streamline pattern of the flow around a body such as an aircraft. If a model having the same shape as an aircraft is placed in a wind tunnel far from the tunnel walls and tested at the same angle of attack, Mach number, and Reynolds number as those prevailing for the aircraft in flight, the streamline pattern of the flow around the model will be geometrically similar to that of the flow around the aircraft. The lift and drag coefficients measured for the model will then be identical to those for the aircraft (equation B-6b).

This condition of dynamic similarity provides the basis for scaling up the forces measured during model testing to estimate those acting on the aircraft in flight. The economy of effort resulting from use of the nondimensional functional relation (B-6a) instead of the dimensional form (B-4) is impressive. A similar economy of description results from use of the nondimensional parameters in dynamical modeling and simulation.

Aerodynamic Force Characteristics

The functional forms of the lift and drag coefficients for representative transport aircraft are illustrated by figure B-2, which shows the variations of these coefficients with angle of attack and Mach number.

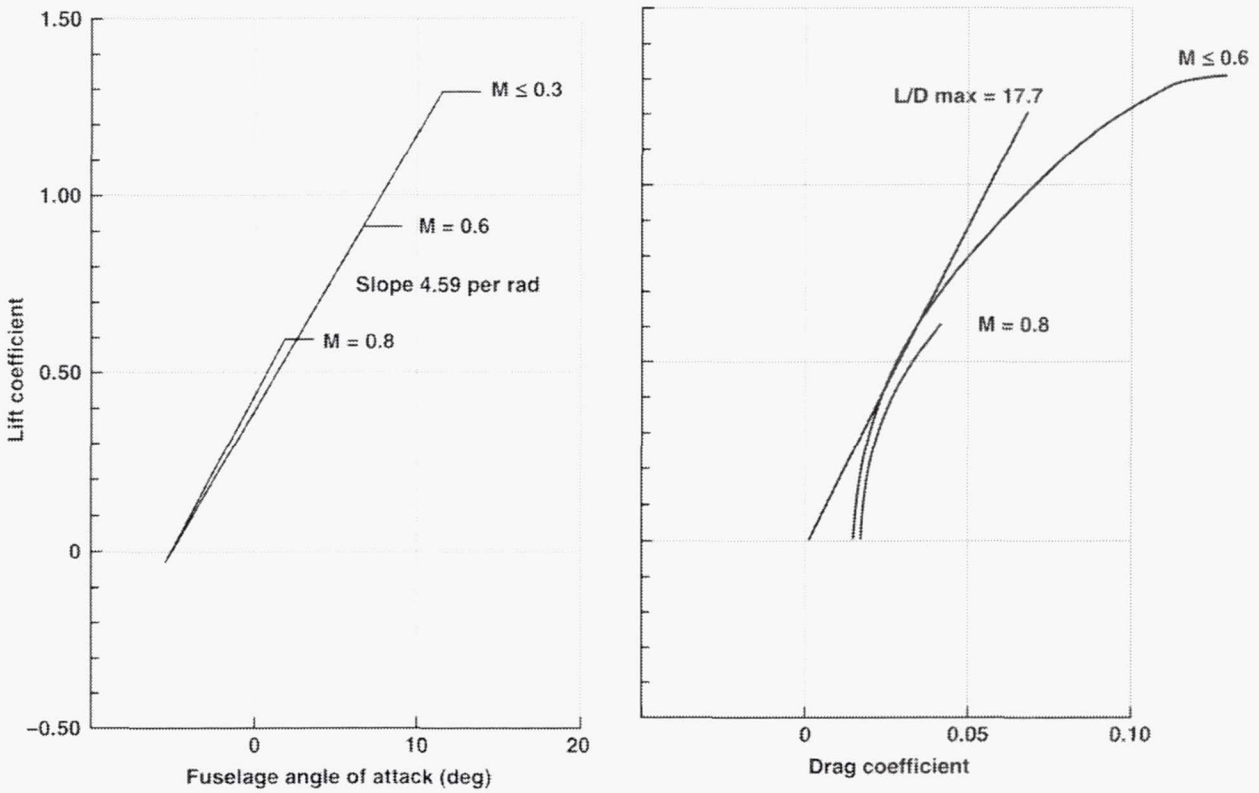

a) Lift curve

b) Drag polar

Figure B-2. Aerodynamic force characteristics.

Lift

It can be seen that the variation of lift coefficient with angle of attack is nearly linear for angles of attack below the stalling angle, which decreases with increasing Mach number (fig. B-2(a)). Therefore, it can be represented by an equation of the form

$$C_L = (dC_L/d\alpha)\,(\alpha - \alpha_0) \tag{B-7a}$$

where α_0 denotes the angle of zero lift, and the lift-curve slope $dC_L/d\alpha$ depends on Mach number. The lift-curve slope can be approximated for transport aircraft by the equation (Shevell, 1989)

$$\frac{dC_L}{d\alpha} = \frac{2\pi\,AR}{2 + 1.03\,AR\sqrt{(1 + \tan^2\Lambda - M^2)}} \tag{B-7b}$$

where Λ is the angle of wing sweep and AR is the wing aspect ratio defined in the next section. Equation (B-7a) is valid for angles of attack less than the stalling angle, for which the lift coefficient takes on its maximum value $C_{L\,MAX}$ (fig. B-2(a)). Representative parameter values for transport aircraft can be found in table B-1.

TABLE B-1. TRANSPORT AIRCRAFT PERFORMANCE PARAMETERS

$M \leq 0.6$ Wing flaps and landing gear retracted			
$C_{L\,MAX} = 1.30$	$C_{DP} = 0.0150$	$AR = 7.2$	$e = 0.83$
$C_{L\,MIN\,DRAG} = 0.53$	$(L/D)_{MAX} = 17.7$	$V_{E\,MAX} = 400$ kt	

	Maximum takeoff weight	**Midcruise weight**	**Maximum landing weight**	**Normal landing weight**
W/S, lb/ft^2	150	125	110	90
T/W (static)	0.25	0.30	0.34	0.42
$V_{E\,STALL}$, kt	184.6	168.5	158.1	143.0
$V_{E\,MIN\,DRAG}$, kt	289.0	263.9	247.5	223.9

Drag

The variation of drag coefficient with lift coefficient is approximately parabolic over the range used in airline service (fig. B-2(b)). Therefore, it can be represented by an equation of the form

$$C_D = C_{DP} + \frac{C_L^{\,2}}{\pi\,AR\,e} \tag{B-7c}$$

where C_{DP} and e depend on the Mach number for $M > 0.6$ (fig. B-2(b)). The parasite drag represented by C_{DP} is due primarily to skin-friction drag independent of lift.

The second right-hand term of equation (B-7c) represents lift-dependent drag termed induced drag, which corresponds to the rate of increase of kinetic energy in the trailing vortices that form in the wake of the aircraft. The dimensionless aspect ratio AR is defined by $AR \equiv b^2/S$, where b is the wing span and S the wing area. The Oswald span efficiency factor e accounts for the differences between practical wings and a hypothetical wing of the same span with elliptic spanwise distribution of lift, for which induced drag is known theoretically to be minimum and the efficiency factor e to be unity. Representative values of AR and e for transport aircraft can be found in table B-1.

Aerodynamic Performance

The aircraft lift and drag characteristics determine several parameters that are important for aerodynamic performance.

Level-Flight Performance

For steady level flight ($dV/dt = d\gamma/dt = 0$), equation (B-2a) shows that the thrust T must equal the drag D. Similarly, equation (B-2b) shows that the lift L must equal the weight W. Expressing the lift in coefficient form (eq. (B-6d)) and using the alternate form for the dynamic pressure q (eq. (B-6f)), the lift equation for steady level flight can be put in the form

$$L = (\gamma_S \, p \, M^2/2) \, S \, C_L = W \tag{B-7d}$$

Solving this equation for M and expressing the atmospheric pressure p in the nondimensional form $\delta \, P_0$ (eqs. (A-6a), (A-9a)), the Mach number required for steady level flight is found to be

$$M = \sqrt{(2/\gamma_S \, p) \, (W/S) \, (1/C_L)} = \sqrt{(2/\gamma_S \, p_0) \, (\frac{W/S}{\delta}) \, (1/C_L)} \tag{B-7e}$$

The important parameter W/S is termed the wing loading. Physically, the wing loading represents the weight supported by each unit area of wing surface. Representative parameter values can be found in table B-1. Similarly, by expressing the dynamic pressure q as $\rho V^2/2$ and solving the lift equation for the airspeed V, the airspeed required for steady level flight is found to be

$$V = \sqrt{(2/\rho) \, (W/S) \, (1/C_L)} = \sqrt{(2/\rho_0) \, (W/S/\sigma) \, (1/C_L)} \tag{B-7f}$$

Stall

The stalling airspeed V_{STALL} is found by substituting the maximum lift coefficient into equation (B-7f):

$$V_{STALL} = \sqrt{(2/\rho_0) \, (W/S/\sigma)/C_{L\,MAX}} \tag{B-7g}$$

Representative values of the parameters C_{LMAX} and V_{STALL} for transport aircraft can be found in table B-1.

Lift/Drag Ratio

The ratio of lift to drag L/D is an important figure of merit for aerodynamic performance. Since it follows from the definitions (B-6d) that this ratio is the same in coefficient form as in dimensional form, it can be seen from figure B-2(b) that the point of maximum L/D is determined by the tangent line from the origin with smallest slope. The corresponding angle of attack can then be found from figure B-2(a).

In dimensional form, the parasite drag corresponding to the first right-hand term of equation (B-7c) is defined from equation (B-6d) to be $D_P = (\rho\ V^2/2)\ S\ C_{DP}$, and similarly the level-flight induced drag corresponding to the second right-hand term is

$$D_I = (\rho\ V^2/2)\ S\ C_L{}^2/\pi AR\ e = (\rho\ V^2/2)\ S\ [W/(\rho V^2/2)\ \ S]^2/\pi AR\ e$$

or

$$D_I = [(W/S)/(\rho V^2/2)]\ [W/\pi AR\ e]$$

Thus D_P is proportional to V^2, and D_I to $1/V^2$. Clearly, the total drag $D = D_P + D_I$ takes on its minimum value at some intermediate airspeed that will be termed $V_{MIN\ DRAG}$.

Minimum Drag

For $M \leq 0.6$ where the parasite drag C_{DP} and the span efficiency e are independent of Mach number, this minimizing airspeed could be found by differentiating the total drag D with respect to the airspeed V. Alternatively, the lift coefficient corresponding to minimum drag can be found by differentiating the ratio C_D/C_L obtained from equation (B-7c) with respect to C_L. This minimizing value is found to be

$$C_{L\ MIN\ DRAG} = \sqrt{(\pi\ AR\ e\ C_{DP})} \qquad \text{(B-7h)}$$

By analogy to equation (B-7g), the level-flight airspeed for minimum drag is then

$$V_{MIN\ DRAG} = \sqrt{(2/\rho_0)(W/S/\sigma)/C_{L\ MIN\ DRAG}} \qquad \text{(B-7i)}$$

Since for steady level flight $D = L/(L/D) = W/(L/D)$, minimizing the total drag D maximizes the lift/drag ratio $L/D = C_L/C_D$.

By substituting $C_{L\ MIN\ DRAG}$ into equation (B-7c), the minimum value of the drag coefficient $C_{D\ MIN\ DRAG}$ is found to be

$$C_{D\ MIN\ DRAG} = C_{DP} + \pi\ AR\ e\ C_{DP}/\pi\ AR\ e = 2\ C_{DP} \qquad \text{(B-7j)}$$

Equation (B-7j) shows that, at the speed for minimum drag, the parasite drag and the induced drag are equal. Representative values of $C_{L\ MIN\ DRAG}$, $V_{MIN\ DRAG}$, and $(L/D)_{MAX}$ for transport aircraft can be found in table B-1.

Equivalent Airspeed

The equivalent airspeed V_E is defined as the product of the true airspeed V and the square root of the nondimensional density ratio $\sigma \equiv \rho/\rho_0$ (app. A), so that equation (B-7f) becomes

$$V_E \equiv V\sqrt{\sigma} = \sqrt{(2/\rho_0)(W/S)/C_L} \tag{B-7k}$$

Expressed in terms of the equivalent airspeed, the stalling speed (equation (B-7g)) becomes

$$V_{E\ STALL} = \sqrt{(2/\rho_0)(W/S)/C_{L\ MAX}} \tag{B-7l}$$

Equation (B-7l) shows that, in terms of equivalent airspeed, the stalling speed is independent of ambient density, and therefore independent of altitude. The same is true for $V_{MIN\ DRAG}$ (eq. (B-7i)).

By substituting $M \equiv V/a$, $a = a_0\sqrt{\theta}$, and $\sigma = \sqrt{(\delta/\theta)}$ (app. A) into equation (B-7k), the relation between equivalent airspeed and Mach number is found to be

$$V_E \equiv V\sqrt{\sigma} = M\,a\left[\sqrt{\sigma}\right] = M\,a_0\sqrt{\theta}\left[\sqrt{(\delta/\theta)}\right] = M\,a_0\sqrt{\delta} \tag{B-7m}$$

where $a_0 = 1116.45$ ft/sec $= 661.48$ kt.

Since the dynamic pressure q is defined by $\rho V^2/2 = \rho_0\,\sigma V^2/2 = \rho_0\,V_E^2/2$, structural loads depend on the square of V_E. At low Mach numbers, the equivalent airspeed V_E is approximately the same as that measured by the aircraft pitot-static system for display to the pilot.

ENGINE MODEL

Thrust Function

The engine thrust can be regarded as a fluid force acting on a submerged body (that is, the engine itself within its nacelle), so that the thrust is related to the size and shape of the engine, its motion, and the physical properties of air as its working fluid by a functional relationship of the same kind as that for the aircraft itself, as discussed previously. Representing the size by a characteristic length that can be taken as the diameter of the inlet, and taking the rotational shaft speed as a separate motion variable and pressure, temperature, and viscosity as fluid properties, the thrust can be expressed symbolically by the following functional equation:

$$\mathbf{f}(T, D, V, N, p, T_a, \upsilon, \text{shape}) = 0 \tag{B-8}$$

where the notation is as follows:

T	Thrust, lb	p_a	Ambient pressure, lb/ft^2
D	Inlet diameter, ft	T_a	Ambient temperature, deg R
V	Airspeed, ft/sec	υ	Viscosity, slug/ft-sec
N	Rotational speed, rev/min (rpm)		

The shape factor can be regarded as a large number of dimensional ratios that, taken together, entirely determine the complex internal geometry of the engine, including all its rotating machinery. By applying dimensional analysis to equation (B-8), it can be shown (Hill and Peterson, 1992) that the thrust can be expressed in nondimensional form by the equation

$$\frac{T}{p\,D^2} = \mathbf{f}\left(M, \frac{ND}{\sqrt{\gamma_S R T_a}}, Re, \text{shape} \right) \tag{B-8a}$$

Since the sonic velocity is given by $a = \sqrt{\gamma_S R T_a}$ (equation (A-4), the nondimensional rotational speed $ND / \sqrt{\gamma_S R T_a}$ can be regarded as a measure of the Mach number at the tips of the turbine blades. Just as for the aerodynamic force functions, it is found that, at the high Reynolds numbers characterizing engine operation, the thrust is nearly independent of the Reynolds number Re, which can therefore be dropped from the functional equation.

For a given engine, the inlet diameter D and the shape factors are fixed constants that can also be removed from the functional equation. Introducing the dimensionless pressure and temperature ratios $\delta \equiv p/p_0$ and $\theta \equiv T_a/T_0$ (app. A), the thrust can be expressed by the equation

$$\frac{T}{\delta} = \mathbf{f}\left(M, \frac{N}{\sqrt{\theta}} \right) \tag{B-8b}$$

where the standard sea-level values of pressure and temperature p_0 and T_0 have been removed. Equation (B-8b) is useful for correlating engine manufacturers' data gathered under various conditions in flight with the static thrust measured under standard sea-level conditions. The quantity T/δ is termed the corrected thrust, and the quantity $N/\sqrt{\theta}$ is termed the corrected rpm.

Thrust Characteristics

Turbofan engines are characterized by their bypass ratio, which is the ratio of the mass airflow passing through the fan to that passing through the core engine. Bypass ratios of 5 to 6 are representative of the engines in use on current transport aircraft. The variation of corrected thrust with corrected rpm typical of such engines during steady-state operation under static conditions (M = 0) is illustrated by figure B-3, which is taken from a NASA-Ames simulation model. Neglecting details such as the minor disturbance owing to compressor bleed-valve operation (fig. B-3), this thrust variation can be represented nondimensionally by the empirical equations

$$N = 51 + 0.5\,\delta_T \qquad 0 \le \delta_T \le 96\% \tag{B-8c}$$

$$(T_0/T_{ST})/\delta = 0.765\left[(N/\sqrt{\theta})/100\right] - 0.34 \qquad 51\% \le N/\sqrt{\theta} < 75\% \tag{B-8d}$$

$$(T_0/T_{ST})/\delta = 17.47\left[1 - N/\sqrt{\theta})/100\right]^3 + 4.04\left[(N/\sqrt{\theta})/100\right] - 3.07 \qquad 75\% \le N/\sqrt{\theta} \le 100\% \tag{B-8e}$$

where the throttle setting δr and the rpm N are expressed in percent of maximum, T_0/δ denotes the corrected static (M = 0) thrust, and T_{ST} denotes the manufacturer's rated thrust. The maximum available thrust is taken as 97% of rated static thrust to account for installation losses (Shevell, 1989).

The variation of nondimensional corrected thrust with Mach number at constant corrected rpm can be approximated by the empirical equations

$$(T/T_{ST})/\delta = [T_0/T_{ST})/\delta][1 - 1.224\ M + 1.398\ M^2] \qquad M < 0.3 \tag{B-8f}$$

$$(T/T_{ST})/\delta = [T_0/T_{ST})/\delta][0.874 - 0.385\ M] \qquad M \ge 0.3 \tag{B-8g}$$

where the nondimensional corrected static thrust $(T_0/T_{ST})/\delta$ is given by equations (B-8d), (B-8e). The characteristic decrease of thrust with increase of Mach number results from momentum loss in the airstream entering the engine owing to deceleration within the inlet, which is termed ram drag.

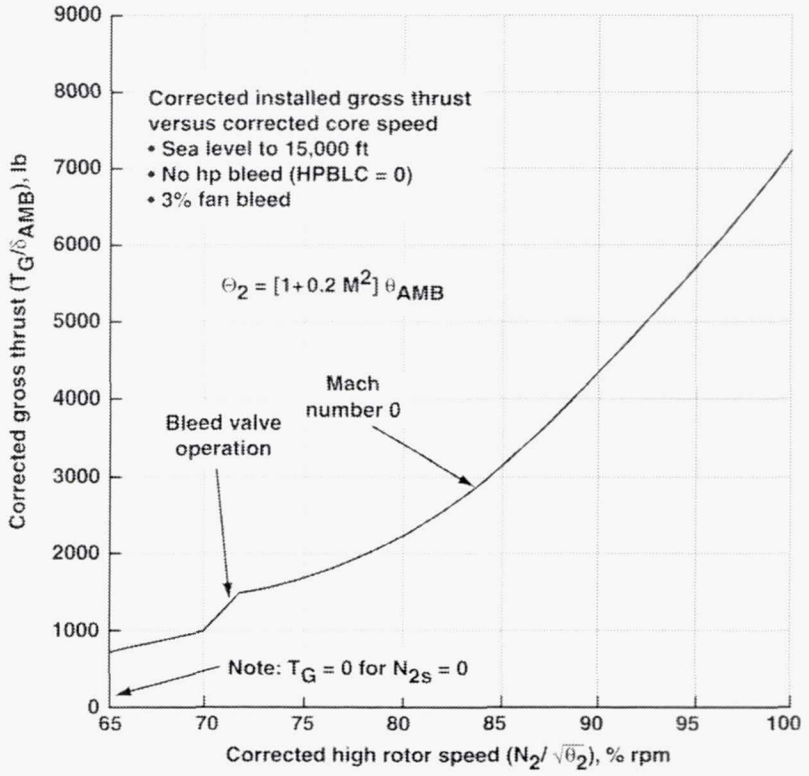

Figure B-3. Variation of corrected thrust with corrected rpm.

Thrust Limits

Equations (B-8d) and (B-8e) do not apply to the maximum available thrust T_{MAX} except at sea level, because at maximum thrust the physical rpm, not the corrected rpm, must be held fixed at its maximum value. With the physical rpm held constant, the corrected rpm varies with altitude, increasing according to equations (B-8d) and (B-8e) as the nondimensional temperature ratio θ decreases with height until it reaches its minimum value in the constant-temperature stratosphere (table A-1). The resulting variation of thrust with Mach number is illustrated by figure B-4 for five altitudes ranging from sea level to 45,000 ft.

The variation of maximum thrust illustrated by figure B-4 is given by the empirical equations

$$(T_{MAX}/T_{ST})/\delta = 0.970 - [1.187 - 7.737\,(\theta^{-1/2} - 1)]\,M + [1.356 - 8.840\,(\theta^{-1/2} - 1)]\,M^2 \qquad M < 0.3 \qquad \text{(B-8h)}$$

$$(T_{MAX}/T_{ST})/\delta = 0.848 - 0.373\,M + (0.796 + 2.433\,M)\,(\theta^{-1/2} - 1) \qquad M \geq 0.3 \qquad \text{(B-8i)}$$

The $(\theta^{-1/2} - 1)$ temperature factors in equations (B-8h) and (B-8i) account for the increase in thrust owing to the increase in corrected rpm. This temperature factor, which is constant at about 15% within the stratosphere, approximately compensates the thrust loss owing to ram drag, so that for $M \geq 0.3$ the maximum thrust is nearly independent of Mach number at 35,000 ft and 45,000 ft (fig. B-4). Other engine limits such as turbine temperature limits (which are not represented in figure B-4) may limit available thrust under some conditions.

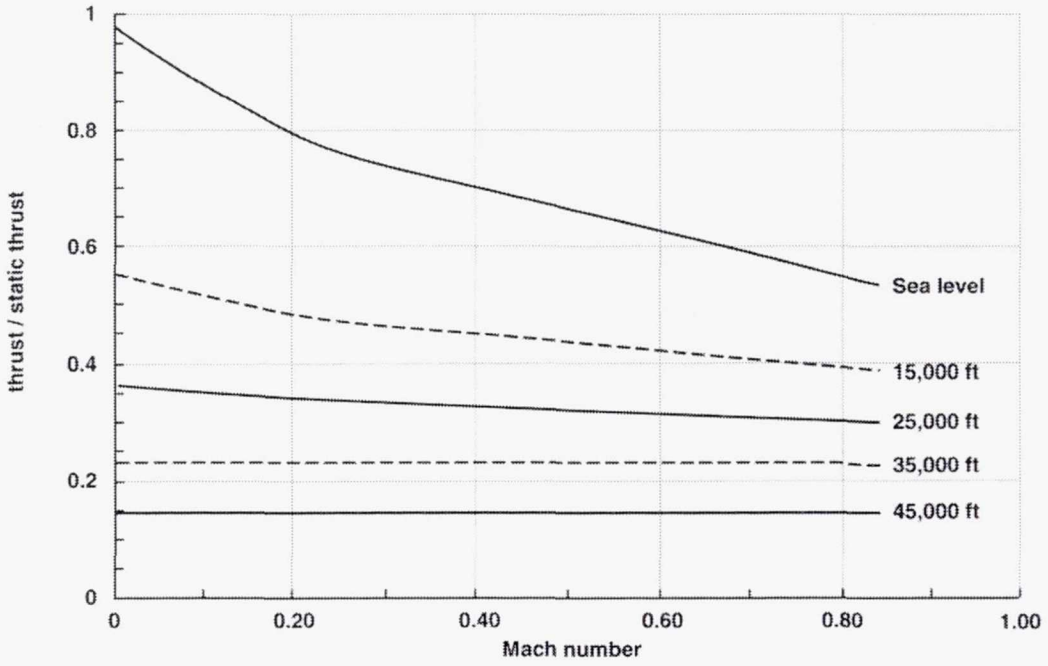

Figure B-4. Variation of maximum thrust with Mach number.

Thrust Lag

The throttle of a turbine engine controls the rate at which fuel is admitted to the combustion chamber, which must be limited within the fuel control to avoid excessive turbine temperature during engine acceleration. The resulting limitation of available shaft torque combines with the inertia of the rotating parts to cause a characteristic lag in the response of rotational shaft speed (rpm) to a throttle command. For correct physical modeling, a dynamical lag function should be applied to the shaft rpm to represent the effects of fuel-control limiting and rotational inertia, and the thrust should then be calculated from this lagged rpm according to the nonlinear equations (B-8c), (B-8d), and (B-8e).

However, for simplicity the lag function can be applied directly to the thrust commanded by the throttle, provided that the time constants and rate limits involved are adjusted to represent the actual lag in the thrust function correctly. Such an adjusted lag function is illustrated by the block diagram of figure B-5, which is taken from a NASA-Ames simulation model. It can be seen that the thrust lag is represented by a critically damped second-order system that is equivalent to two first-order exponential lags in cascade, each with a characteristic time constant of 0.5 sec.

The thrust response to abrupt full-throttle step commands, including the effects of the acceleration and rate limiters (fig. B-5), is illustrated by figure B-6(a). It can be seen that, starting from at least 85% rpm (50% thrust), the thrust response is crisp, reaching full thrust in slightly more than 2 sec.

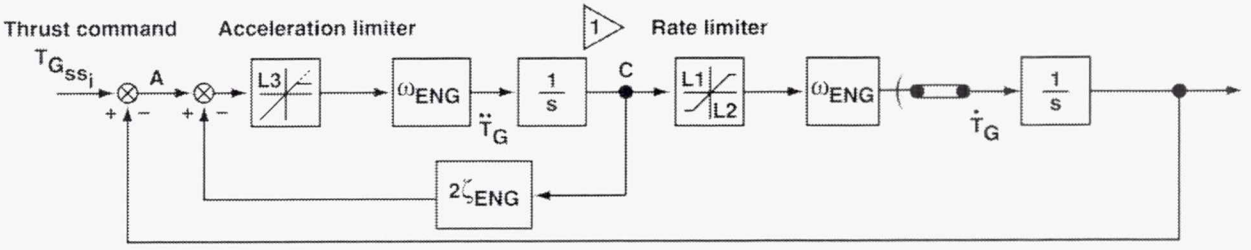

Engine respoonse characterisitcs

- ω_{ENG} = 4.0 rad/sec, ζ_{ENG} = 1.0
- Limiters:

  Acceleration

  - Upper limit L3 = FCN $\left(T_{G_i}, T_{G_{SS_i}} \right)$ See logic diagram, figure B-5b, for rules on use of this limiter.
  - No lower limit

  Rate

  - Upper limit L1 = 0.0925 • $\left(T_{G_{MAX}} \right)$

    $$T_{G_{MAX}} = \left(T_G / \delta_{AMB} \right)_{MAX} \delta_{AMB}$$

  - Lower limit L2 = –0.020 * $\left(T_{G_{MAX}} \right)$

Figure B-5(a). Thrust response block diagram.

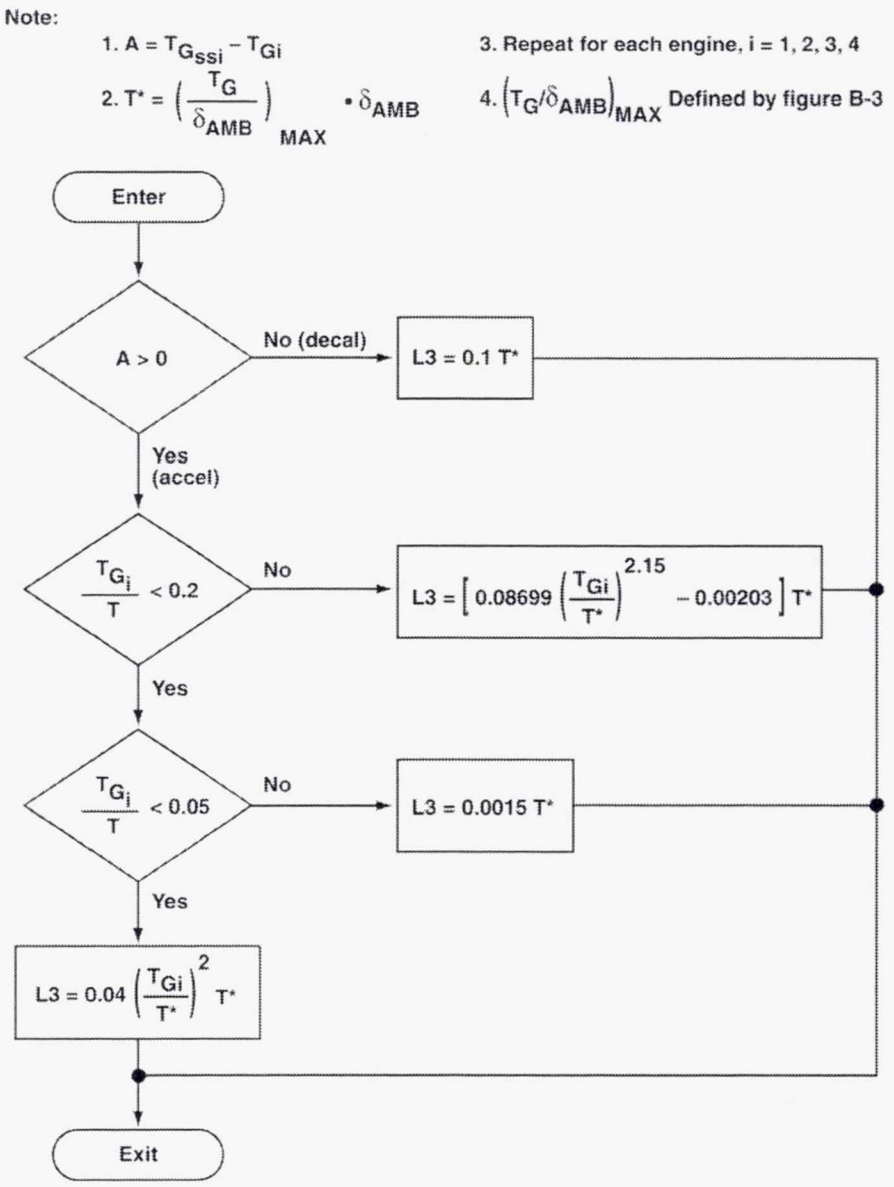

Figure 5(b). Acceleration limit logic.

With initial rpm below 78% (30% thrust), fuel limiting increases the lag substantially, with about 8 seconds required to reach full thrust when starting from idle. The thrust response to abrupt reduced-thrust step commands is illustrated by figure B-6(b).

The degrading effect of thrust lag on control of airspeed is most critical during landing approach, when the need for precise airspeed control is greatest. During landing approach, extension of landing gear and wing flaps reduces the lift/drag ratio to about 7 (not represented in table B-1). For a wing loading of 110 lb/ft^2 at landing weight, about 26.5% of maximum thrust is required for steady flight on a standard three-degree approach flightpath angle (equation B-2(a)). It can be seen from figure B-6 that thrust response would then be somewhat degraded.

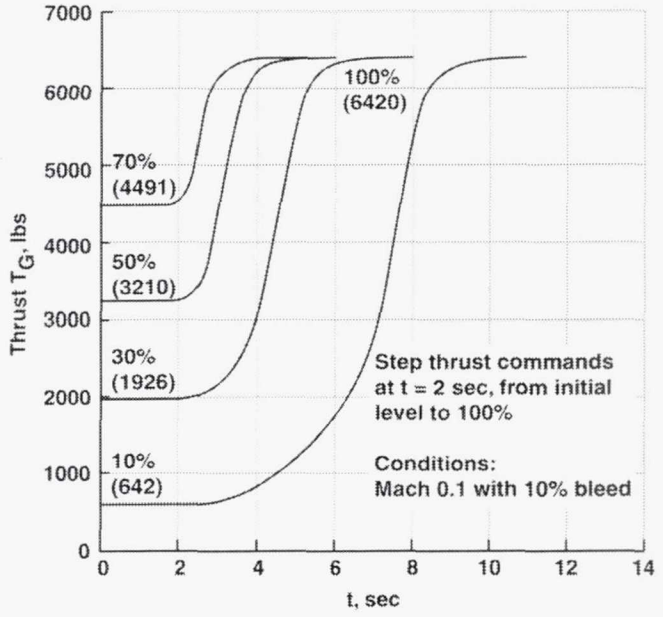

a) Acceleration

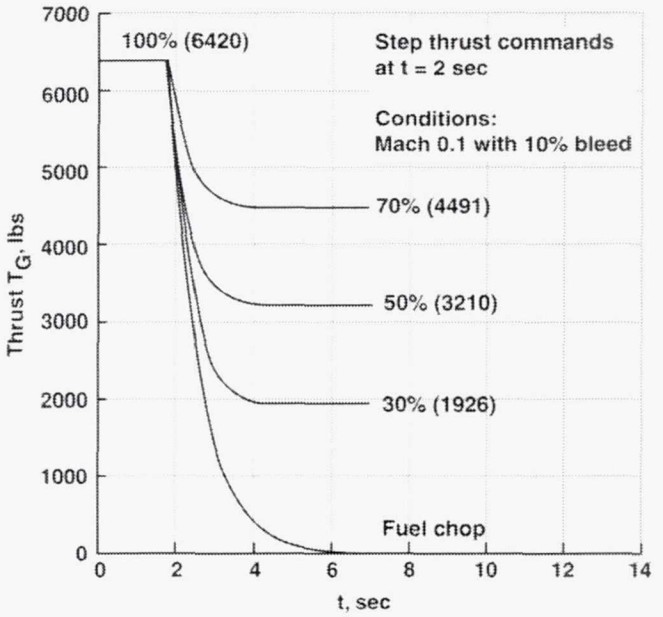

b) Deceleration

Figure B-6. Thrust response to throttle steps.

AIRPLANE PERFORMANCE

Performance of an aircraft in steady flight is determined by the steady-state (equilibrium) solution of the streamwise and normal force equations (B-2a) and (B-2b). For simplicity, flight in still air is assumed. However, as noted previously, the equations of motion remain unchanged in form for flight in a steady wind, provided that the speed V and the flightpath angle γ are measured with respect to the airmass (eq. (B-3)). In still air, the airspeed V and the aerodynamic flightpath angle γ coincide with their inertial counterparts. In equilibrium flight, the longitudinal acceleration dV/dt and the normal acceleration V(dγ/dt) must vanish, so that, denoting the equilibrium (trim) flightpath angle by γ_{TRIM}, the force equations become

$$\sin \gamma_{TRIM} = (T - D)/W \tag{B-9a}$$

and

$$\cos \gamma_{TRIM} = L/W \tag{B-9b}$$

Expressing the lift, drag, and weight forces in coefficient form (equations (B-6c), (B-6d)), the force equations become

$$\sin \gamma_{TRIM} = \frac{T}{W} - \frac{C_D}{C_W} \tag{B-9c}$$

and

$$\cos \gamma_{TRIM} = \frac{C_L}{C_W} \tag{B-9d}$$

where $C_L \equiv L/qS$, $C_D \equiv D/qS$, and $C_W \equiv W/qS$, and the dynamic pressure q is defined as usual by $q \equiv \rho V^2/2$, or alternatively by $q \equiv \gamma_S p M^2/2$ (eq. (B-6f)).

Assuming for simplicity that the drag characteristic of the aircraft can be represented by a parabolic polar curve (Shevell, 1989), the drag coefficient C_D is given by:

$$C_D = C_{DP} + C_L{}^2/\pi AR\, e \tag{B-7c}$$

Performance Envelope

The performance envelope of the aircraft is determined by the variation of γ_{TRIM} with equivalent airspeed or with Mach number, which can be calculated as follows. Substitute equation (B-7c) into equation (B-9c):

$$\sin \gamma_{TRIM} = \frac{T}{W} - \frac{C_{DP}}{C_W} - \frac{1}{C_W}\frac{C_L{}^2}{\pi AR\, e} \tag{B-10a}$$

Substitute equation (B-7c) into equation (B-10a) to eliminate C_L:

$$\sin\gamma_{TRIM} = \frac{T}{W} - \frac{C_{DP}}{C_W} - \frac{C_W}{\pi AR\, e}\cos^2\gamma_{TRIM} \qquad \text{(B-10b)}$$

With the identity $\cos^2\gamma_{TRIM} = 1 - \sin^2\gamma_{TRIM}$, equation (B-10b) becomes

$$\sin\gamma_{TRIM} - \frac{C_W}{\pi AR\, e}\sin^2\gamma_{TRIM} = \frac{T}{W} - \frac{C_{DP}}{C_W} - \frac{C_W}{\pi AR\, e} \qquad \text{(B-10c)}$$

With $C_W \equiv W/qS$ and $q = \rho_0 V_E^2/2$, equation (B-l0c) becomes, finally,

$$\sin\gamma_{TRIM} - \frac{1}{\pi AR\, e}\frac{W/S}{\rho_0 V_E^2/2}\sin^2\gamma_{TRIM} = \frac{T}{W} - \frac{C_{DP}}{W/S}\rho_0 V_E^2/2 - \frac{1}{\pi AR\, e}\frac{W/S}{\rho_0 V_E^2/2} \qquad \text{(B-10d)}$$

For convenience, the notation is repeated as follows:

English symbols

A	=	a(H)	Sonic velocity, ft/sec
AR	≡	b^2/S	Wing aspect ratio, dimensionless
b			Wing span, ft
C_{DP}	=	C_{DP} (M)	Parasite drag coefficient, dimensionless
e	=	e (M)	Span efficiency, dimensionless
H			Height in standard atmosphere, ft
M	≡	V/a	Mach number, dimensionless
N			Engine rpm, percent
p_0			Standard sea-level barometric pressure, 2116.22 lb/ft^2
q			Dynamic pressure, lb/ft^2
S			Wing area, ft^2
T/δ	=	fn (N, M)	Corrected thrust, lb
V_E	=	$V\sqrt{\sigma}$	Equivalent airspeed, ft/sec
W/S			Wing loading, lb/ft^2

Greek symbols

$\delta \equiv p/p_0 = \delta(H)$			Ambient pressure ratio, dimensionless
γ_{TRIM}			Trim (equilibrium) flightpath angle, deg
ρ_0			Standard sea-level density, 0.00237 691 sl/ft^3
$\sigma \equiv \rho/\rho_0 = \sigma(H)$			Ambient density ratio, dimensionless

Equation (B-10d) gives the variation of the equilibrium (steady-state) flightpath angle γ_{TRIM} with equivalent airspeed V_E, with the thrust T (or, alternatively, engine rpm N) as parameter. It can be seen that, at a known height H in the standard atmosphere (app. A) and at a selected equivalent airspeed V_E, and with known aircraft parameters T/W, W/S, C_{DP} , AR, and e, equation (B-10d) is quadratic in sin γ_{TRIM} and can be solved for γ_{TRIM} in closed form. The following parameter values are representative for a transport aircraft climbing with maximum thrust at sea level at the minimum-drag airspeed (table B-1):

$W/S = 150$ lb/ft^2	$C_{DP} = 0.0150$	$AR = 7.19$	$e = 0.83$
$V = 487.9$ ft/sec	$V_E = 289.1$ kt	$M = 0.437$	$T/W = 0.1765$

With these parameter values, equation (B-10d) becomes

$$\sin \gamma_{TRIM} - 0.028\,286 \sin^2 \gamma_{TRIM} = 0.1200 \qquad \text{(B-10e)}$$

The numerical solution for sin γ_{TRIM} is 17.6766 ± 17.5562, or, since the property sin $(\cdot) \leq 1$ rules out the positive sign,

$$\sin \gamma_{TRIM} = 0.1204 \qquad \gamma_{TRIM} = 6.92 \text{ deg}$$

Since γ_{TRIM} is small, the exact result differs trivially from the approximation obtained by neglecting the small $\sin^2 \gamma_{TRIM}$ term. At this climb angle and airspeed, the lift coefficient, the drag coefficient, the lift/drag ratio, and the rate of climb are found for reference to be

$$C_L = 0.53 \qquad C_D = 0.0298 \qquad L/D = 17.7 \qquad dH/dt = 3524 \text{ ft/min}$$

Repeating the calculation over the airspeed range of interest and plotting γ_{TRIM} against V_E or M (eq. (B-7m) defines the contour for maximum thrust, which forms the upper boundary of the flight envelope. The contour for minimum (idle) thrust forms the lower boundary. Contours for intermediate values of thrust can be added as desired to complete the diagram for the aircraft performance envelope (Innis, Holzhauser, and Quigley, 1970).

A second set of contours corresponding to constant pitch attitude can be constructed in the following way. Solve equation (B-9d) for the lift coefficient

$$C_L = C_W \cos \gamma_{TRIM} = (W/q\,S) \cos \gamma_{TRIM} \qquad \text{(B-10f)}$$

which determines the lift coefficient for any point (V_E, γ_{TRIM}) within the flight envelope, since γ_{TRIM} is given by the ordinate and the dynamic pressure q is determined by the abscissa V_E or M. Now, the lift coefficient is related to angle of attack by equation (B-7a), which can be solved to find the angle of attack corresponding to the selected point. With both the flightpath angle γ_{TRIM} and the angle of attack α known, the pitch attitude θ can be found from equation (B-1)

$$\theta = \alpha + \gamma \tag{B-1}$$

which is valid for wings-level flight.

A representative flight envelope is illustrated by figure B-7. The left-hand boundary corresponds to the stalling speed, or to the minimum-control speed. The right-hand boundary is determined by structural limits at low altitude, and by compressibility (Mach) effects at high altitude. The upper and lower boundaries are determined by the maximum and minimum thrust limits, respectively, as noted previously. Because at any fixed throttle setting (constant engine rpm) thrust decreases with speed (eqs. (B-8f) and (B-8g)), the thrust contours take on their maximum values of γ_{TRIM} at airspeeds slightly below the speed for minimum drag.

During manual flight, the pilot controls pitch with elevator and engine rpm with throttle. It can be seen from figure B-7 that the steady-state solution of the force equations (B-2a), (B-2b) for any combination of control inputs is determined by the intersection of the pitch and rpm contours corresponding to those control inputs. The desired steady-state solution will be termed the target operating point. The next sections discuss the selection of operating points within the performance envelope so as to optimize climb, cruise, and descent performance.

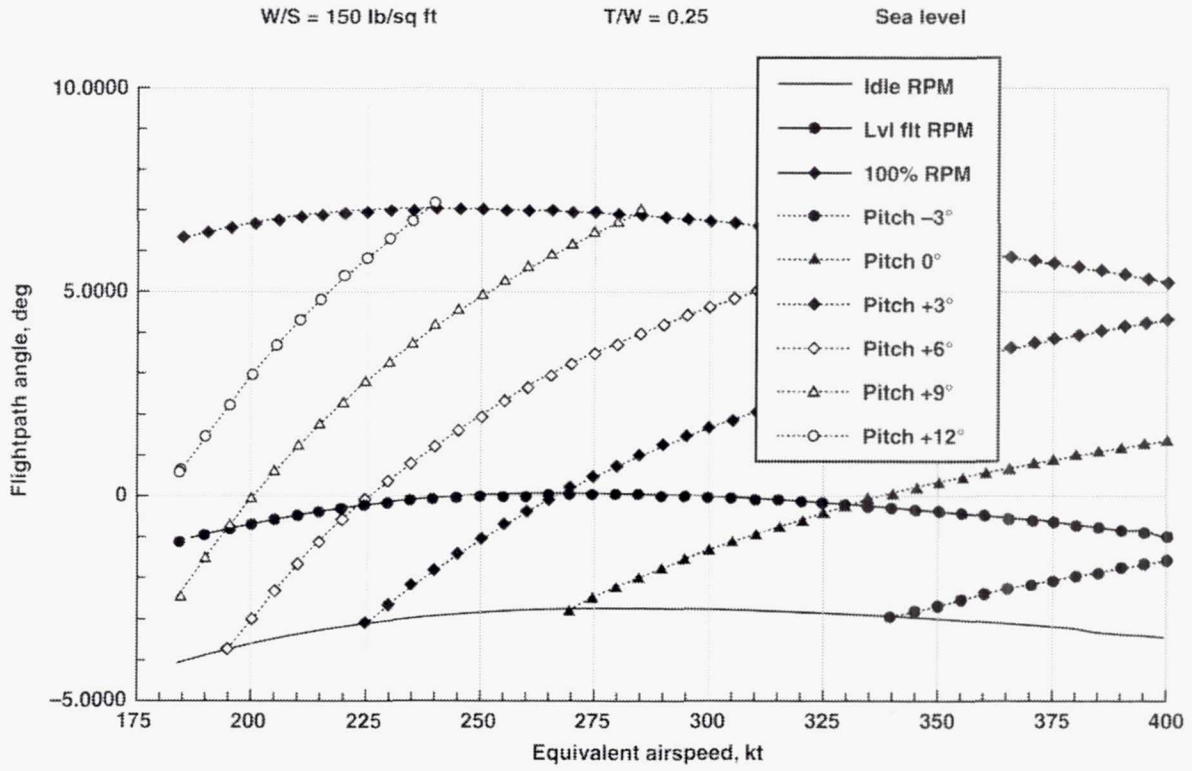

Figure B-7. Performance envelope.

Cruise Performance

Optimization of cruise performance is a dominant influence in the design of transport aircraft, reflecting the importance of economic factors. Selection of the cruise operating point, which is based on maximizing specific range, is examined first.

Specific range

The specific range is defined as the distance flown in still air per unit weight of fuel consumed, which is found by dividing airspeed by the fuel flow rate:

$$sr \equiv dR/dF = (dR/dt) / (dF/dt) = V/(dF/dt) = V/c\,T \qquad \text{(B-11a)}$$

where the notation is as follows:

F	Fuel quantity, lb	dF/dt	Fuel flow rate, lb/hr
R	Range, nautical miles (nm)	T	Thrust, lb
sr	Specific range, nm/lb	V	Airspeed, knots (nm/hr)
c	Specific fuel consumption, lb/hr per lb thrust		

Since cruise operation takes place in steady level flight, lift must equal aircraft weight and thrust must equal drag (eqs. (B-2a), (B-2b), and (B-7c)). The fuel flow rate is proportional to thrust, so that

$$dF / dt = c\,T = c\,D = c\,L / (L/D) = c\,W / (L/D) \qquad \text{(B-11b)}$$

By substituting equation (B-11b) into equation (B-11a) and putting V = M a (eq. (B-5)), the specific range equation can be put in the form

$$sr = (a/c)\,M\,(L/D)\,(1/W) \qquad \text{(B-11c)}$$

Since at any fixed altitude the sonic velocity a is constant (eqs. (A-8) and (A-12)), and since for simplicity the specific fuel consumption c is assumed constant, equation (B-11c) shows that maximizing the specific range requires maximizing the nondimensional product M(L/D).

If the Mach number is restricted to lie below M = 0.6, in the range where compressibility drag is unimportant and an analytic representation of the drag polar is available (eq. (B-7c), then by expressing M as a function of the lift coefficient C_L (eq. (B-7e)), the product M(L/D) could be maximized by differentiation with respect to C_L (compare equation (B-7h)). However, such a result would be invalidated by the restriction to $M \leq 0.6$, because the maximum M(L/D) product is reached for $M > 0.6$ in the range where compressibility effects on drag are important. For the drag characteristics illustrated by figure B-2, it can be shown by numerical optimization that the product M(L/D) takes on its maximum value at M = 0.825, $C_L = 0.46$. For these conditions, the lift/drag ratio is 15.8 and the product M(L/D) is 13.035.

Optimal Altitude

Since most transport aircraft operation takes place in the stratosphere where the sonic velocity a is constant (eq. (A-12)), for simplicity the variation of a at slightly lower altitudes is neglected. Since the specific fuel consumption c has already been assumed constant, equation (B-11c) shows that maximum specific range is obtained for maximum M(L/D) independent of altitude. With the maximizing values of M and C_L known, equation (B-7e) can be solved for the parameter $(W/S)/\delta$, which will be termed normalized wing loading:

$$(W/S)/\delta = (\gamma_S \, p_0 \, M^2/2) \, C_L \tag{B-12a}$$

Numerically, since $\gamma_S = 1.40$ for air and $p_0 = 2116.22$ lb/ft^2 (app. A), for an aircraft with the drag characteristics illustrated by figure B-2, and for $M = 0.825$, $C_L = 0.46$ at the point of maximum M(L/D), equation (B-12a) becomes

$$(W/S)/\delta = (0.7)\,(2116.22)\,(0.825)^2\,(0.46) = 463.8 \text{ lb/ft}^2 \tag{B-12b}$$

This equation shows that, to maintain the normalized wing loading constant as the aircraft weight is reduced by fuel consumption, the aircraft should climb to a higher altitude at which the normalized pressure δ is reduced proportionately. To illustrate this process, several representative combinations of wing loading and cruising altitude are tabulated in table B-2, relating the altitude to the normalized pressure δ by solving the standard atmosphere equations (A-6a) and (A-9a) for the altitude H. The corresponding equivalent airspeed V_E is given by equation (B-7m).

TABLE B-2. OPTIMAL CRUISE ALTITUDE

W/S, lb/ft^2	150	125	100	75
δ	0.323 415	0.269 513	0.215 610	0.161 708
H, ft	28,110	32,110	36,824	42,809
V_E, kt	310.3	283.3	253.4	219.5

Fortunately, as Shevell points out (Shevell, 1989), the altitude optimum is broad, so that near-maximum specific range can be achieved without adhering closely to the optimal altitude. In practice, the optimal altitude is approximated by a step-climb procedure.

Maximum range

Since the aircraft weight is reduced as fuel is consumed, so that $dF = -dW$, in differential form equation (B-11a) becomes

$$dR = sr \, dF = -dW$$

Eliminating the specific range sr with the help of equation (B-11c), this becomes

$$dR = (a/c)\, M\, (L/D)\, (-dW/W) \tag{B-13a}$$

Provided that the parameters a, c, and M(L/D) remain constant, equation (B-13a) can be integrated to obtain the range:

$$R = (a/c)\, M\, (L/D)\, \ln\, (W_0/W_F) \qquad \text{(B-13b)}$$

where W_0 denotes the initial weight and W_F the final weight. Equation (B-13b) is known as the Breguet range equation. In practice, the integration interval is broken into small weight intervals representing about 1 hour of flight. Within each interval, the integrand parameters can be taken as constant with good accuracy.

Since $W_F = W_0 - F_0 = W_0\,(1 - F_0/W_0)$, where F_0 denotes the initial fuel load, the range equation (B-13b) can be put in the form

$$R = (a/c)\, M\, (L/D)\, \ln\, [W_0/(1 - F_0/W_0)] \qquad \text{(B-13c)}$$

The parameter F_0/W_0 is termed the fuel fraction (of the total weight W_0). Similarly defining the payload fraction by W_P/W_0 and the structure fraction by W_S/W_0, the fuel fraction is given by

$$F_0/W_0 = 1 - (W_P/W_0 + W_S/W_0) \qquad \text{(B-13d)}$$

where W_P is the weight of the payload and W_S that of the empty aircraft with no fuel and only the crew on board.

Economic influences

To illustrate economic influences on design, the range performance is calculated from equation (B-13c) for a representative transport aircraft. The following parameter values are assumed for a maximum-range flight with maximum payload, but with fuel quantity limited by maximum takeoff weight:

$$W_P/W_0 = 0.20 \qquad W_S/W_0 = 0.46 \qquad F_0/W_0 = 0.34 \qquad c = 0.65\ \text{(lb/hr)/lb}$$

Allowing for fuel reserves equal to 8% of the zero-fuel weight and for climb and maneuver fuel equal to 2.45% of the takeoff weight (Shevell, 1989), the fuel fraction available for cruise becomes

$$(F_0/W_0)_{\text{CRUISE}} = 0.34 - 0.08\ (0.20 + 0.46) - 0.0245 = 0.2627$$

Assuming for simplicity that optimal cruise altitude is maintained and that cruise takes place in the stratosphere, for which (app. A)

$$a = \mu\, a_0 = (0.867\,101)\,(1116.45\ \text{ft/sec}) = 573.6\ \text{kt}$$

the range is given by

$$R = (573.6/0.65)\,(0.825)\,(15.8)\,\ln\,[1/(1 - 0.2627)] \qquad \text{(B-13c)}$$

or

$$R = 11{,}500 \ln 1.3563 = 3505 \text{ nm}$$

for maximum payload and maximum takeoff weight.

Assume now that the fuel tanks can be filled to capacity without exceeding the maximum takeoff weight limit by exchanging half the payload for additional fuel, so that the payload fraction becomes $W_P/W_0 = 0.10$ and the fuel fraction becomes $F_0/W_0 = 0.44$. Repeating the calculation as before,

$$(F_0 / W_0)_{CRUISE} = 0.44 - 0.08\,(0.10 + 0.46) - 0.0245 = 0.3707$$

and

$$R = 11{,}500 \ln\,[1/(1 - 0.3707)] = 5326 \text{ nm}$$

with maximum fuel and half the maximum payload.

Finally, assume that the fuel tanks are full with $F_0/W_0 = 0.44$, but that it is desired to ferry the aircraft without payload. After reducing the takeoff weight 10% by removing the half payload of the previous case, the fuel fraction becomes $F_0/W_0 = 0.44/0.9 = 0.4889$ and the structure fraction becomes $W_S/W_0 = 0.46/0.9 = 0.5111$. Repeating the calculation,

$$(F_0 / W_0)_{CRUISE} = 0.4889 - 0.08\,(0 + 0.5111) - 0.0245 = 0.4235$$

and

$$R = 11{,}500 \ln\,[1/(1 - 0.4235)] = 6334 \text{ nm}$$

The additional thousand miles of range relative to the case with half payload results entirely from the reduction of weight.

These results can be summarized in the form of a payload-vs-range diagram (fig. B-8). Despite the errors resulting from several simplifying assumptions, this diagram gives a good estimate of the range capabilities of transport aircraft designed for medium to long (transcontinental) range. Very long range (intercontinental) transports would have a somewhat larger fuel fraction and a smaller structure fraction, while short range transports would have a smaller fuel fraction, a larger structure fraction, and a much larger payload fraction.

The sensitivity of operating economics to payload requires that cruise performance be balanced appropriately with airport performance during the design process, since airport performance (discussed in the next section) limits the maximum takeoff weight. Because the specific range depends on both aerodynamic and propulsion efficiency factors, as already discussed, and because the structure fraction is an inverse measure of structural efficiency, the payload-vs-range characteristic can be regarded as a bottom-line indicator of design excellence.

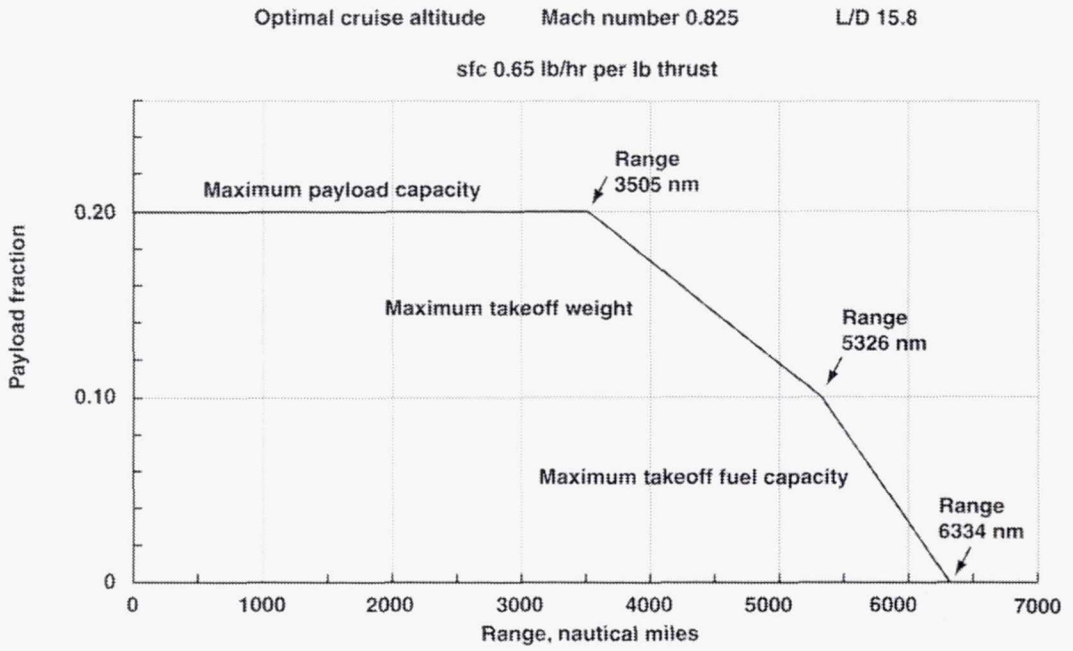

Figure B-8. Variation of payload fraction with range.

Airport Performance

In addition to the optimization of cruise performance just discussed, a second dominant influence on transport aircraft design is the need for adequate airport performance, which is subject to safety requirements imposed by the Federal Air Regulations.

Takeoff field length

The distance X required to accelerate from rest to a speed V_X under constant acceleration a_X is given by the well-known formula $X = V_X^2/2a_X$. The lift-off speed V_X is nominally 1.2 V_{STALL}. With the stall speed given by equation (B-7g), V_X becomes

$$V_X = 1.2\, V_{STALL} = 1.2 \sqrt{(2/\rho)\,(W/S)/C_{L\,MAX}} \qquad \text{(B-14a)}$$

Disregarding drag and assuming still air for simplicity, the acceleration during the takeoff ground run is obtained by substituting $D = 0$ and $\gamma = 0$ into equation (B-2a):

$$a_X = dV_{IN}/dt = (T/W)\, g \qquad \text{(B-14b)}$$

Since thrust decreases with speed during the ground run (equations (B-8d) and (B-8f)), the thrust available at 0.7 V_X should be used in equation (B-14b) to obtain the average acceleration (Shevell, 1989). By substituting equations (B-14a) and (B-14b) into the formula for constant-acceleration distance, the takeoff distance required to reach lift-off speed is found to be

$$X = [1.44\ (W/S)/C_{L\ MAX}]/\rho g\ (T/W) = (1.44/\rho g)\ [((W/S)/(T/W))/C_{L\ MAX}] \qquad \text{(B-14c)}$$

Despite the errors introduced by simplifying assumptions, it is found that actual takeoff distances are roughly proportional to the bracketed quantity in equation (B-14c), which is widely used within the industry to predict takeoff performance during preliminary design. Even after accounting for the failure of one engine as required by the Federal Air Regulations, the bracketed quantity serves as a field-length correlation parameter with surprising accuracy (Shevell, 1989).

Climb Gradient

To ensure safe obstacle clearance after takeoff, the Federal Air Regulations specify the minimum climb gradient ($\tan \gamma$) that must be demonstrated both with and without failure of one engine. With the aircraft drag D and weight W known, the thrust loading T/W necessary to achieve the required steady climb gradient is found by solving equation (B-2a) for T/W with $dV_{IN}/dt = 0$:

$$T/W = D/W + \sin \gamma_{REQ} \qquad \text{(B-15)}$$

With the thrust loading T/W fixed by the climb gradient requirements, equation (B-14c) shows that the takeoff field length is then proportional to the wing loading W/S.

Landing Field Length

Although the takeoff is essentially a Newtonian process, landing is much more dependent on pilot technique. The Federal Air Regulations require that a generous safety factor (67%) be added to the demonstrated landing distance to account for uncertainties. An additional 15% is added for wet pavement, and an additional safety factor results from prohibiting the use of reverse thrust during flight-test demonstrations of landing distance. Fortunately, landing field lengths are almost always shorter than takeoff field lengths, so that landing distance is seldom safety-critical.

Design Overview

Taken together, the desired cruise performance and the necessary airport performance determine the major elements of transport aircraft design. Readers wishing to supplement the following brief comments with more detailed discussion can consult Shevell's 1989 text (Shevell, 1989), which draws on the author's experience as an industry designer to provide an especially clear account. Readers desiring discussion of operational matters involving pilot technique can consult Davies's classic *Handling the Big Jets* (Davies, 1969), which draws on the author's experience as chief test pilot for the Air Registration Board (U.K.) to provide an interesting discussion of jet transport flying qualities. Davies's treatment of airworthiness matters is authoritative.

Design for Cruise Performance

Considering first the major design elements determined by optimization of cruise performance, the parasite drag C_{DP} is proportional to wing thickness, and to the total wetted area of the wing, fuselage, and tail. Induced drag is determined primarily by the wing aspect ratio AR, and by wing taper and twist, which determine the span efficiency factor e. Compressibility drag at cruising speed is determined primarily by the airfoil shape and by the angle of wing sweep.

Design for Airport Performance

The major design elements determined by the required airport performance are the wing loading W/S and the thrust loading T/W. As already noted, the thrust loading is determined primarily by the engine-out climb gradient required for safe obstacle clearance after takeoff. Representative thrust loadings lie near T/W = 0.25 at maximum takeoff weight, slightly less for four-engine aircraft and slightly more for twin-engine or three-engine aircraft to compensate for their larger engine-out thrust loss. Since the induced drag dominates the total drag characteristic at takeoff speed, the engine-out climb gradient of twin-engine aircraft is often improved by increasing the aspect ratio, enabling the required thrust loading to be decreased. Increasing the installed thrust would increase engine weight and cost, and could degrade the specific fuel consumption during cruise if the required cruise thrust were less than about 80% of the maximum thrust available at cruise altitude. Cruise thrust requirements seldom size the engine.

With the thrust loading fixed by climb gradient requirements, the takeoff field length is proportional to the wing loading W/S (eq. (B-14c)), as already noted. As increased thrust becomes available through engine development, economic pressure for increased payload tends to increase maximum takeoff weight proportionately, while maintaining thrust loading constant. If sufficient structural growth capability ("stretch") is available, wing loading increases significantly as later models of the aircraft enter airline service, until practical field length limits are reached. As a rough guide, short-range transports are designed for ranges of 1000 to 2500 nm and takeoff field lengths of 6000 to 8000 ft, with wing loadings up to 120 lb/ft^2. Medium- and long-range transports are designed for transcontinental ranges of 2500 to 5000 nm and takeoff field lengths of 8000 to 10,000 ft, while very long range transports are designed for intercontinental ranges of 5000 to 7000 nm and takeoff field lengths of 10,000 to 12,000 ft, with wing loadings near 150 lb/ft^2.

Balance of Design Factors

A successful transport aircraft design results from balancing competing requirements. To maximize the M(L/D) product in cruise, the aerodynamicist would like long, thin, highly swept wings with small surface area, and the smallest practical tail.

To reduce wing structural weight and provide space for fuel tanks, the structural designer would like short, thick wings, and prefers small sweep angles to avoid problems with structural flexibility. Resolution of the conflicts between aerodynamic and structural designers for subsonic transport aircraft usually results in wing thickness about 10% of chord, aspect ratios in the range of 7 to 8, and sweep angles of 25 to 35 degrees.

To reduce avionics weight and cost and to improve reliability, avionics and flight control designers would like a large tail that avoids the need for stability augmentation. Resolution of their conflict with the aerodynamicists is not yet clear, although transport aircraft with near-neutral natural stability are currently in service, and designs that would be unstable without augmentation are being proposed.

To mitigate the operational penalties for engine failure and avoid the need for extremely high engine reliability for over-water flight, the propulsion designer would like several small engines, but reducing the customer's maintenance costs favors two large ones. This conflict seems likely to be resolved in favor of large twin-engine designs by steady improvement in engine reliability.

As noted previously, the payload-vs-range characteristic of a transport aircraft is a primary economic indicator of the capability of the aircraft for its intended purpose, and therefore constitutes an overall measure of its design excellence. The factors just discussed determine the major elements of each transport aircraft design. The following section discusses operation of the aircraft so as to minimize overall time and cost.

AIRPLANE OPERATION

Climb and Descent Operation

The climb and descent operation of transport aircraft is often optimized so as to minimize total fuel consumption for each flight. For climb, thrust is reduced slightly from takeoff thrust in order to extend engine life. This reduced thrust setting is termed maximum continuous thrust. Idle thrust is used for the descent. With the thrust setting determined, climb and descent trajectories are optimized by selecting the appropriate airspeeds.

Climb

Three different airspeeds may be selected for climb, the choice depending on the quantity to be maximized. If climb gradient is to be maximized for obstacle clearance after takeoff or for some noise-abatement procedures, the airspeed for best angle of climb can be obtained from the performance envelope diagram (fig. B-7). As noted previously, the airspeed for best angle of climb lies slightly below the speed for minimum drag. (Since minimizing drag also minimizes the rate of fuel consumption, the speed for minimum drag is also the speed that maximizes the time of flight available with a fixed fuel quantity, which is termed endurance. For example, the speed selected for holding lies near the speed for minimum drag.)

Since the vertical velocity dH/dt is equal to V sin γ, the airspeed for best rate of climb lies above that for best angle of climb. The former airspeed can be found graphically by adding dH/dt contours to the performance envelope, as illustrated by figure B-9. The airspeed for best rate of climb lies at the point for which the contour for maximum continuous thrust is tangent to the hyperbolic dH/dt contours (fig. B-9).

It can be seen that, as available thrust decreases with altitude, the speed for best rate of climb is reduced, approaching the speed for best angle of climb as the aircraft approaches its ceiling, where $\gamma_{MAX} = 0$. In practice, the maximum altitude is usually determined by the need for a small amount of reserve thrust, which is necessary to enable the aircraft to maneuver. It can be shown that, for coordinated turns, the increased lift required is found by dividing the lift for wings-level flight by the cosine of the bank angle (app. C). The resulting increase of induced drag (eq. (B-7c)) must be compensated by increased thrust to avoid loss of airspeed during turns. Independent of excess thrust, the aircraft's ceiling is limited by stalling or by Mach buffet, because for fixed weight and Mach number the lift coefficient increases with altitude as atmospheric pressure decreases (eq. (B-7c)).

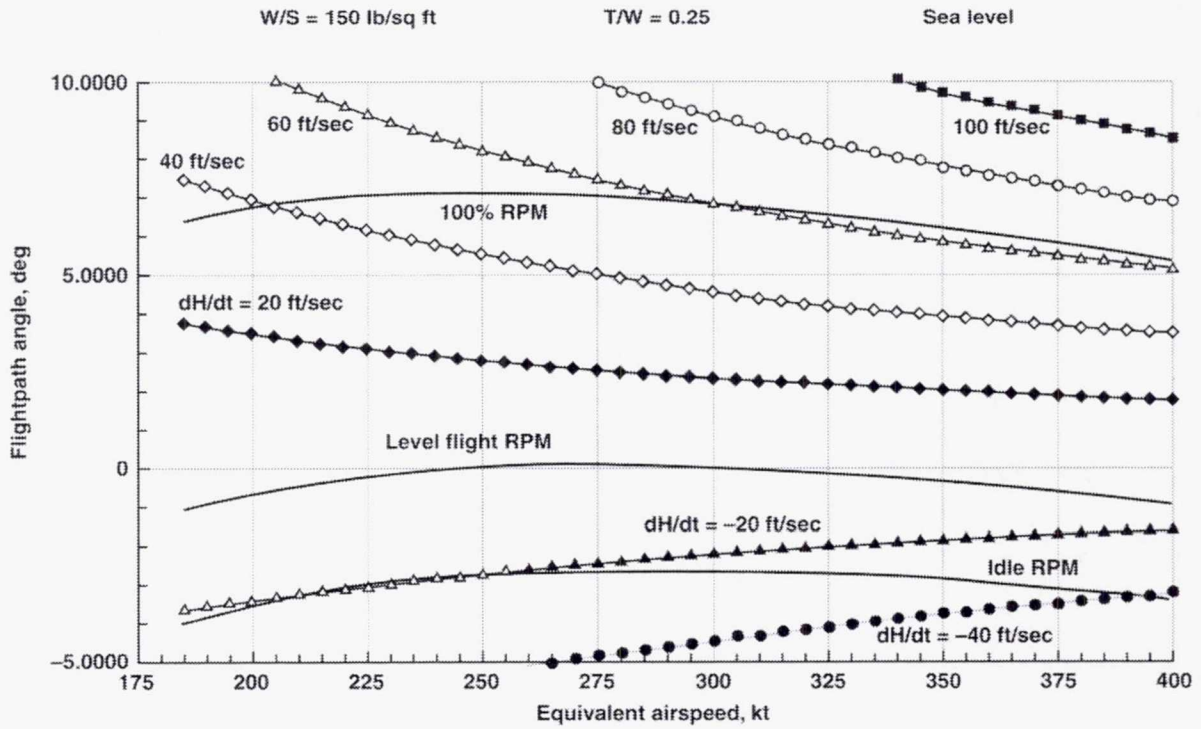

Figure B-9. Performance envelope with vertical velocity contours.

The climb airspeed that minimizes total fuel consumption lies above that for best rate of climb, since the distance traveled during the climb is directly proportional to the climb speed, while the vertical velocity is reduced only slightly at speeds somewhat higher than that for best rate of climb (fig. B-9). In practice, transport aircraft usually climb at constant equivalent airspeed at low altitudes and constant Mach number at high altitudes. Shevell gives the following schedule for a high-speed climb for the DC-l0 series 10 aircraft (Shevell, 1989):

Altitude, ft	0–10,000	10,000–27,880	> 27,880
V_{IAS} or M	250 kt	340 kt	0.85 M

At the "cross-over" altitude of 27,880 ft, at M = 0.85 the equivalent airspeed is 321.4 kt (eqs. (B-7m) and (A-6a)). The pilot's indicated airspeed (IAS) is 19 kt higher than the equivalent airspeed in this case because of the effect of compressibility on the aircraft pitot pressure.

The time to climb is found by evaluating the integral

$$t = \int dH/(dH/dt)$$

over the altitude range of interest. It is found that the initial climb to the optimal cruise altitude tends to require about 30 minutes, independent of aircraft weight.

Descent

As already noted, idle thrust is used for descent. The residual thrust at idle can be neglected. With T = 0, equation (B-9a) shows that the descent angle is proportional to D/W, so that the distance traveled during descent is maximized by minimizing drag. Therefore, the descent airspeed is usually near the speed for minimum drag.

The descent gradient is found by dividing equation (B-9a) by equation (B-9b), which results in the equation

$$\tan \gamma_{TRIM} = (T - D)/L = (0 - D)/L = -1/(L/D) \tag{B-16}$$

Since the angle of descent is small, the lift is approximately equal to the weight (equation (B-9b)). With L/D = 17.7 for M ≤ 0.6 (table B-1), the descent gradient is 1/17.7, or, since 1 nm equals 1852 m or 6076.1 ft, the gradient is 6076.1/17.7 = 343.3 ft/nm. Therefore, the distance traveled per 1000 ft of descent is 1000/343.3 = 2.91 nm/10^3 ft. In practice, it is found that 3 nm per 1000 ft is a good estimate of the descent gradient for most transport aircraft.

Trajectory Optimization

Optimization of climb, cruise, and descent by the methods just discussed does not, in general, result in the best complete flight profile from takeoff to landing, for two reasons. First, the methods presented have concentrated on minimizing fuel consumption and fuel cost for a fixed range, but have not considered the cost of time. It is immediately obvious that combining the cost of time with fuel cost to form a weighted total cost that is to be minimized will lead to scheduled speeds higher than those that minimize fuel cost alone.

Second, independent optimization of the climb, cruise, and descent flight segments does not necessarily result in optimization of the complete flight profile. In particular, optimization of the cruise segment has assumed that cruising flight should take place at the optimal cruise altitude. This assumption is correct for long flights that are dominated by the cruise segment, but for shorter flights it is found that optimization of a short cruise segment may not determine the optimal profile for the entire flight. Indeed, since about 30 min is usually required for climb to the optimal altitude, as already noted, very short trips may not contain any cruise segment whatever. Thus the classical, quasi-steady optimization methods presented previously can be regarded as approximations valid for long flights dominated by the cruise segment when fuel cost dominates the total cost.

Modern Optimization

The modern approach to trajectory optimization, which accounts specifically for interaction between climb, cruise, and descent segments, is accomplished by application of optimal control theory based on calculus of variations (Erzberger and Lee, 1978; Lee and Erzberger, 1980; Erzberger, 1982). Fuel savings of 2 to 3 percent can be achieved for short trips, for which quasi-steady approximations are especially inaccurate. Although the modem approach leads to a mathematically complex problem that lies beyond the scope of this appendix, the following brief comments indicate the problem formulation. Readers desiring a detailed treatment can consult the references provided.

The cost function J to be minimized consists of the sum of the fuel cost and the time cost integrated over the time of flight:

$$J = \int_{TIME} (f_c \, dF/dt + t_c) \, dt \qquad \text{(B-17a)}$$

where f_c and t_c are the unit costs of fuel and time and F denotes fuel quantity. Time is now replaced as the independent variable in equation (B-17a) by the total energy of the aircraft. This energy-state approach to performance optimization recognizes that the total energy of the aircraft is increased not just by climbing, but also by accelerating to cruising speed. The resulting cruise energy is dissipated during descent and landing. The objective of optimization can then be regarded as the increase and decrease of total energy in the most desirable way; that is, at least cost (Shevell, 1989).

Specific energy– The total specific energy e of the aircraft per unit weight is the sum of its potential energy and its kinetic energy:

$$e = H + V^2/2g \qquad \text{(B-17b)}$$

where H denotes altitude, V denotes airspeed, and g denotes gravitational acceleration. Differentiating equation (B-17b), the specific energy rate is given by

$$de/dt = dH/dt + (V/g)(dV/dt) \qquad \text{(B-17c)}$$

Substituting $dH/dt = V \sin \gamma$, equation (B-17c) becomes

$$de/dt = V [\sin \gamma + (1/g)(dV/dt)] \qquad \text{(B-17d)}$$

Recognizing the bracketed quantity in equation (B-17d) as the quantity $(T - D)/W = \sin \gamma_{TRIM}$ (eqs. (B-2a) and (B-9a)), the specific energy rate becomes

$$de/dt = V (T - D)/W = V \sin \gamma_{TRIM} \qquad \text{(B-17e)}$$

By replacing time as the independent variable using the transformation $dt = de/(de/dt)$, equation (B-17a) becomes

$$J = f_c \int_{ENERGY} (dF/dt)/(de/dt) \, de + t_c \int_{ENERGY} 1/(de/dt) \, de \qquad \text{(B-17f)}$$

The integration limits in equation (B-17f) are the initial and final values of specific energy, which are found from the initial and final altitudes and airspeeds using equation (B-17b), and the maximum energy, which is discussed next.

Numerical optimization– It is now assumed that the optimal trajectory, which minimizes the cost function J, consists of, at most, three segments: (1) a climb segment characterized by monotonically increasing specific energy; (2) a constant-energy cruise segment, if any; and (3) a descent segment characterized by monotonically decreasing specific energy. Within each segment, the scheduled

airspeed is selected numerically so as to minimize the cost function at each energy level. The optimal thrust schedule can be determined numerically in the same way, but it is found that using maximum continuous thrust for the climb and idle thrust for the descent is nearly optimal.

The climb segment begins at the initial energy and ends at the maximum (cruise) energy, and the descent segment begins at the maximum energy and ends at the final energy. The maximum energy increases with range until the optimal cruise energy is reached, as determined from equation (B-17b) for the optimal cruise altitude and speed. For shorter trips without a cruise segment, the maximum energy is determined by the desired total range.

Graphical optimization– Shevell presents a relatively simple graphical treatment of the minimum-time and minimum-fuel climb trajectories that provides insight into the nature of the optimal solutions (Shevell, 1989). The corresponding descent problems could be handled in the same way. For supersonic aircraft, it is shown that energy-state methods have decisive advantages over classical methods for trajectory optimization, defining entirely different trajectories that are much more efficient.

Operation Overview

The planned trajectory of a transport aircraft in space and time can be determined almost entirely by the considerations of optimization just discussed, which determine the selection of operating points within the aircraft performance envelope and the schedules of airspeed and thrust to be employed. Appropriate trajectory-planning optimization algorithms are incorporated within the flight management systems on board current transport aircraft. However, the minimization of cost is also subject to external constraints imposed by Air Traffic Control (ATC) to provide separation from other air traffic. In the absence of such external constraints, trajectories can be selected to achieve the unconstrained optimum determined by the methods just discussed. As traffic density increases, optimality must be sacrificed to a greater or lesser extent as required for separation. In heavy traffic situations, feasible trajectories can be determined almost entirely by traffic constraints, leaving little freedom for optimization.

The global problem of optimizing trajectories subject to traffic constraints is extremely complex, involving, in principle, the trajectories of all aircraft operating within the worldwide air traffic control system. Global optimization must consider criteria related to system capacity and safety, in addition to the costs borne by aircraft operators. These problems are currently being addressed at the research level (Erzberger and Nedell, 1989; Erzberger, Davis, and Green, 1993).

Current research indicates that efficient global optimization will require exchange of trajectory specifications between airborne and ground-based computers. With concurrence of pilots and air traffic controllers, profile negotiation algorithms will be iterated until convergence is achieved (Green, Den Braven, and Williams, 1993). It is hoped that future development of well-coordinated airborne and ground-based systems will enable significant increases in system capacity, improvements in operational safety, and reductions in cost.

AIRPLANE DYNAMIC RESPONSE

The dynamic response of a transport aircraft to elevator and throttle control depends on the initial operating point within the aircraft performance envelope. Operating points are selected to realize the flight profile summarized by the flight plan, as already discussed. Each operating point corresponds to a steady-state solution of the equations of motion for specified elevator and throttle control inputs, and the transitions from one operating point to the next correspond to transient solutions of the equations of motion. Flying-qualities criteria based on pilot evaluation define what is meant by well-shaped responses, which enable smooth, rapid capture of the desired (target) operating point during manual control.

The following sections examine dynamic response by means of simulation (that is, by numerical solution of the equations of motion) at three different levels of dynamical fidelity, and interpret various flying-qualities criteria that guide stability and control aspects of aircraft design. Automatic systems should be designed to achieve response shapes similar to those desired for manual control, since from the flying-qualities viewpoint it can be taken as axiomatic that behavior that is difficult to anticipate is difficult to monitor. Readers who wish to skip the details of the simulation calculations can turn immediately to the discussion in the section "Aircraft Response Characteristics."

Three-Degree-of-Freedom Model

At airspeeds below $M = 0.6$, compressibility effects are unimportant, as previously noted. In this speed range, the aircraft lift coefficient is a linear function of angle of attack (eqs. (B-7a) and (B-7b)), and its pitching moment coefficient can be represented as a linear function of elevator and stabilizer deflections and of pitch rate, which is proportional to tail angle of attack (eq. (B-6e)). For $M \leq 0.6$, the drag coefficient is a nonlinear function of lift coefficient (eq. (B-7c)), and the dimensional aerodynamic forces and moments are nonlinear functions of airspeed (eqs. (B-6d) and (B-6e)). At higher Mach numbers, compressibility effects would contribute other Mach-dependent nonlinearities.

Stability and Control Parameters

For simplicity, it is assumed that the aircraft is initially trimmed in level flight in still air at the minimum-drag airspeed. The trim condition is specified by the steady-state solution of the equations of motion (B-2a), (B-2b), and (B-2c). The stabilizer is adjusted to balance the total pitching moment with the elevator faired ($\delta_e = 0$). Representative parameter values for a transport aircraft at normal landing weight at 15,000 ft can be found in table B-3, which also shows how the various partial derivatives vary with airspeed, V_{MD} denoting the minimum-drag speed. Estimation of these parameters, which makes use of available transport aircraft data, lies beyond the scope of this appendix. Readers desiring a more detailed discussion can consult standard engineering references dealing with aircraft stability and control (McRuer, Ashkenas, and Graham, 1973). For simplicity, small contributions to the aerodynamic forces and to the pitching moment have been neglected. With these assumptions, the dynamical system corresponding to the longitudinal equations of motion (B-2a), (B-2b), and (B2c) can be represented by the block diagram of figure B-l0(a).

TABLE B-3. TRANSPORT AIRCRAFT STABILITY AND CONTROL PARAMETERS

$(1/I_Y)\,\partial M/\partial\delta_e = +3.61\,(V/V_{MD})^2$ rad/sec^2 per rad $= +3.61\,(V/V_{MD})^2$ deg/sec^2 per deg

$(1/I_Y)\,\partial M/\partial\alpha = -3.03\,(V/V_{MD})^2$ rad/sec^2 per rad $= -3.03\,(V/V_{MD})^2$ deg/sec^2 per deg

$(1/I_Y)\partial M/\partial(d\alpha/dt) = -0.554\,(V/V_{MD})$ rad/sec^2 per rad $= -0.554\,(V/V_{MD})$ deg/sec^2 per deg

$(1/I_Y)\partial M/\partial q = -1.66\,(V/V_{MD})$ rad/sec^2 per rad/sec $= -1.66\,(V/V_{MD})$ deg/sec^2 per deg/sec

$(1/W)\partial L/\partial\delta_e = -0.97\,(V/V_{MD})^2$ g's per rad $= -0.0169\,(V/V_{MD})^2$ g's per deg

$(1/W)\,\partial L/\partial\alpha = +8.65\,(V/V_{MD})^2$ g's per rad $= +0.151\,(V/V_{MD})^2$ g's per deg

$g/V = 0.0675\,(V_{MD}/V)$ rad/sec per g unit $= 3.87\,(V_{MD}/V)$ deg/sec per g unit

$\alpha_i = -4.84$ deg $\qquad \alpha_{trim} = +1.7825$ deg $\qquad V_{MD} = 476.39$ ft/sec

$(1/W)\,T_{trim} = 0.07058$ $\qquad (1/W)\,\partial T/\partial(V/V_{MD}) = -1/71.387$

$(1/2)\,(L/D)_{MAX} = 0.028\,286$ $\qquad g = 32.174$ ft/sec^2

Block Diagram

The simplified block diagrams of figures B-l0(b), B-l0(c), and B-l0(d) are discussed later, and should be ignored for the present. In figure B-l0(a), the solid lines denote parameters appearing in the equations of motion, starting with the elevator and throttle control inputs at the left. The arrows indicate the sequence of computation. Each block indicates that the quantity entering that block is to be multiplied by the parameter within the block. Addition of signals is indicated by small circles containing a plus sign, with subtraction denoted by minus signs adjacent to the appropriate arrows. Time integration of the quantity entering a block is indicated by an integral sign within the block. The symbol *D* within a block denotes a one-frame delay. (In the spread-sheet implementation to be described, delayed quantities are taken from the previous row of the spread-sheet table.)

Terminology

It can be seen that the increment of total pitching moment M contributed by the elevator deflection δ_e is specified by the parameter $\partial M/\partial\delta_e$, which is termed elevator effectiveness. Similarly, the contribution of elevator deflection to the tail download, which reduces total lift, is specified by the parameter $\partial L/\partial\delta_e$. The contribution of angle of attack to total pitching moment is specified by the parameter $\partial M/\partial\alpha$, which is termed static stability. The contribution of pitch rate to total pitching moment is specified by the parameter $\partial M/\partial q$, which is termed pitch damping. The contribution of angle-of-attack rate to total pitching moment owing to down wash lag at the tail is specified by the parameter $\partial M/\partial(d\alpha/dt)$. The primary contribution to total lift is that owing to the wing, which is proportional to the lift-curve slope specified by the parameter $\partial L/\partial\alpha$. Representative numerical values of these parameters, which are marked on figure B-10(a), can be found in table B-3, as already noted.

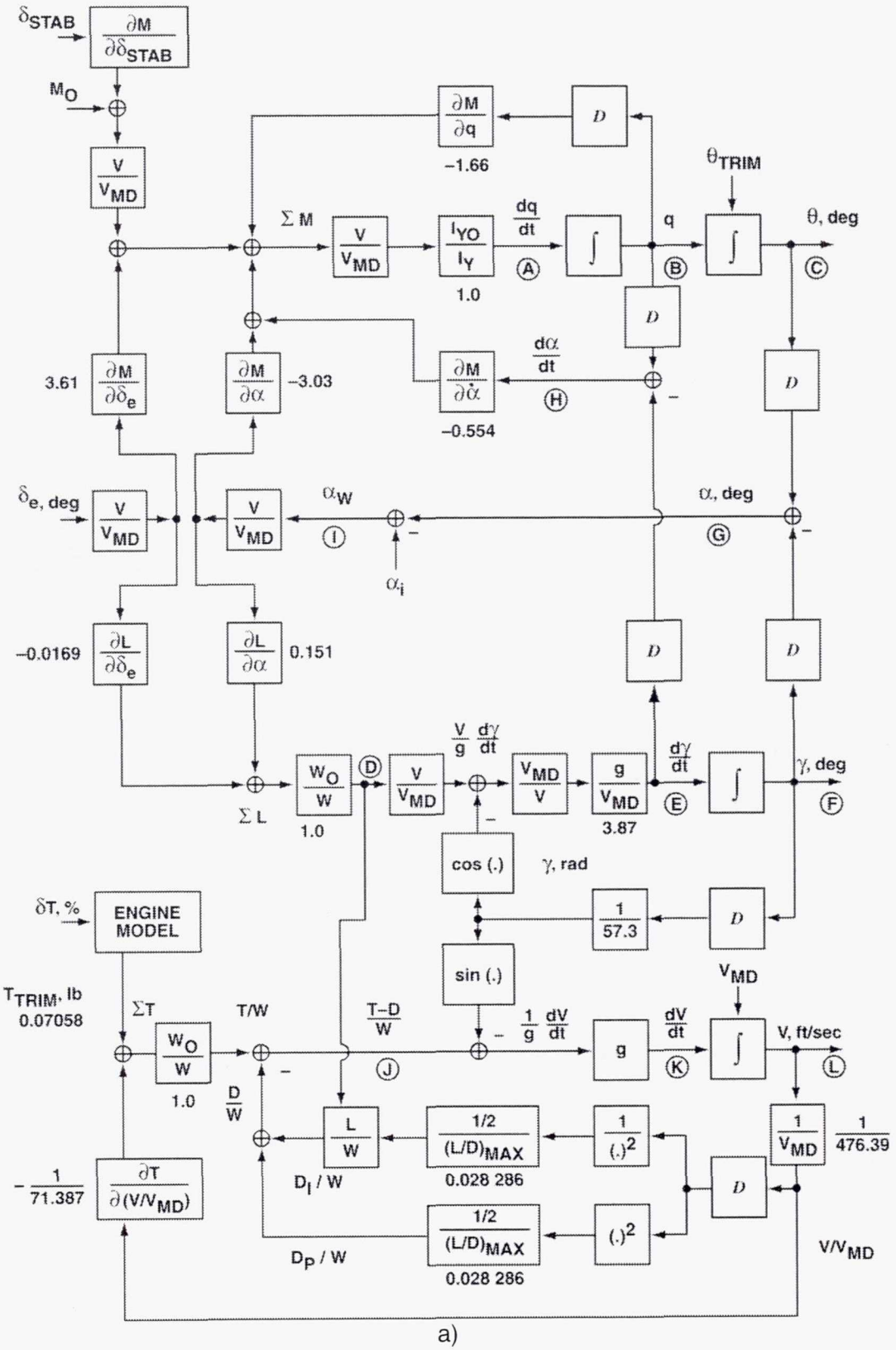

a)

Figure B-10. Longitudinal dynamical system.

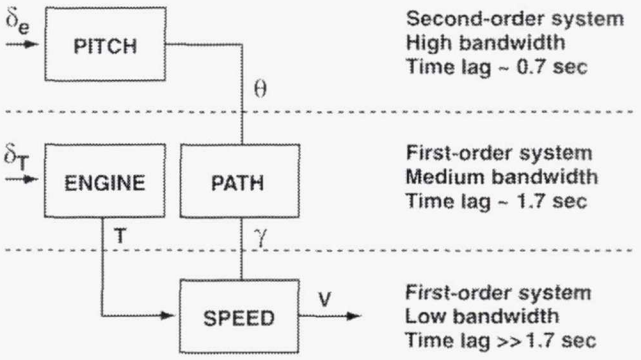

b) Three-degree-of-freedom model.

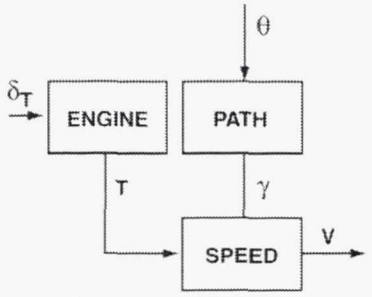

c) Two-degree-of-freedom-model.

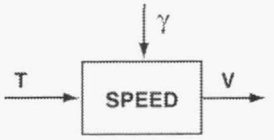

d) Single-degree-of-freedom model.

Figure B-10. Longitudinal dynamical system (concluded).

Functional Description

The arrangement of the block diagram of figure B-10(a) follows certain conventions related to physical significance. It can be seen that each of the forward paths leading from the elevator and throttle control inputs δ_e and δ_T on the left through the integrators to the controlled variables (that is, the pitch angle θ, the flightpath angle γ, and the airspeed V) is drawn from left to right in the diagram. The other paths drawn from right to left represent feedback that modifies the forces and moments generated by the control inputs. Considering the forward paths first, the path at the top of the diagram leading from the pitching moment summation point (marked ΣM in the diagram) to the pitch angle θ on the right corresponds to the solution of the pitching moment equation (B-2c)

$$dq/dt = M/I_Y \qquad \text{(B-2c)}$$

since integrating equation (B-2c) twice yields the equation

$$\theta = \theta_{TRIM} + \int q\, dt = \theta_{TRIM} + \int\int (dq/dt)\, dt = \theta_{TRIM} + \int\int (M/I_Y)\, dt$$

Similarly, the forward path at the center of the diagram leading from the lift summation point marked ΣL to the flightpath angle γ on the right corresponds to the solution of equation (B-2b) in the form

$$\gamma = \gamma_{TRIM} + \int (g/V)\,[L/W - \cos\gamma]\,dt$$

where γ_{TRIM} vanishes for initialization in level flight. At the bottom of the diagram, the forward path leading from the streamwise force summation marked $(T - D)/W$ to the airspeed V on the right corresponds to the solution of equation (B-2a) in the form

$$V = V_{TRIM} + \int g\,[(T - D)/W - \sin\gamma]\,dt$$

where $V_{TRIM} = V_{MIN\ DRAG} = V_{MD}$.

To derive the angle of attack feedback, the fuselage angle of attack α is formed according to equation (B-1):

$$\alpha = \theta - \gamma \qquad \text{(B-1)}$$

The aerodynamic (wing) angle of attack is obtained by correcting for the wing incidence angle α_i between wing and fuselage. The angle of attack feedback contributes to the total pitching moment ΣM through the static stability parameter $\partial M/\partial\alpha$, and contributes to the total lift ΣL through the lift-curve slope $\partial L/\partial\alpha$. Numerically, the pitching moment of inertia I_Y and the weight W are included in these parameter values. As already noted, the time derivative of angle of attack $d\alpha/dt$ contributes to the total pitching moment ΣM through the downwash lag parameter $\partial M/\partial(d\alpha/dt)$.

At the bottom of the diagram, the airspeed V is fed back to determine the drag/weight ratio D/W as follows. Expressing this ratio in coefficient form with the help of equation (B-7c),

$$D/W = C_D/C_W = C_{DP}/C_W + (C_L/C_W)\,C_L/\pi\,AR\,e$$

Normalizing by the minimum-drag lift coefficient $C_{L\ MIN\ DRAG} = C_{L\ MD}$,

$$D/W = (C_{DP}/C_{L\ MD})\,(C_{L\ MD}/C_W) + (C_L/C_W)\,(C_{L\ MD}/\pi\,AR\,e)\,(C_L/C_{L\ MD})$$

According to equation (B-7j),

$$C_{DP}/C_{L\ MD} = (C_{D\ MIN}/2)/\,C_{L\ MD} = (1/2)\,(D/L)_{MIN} = (1/2)/(L/D)_{MAX}$$

Also, $C_{L\ MD}/C_W = (V/V_{MD})^2$ (eq. (B-7f)), and $C_L/C_W = L/W$. Therefore,

$$D/W = (1/2)\,(V/V_{MD})^2/(L/D)_{MAX} + (1/2)\,(L/W)\,(V_{MD}/V)^2/(L/D)_{MAX}$$

where the first term on the right represents the contribution of parasite drag and the second term that of induced drag, as shown in the block diagram. The remaining airspeed feedback modifies the thrust according to equation (B-8g), which is valid for $M \geq 0.3$ ($V \geq 187.9$ kt).

Numerical Integration

The equations of motion can be solved numerically to determine the dynamic response of the aircraft to any physically realizable elevator and throttle control inputs. If this solution is carried out in real time, it can provide the basis for piloted simulation. Two numerical integration methods commonly used for real-time simulation are second-order Adams-Bashforth prediction with Adams-Moulton correction, or for simplicity, Adams-Bashforth prediction alone (Press et al, 1986). These second-order prediction-correction methods, which are based on the well-known trapezoidal rule, are much more accurate for smooth input functions than first-order numerical methods such as Euler integration, and they are also more accurate than higher-order prediction-correction methods for impulsive inputs such as landing gear loads at touch-down. High-accuracy methods such as fourth-order Runge-Kutta integration (often available in computation libraries) are too slow for real-time simulation because they require more function evaluations (which must, in general, be performed by time-consuming table look-up). The integration time step should be made as short as practicable, since excessive step length degrades accuracy and numerical stability.

In practice, step lengths of 25 msec are representative for transport aircraft simulation. The following sections describe dynamic responses calculated with 25-msec time steps, as implemented by means of a widely available general-purpose spread-sheet package. The Adams-Bashforth prediction method is illustrated by example. The response of the aircraft to an abrupt change of elevator deflection, termed an elevator step, is calculated first. To ensure physical realizability, the mathematically discontinuous step is shaped by multiplying it by a half-period cosine bell of 0.5-sec duration, which is representative of an abrupt pilot control input.

Calculation of Elevator Step Response

The quantities to be calculated are the aircraft state variables, which are the outputs of the four integrators shown in figure B-10(a). It may be seen that these four quantities are pitch rate, pitch angle, flightpath angle, and airspeed.

Pitch response– Since the pitch response has the widest bandwidth and the shortest time scale, pitch rate and pitch angle are calculated first. The first step is to sum the contributions to total pitching moment, dividing by the moment of inertia I_Y to obtain the pitch acceleration dq/dt (point A in figure B-10(a)). Since the aircraft is assumed to be in equilibrium (trim) initially, the initial pitching-moment contributions from pitch rate q and angle-of-attack rate $d\alpha/dt$ both vanish, and the stabilizer deflection δ_{STAB} is adjusted so as to balance the contribution from angle of attack. The pitch acceleration dq/dt at point A corresponds to that on the left side of the pitching-moment equation (B-2c). Next, the pitch rate q at time $t = 0.025$ sec (point B in figure B-10(a)) is found by Adams-Bashforth prediction.

If the pitch acceleration were known at time t = 0.025 sec, then the desired pitch rate could be found by numerical integration of equation (B-2c) using the trapezoidal rule:

$$q_1 = q_0 + \int_{\Delta t} (dq/dt)\, dt = q_0 + [(dq/dt)_1 + (dq/dt)_0]\, \Delta t/2 \qquad \text{(B-18a)}$$

where the subscript 0 denotes the time t = 0, the subscript 1 denotes the time t = 0.025 sec, and Δt denotes the 0.025-sec time step. Since the pitch acceleration $(dq/dt)_1$ is not known, the Adams-Bashforth prediction method estimates it by linear extrapolation:

$$(dq/dt)_1 = (dq/dt)_0 + [(dq/dt)_0 - (dq/dt)_{-1}] \qquad \text{(B-18b)}$$

where the subscript –1 has the obvious significance. Collecting terms and substituting equation (B-18b) into equation (B-18a), the pitching velocity q_1 becomes

$$q_1 = q_0 + (3\ \Delta t/2)\, (dq/dt)_0 - (\Delta t/2)\, (dq/dt)_{-1} \qquad \text{(B-18c)}$$

Applying the Adams-Bashforth integration formula (B-18c) to the first time step, for which both $(dq/dt)_{-1}$ and $(dq/dt)_0$ vanish by the assumption of initial equilibrium, the pitching velocity after the first step at time t = 0.025 sec is found to be

$$q_1 = 0 + (3\ \Delta t/2)\, (dq/dt)_0 = (3/2)\, (0.025)\, (0.0889) = 0.0033 \text{ deg/sec}$$

Next, the pitch angle at time t = 0.025 sec (point C in figure B-l0(a)) is found by evaluating the second integral, again using the Adams-Bashforth prediction formula. By analogy to equation (B-18c),

$$\theta_1 = \theta_0 + \int_{\Delta t} q\, dt = \theta_0 + (3\ \Delta t/2)\, q_0 - (\ \Delta t/2)\, q_{-1}$$

where $\theta_0 = 1.7825$ deg (table B-3), and both q_0 and q_{-1} vanish by initial assumption. The pitch angle θ_1 at time t = 0.025 sec (point C) is found to be

$$\theta_1 = 1.7825 + (3/2)\, (0.025)\, (0.0033) - (1/2)\, (0) = 1.7826 \text{ deg}$$

This completes the: pitch response calculation for the first time step. The results are summarized by table B-4. It can be seen that, with certain exceptions, the columns of the table correspond to the lettered points A, B, and C identified on figure B-10(a), and that each row corresponds to one time step.

TABLE B-4. ELEVATOR STEP RESPONSE

Three Degrees of Freedom

Time sec	Elev defl deg	Pitch accel deg/s/s	Pitch rate deg/sec	Pitch angle deg	Fltpath rate deg/sec	Fltpath angle deg	Angle of attack deg	Elev defl deg
–0.025	0.000	0.0000	0.0000	1.7825	0.0000	0.0000	1.7825	0.000
0.000	0.000	0.0000	0.0000	1.7825	0.0000	0.0000	1.7825	0.000
0.025	0.025	0.0889	0.0033	1.7826	–0.0016	–0.0001	1.7827	0.025
0.050	0.098	0.3446	0.0151	1.7832	–0.0063	–0.0003	1.7834	0.098
0.075	0.218	0.7471	0.0389	1.7844	–0.0137	–0.0007	1.7851	0.218
0.100	0.382	1.2773	0.0774	1.7868	–0.0235	–0.0014	1.7883	0.382
0.125	0.586	1.9129	0.1332	1.7909	–0.0350	–0.0024	1.7933	0.586
0.150	0.824	2.6293	0.2079	1.7970	-0.0476	-0.0038	1.8008	0.824
0.175	1.092	3.4002	0.3025	1.8057	-0.0607	-0.0055	1.8112	1.092
0.200	1.382	4.1986	0.4175	1.8176	-0.0736	-0.0075	1.8251	1.382
0.225	1.687	4.9966	0.5523	1.8331	-0.0854	-0.0098	1.8429	1.687
0.250	2.000	5.7670	0.7061	1.8527	-0.0955	-0.0123	1.8650	2.000
0.275	2.313	6.4834	0.8772	1.8768	-0.1030	-0.0149	1.8917	2.313
0.300	2.618	7.1213	1.0632	1.9057	-0.1074	-0.0177	1.9233	2.618
0.325	2.908	7.6579	1.2614	1.9397	-0.1078	-0.0204	1.9600	2.908
0.350	3.176	8.0738	1.4684	1.9790	-0.1039	-0.0229	2.0019	3.176
0.375	3.414	8.3523	1.6807	2.0236	-0.0950	-0.0252	2.0488	3.414
0.400	3.618	8.4809	1.8943	2.0737	-0.0809	-0.0270	2.1007	3.618
0.425	3.782	8.4505	2.1052	2.1289	-0.0613	-0.0283	2.1572	3.782
0.450	3.902	8.2567	2.3092	2.1892	-0.0361	-0.0289	2.2181	3.902
0.475	3.975	7.8991	2.5022	2.2542	-0.0053	-0.0287	2.2828	3.975
0.500	4.000	7.3817	2.6803	2.3234	0.0309	-0.0274	2.3508	4.000
0.525	4.000	6.8014	2.8431	2.3965	0.0707	-0.0252	2.4217	4.000
0.550	4.000	6.2483	2.9924	2.4732	0.1121	-0.0218	2.4950	4.000
0.575	4.000	5.7184	3.1287	2.5531	0.1549	-0.0174	2.5706	4.000
0.600	4.000	5.2115	3.2526	2.6360	0.1991	-0.0119	2.6479	4.000
0.625	4.000	4.7271	3.3648	2.7215	0.2442	-0.0052	2.7267	4.000
0.650	4.000	4.2649	3.4656	2.8094	0.2903	0.0026	2.8068	4.000
0.675	4.000	3.8245	3.5557	2.8994	0.3370	0.0116	2.8878	4.000
0.700	4.000	3.4053	3.6356	2.9913	0.3843	0.0218	2.9695	4.000
0.725	4.000	3.0071	3.7058	3.0848	0.4320	0.0332	3.0516	4.000
0.750	4.000	2.6291	3.7668	3.1798	0.4799	0.0458	3.1340	4.000
0.775	4.000	2.2711	3.8191	3.2759	0.5280	0.0596	3.2163	4.000
0.800	4.000	1.9323	3.8632	3.3730	0.5760	0.0746	3.2984	4.000
0.825	4.000	1.6124	3.8995	3.4710	0.6239	0.0908	3.3802	4.000
0.850	4.000	1.3107	3.9285	3.5695	0.6716	0.1082	3.4614	4.000
0.875	4.000	1.0268	3.9506	3.6686	0.7189	0.1267	3.5418	4.000
0.900	4.000	0.7601	3.9663	3.7679	0.7658	0.1465	3.6215	4.000
0.925	4.000	0.5101	3.9759	3.8675	0.8122	0.1674	3.7001	4.000
0.950	4.000	0.2761	3.9799	3.9670	0.8579	0.1894	3.7776	4.000
0.975	4.000	0.0576	3.9786	4.0665	0.9031	0.2125	3.8539	4.000
1.000	4.000	-0.1458	3.9724	4.1657	0.9475	0.2368	3.9289	4.000

TABLE B-4. ELEVATOR STEP RESPONSE (concluded)

Three Degrees of Freedom

Time sec	Airspeed change kt	Long accel g	Normal accel g	Airspeed kt	Airspeed ratio
-0.025	0.00	0.0000	0.0000	282.25	1.0000
0.000	0.00	0.0000	0.0000	282.25	1.0000
0.025	0.00	0.0000	-0.0004	282.25	1.0000
0.050	0.00	0.0001	-0.0016	282.25	1.0000
0.075	0.00	0.0001	-0.0035	282.25	1.0000
0.100	0.00	0.0002	-0.0061	282.25	1.0000
0.125	0.00	0.0003	-0.0090	282.25	1.0000
0.150	0.00	0.0004	-0.0123	282.25	1.0000
0.175	0.00	0.0005	-0.0157	282.25	1.0000
0.200	0.00	0.0007	-0.0190	282.25	1.0000
0.225	0.00	0.0008	-0.0221	282.25	1.0000
0.250	0.00	0.0009	-0.0247	282.25	1.0000
0.275	0.00	0.0010	-0.0266	282.25	1.0000
0.300	0.00	0.0011	-0.0277	282.25	1.0000
0.325	0.00	0.0011	-0.0279	282.25	1.0000
0.350	0.00	0.0012	-0.0268	282.25	1.0000
0.375	0.00	0.0011	-0.0245	282.25	1.0000
0.400	0.01	0.0011	-0.0209	282.26	1.0000
0.425	0.01	0.0009	-0.0158	282.26	1.0000
0.450	0.01	0.0008	-0.0093	282.26	1.0000
0.475	0.01	0.0005	-0.0014	282.26	1.0000
0.500	0.01	0.0003	0.0080	282.26	1.0000
0.525	0.01	-0.0001	0.0183	282.26	1.0000
0.550	0.01	-0.0004	0.0290	282.26	1.0000
0.575	0.01	-0.0008	0.0400	282.26	1.0000
0.600	0.00	-0.0012	0.0514	282.25	1.0000
0.625	0.00	-0.0017	0.0631	282.25	1.0000
0.650	0.00	-0.0022	0.0750	282.25	1.0000
0.675	0.00	-0.0027	0.0871	282.25	1.0000
0.700	0.00	-0.0032	0.0993	282.25	1.0000
0.725	0.00	-0.0037	0.1116	282.25	1.0000
0.750	0.00	-0.0043	0.1240	282.25	1.0000
0.775	-0.01	-0.0049	0.1364	282.24	1.0000
0.800	-0,01	-0.0055	0.1488	282.24	1.0000
0.825	-0.01	-0.0061	0.1612	282.24	1.0000
0.850	-0.02	-0.0068	0.1735	282.23	0.9999
0.875	-0.02	-0.0075	0.1858	282.23	0.9999
0.900	-0.02	-0.0082	0.1979	282.23	0.9999
0.925	-0.03	-0.0089	0.2099	282.22	0.9999
0.950	-0.03	-0.0096	0.2217	282.22	0.9999
0.975	-0.04	-0.0103	0.2334	282.21	0.9999
1.000	-0.04	-0.0111	0.2449	282.21	0.9998

Flightpath response– The flightpath response is calculated next, because its bandwidth is wider (and its time scale shorter) than that of airspeed. To begin the calculation of flightpath response, the lift contributions from angle of attack and from elevator deflection are summed to obtain the total lift, and divided by weight to find the load factor L/W (point D). After subtracting the cosine of the flightpath angle γ to form the normal acceleration (V/g) (dγ/dt) (equation (B-2b)), the normal acceleration is multiplied by g/V to obtain the flightpath rate dγ/dt (point E). Finally, the flightpath rate is integrated using the Adams-Bashforth formula (B-18c) to obtain the flightpath angle γ at time t = 0.025 sec (point F). To complete the calculation, the angle of attack α (point G) and angle-of-attack rate dα/dt (point H) are updated to time t = 0.025 sec using equation (B-1):

$$\alpha_1 = \theta_1 - \gamma_1 \qquad (d\alpha/dt)_1 = q_1 - (d\gamma/dt)_1$$

The wing (aerodynamic) angle of attack (point I) is found by subtracting the fixed wing incidence α_i (table B-3) from the fuselage angle of attack α. This completes the calculation of the flightpath and angle-of-attack responses for time t = 0.025 sec.

Airspeed response– The airspeed response is calculated last, because it has the narrowest bandwidth and the longest time-scale. The thrust is evaluated first. It is assumed for simplicity that the throttle setting and engine rpm are constant, so that thrust is a function of Mach number (or airspeed) and of altitude (eqs. (B-8d) and (B-8e)). Next, the lift coefficient is found from the load factor L/W calculated previously (eq. (B-6d)), the drag coefficient is found as a parabolic function of lift coefficient (eq. (B-7c)), and the dimensional drag force is found as a function of drag coefficient and airspeed (eq. (B-6d)). The excess thrust T – D is formed and divided by weight to obtain the quantity (T – D)/W (point J). After subtracting the sine of the flightpath angle γ to form the normalized longitudinal acceleration (1/g) (dV/dt) (eq. (B-2a)), the latter quantity is multiplied by g to obtain the dimensional acceleration dV/dt (point K). Finally, the acceleration is integrated using the Adams-Bashforth formula (B-18c) to obtain the airspeed V at time t = 0.025 sec (point L). The airspeed ratio V/V_{MD} is now updated throughout the simulation using the airspeed at time t = 0.025 sec, completing the response calculations for the first time step. The results thus far are tabulated in the first three rows of table B-4.

By repeating the entire calculation for 199 subsequent time steps, the first 5 sec of the response of the aircraft to the specified elevator step is tabulated. The calculations were performed in a few seconds by a Microsoft Excel 3.0 spread-sheet package running on a Macintosh IIsi computer. The dynamic response of the aircraft to any other desired elevator control input could be calculated in a similar way. The resulting parameter variations are illustrated by figure B-11, which is discussed next.

Aircraft Response Characteristics

The dynamic response characteristics of the aircraft are presented in the form of time histories, that is, by the variations of the primary response variables with time. The variations of pitch rate, pitch angle, flightpath rate, flightpath angle, and angle of attack in response to a nose-up step in elevator deflection are illustrated by figures B-11(a) and B-11(c), and the associated variations of airspeeed relative to its initial value and of longitudinal and normal acceleration are illustrated by

figure B-11(b). Figure B-11(d) shows the dynamic variation of flightpath angle with equivalent airspeed in the same form as that of the performance envelope of figure B-7.

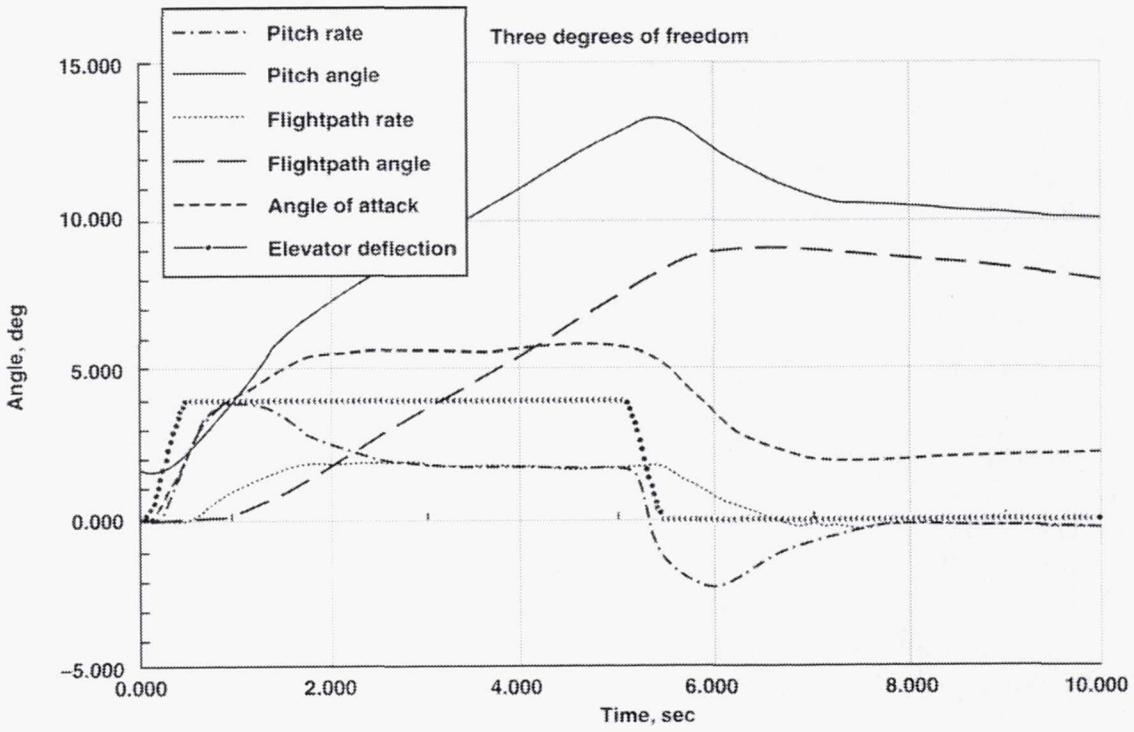

a)

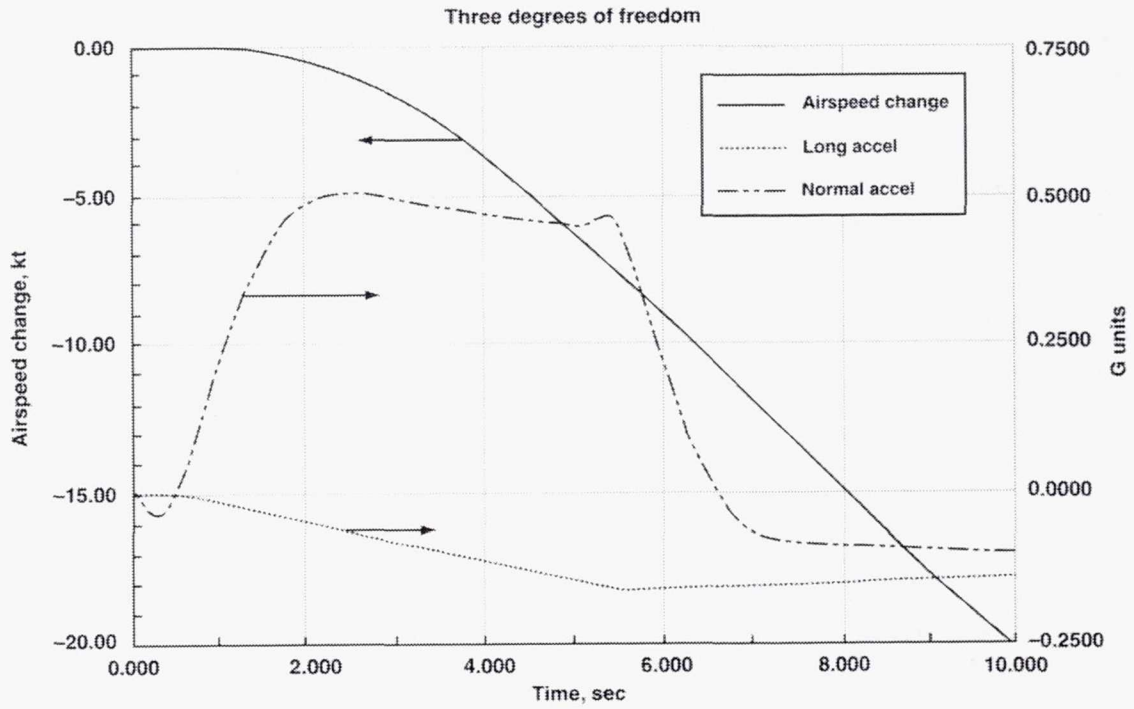

b)

Figure B-11. Elevator step response, 10 sec.

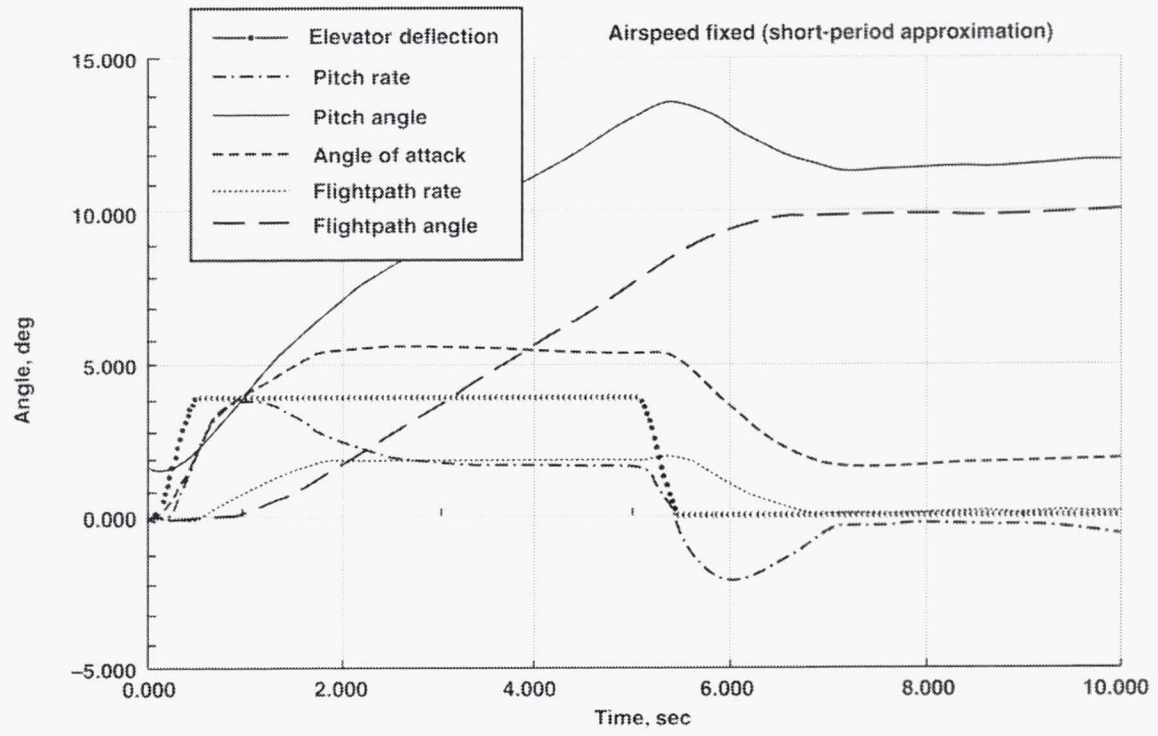

c)

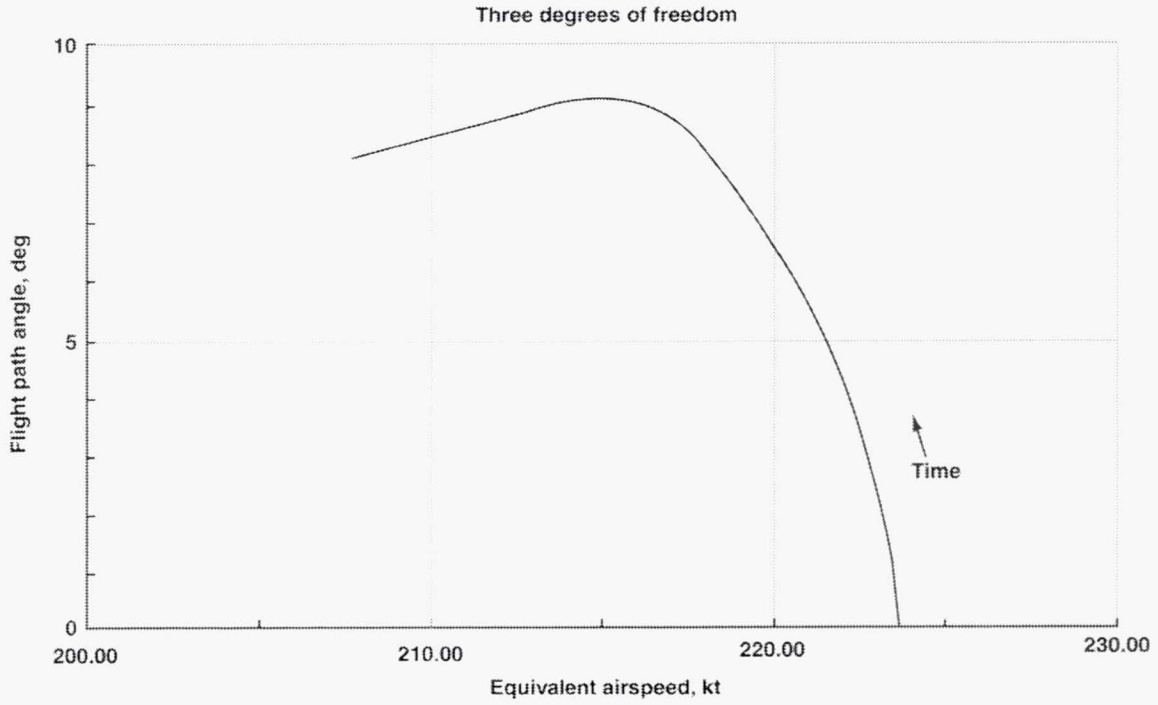

d)

Figure B-11. Elevator step response, 10 sec (concluded).

Elevator step response characteristics– It can be seen from figure B-11 that the angle-of-attack response (fig. B-11(a)) and the resulting normal acceleration (fig. B-11(b)) and flightpath angle rate (fig. B-11(a)) responses all have the same form as that of the initial step in elevator (fig. B-11(a)), but exhibit a time lag of about 1.7 sec relative to the elevator control input. Therefore, *elevator deflection commands normal acceleration.* One of the oldest and most important flying qualities criteria specifies the pilot stick force per g. Desirable values are 6 lb/g for stick-equipped high-performance aircraft, and 30 to 40 lb/g for transport aircraft equipped with wheel and column.

Figure B-11(a) shows that, after an initial transient of about 2.5 sec, pitch rate becomes equal to the (constant) flightpath angle rate. Therefore, *elevator deflection commands pitch rate.* Since both pitch angle and flightpath angle become parallel, steadily increasing ramp functions in the medium term after the initial transient, figure B-11(a) shows that *flightpath angle can be controlled by means of pitch angle.* During almost all flying, the fundamental control task is control of the flightpath; control of the aircraft pointing attitude should be regarded as a means to that end. The exceptions are takeoff and landing, for which the attitude is important in itself to avoid scraping the tail or an engine nacelle, or landing on the nose gear.

The lag of normal acceleration and flightpath rate relative to elevator deflection, which is inversely proportional to lift-curve slope, characterizes each aircraft. Since after integration the flightpath angle response exhibits the same lag relative to that of pitch angle, which is directly visible to the pilot, *control of flightpath angle requires compensation by the pilot for this characteristic lag.* The small initial reversal noticeable in the flightpath response (see the normal acceleration time history in figure B-11 (b)) results from the increase of tail download owing to elevator deflection, which reduces total lift. This reversal contributes to the total lag of the flightpath response relative to pitch, and can degrade the flying qualities of some transport aircraft configurations with small tail arms, especially during high-bandwidth maneuvers such as landing flare that require rapid response. To summarize, *flightpath follows pitch with a time lag that characterizes the aircraft.*

At time t = 5 sec an equal and opposite elevator step is applied, which returns the elevator to the faired position (fig. B-11(a)). After the elevator control is neutralized, the pitching motion damps out smoothly without significant overshoot, and the pitch angle stabilizes in about 2 sec. In the long term after 7 sec, it can be seen that the aircraft holds the pitch attitude approximately constant. Therefore, *neutral elevator commands constant pitch angle.*

These well-shaped, well-damped responses characterize transport aircraft considered to possess good flying qualities, which facilitate rapid, precise manual control of pitch attitude. These desirable response characteristics provide the motivation for rate command, attitude hold control augmentation, which can be used to improve the flying qualities of aircraft not possessing desirable natural response characteristics.

The substantial increase in flightpath angle relative to its initial equilibrium value produces negative longitudinal acceleration according to equation (B-2a), which is illustrated by the inverse correlation of longitudinal acceleration in figure B-11(b) with flightpath angle in figure B-11(a). This sustained longitudinal deceleration integrates to cause airspeed decay (fig. B-11(b)). The resulting lift loss (eq. (B-6(d)) produces the slight droop in pitch angle and flightpath angle visible in figure B-11(a)

for times after 7 sec. If the thrust were adjusted so as to hold airspeed fixed, the pitch angle and flightpath angle would remain constant in the long term (fig. B-11(c)).

The variation of flightpath angle with equivalent airspeed during the first 10 sec is illustrated by figure B-11(d). It can be seen that the initial trajectory in the (V, γ) plane is vertically upward in the short term, rounding over to the left in the medium term and becoming roughly horizontal in the long term.

Figures B-12(a), (b), and (c) illustrate extension of the time histories of figure B-11 to include one minute of the response. The most striking feature of figure B-12 is the sustained long-period oscillation of pitch angle, flightpath angle, and airspeed, which is termed the phugoid oscillatory mode. It can be seen from figure B-12(a) that the angle of attack remains nearly constant throughout the phugoid oscillation.

The elevator steps of figures B-11 and B-12 are representative of large, coarse maneuvers such as glide-slope capture at the start of a landing approach. The small, precise modulations of flightpath angle needed for glide-slope tracking can be achieved by means of elevator pulses, which are discussed next, after presenting an interpretation of figures B-11 and B-12 from an alternative viewpoint.

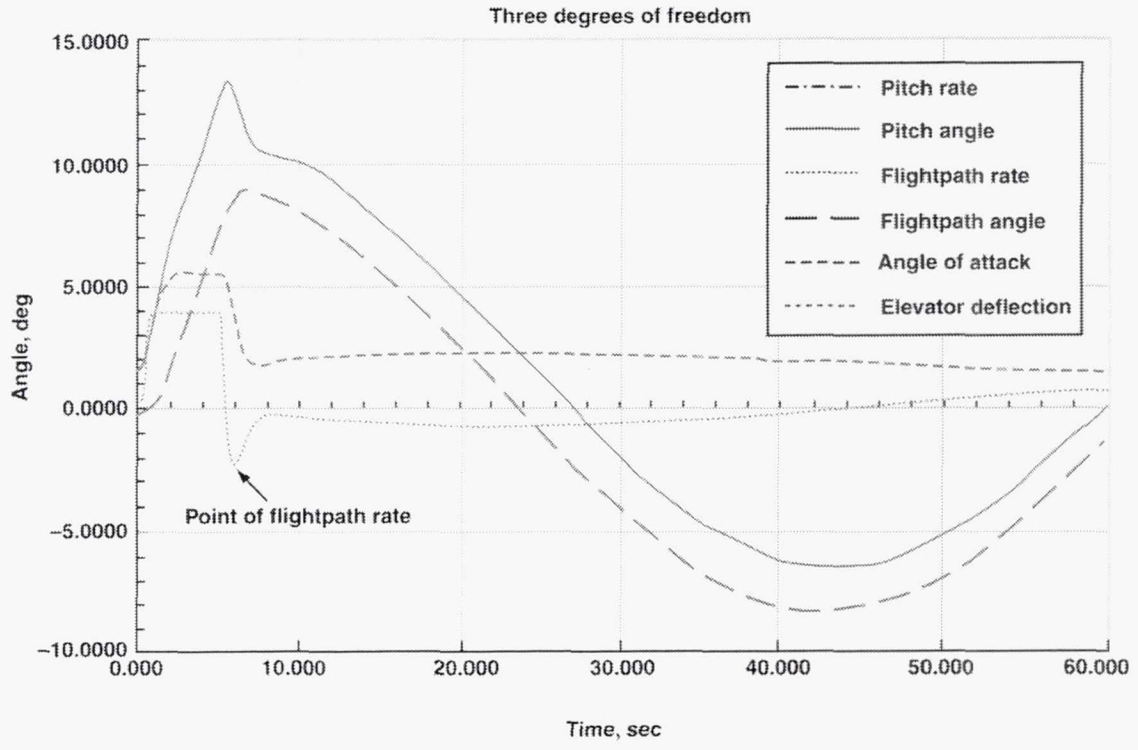

a)

Figure B-12. Elevator step response, 60 sec.

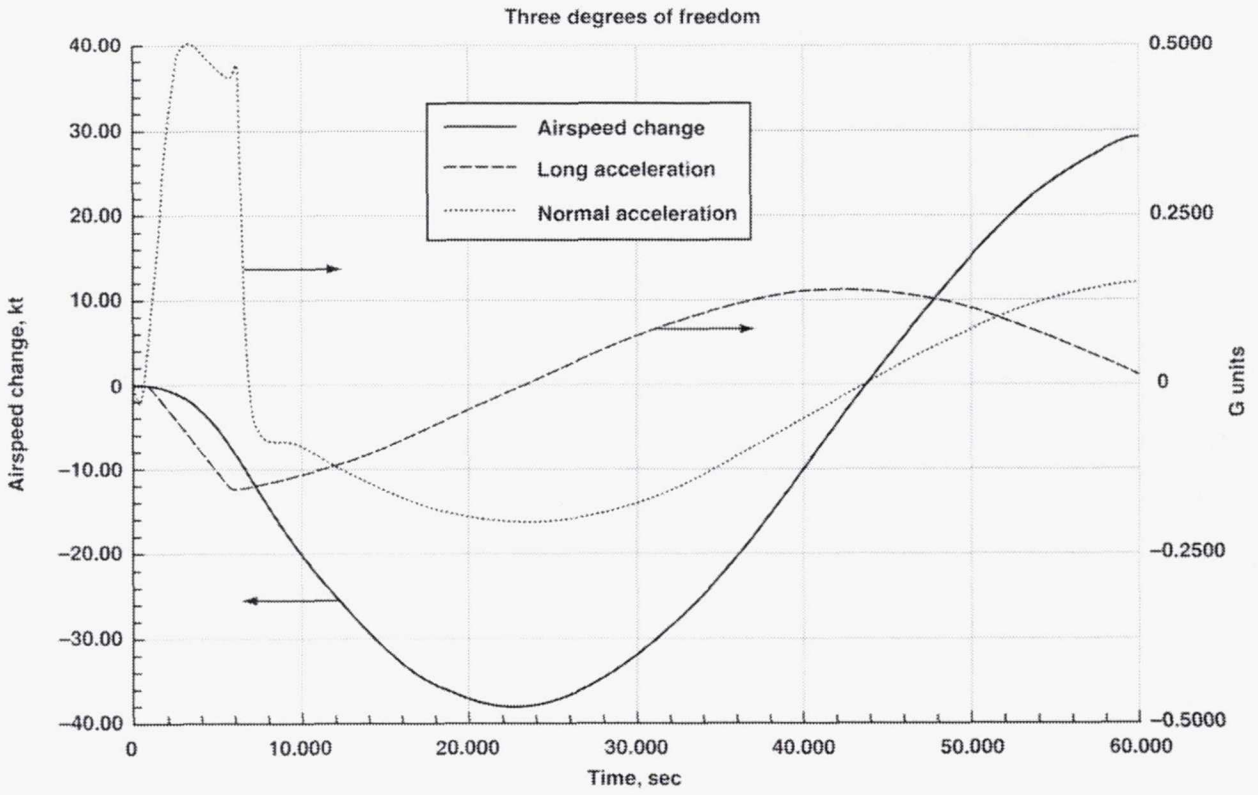

b)

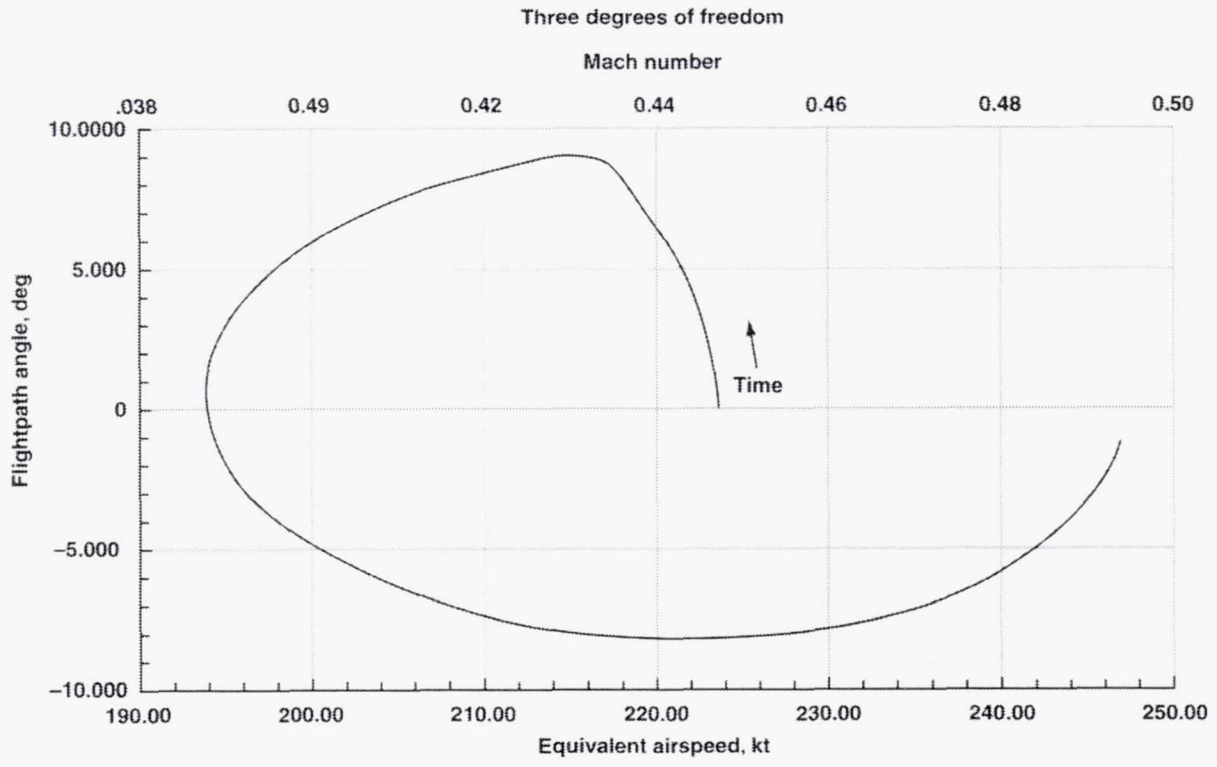

c)

Figure B-12. Elevator step response, 60 sec (concluded).

Frequency domain– In addition to the time-domain representation of the aircraft dynamical system made explicit by the block diagram of figure B-10(a), there is a complementary frequency-domain representation that is discussed in this section. This frequency-domain representation provides an alternative view of aircraft dynamic response that should be of interest to readers familiar with simple electrical filters, and also motivates the simplifications of the dynamic model to be discussed later. The discussion begins by simplifying the block diagram of figure B-10(a).

It can be seen from figure B-10(a) that a forward path leads from the elevator control input to the pitch angle output. A direct path then continues from the pitch angle through the angle-of-attack feedback to the lift summation point marked ΣL. When considering total lift, the pitch angle contribution to angle of attack can be regarded as a forward path contribution from elevator control, although the flightpath angle contribution to angle of attack is a feedback signal. The second contribution of elevator control to total lift via the tail download is much smaller than the wing lift contribution, and is neglected for simplicity in the present frequency-domain treatment.

By representing only the forward path from the elevator control input to the pitch angle and then continuing to the flightpath angle and airspeed outputs, the dynamical system of figure B-10(a) can be separated into its essential elements, as illustrated by the simplified diagram of figure B-10(b). It can be seen that the forward path leading from the throttle control input through the engine model to its thrust output, and then to the airspeed output, has been treated in the same manner as elevator control. In figure B-10(b), the same feedback structure as that in figure B-10(a) is implicit.

From the frequency-domain viewpoint, each of the elementary dynamical systems corresponding to the blocks in figure B-10(b) can be regarded as a first or second order low-pass filter that acts on its input signal just as the corresponding electrical filter would, smoothing the input signal by filtering out its high-frequency components and imparting a characteristic time lag. Numerically, this characteristic lag is the time required for the exponential response to an abrupt, mathematically discontinuous input step to reach 63 percent of its steady-state value. As indicated on the diagram (fig. B-10(b)), the second-order pitch filter has the widest bandwidth and the shortest lag, the first-order path filter and the second-order engine filter have intermediate bandwidth with a lag in the order of 2 sec, and the first-order airspeed filter has the narrowest bandwidth and the longest lag.

The dynamic effects of these filters on the response to an elevator step can be seen in figures B-11 and B-12, which have already been discussed from the time-domain perspective. Regarding the elevator deflection time history illustrated by figure B-11(a) as a long pulse formed by the two equal and opposite steps discussed previously, it can be seen from figure B-11(a) that the pitch filter smooths this elevator pulse and extends its time duration, with a characteristic overshoot of the steady-state value and a heavily damped oscillation that results from its second-order nature. The path filter then acts on the pitch angle input signal, smoothing it heavily to generate the flightpath angle signal. The overshoot in the pitch-angle signal is filtered out, but serves to quicken the flightpath response so as to make its lag relative to pitch less noticeable than it would be in the absence of pitch overshoot.

The first-order speed filter then acts on the flightpath angle signal to generate the airspeed signal (fig. B-11(b)). The airspeed signal is smoothed too heavily for its dynamics to be visible on the short

time-scale of figure B-11(b), but the long-period phugoid oscillation seen in figure B-12 results from the long lag of the speed filter, which couples dynamically with the pitch filter and the path filter by means of the implicit feedback paths to generate the phugoid oscillation.

The same kind of frequency-domain analysis could be applied to the response of the aircraft to a short elevator pulse, which is discussed in the next section from the time-domain perspective. The frequency-domain viewpoint is addressed again later to enable further simplifications of the dynamic model.

Elevator pulse response at airspeeds above the speed for minimum drag– The first 5 sec of the response to a short (1 sec) 1-deg elevator pulse that pitches the aircraft nose-down is illustrated by figure B-13. The figure shows that, in the medium term after 2.5 sec, both pitch angle and flightpath angle remain constant after decreasing by about 1/4 deg relative to their initial values. This 1-deg elevator pulse is representative of the control inputs required to achieve small, precise changes in flightpath angle during high-precision tasks such as glide-slope tracking. The associated airspeed increase (fig. B-13(b)) is too small for the resulting lift increase to affect the pitch angle, flightpath angle, and angle-of-attack responses seen in figure B-13(a).

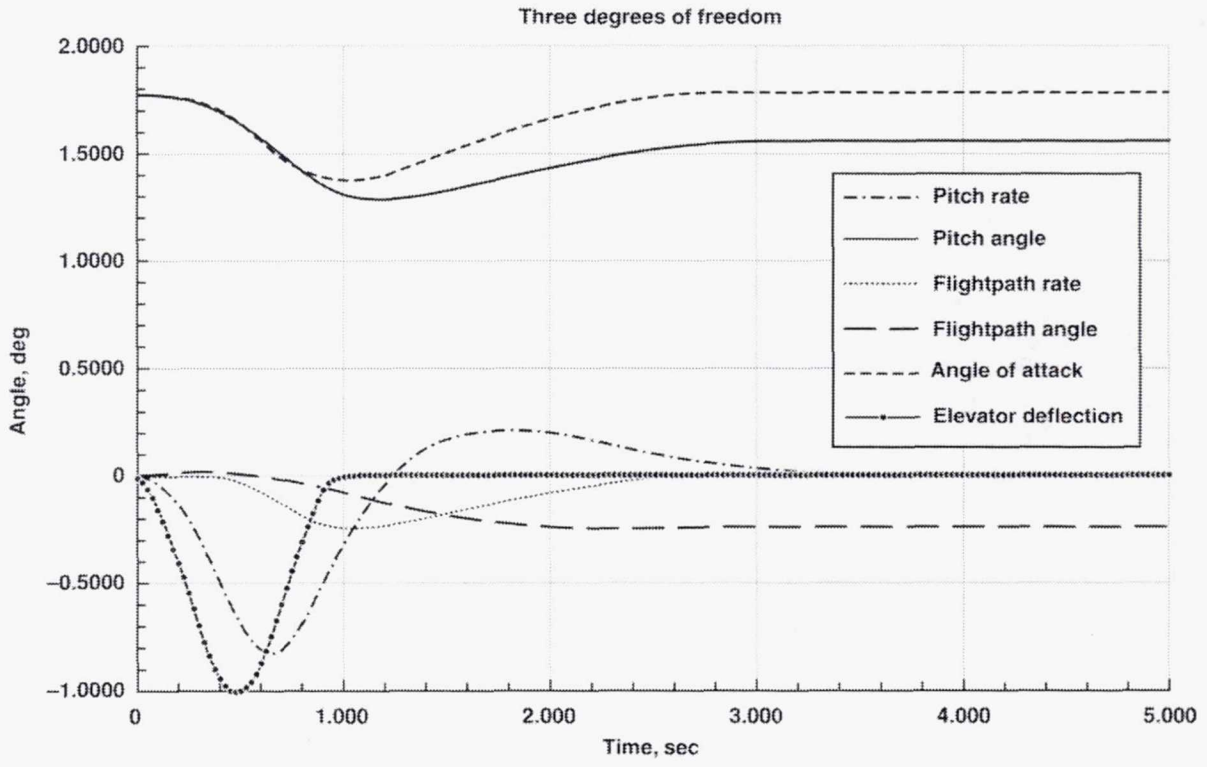

a)

Figure B-13. Elevator pulse response, 5 sec.

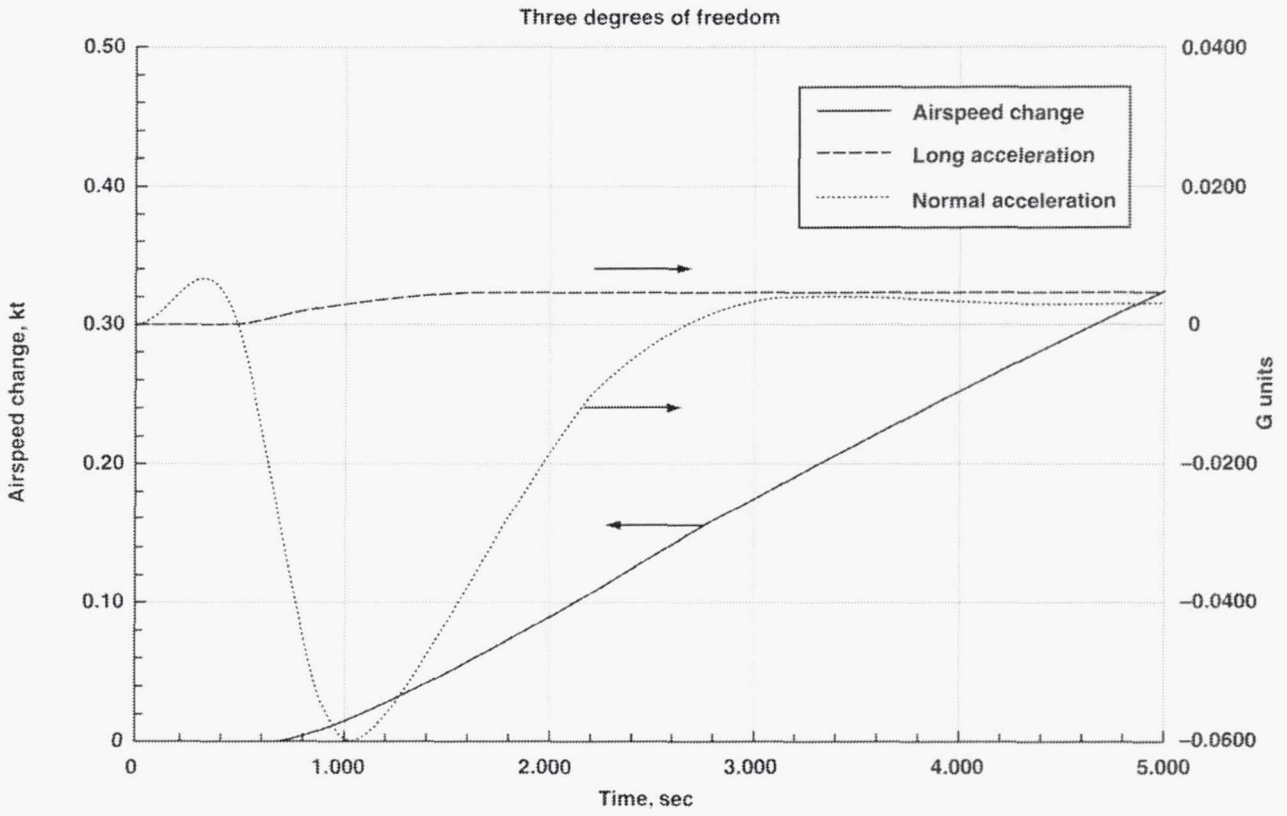

b)

Figure B-13. Elevator pulse response, 5 sec (concluded).

However, extending the time histories of figure B-13 to include 60 sec of response, as illustrated by figure B-14, reveals the characteristic phugoid oscillation seen previously in figure B-12. Pilots suppress this phugoid oscillation by applying elevator control so as to stabilize pitch angle. This pilot control input can be approximated by holding pitch angle fixed for all times after 4.65 sec, as illustrated by figure B-15. (The time 4.65 sec was selected by choosing a time before the phugoid response has developed significantly, and for which the pitch rate vanishes.) It can be seen from figure B-15(a) that stabilizing the pitch angle completely suppresses the phugoid oscillation. As the airspeed increases because of the sustained longitudinal acceleration resulting from the decrease in flightpath angle (fig. B-15(b)), the long-term increase in lift causes the flightpath angle to increase (fig. B-15(a)). With pitch fixed, the angle of attack decreases, reducing lift until the decreased lift resulting from the angle of attack decrease equilibrates the increased lift resulting from the airspeed increase. In the long term, it can be seen that the flight condition becomes stable, with the aircraft in equilibrium at the higher airspeed. It should be noted from figure B-15(a) that, with pitch stabilized, most of the initial flightpath increment is destroyed by the long-term response, almost nulling the effect of the control input.

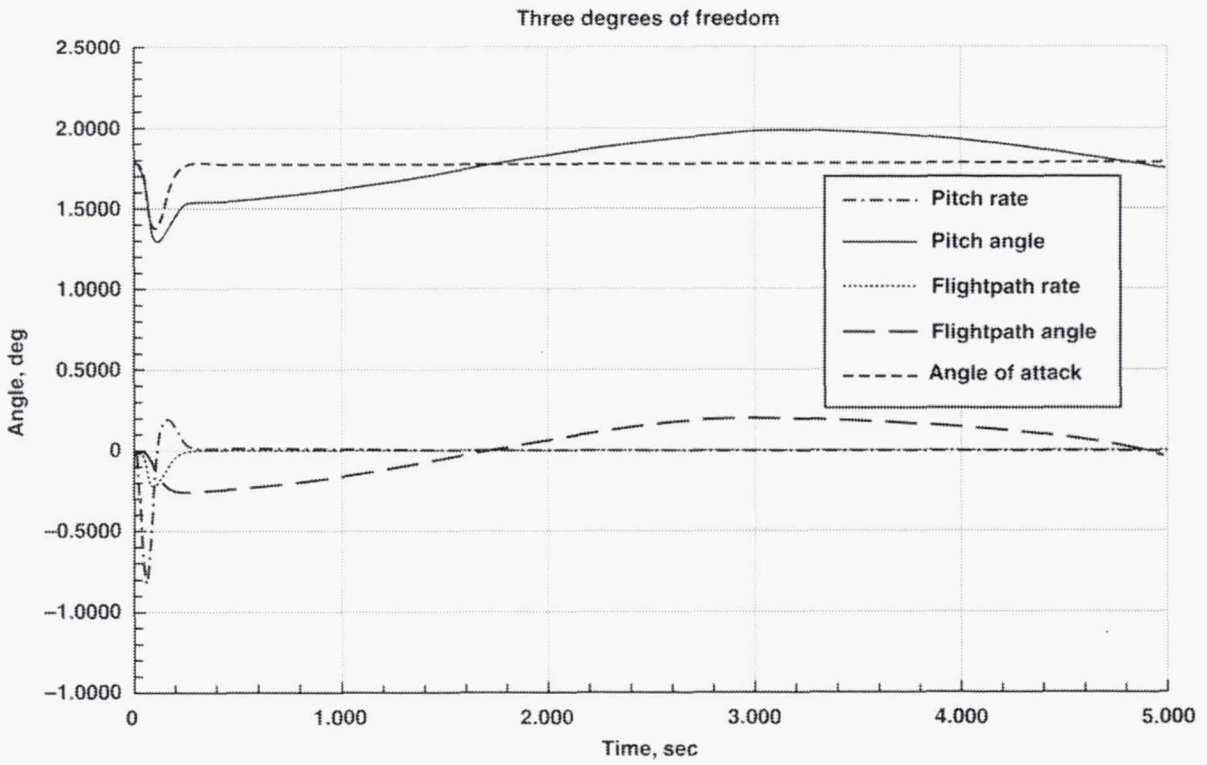

a)

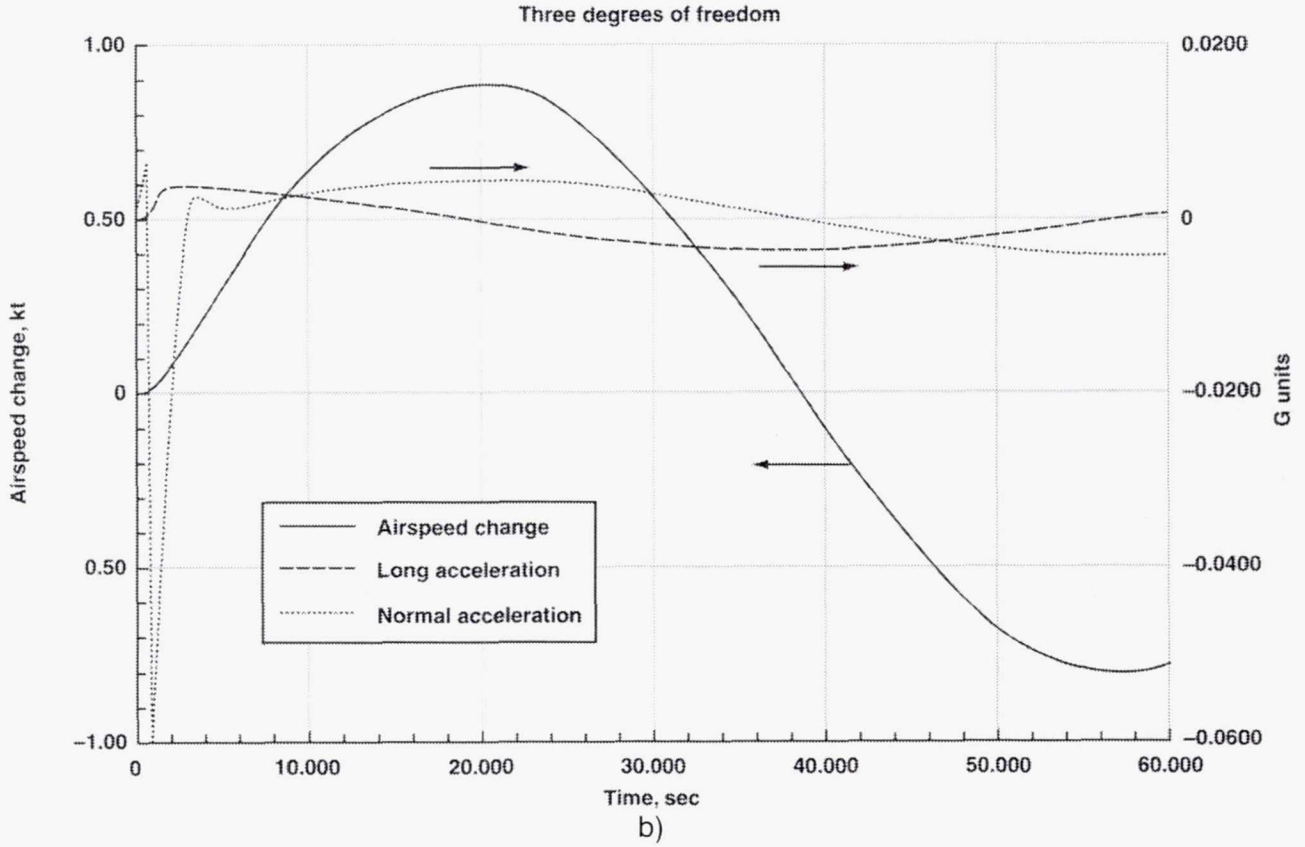

b)

Figure B-14. Elevator pulse response, 60 sec.

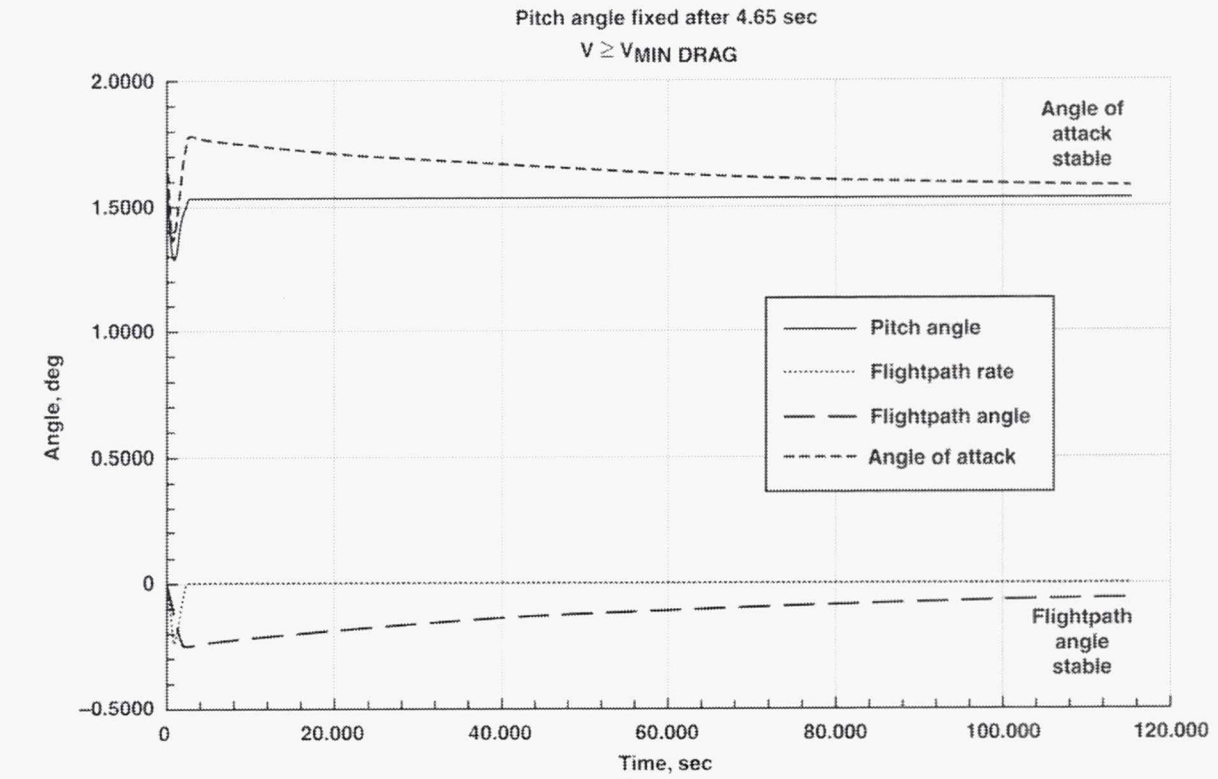

a)

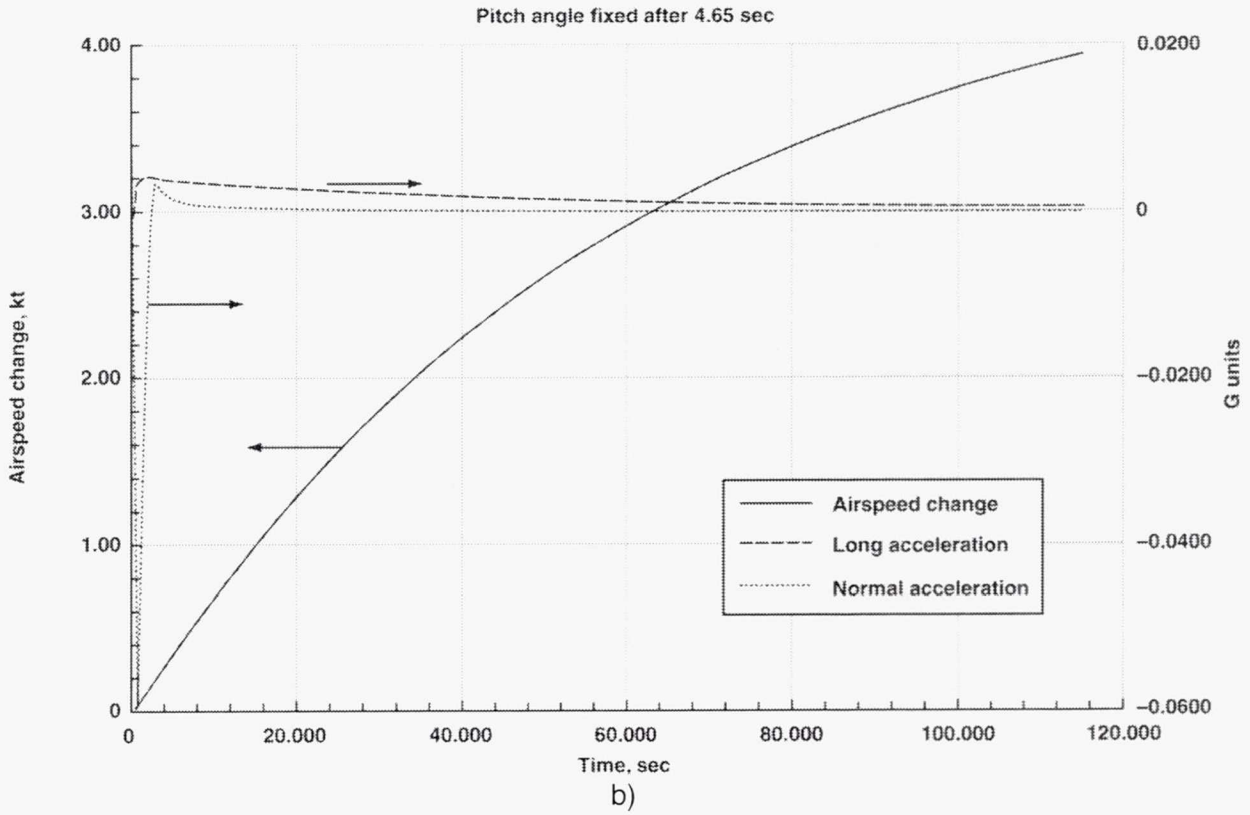

b)

Figure B-15. Elevator pulse response, 115 sec, θ fixed after 4.65 sec, $V \geq V_{MIN\ DRAG}$.

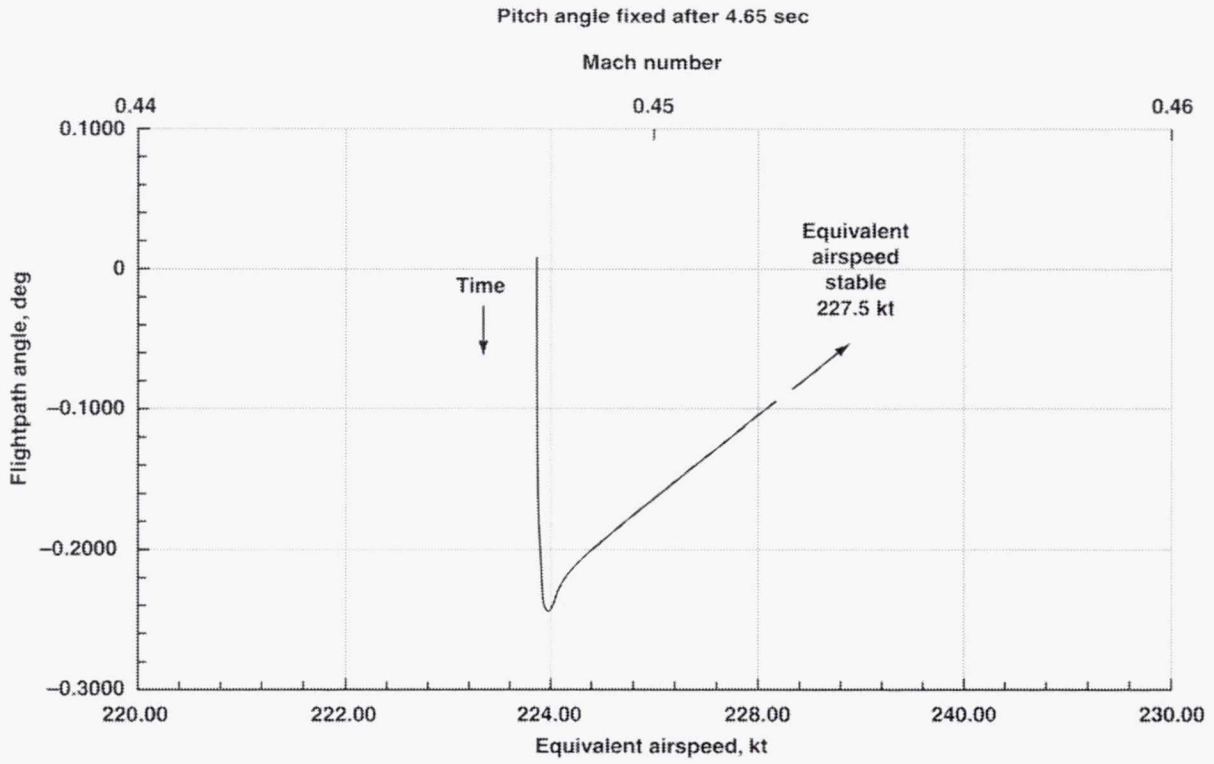

c)

Figure B-15. Elevator pulse response, 115 sec, θ fixed after 4.65 sec, $V \geq V_{MIN\ DRAG}$ (concluded).

If the pitch angle is controlled so as to maintain this flightpath increment fixed, the response of the aircraft is illustrated by figure B-l6. The figure shows that, in the medium and long term after time 2.7 sec (selected for vanishing flightpath rate), the flightpath angle remains fixed. Figure B-16(a) shows that a slow decrease in angle of attack is required to hold flightpath angle fixed. With path angle fixed, the time history of pitch angle (not illustrated) has the same form as that of angle of attack. Again the aircraft stabilizes in the long term just as for fixed pitch (compare figure B-15), although a much longer time is required to reach equilibrium. (The very long 10-sec integration step used after time 5 sec was selected for computational convenience in the spread-sheet implementation. With these smooth functions, trials with shorter steps showed no significant error owing to the long step, and in any case, the final equilibrium condition is independent of the trajectory by which it is reached.) The variation of flightpath angle with airspeed illustrated by figure B-16(c) consists of an initial vertical segment and a final horizontal segment without visible rounding, a consequence of the effect of the large airspeed change on the scaling of the abscissa.

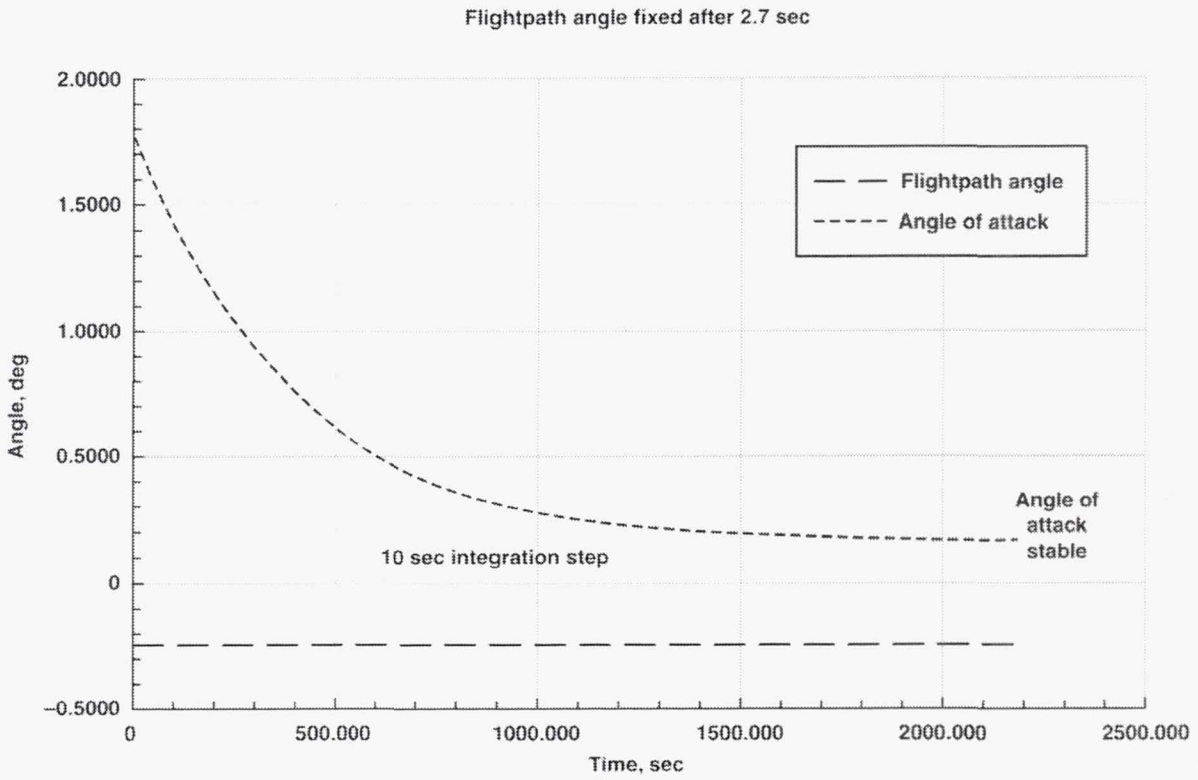

a)

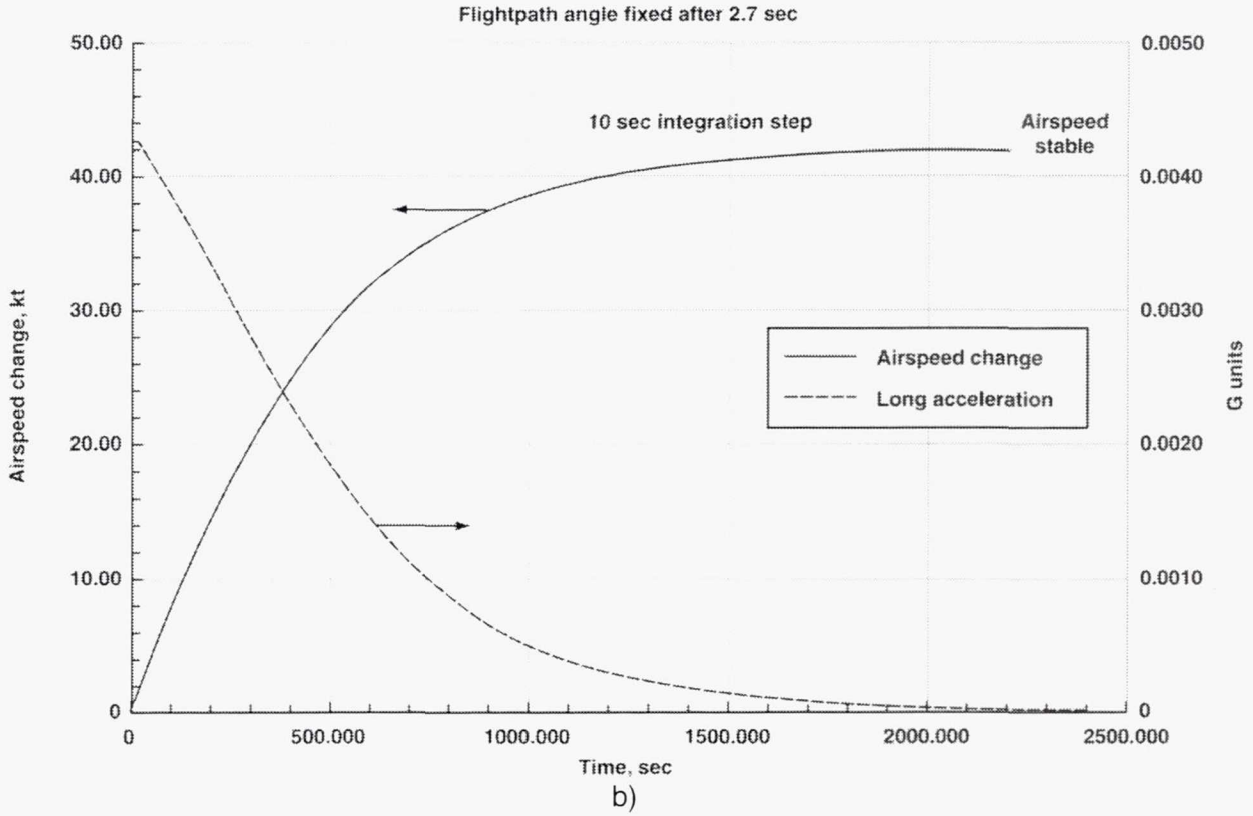

b)

Figure B-16. Elevator pulse response, 2205 sec, γ fixed after 2.7 sec, $V \geq V_{MIN\ DRAG}$.

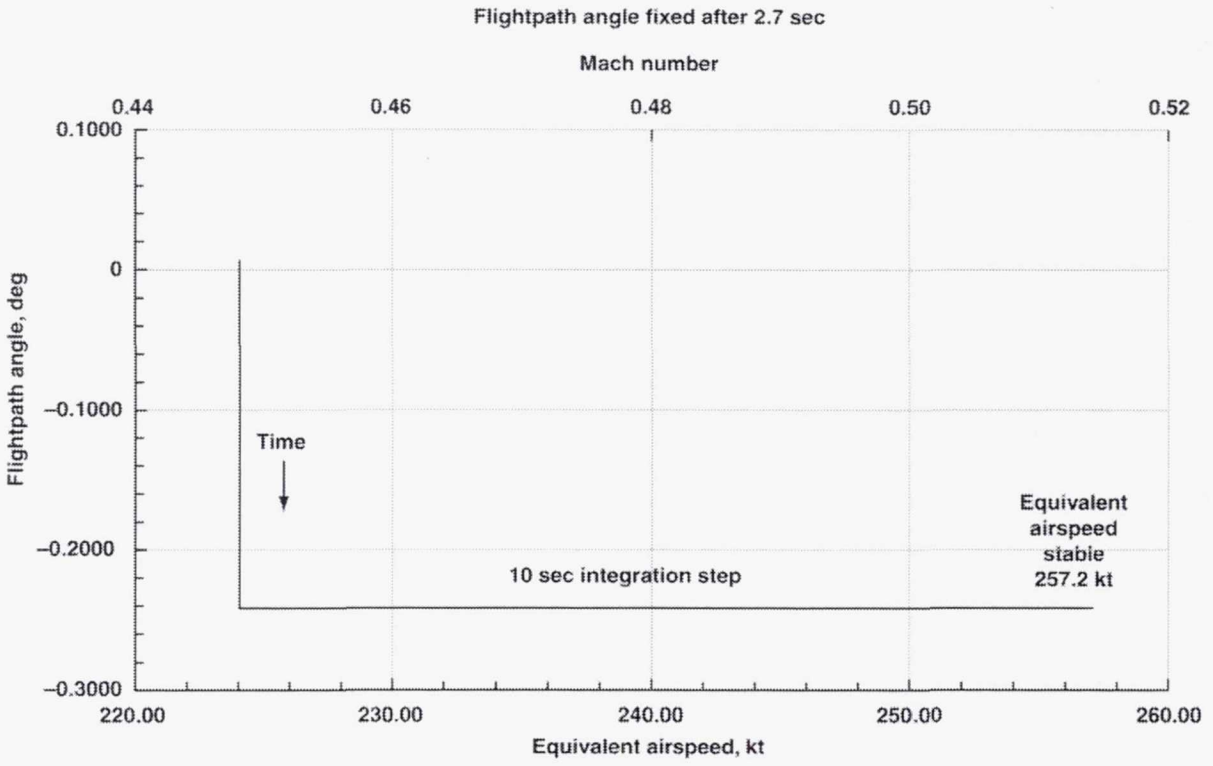

c)

Figure B-16. Elevator pulse response, 2205 sec, γ fixed after 2.7 sec, $V \geq V_{MIN\ DRAG}$ (concluded).

For fixed flightpath angle (horizontal segment of figure B-16(c)) lift is equal to aircraft weight (eq. (B-2b)), so that the normal forces are in equilibrium during the whole time after the path is fixed at 2.7 sec. The longitudinal acceleration resulting initially from the decrease in flightpath angle is sustained until it is equilibrated by the increase of parasite drag owing to the airspeed increase (fig. B-16(b)). The airspeed increase required to reach equilibrium of the longitudinal forces can be determined from the performance envelope, such as that illustrated by figure B-7. The point of final equilibrium is defined by the intersection of the appropriate constant-rpm contour with the horizontal line corresponding to the fixed flightpath angle. To summarize, figure B-16 shows that, *in the region above the speed for minimum drag, the flightpath can be controlled by means of pitch control alone, with thrust setting (rpm) fixed.* It is otherwise below the speed for minimum drag.

Elevator pulse response at airspeeds below the speed for minimum drag– If the elevator pulse is reversed in sign so that the aircraft pitches nose-up, its response with pitch fixed after 4.65 sec is illustrated by figure B-17. It can be seen that, after accounting for the elevator sign reversal, the response is similar in form to that for the nose-down elevator pulse (compare figure B-15). In particular, figure B-17 shows that, *with pitch fixed, the aircraft stabilizes in the long term at an airspeed slightly below the speed for minimum drag.*

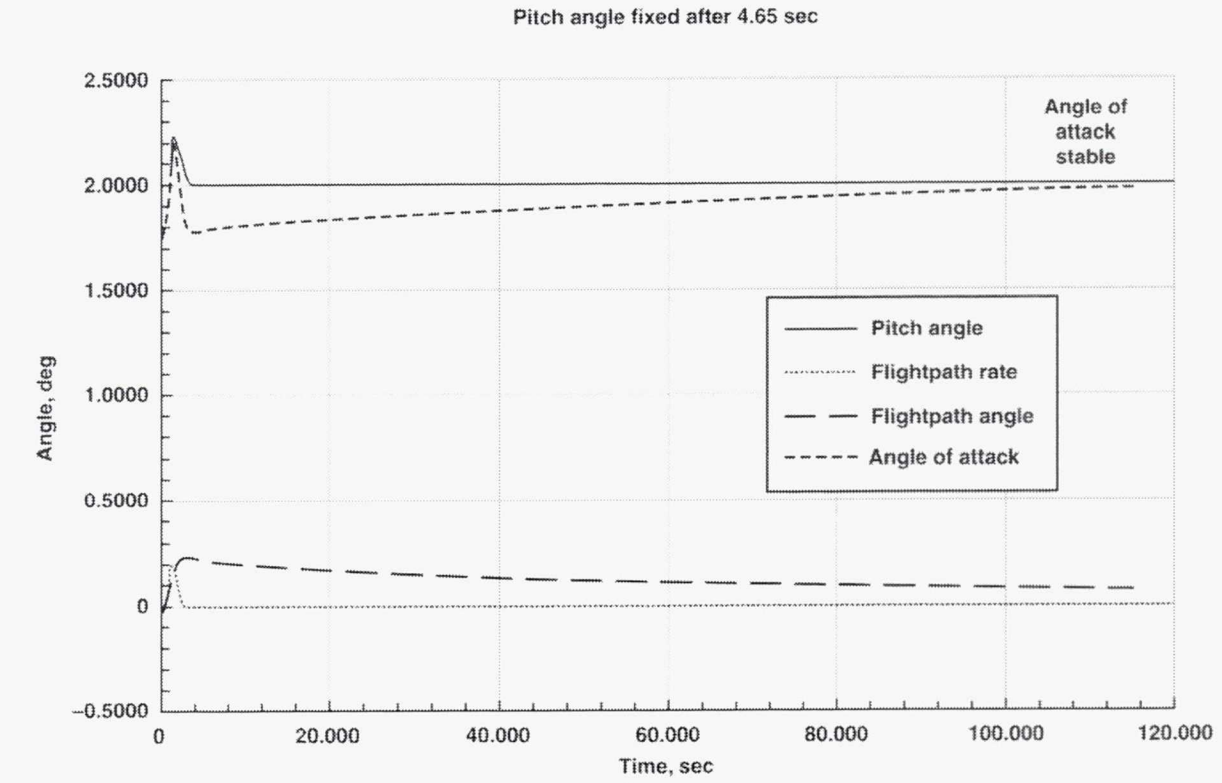

a)

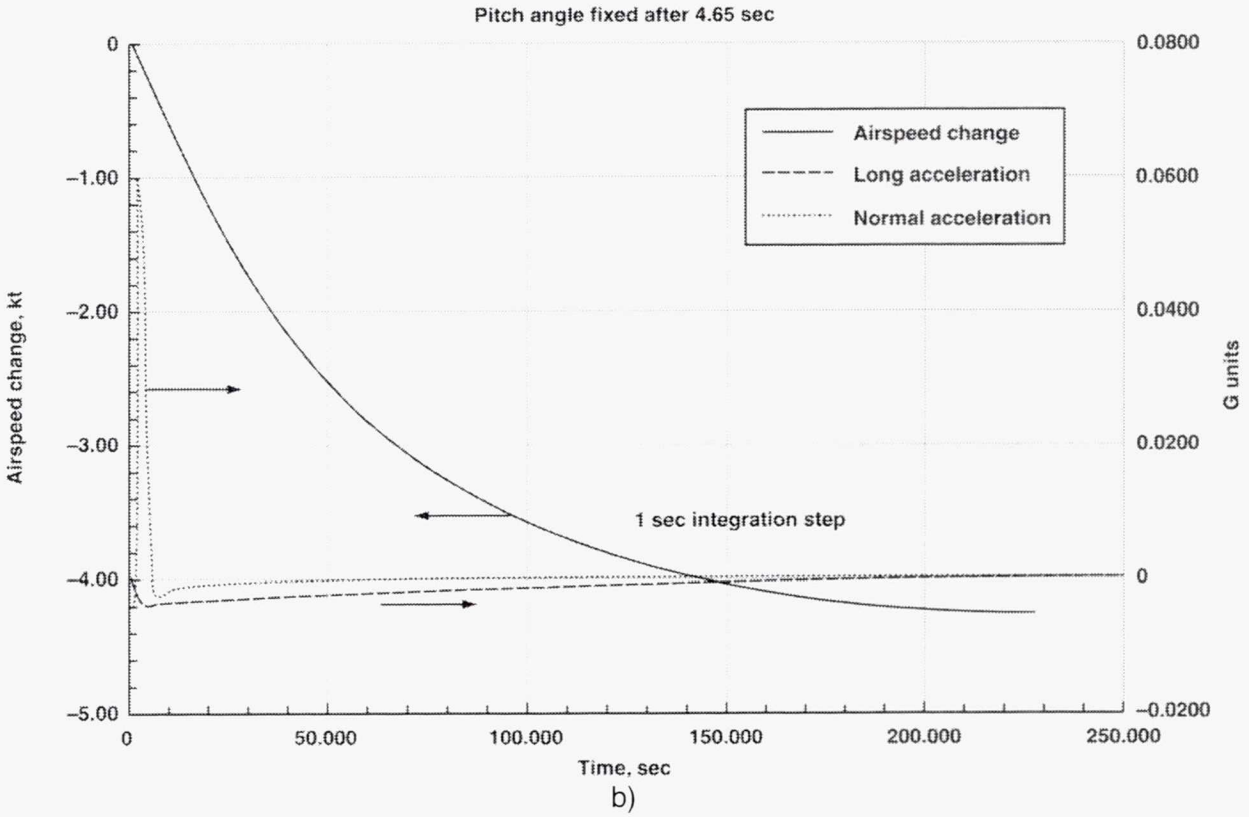

b)

Figure B-17 Elevator pulse response, 115 sec, θ fixed after 4.65 sec, $V \leq V_{MIN\ DRAG}$.

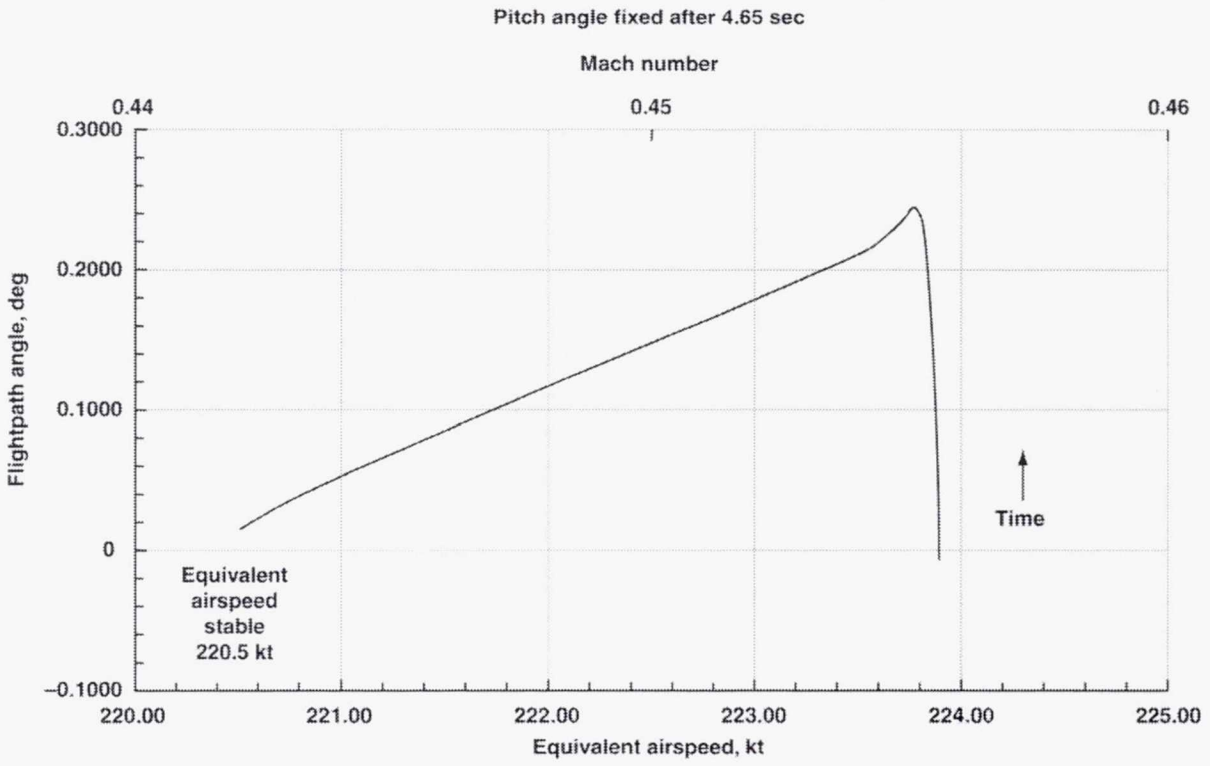

c)

Figure B-17 Elevator pulse response, 115 sec, θ fixed after 4.65 sec, $V \leq V_{MIN\ DRAG}$ (concluded).

In contrast, if pitch is controlled so as to hold the flightpath angle fixed after 2.7 sec, the response of the aircraft is illustrated by figure B-18. It can be seen that the aircraft never reaches a stable equilibrium of longitudinal forces. The longitudinal deceleration owing to the initial increase in flightpath angle is sustained by the contribution of induced drag, which as previously noted increases with decreasing airspeed (fig. B-18(b)). The result is that, with both flightpath angle and thrust setting held fixed below the speed for minimum drag, the airspeed decreases (fig. B-16(b)) and the angle of attack increases (fig. B-16(a)) until the aircraft stalls. The time history of the pitch angle required to hold the flightpath fixed (not illustrated) has the same form as that of angle of attack (fig. B-16(a)). The important conclusion is that, *below the speed for minimum drag, the flightpath angle cannot be controlled by means of pitch control alone with thrust setting fixed.*

By making thrust adjustments that compensate for the increase of induced drag (eq. (B-2a)), the aircraft can be stabilized at a target (V, γ) operating point below the speed for minimum drag. On the performance envelope chart of figure B-7, such a target operating point is defined by the intersection of the horizontal line corresponding to the selected flightpath angle with the vertical line corresponding to the selected airspeed. It can be shown that, below the speed for minimum drag, such points are points of unstable equilibrium. To verify this property, note that displacement to a slightly lower airspeed by some disturbance would result in airspeed divergence to the stall, just as that illustrated by figure B-18. Therefore, *below the speed for minimum drag, active control of thrust is required for stability*, with significantly increased pilot workload during manual control.

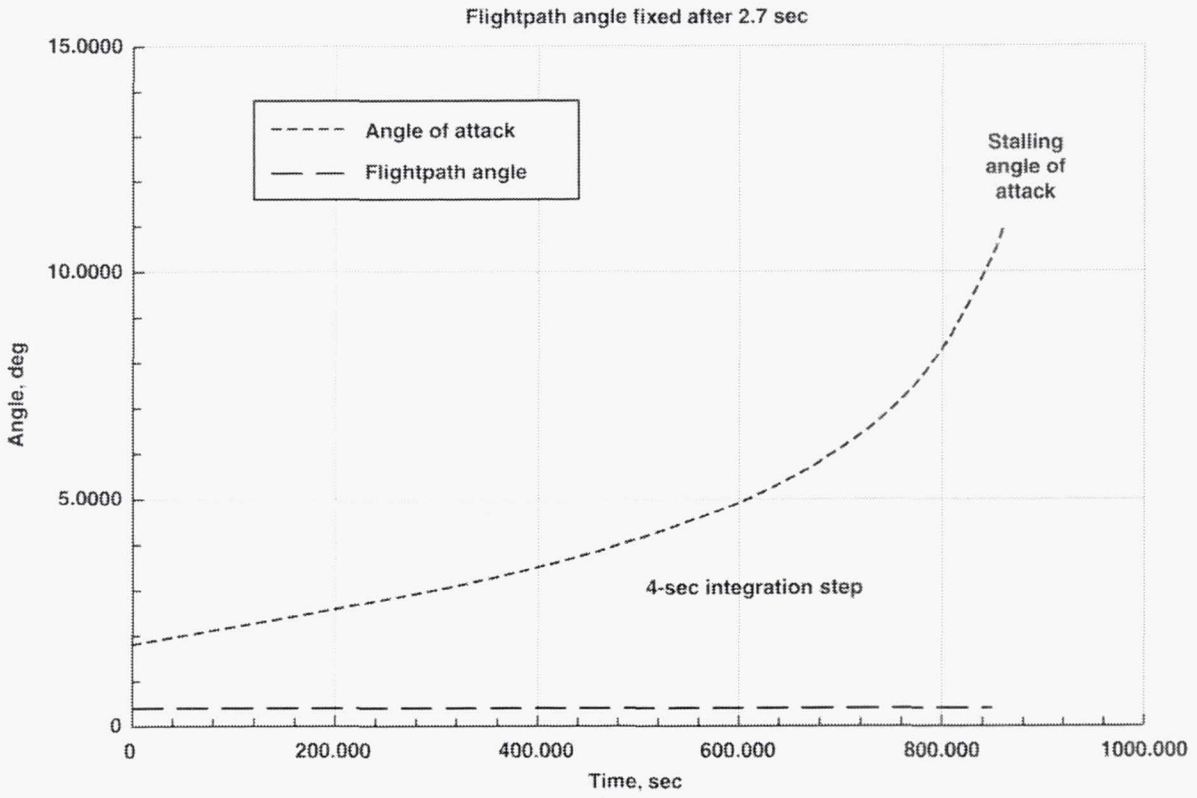

a)

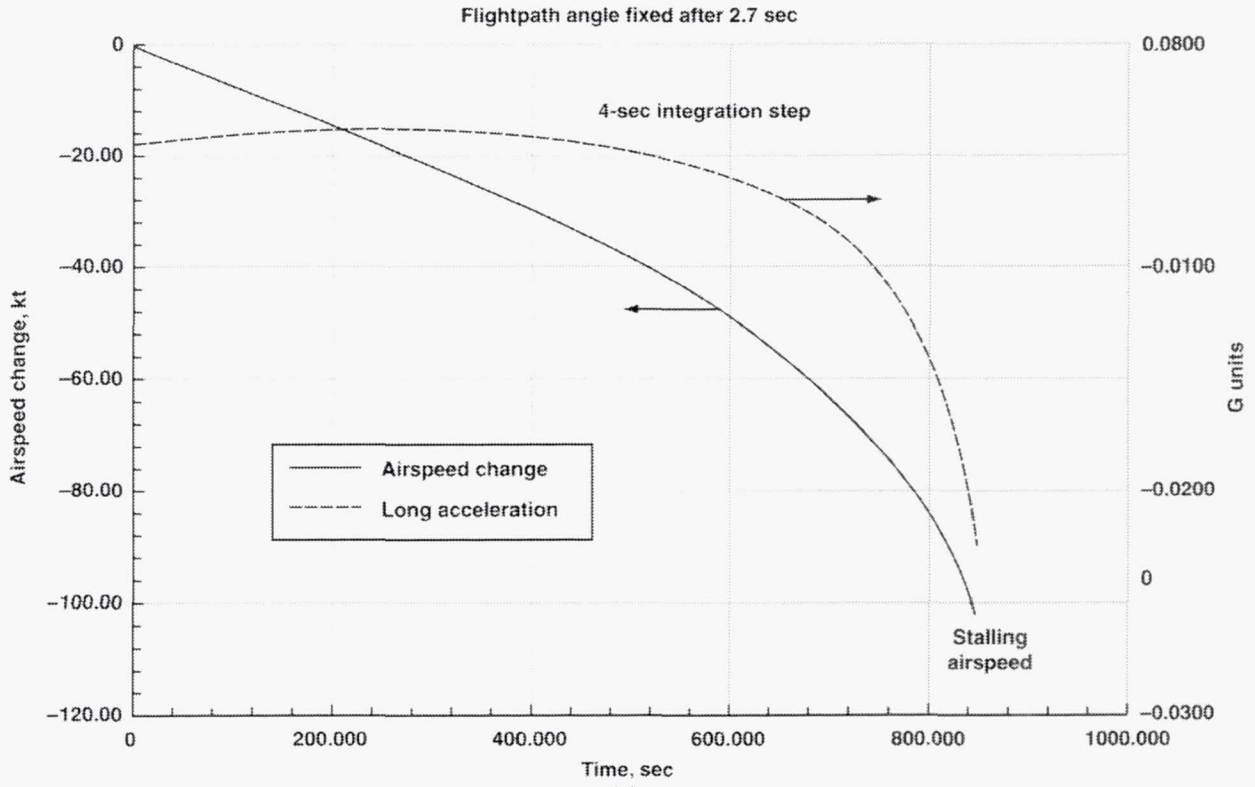

b)

Figure B-18. Elevator pulse response, 885 sec, γ fixed after 2.7 sec, $V \geq V_{MIN\ DRAG}$.

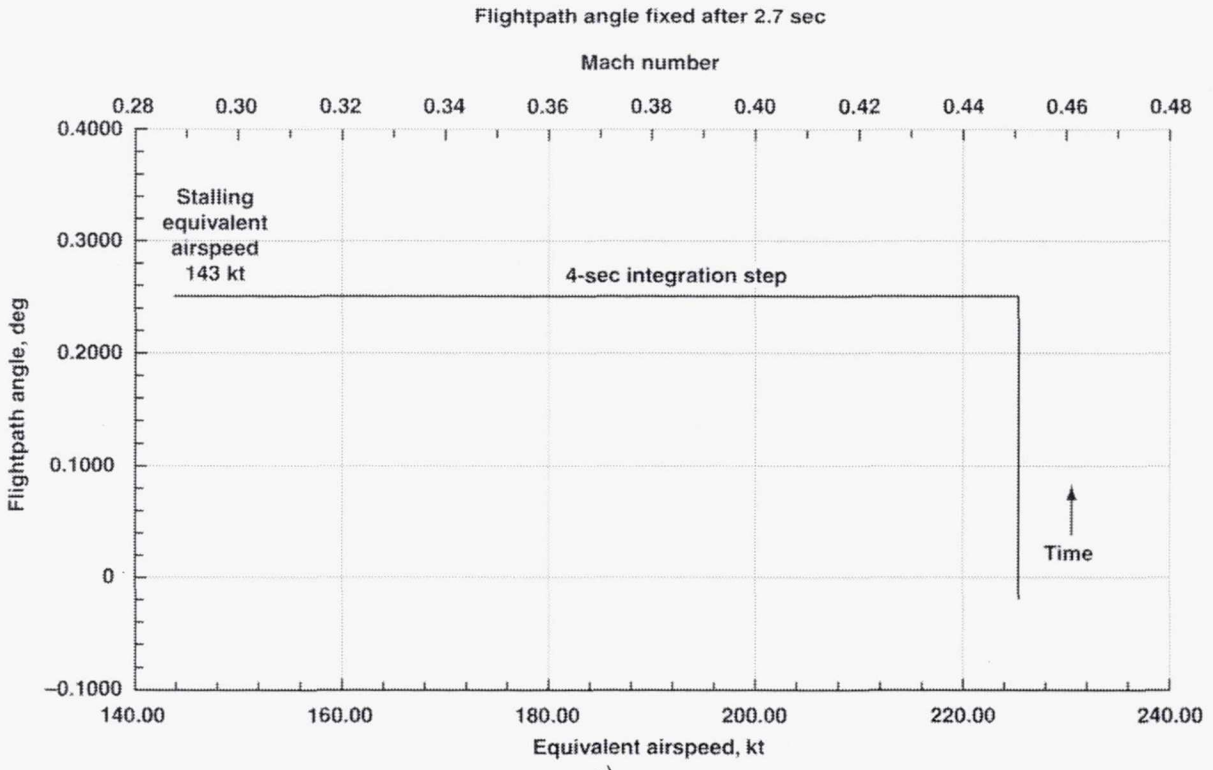

c)

Figure B-18. Elevator pulse response, 885 sec, γ fixed after 2.7 sec, $V \geq V_{MIN\ DRAG}$ (concluded).

The pilot technique actually used for glide-slope tracking below the speed for minimum drag, such as for aircraft carrier landing approach, can be discussed by referring to the performance envelope chart of figure B-7. It can be seen that any target operating point can be defined by the intersection of the contour corresponding to the selected thrust setting (rpm) with that corresponding to the selected pitch angle. Since all points within the performance envelope are points of equilibrium, the forms of these contours imply that, in the long term, flightpath angle can be controlled by means of thrust. If flightpath angle is varied by 1/4-deg increments for glide-slope tracking by adjusting thrust, while pitch angle is held fixed, then figure B-7 shows that the resulting airspeed excursions are small in the long term. These small airspeed excursions can be controlled as necessary by adjusting pitch, and the time histories of figure B-17 show that the resulting response is stable. In practice, pitch control is coordinated with thrust in order to obtain more rapid flightpath response than that resulting from thrust modulation alone.

Pilots often refer to the airspeed region below the speed for minimum drag, in which total drag is dominated by the induced drag contribution, as the "back side of the drag curve," and to the control of flightpath angle by means of thrust and control of airspeed and angle of attack by means of pitch as "back-side technique." The region below the speed for minimum drag is also termed the region of reversed command, since above that speed path is controlled with pitch and speed with thrust, as already discussed. In order to limit the increase in pilot workload required for thrust coordination below the speed for minimum drag, flying qualities criteria for manual control specify the maximum slope (that is, $d\gamma/dV$) of the constant-rpm contours in the neighborhood of the target operating point

(fig. B-7). Pilot workload can be reduced significantly by means of an autothrottle. The characteristic differences in dynamic response above and below the speed for minimum drag just discussed for manual control also have fundamental significance for the choice of feedback loop structure within such automated systems.

Automated control systems– In particular, referring to the three primitive control modes discussed in the main report, the loop structure chosen for the γ-V Command mode feeds back path error to pitch control and speed error to thrust control. In the γ-V Command mode, active thrust control enables stability to be achieved both above and below the speed for minimum drag. If the thrust saturates so that active thrust control is no longer available, then the γ-V Command mode is invalid, and one of the other two primitive modes must be selected.

The loop structure chosen for the V Command mode feeds back speed error to pitch control, while thrust (rpm) remains fixed. The resulting response is qualitatively similar to that illustrated by figures B-15 and B-17, so that the V Command mode is stable both above and below the speed for minimum drag, although the path is not constrained.

The other primitive mode available when thrust is saturated is the γ Command mode, which feeds back path error to pitch control while thrust remains fixed. Above the speed for minimum drag, the resulting response is qualitatively similar to that of figure B-16, so that the γ Command mode is stable, although speed is not constrained. Below the speed for minimum drag, the response in the γ Command mode is qualitatively similar to that of figure B-18. It has already been noted that this response is unstable. If the γ Command mode were engaged below the speed for minimum drag, the resulting airspeed divergence could lead to a potentially catastrophic stall. Therefore, *flight safety requires that the associated mode selection logic must prevent its engagement under these invalid conditions*. It is clear that the dynamical behavior illustrated by figures B-15, B-16, B-17, and B-18 is of fundamental importance for the design of automated control systems.

Simplified Models

The remaining task is the development of simplified dynamic models; simplification is facilitated by returning to the frequency-domain viewpoint discussed previously. Since the three filters for pitch, path, and speed illustrated by figure B-10(b) act in cascade, the bandwidth of the response signal at any point in the diagram is dominated by the bandwidth of the lowest-bandwidth filter upstream of that point. Stating the same property in time-domain terms, the high-frequency fluctuations present in the pitch angle signal at the output of the pitch filter are not observable in the flightpath response, because these high-frequency details are filtered out by the heavy smoothing of the path filter that lies immediately downstream of the pitch filter. Similarly, intermediate-frequency fluctuations present in the flightpath signal at the output of the path filter are not observable in the airspeed signal, because they are filtered out by the extremely heavy smoothing of the speed filter. These summary statements are justified by the detailed discussion of the time histories of figures B-11 and B-12 presented previously.

Two-Degree-of-Freedom Model

It follows that little change in the flightpath and airspeed signals would result if the pitch angle signal were drastically simplified. For the aircraft response to the short nose-up elevator pulse illus-

trated by figure B-13(a), if the details of the pitch overshoot and oscillation are neglected, the pitch response can be approximated by a pitch step shaped by a cosine bell. It was pointed out previously that the pilot shapes the elevator control input so as to obtain just such a pitch response, thereby enabling small, precise changes in flightpath angle in the medium term and suppressing the phugoid oscillation in the long term. If the pitch angle thus specified is regarded as the control input, then the dynamical system can be represented by the two-degree-of-freedom model illustrated by the simplified block diagram of figure B-10(c). (Throttle control, which is not treated in the examples selected for this appendix, would add another degree of freedom for thrust, so that the system of figure B-10(c) would have a total of three degrees of freedom.) The response of this two-degree-of-freedom model to the nose-up elevator pulse of figure B-13(a) is illustrated by figures B-19 and B-20.

Pitch step response – In figure B-19(a), the actual pitch time history of figure B-13(a) is approximated by a step shaped by a 0.5-sec cosine bell. The magnitude of this pitch step is chosen so that the initial pitch angle and that at time 4.65 sec coincide on the two charts. It can be seen that the two pitch-angle time histories are nearly coincident over the medium term after 3 sec. Furthermore, the angle of attack responses seen in the two charts also match fairly well in the medium term. The two flightpath-angle responses match fairly well over the whole 5-sec interval, with errors that do not exceed about 0.1 deg anywhere. Comparison of figure B-19(b) with figure B-13(b) shows that the longitudinal acceleration and airspeed responses match very well over the whole 5-sec interval (note the expanded airspeed scale).

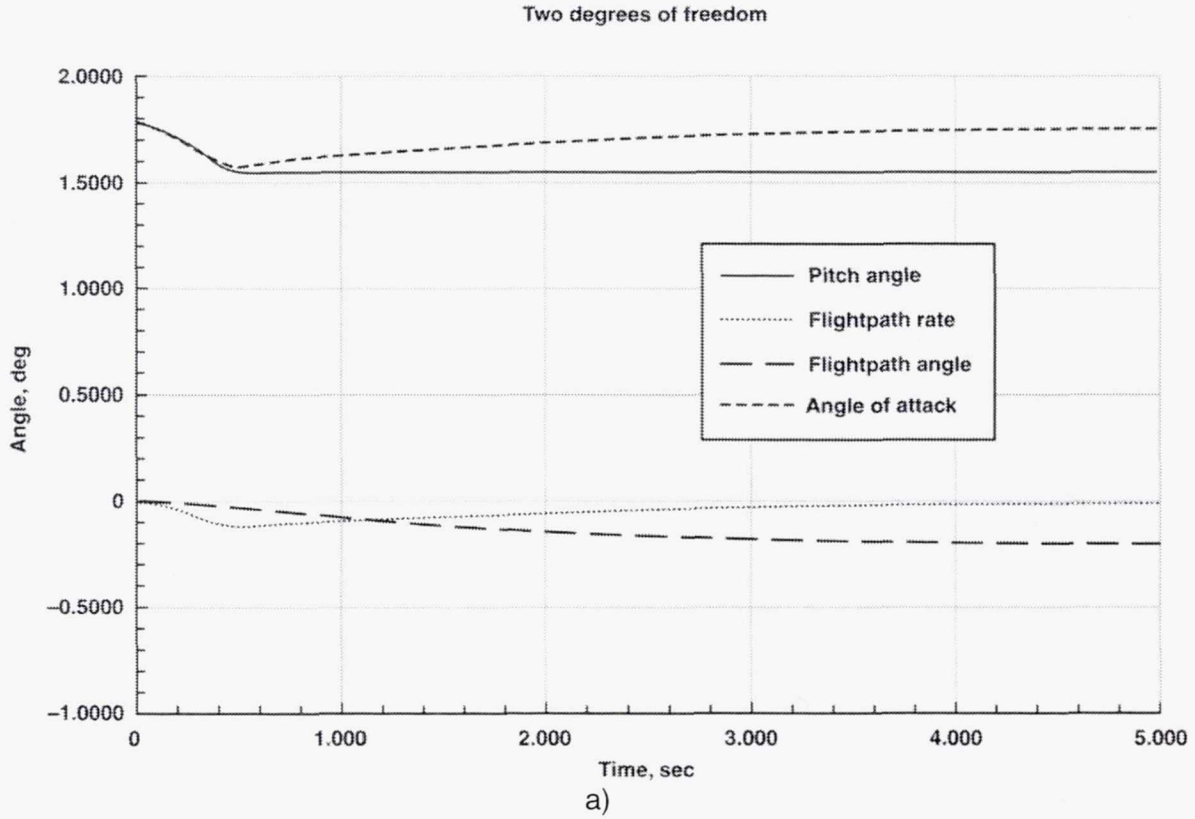

a)

Figure B-19. Pitch step response, 5 sec, two degrees of freedom.

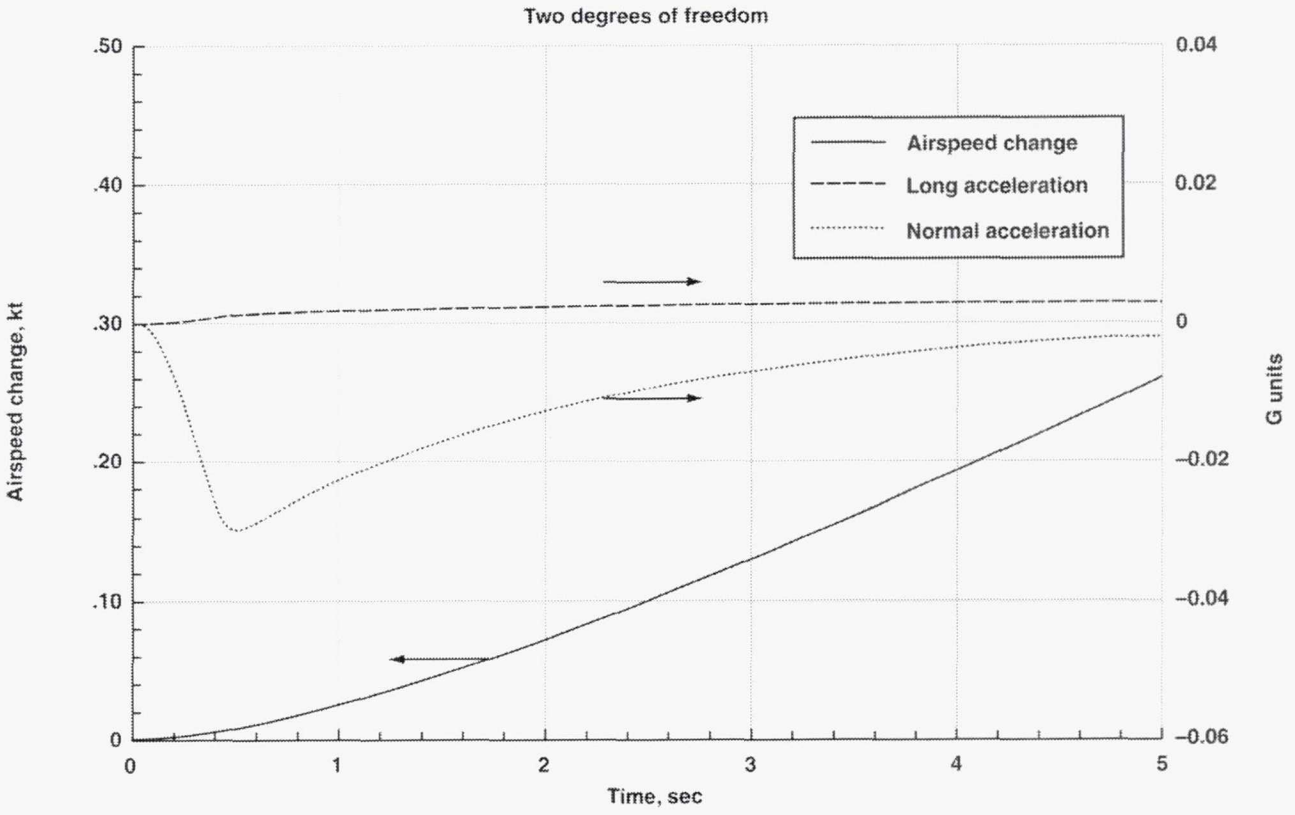

b)

Figure B-19. Pitch step response, 5 sec, two degrees of freedom (concluded).

When the time interval is extended to 115 sec, comparison of figure B-20(a) with figure B-15(a) shows that, in the medium and long term after 5 sec, the two-degree-of-freedom approximation is nearly exact for both angle of attack and flightpath angle. Comparison of figure B-20(b) with figure B-15(b) shows that the same is true for longitudinal acceleration and airspeed. *Therefore, if one is interested chiefly in the flightpath angle and airspeed responses to pitch control, it is evident that the two-degree-of-freedom model will serve very well.*

Discussion– In particular, this demonstration justifies use of the two-degree-of-freedom approximation for the analysis of mode validity discussed in the main report. For the control system described there, the γ Command mode corresponds to control of flightpath angle by means of elevator control with fixed throttle setting, and the V Command mode corresponds to control of airspeed by means of elevator control with fixed throttle setting. It has just been demonstrated that, with fixed throttle setting, both flightpath angle and airspeed responses to elevator control can be approximated satisfactorily by the two-degree-of-freedom model, which replaces specification of the form of the elevator control time history with specification of the resulting medium-term and long-term pitch response. The two-degree-of-freedom approximation is therefore valid for both the γ Command and the V Command modes.

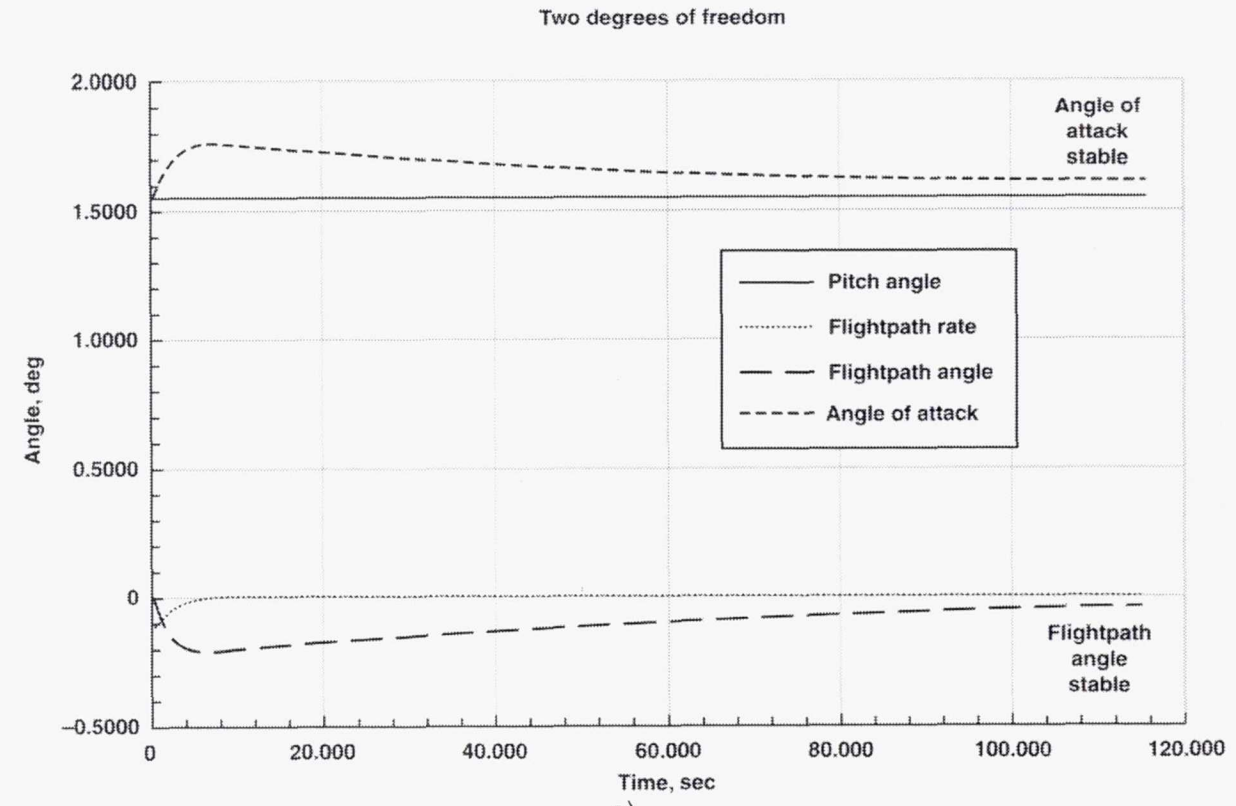

a)

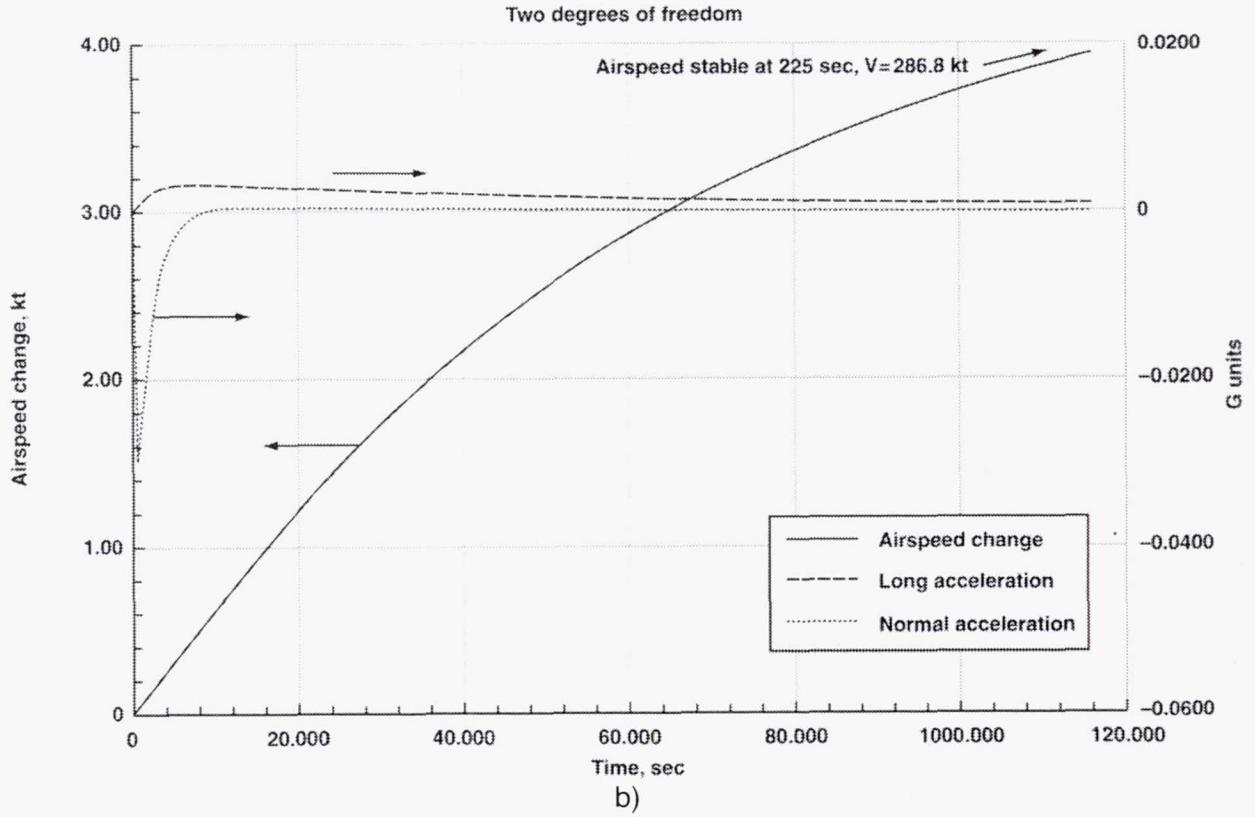

b)

Figure B-20. Pitch step response, 115 sec, two degrees of freedom.

In a similar way, the two-degree-of-freedom model can be extended to include control of both flightpath angle and airspeed by simultaneous elevator and throttle control, which corresponds to the γ-V Command mode. This extension is accomplished by replacing specification of the form of the throttle control time history with specification of the resulting medium-term and long-term thrust response generated by the engine model. Because the dynamic thrust lag within the engine model has a narrower bandwidth and a longer time scale than that of the pitch response to elevator deflection, it follows that neglect of thrust dynamics presents a less critical challenge to validity of the two-degree-of-freedom model than does the neglect of pitch dynamics already demonstrated.

One-Degree-of-Freedom Model

If flightpath angle is controlled by means of pitch (that is, elevator deflection) and thrust is controlled by means of throttle so that the forms of both the flightpath angle and thrust time histories are specified, then the airspeed response can be approximated by making use of the one-degree-of-freedom model illustrated by figure B-l0(d). This drastically simplified model, which neglects the dynamics of pitch, flightpath, and thrust, nevertheless retains the important quadratic nonlinearity resulting from the variation of drag with speed.

Path step response– To specify the flightpath angle time history for the single-degree-of-freedom model, the flightpath angle step is shaped by a 2-sec cosine bell that approximates the flightpath lag relative to elevator deflection (fig. B-13(a)). The resulting responses of longitudinal acceleration and airspeed are illustrated by figures B-21(a) and B-21(b). Comparison of figure B-21(a) with figure B-13(b) shows that the single-degree-of-freedom approximation provides a nearly exact match of the two time histories during the first 5 sec, and comparison of figure B-2l(b) with figure B-16(b) shows that this excellent agreement extends over the long term. Since the engine thrust lag (figs. B-5 and B-6) is of the same order as that of the flightpath response (fig. B-l0(b)), the thrust input for figure B-l0(d) could be specified in a similar manner by shaping a thrust step of the desired magnitude with a 2-sec cosine bell to approximate the engine thrust lag. It is clear that, *if one is interested chiefly in the airspeed response to flightpath angle and thrust control, the single-degree-of-freedom model will serve very well.* This somewhat surprising result reduces the entire aircraft model to a very simple dynamical system governed by the nonlinear differential equation (B-2a) for longitudinal forces, which can be solved numerically by a single integration for each time step.

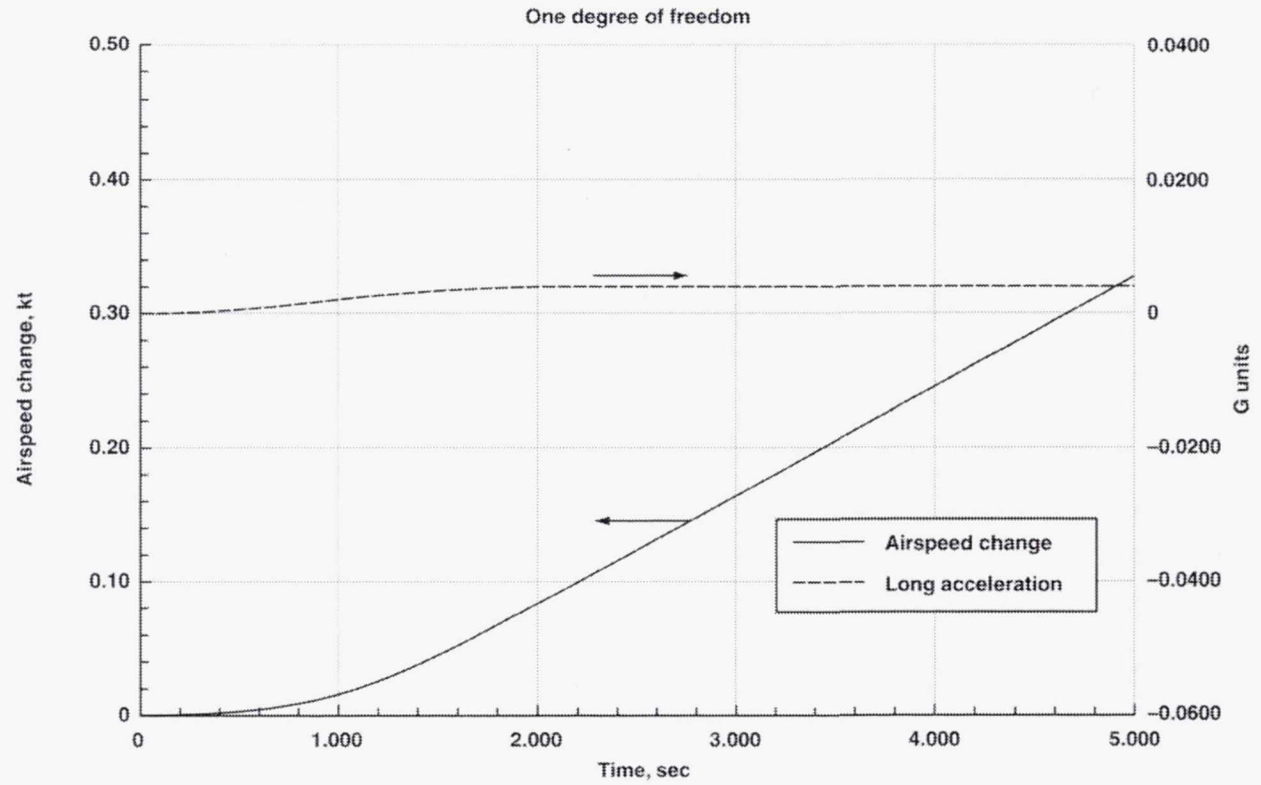

a)

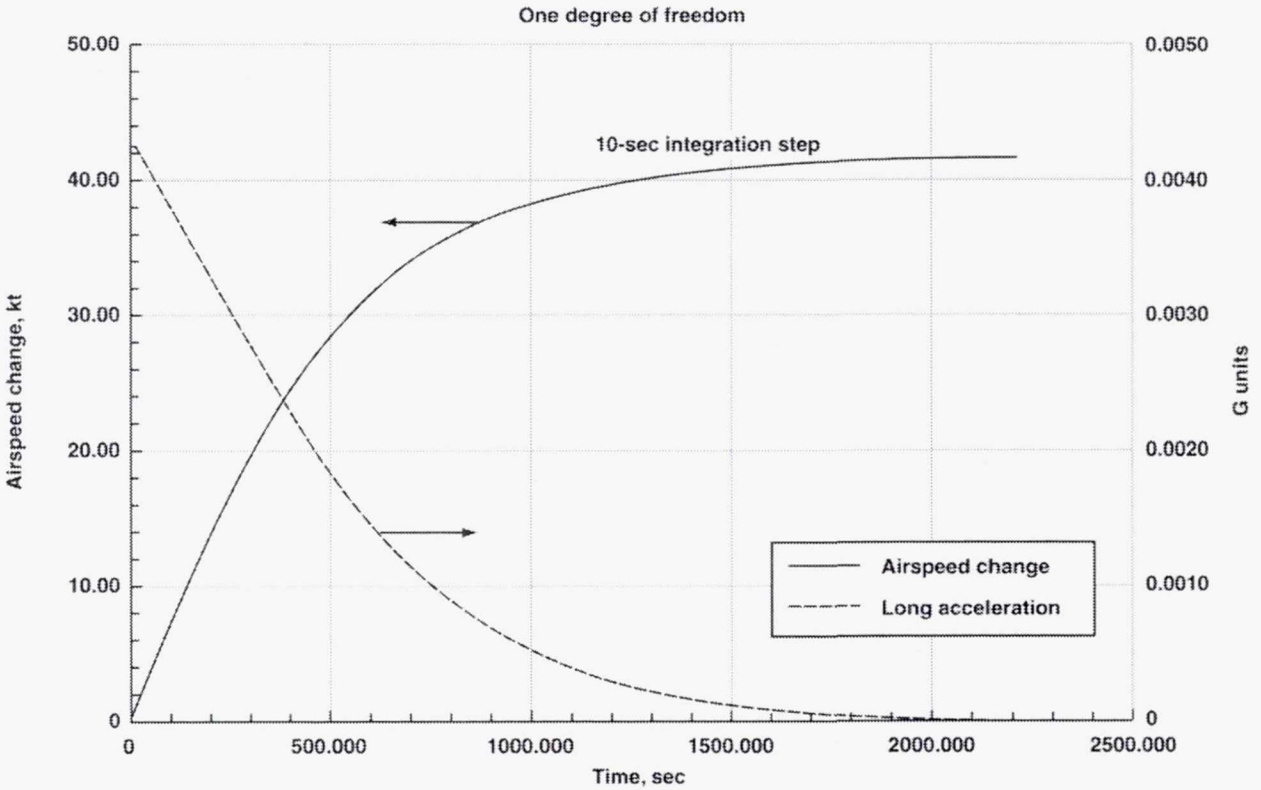

b)

Figure B-21. Path step response, 5 sec and long term, single degree of freedom.

REFERENCES

Bridgman, P. W.: Dimensional Analysis. Encyclopedia Britannica, vol. 7, pp. 439–449, 1970.

Davies, D. P.: Handling the Big Jets. Air Registration Board, Brabazon House (England), 1969.

Erzberger, Heinz; and Lee, Homer Q.: Characteristics of Constrained Optimum Trajectories with Specified Range. NASA TM 78519, Sept. 1978.

Erzberger, Heinz: Automation of On-Board Flightpath Management. Tenth von Karman Memorial Lecture presented at 24th Israel Annual Conference on Aviation and Astronautics, Tel Aviv and Haifa, Israel, Feb. 17–18, 1982.

Erzberger, Heinz; and Nedell, William: Design of Automated System for Management of Arrival Traffic. NASA TM 102201, June 1989.

Erzberger, Heinz; Davis, Thomas J.; and Green, Steven: Design of CenterTRACON Automation System. AGARD CP-538, AGARD Guidance and Control Panel 56th Symposium, Berlin, Germany, May 1993.

Green, Steven M.; Den Braven, Wim; and Williams, David. H.: Development and Evaluation of a Profile Negotiation Process for Integrating Aircraft and Air Traffic Control Automation. NASA TM 4360, April 1993.

Hill, Philip G.; and Peterson, Carl R.: Mechanics and Thermodynamics of Propulsion, 2nd ed. Addison-Wesley (Mass.), 1992.

Innis, Robert C.; Holzhauser, Curt A.; and Quigley, Hervey C.: Airworthiness Considerations for STOL Aircraft. NASA TN D-5594, Jan. 1970.

Lee, Homer Q.; and Erzberger, Heinz: Algorithm for Fixed-Range Optimum Trajectories. NASA TP-1565, July 1980.

McRuer. D. T.; Ashkenas, I. L.; and Graham, D.: Aircraft Dynamics and Automatic Control. Princeton University Press (New Jersey), 1973.

Press, W. H.; Flannery, B. P.; Teukolsky, S. A.; and Vetterling, W. T.: Numerical Recipes: The Art of Scientific Computing. Cambridge University Press (New York), 1986.

Shevell, Richard S.: Fundamentals of Flight, 2nd ed. Prentice Hall (New Jersey), 1989.

Taylor, E. S.: Dimensional Analysis for Engineers. Clarendon Press (England), 1974. (Quoted by Hill and Peterson, 1992.)

APPENDIX C
SYMMETRIC (COORDINATED) TURNING FLIGHT

This appendix generalizes the longitudinal equations of motion for symmetric (coordinated) turning flight, in order to provide results needed for the main report. The main report uses the two-degree-of-freedom model presented in appendix B, which eliminates the pitching moment equation from the dynamic model by the assumption of effectively infinite pitch bandwidth and control power. Therefore, only the two longitudinal force equations require generalization for turning flight.

In order to achieve a concise but rigorous treatment, the development that follows makes extensive use of vector/matrix methods, and limited use of spherical trigonometry. It will be shown that, for straight wings-level flight, the generalized equations reduce to those already obtained (app. B) by elementary methods. The aircraft structural, aerodynamic, and propulsive models, together with those for the Earth and the atmospheric environment, remain the same as those discussed in appendix B. For the generalized treatment that follows, flight is assumed to take place in still air.

GENERAL VECTOR FORCE EQUATION

The equation of motion for a rigid aircraft subject to aerodynamic, propulsive, and gravitational forces is obtained directly in vector form from Newton's second law:

$$m\,\mathbf{a}_{path} = \mathbf{F}^{aero} + \mathbf{F}^{prop} + \mathbf{F}^{grav} \tag{C-1}$$

where m denotes the aircraft mass, **a** its kinematic acceleration, and **F** the external force acting on the aircraft. The superscripts indicate the nature of each force, and the subscript indicates the reference frame in which each quantity is described. In equation (C-1), the path-frame components of the aerodynamic and propulsive forces are the lift L, the drag D, the side force Y, and the thrust T, as discussed previously (app. B). The path-frame components of the aircraft weight W must be found by trigonometric resolution. To accomplish this task, the spatial orientation of the path frame can be specified relative to the Earth by defining three Eulerian angles.

Eulerian Angles for Path Frame

These three Eulerian angles are defined as follows (fig. C-l). The process starts with the orthogonal right-handed local Earth frame N E D (that is, the directions North, East, and Down) with its origin fixed at the aircraft center of gravity. The frame X″ Y″ Z″ is generated by positive rotation about the D axis through the aircraft track angle ψ_T (fig. C-1(a)). It can be seen that the Z″ axis coincides with the D axis. Next, the frame X′ Y′ Z′ is generated by positive rotation about the Y axis through the aircraft flightpath angle γ (fig. C-1(b)). It can be seen that the Y′ axis coincides with the Y″ axis. Finally, the path frame T L N (that is, the tangent direction along the aircraft velocity vector, the normal to the velocity vector in the negative lift direction, and the lateral axis in the direction of the side force) is generated by positive rotation about the X′ axis through the roll angle ϕ' (fig. C-l(c)).

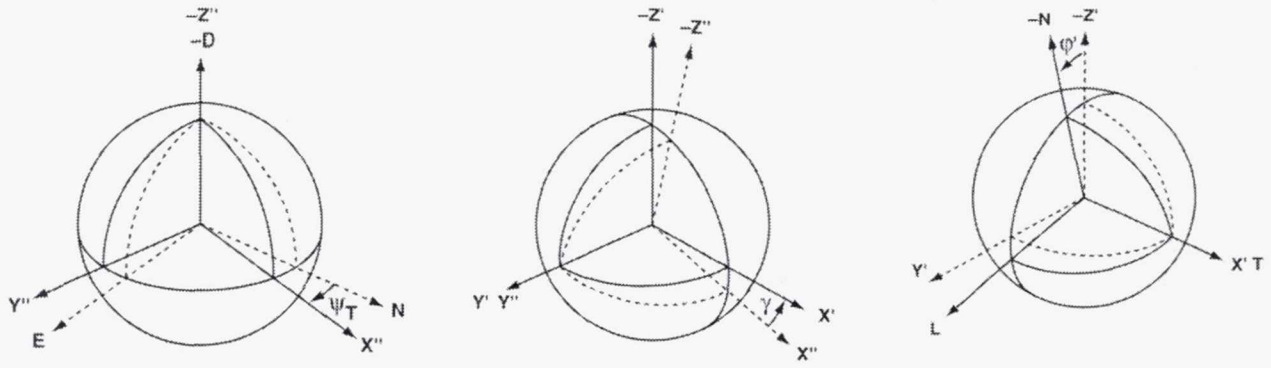

a) Definition of track angle ψ_T. b) Definition of flightpath angle γ. c) Definition of roll angle ϕ'.

Figure C-1. Spatial orientation of path frame.

It can be seen that the T axis coincides with the X′ axis. The N axis is taken as the negative lift direction in order to preserve the right-handedness of the path frame.

Weight Components

With the Eulerian angles ψ_T, γ, and ϕ' specified, the path-frame components of the aircraft weight **W** are given by the matrix equation

$$[W_T \; W_L \; W_N]^T = [\phi'][\gamma][\psi_T] \; [0 \; 0 \; W]^T \tag{C-2}$$

In equation (C-2), the direction cosine matrices $[\psi_T]$, $[\gamma]$, and $[\phi']$ are specified by symmetric nine-element arrays as follows:

$$[\boldsymbol{\psi_T}] = \begin{bmatrix} \cos\psi_T & \sin\psi_T & 0 \\ -\sin\psi_T & \cos\psi_T & 0 \\ 0 & 0 & 1 \end{bmatrix} \tag{C-2a}$$

$$[\boldsymbol{\gamma}] = \begin{bmatrix} \cos\gamma & 0 & -\sin\gamma \\ 0 & 1 & 0 \\ \sin\gamma & 0 & \cos\gamma \end{bmatrix} \tag{C-2b}$$

$$[\boldsymbol{\phi'}] = \begin{bmatrix} 1 & 0 & 0 \\ 0 & \cos\phi' & \sin\phi' \\ 0 & -\sin\phi' & \cos\phi' \end{bmatrix} \tag{C-2c}$$

In equation (C-2), the first matrix multiplication yields

$$[\psi_T][0 \quad 0 \quad W]^T = [0 \quad 0 \quad W]^T \tag{C-2d}$$

Equation (C-2d) shows that, because the ψ_T rotation is taken about the D axis, which coincides with the direction of the gravity vector, the path-frame components of the weight vector are independent of the aircraft track direction ψ_T. Therefore, the track angle can be taken as North (that is, $\psi_T = 0$) without loss of generality. With equation (C-2d), equation (C-2) becomes

$$[W_T \; W_L \; W_N]^T = [\phi'][\gamma][0 \quad 0 \quad W]^T \tag{C-2e}$$

The indicated matrix multiplication on the right side of equation (C-2e) results in the product

$$[\phi'][\gamma] = \begin{bmatrix} \cos\gamma & 0 & -\sin\gamma \\ \sin\phi'\sin\gamma & \cos\phi' & \sin\phi'\cos\gamma \\ \cos\phi'\sin\gamma & -\sin\phi' & \cos\phi'\cos\gamma \end{bmatrix} \tag{C-2f}$$

With equation (C-2f), the path-frame components of the weight **W** are found from equation (C-2e) to be

$$[W_T \; W_L \; W_N]^T = W[-\sin\gamma \quad \sin\phi'\cos\gamma \quad \cos\phi'\cos\gamma]^T \tag{C-2g}$$

After substituting equation (C-2g) and putting m = W/g, equation (C-1) becomes, in matrix form,

$$\begin{aligned}(W/g)[a_T \quad a_L \quad a_N]^T = {} & [-D \quad Y \quad -L]^{T\,\text{aero}} \\ & + [T \quad 0 \quad 0]^{T\,\text{prop}} \\ & + W[-\sin\gamma \quad \sin\phi'\cos\gamma \quad \cos\phi'\sin\gamma]^{T\,\text{grav}}\end{aligned}$$

or, combining terms and dividing by **W**,

$$\begin{aligned}&(1/g)[a_T \quad a_L \quad a_N]^T \\ &\quad = [(T-D)/W - \sin\gamma) \quad (Y/W + \sin\phi'\cos\gamma) \quad (-L/W + \cos\phi'\cos\gamma]^T\end{aligned} \tag{C-3}$$

Kinematic Acceleration Components

The next task is to calculate the path-frame components of the kinematic acceleration a on the left side of equation (C-3). In general, the path frame rotates with respect to the Earth with an angular velocity that is denoted by ω. Since by assumption the Earth frame is inertial, the path frame rotates with angular velocity ω relative to inertial space. In such a rotating frame, the kinematic acceleration **a** is given by the well-known formula for vector differentiation of velocity (Wills, 1958; Etkin, 1959; McRuer, Ashkenas, and Graham, 1973):

$$\mathbf{a} = \mathbf{dV/dt} = \boldsymbol{\delta}\mathbf{V/\delta t} + \omega \times \mathbf{V} \tag{C-4}$$

where **dV/dt** denotes the time derivative of the velocity vector **V** measured in the inertial (Earth) frame, and **δV/δt** denotes the time derivative of the scalar magnitude V measured in the path frame. Equation (C-4) has the physical interpretation that, at constant speed, the **δV/δt** term vanishes, but the centripetal acceleration owing to curvature of the flightpath is accounted for by the vector cross-product term $\omega \times \mathbf{V}$.

In equation (C-4), the total angular velocity ω is found by vectorial summation of the Eulerian angular rates $d\psi_T/dt$, $d\gamma/dt$, and $d\phi'/dt$. This summation is complicated by the fact that the axes about which the Eulerian rotations ψ_T, γ, and ϕ' are taken are not, in general, orthogonal (fig. (C-l)). It follows from the definitions of these angles that the path-frame components of the angular velocity vector ω are given by the matrix equation

$$[\omega_T \quad \omega_L \quad \omega_N]^T = [d\phi'/dt \quad 0 \quad 0]^T + [\phi']\left\{[0 \quad d\gamma/dt \quad 0]^T + [\gamma][0 \quad 0 \quad d\psi_T/dt]^T\right\}$$

or (C-5)

$$[\omega_T \quad \omega_L \quad \omega_N]^T = [d\phi'/dt \quad 0 \quad 0]^T + [\phi'][0 \quad d\gamma/dt \quad 0]^T + [\phi'][\gamma][0 \quad 0 \quad d\psi_T/dt]^T$$

After carrying out the indicated matrix multiplications on the right side of equation (C-5), the path-frame components of the angular velocity vector ω are found to be

$$[\omega_T \quad \omega_L \quad \omega_N]^T = [(d\phi'/dt \quad -d\psi_T/dt \sin\gamma) \quad (d\gamma/dt \cos\phi' + d\psi_T/dt \sin\phi' \cos\gamma) \quad (-d\gamma/dt \sin\phi' + d\psi_T/dt \cos\phi' \cos\gamma)]^T \tag{C-5a}$$

In equation (C-4), the path-frame components of the **δV/δt** term on the right are given by

$$\boldsymbol{\delta}\mathbf{V/\delta t} = [\delta V/\delta t \quad 0 \quad 0]^T \tag{C-5b}$$

With equations (C-5a) and (C-5b), equation (C-4) becomes

$$\begin{bmatrix} a_T \\ a_L \\ a_N \end{bmatrix} = \begin{bmatrix} (dV/dt) \\ (-V\, d\gamma/dt \sin\phi' + V\, d\psi_T/dt \cos\phi' \cos\gamma) \\ (-V\, d\gamma/dt \cos\phi' - V\, d\psi_T/dt \sin\phi' \cos\gamma) \end{bmatrix} \tag{C-5c}$$

All the elements of the path-frame longitudinal force equations have now been found. After substituting equation (C-5c) into the left side of equation (C-3), the general vector equation of motion becomes

$$\frac{1}{g}\begin{bmatrix} (dV/dt) \\ (-V\ d\gamma/dt \sin\phi' + V\ d\psi_T/dt \cos\phi' \cos\gamma) \\ (-V\ d\gamma/dt \cos\phi' - V\ d\psi_T/dt \sin\phi' \cos\gamma) \end{bmatrix} = \begin{bmatrix} (T - D)/W - \sin\gamma) \\ (Y/W + \sin\phi' \cos\gamma) \\ (-L/W + \cos\phi' \cos\gamma) \end{bmatrix} \qquad \text{(C-6)}$$

When expressed in scalar form, the vector equation (C-6) is equivalent to three scalar equations for longitudinal (streamwise) force, side force, and normal force (lift):

$$(1/g)[(dV/dt) = (T - D)/W - \sin\gamma \qquad \text{(C-6a)}$$

$$-(V/g)\ d\gamma/dt \sin\phi' + (V/g)\ d\psi_T/dt \cos\phi' \cos\gamma = Y/W + \sin\phi' \cos\gamma \qquad \text{(C-6b)}$$

$$-(V/g)\ d\gamma/dt \cos\phi' - (V/g)\ d\psi_T/dt \sin\phi' \cos\gamma = -L/W + \cos\phi' \cos\gamma \qquad \text{(C-6c)}$$

COORDINATED TURNING FLIGHT

In coordinated (symmetric) turning flight, the side force Y vanishes. After imposing this condition, equation (C-6b) can be solved for the quantity $(V/g)\ d\psi_T/dt$ to obtain

$$(V/g)\ d\psi_T/dt \cos\phi' \cos\gamma = \sin\phi' \cos\gamma + (V/g)\ d\gamma/dt \sin\phi'$$

or

$$(V/g)\ d\psi_T/dt = \tan\phi' + (V/g)\ d\gamma/dt \tan\phi'/\cos\gamma \qquad \text{(C-7a)}$$

In level flight, or in a steady climb or descent, the flightpath rate $d\gamma/dt$ vanishes, and the turn rate equation (C-7a) reduces to a well-known formula for a steady coordinated turn:

$$(V/g)\ d\psi_T/dt = \tan\phi' \qquad \text{(C-7b)}$$

Returning to the general coordinated turn, the quantity $(V/g)\ d\psi_T/dt$ can be eliminated from the lift equation (C-6c) by substituting equation (C-7a). After simplifying with the help of the identity $1/\cos^2\phi' = 1 + \tan^2\phi'$, the lift equation for the coordinated turn is finally obtained:

$$(V/g)\ d\gamma/dt + \cos\gamma = (L/W)\cos\phi' \qquad \text{(C-7c)}$$

The longitudinal (streamwise) force equation (C-6a) can be written

$$(1/g)\ (dV/dt) + \sin\gamma = (T - D)/W \qquad \text{(C-7d)}$$

It should be noted that the streamwise force equation (C-7d) holds in general, but the lift equation (C-7c) is restricted to coordinated flight.

By comparing equation (C-7c) with equation (B-2b) (app. B), and comparing equation (C-7d) with equation (B-2a) (app. B), it can be seen that, for wings-level flight (that is, $\phi' = 0$), the generalized equations reduce to those obtained previously by elementary methods. (As noted in appendix B, for flight in still air the inertial velocity and inertial flightpath angle coincide with their airmass counterparts.)

KINEMATIC EQUATIONS FOR COORDINATED TURNING FLIGHT

Although equation (C-7c) is exact, it involves the roll angle ϕ' taken about the velocity vector (fig. C-l(c)). This definition of the roll angle differs from the conventional one, which takes the roll rotation about the longitudinal fuselage axis (that is, the X axis of the body frame). It will be shown that, in coordinated (symmetric) flight, the direction of the fuselage axis differs from that of the velocity vector by the angle of attack α. Therefore, for small angles of attack, it is immediately obvious that the lift equation (C-7c) holds approximately if the roll angle ϕ' taken about the velocity vector is replaced by the conventionally defined bank angle ϕ taken about the fuselage axis. The region of validity of this approximation can be determined by finding the exact relation between the two roll angles ϕ' and ϕ. This problem is considered next.

Eulerian Angles for Body Frame

The first task is to specify the spatial orientation of the body frame, which can be achieved by defining the Eulerian aircraft heading angle ψ, the pitch angle θ, and the bank angle ϕ (fig. C-2). It can be seen that the aircraft heading angle ψ specifies the azimuth direction relative to north of the projection of the fuselage axis X onto the horizontal plane (fig. C-2), while the track angle ψ_T defined previously specifies the direction of the horizontal projection of the aircraft velocity vector (fig. C-1).

Starting from the Earth frame N E D as before, the frame X'' Y'' Z'' is generated by positive rotation about the D axis through the heading angle ψ (fig. C-2(a)). It can be seen that the Z'' axis coincides with the D axis. Next, the frame X' Y' Z' is generated by positive rotation about the Y'' axis through

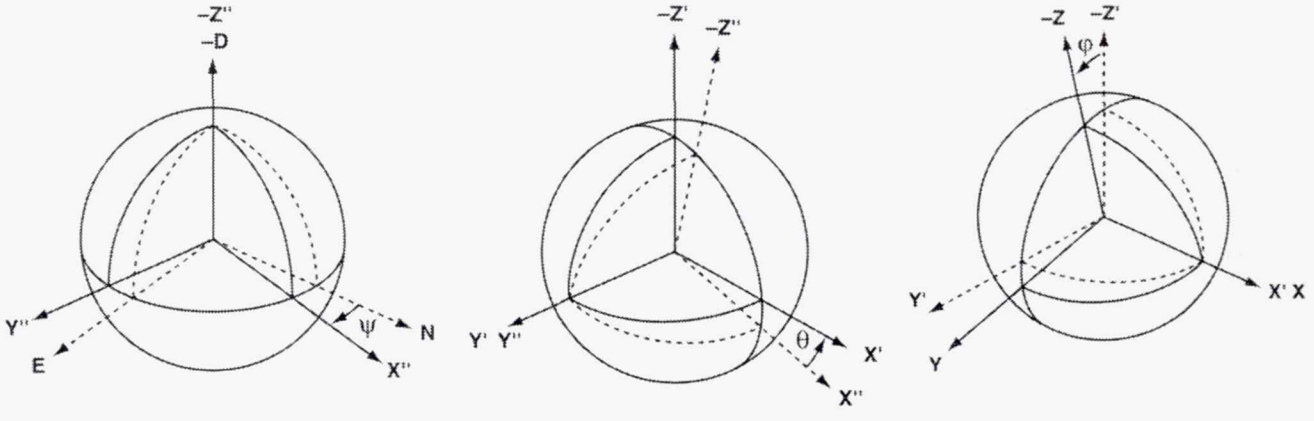

a) Definition of heading angle ψ. b) Definition of pitch angle θ. c) Definition of bank angle ϕ.

Figure C-2. Spatial orientation of body frame.

the pitch angle θ (fig. C-2(b)). It can be seen that the Y′ axis coincides with the Y″ axis. Finally, the body frame X Y Z is generated by positive rotation about the X′ axis through the roll angle ϕ (the conventionally defined bank angle). It can be seen that the fuselage axis X coincides with the X′ axis. To summarize, the body frame is related to the Earth frame by the Eulerian angles ψ, θ, and ϕ (fig. C-2), and the path frame is related to the Earth frame by the angles ψ_T, γ, and ϕ' (fig. C-1).

The path frame is related to the body frame by the angle of attack α and the angle of sideslip β (fig. C-3(a)). It can be seen from figure C-3(a) that the body-axis velocity components u, v, w are related to the total velocity V by the equations

$$\begin{aligned} u &= V \cos\beta \cos\alpha \\ v &= V \sin\beta \\ w &= V \cos\beta \sin\alpha \end{aligned} \tag{C-8}$$

In coordinated flight, the sideslip angle β vanishes together with the side force Y because of the assumed aerodynamic and propulsive bilateral symmetry (app. B), so that the velocity vector lies in the body-frame plane of symmetry X Z (fig. C-3(a)). It can be seen that, in the plane of symmetry, the projection of the velocity vector intersects the fuselage axis in the angle of attack α, as stated previously.

Kinematic Relationships

The relationship of the body frame to the path frame in coordinated flight is illustrated by figure C-3(b), which depicts the surface of the sphere of unit radius whose origin lies at the aircraft center of gravity. The North direction N intersects the spherical surface at point D, the gravitational vertical –D intersects it at point A, the aircraft velocity vector T intersects it at point B, and the fuselage axis X intersects it at point C. The horizontal plane cuts the sphere in arc DE. The vertical plane containing the velocity vector T cuts the sphere in arc ABD, and that containing the fuselage axis cuts it in arc ACE. The two vertical planes are orthogonal to the horizontal plane, so that the angles ADE and AED are right angles. The aircraft plane of symmetry contains both its fuselage

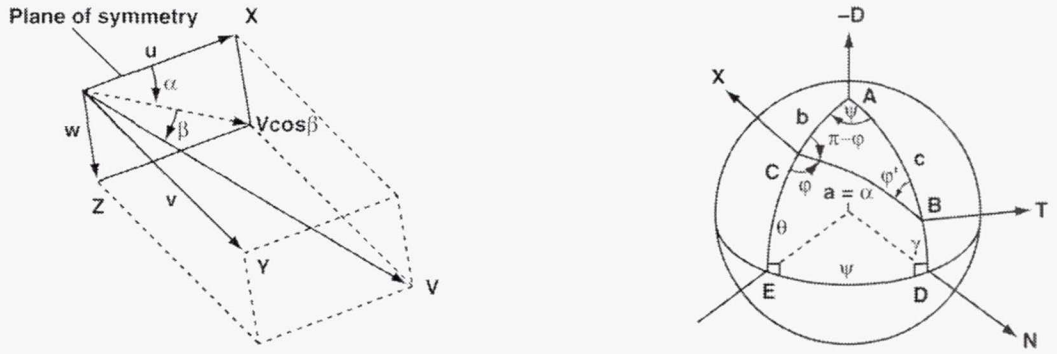

a) Definition of angle of attack α and angle of sideslip β.

b) Relation of body frame to path frame in symmetric (coordinated) flight.

Figure C-3. Orientation of body frame to path frame.

axis X and its velocity vector T, and cuts the sphere in the arc BC, which by definition (fig. C-3(a)) measures the angle of attack α. Since all these planes contain the origin, their intersecting arcs are therefore great-circle arcs. In figure C-3(b), the direction of the aircraft track is north, so that $\psi_T = 0$. Its heading angle ψ coincides with the angle CAD, and is measured by the arc DE. Its pitch angle θ is measured by the arc CE, and its flightpath angle γ by the arc BD. The roll angle ϕ' about the velocity vector T and the bank angle ϕ about the fuselage axis X are illustrated by figure C-3(b). The pilot, of course, observes these relationships from inside the sphere.

Instead of multiplying out the direction-cosine matrices as done previously in deriving equation (C-6), the desired relation between the roll angle ϕ' and the bank angle ϕ will be obtained in a simpler way by making use of spherical trigonometry. In the spherical triangle ABC, the angles A, B, and C and the opposite sides a, b, and c can be identified as follows (fig. C-3(b)):

$$\begin{aligned} A &= \psi \qquad B = \phi' \qquad C = \pi - \phi \\ a &= \alpha \qquad b = \pi/2 - \theta \qquad c = \pi/2 - \gamma \end{aligned} \tag{C-9}$$

The law of sines gives immediately the relations

$$\sin A/\sin a = \sin B/\sin b = \sin C/\sin c \tag{C-9a}$$

After substituting the identities (C-9), the second equality (C-9a) becomes

$$\sin \phi'/\sin (\pi/2 - \theta) = \sin (\pi - \phi)/\sin (\pi/2 - \gamma)$$

which reduces to

$$\sin \phi'/\cos \theta = \sin \phi/\cos \gamma$$

or, finally,

$$\sin \phi' = (\cos \theta/\cos \gamma) \sin \phi \tag{C-9b}$$

Equation (C-9b) is exact, and holds for coordinated flight without restriction to first-quadrant angles. It gives the desired relationship between the two roll angles ϕ' and ϕ for coordinated flight.

Another exact relationship between θ, γ, α, and ϕ can be obtained from the law of cosines for side c of the spherical triangle ABC:

$$\cos c = \cos a \cos b + \sin a \sin b \cos C \tag{C-9c}$$

Upon substituting the identities (C-9) into equation (C-9c), it is found that

$$\sin \gamma = \sin \theta \cos \alpha - \cos \theta \sin \alpha \cos \phi \tag{C-9d}$$

The kinematic equation (C-9d) is exact, and holds for coordinated flight without restriction to first-quadrant angles.

For wings-level flight ($\phi = 0$), equation (C-9d) reduces to

$$\sin \gamma = \sin \theta \cos \alpha - \cos \theta \sin \alpha = \sin (\theta - \alpha)$$

or

$$\gamma = \theta - \alpha \tag{C-9e}$$

in agreement with the elementary definitions of these angles (app. B).

Kinematic Approximations

If the angles α, γ, and θ are small, then equation (C-9d) can be simplified to obtain the approximate relation

$$\theta - \gamma = \alpha \cos \phi \tag{C-9f}$$

Equation (C-9f) is useful for the inverse control system described in the main report, where it enables the pitch command to be computed conveniently in closed form. It will be shown in the next two sections that the approximation (C-9f) remains valid even under the most extreme flight conditions encountered during controlled flight of transport aircraft.

If the difference $\theta - \gamma$ is small, then it is clear from equation (C-9b) that, for roll angles in the first quadrant, ϕ' can be approximated by ϕ:

$$\phi = \phi' \tag{C-9g}$$

Substitution of the approximation (C-9g) into the lift equation (C-7c) eliminates dependence of the equations of motion for coordinated turning flight on the roll angle ϕ' taken about the velocity vector, which is not measured by conventional onboard instrumentation.

Alternatively, if the pitch angle θ, the flightpath angle γ, and the bank angle ϕ are known from in-flight measurements or simulation computations, then the roll angle ϕ' can be found from the exact equation (C-9b). Use of the exact roll angle in the lift equation (C-7c) could improve the accuracy of the lift command calculation for the inverse control system described in volume one of this report. It will be shown in the next two sections that use of the approximation (C-9g) is justified for coordinated flight over the range of bank angles extending from 0 to about 40 deg, which includes the range normally encountered in airline service. At larger bank angles, its use in the lift equation could result in significant lift error.

Limiting Flight Conditions for Transport Aircraft

In order to test the validity of the approximations (C-9e) and (C-9g) with the largest practical values of α, γ, θ, and ϕ, a minimum-radius climbing turn that is representative of a collision-avoidance maneuver is calculated as an example using the generic transport aircraft model developed in appendix B. It will be shown that this maneuver results in flight conditions that reach both structural and aerodynamic limits for transport aircraft.

The aircraft load factor (denoted by n) is defined by the expression n = L/W. For a steady climbing turn, the flightpath rate $d\gamma/dt$ vanishes, and the load factor is found from equation (C-7c) to be

$$n = L / W = \cos \gamma / \cos \phi' \qquad \text{(C-10)}$$

It is assumed that the design limit load factor n_{MAX} is 2.5 g, as is usual for transport aircraft (Shevell, 1989).

For a level turn ($\gamma = 0$), equation (C-l0) shows that the maximum roll angle ϕ' is then given by $\cos \phi' = 1/n_{MAX} = 1/2.5$, or $\phi' = 66.4$ deg. Since the turn radius R is equal to the quotient $V/d\psi_T/dt$, it is given by (eq. (C-7b))

$$R = V^2/g \tan \phi'$$

Since $n^2 = 1/\cos^2 \phi' = 1 + \tan^2 \phi'$, so that $\tan^2 \phi' = n^2 - 1$, eliminating the roll angle ϕ' results in the expression

$$R = V^2 / g \sqrt{(n^2 - 1)}$$

It is clear that the turn radius R is minimized by choosing the maximum load factor and the minimum airspeed, which corresponds to the maximum lift coefficient (app. B), and results in flight near the stalling angle of attack. It is assumed that the corresponding fuselage angle of attack is 15 deg.

For a steady climbing turn, since the velocity component in the horizontal plane is $V \cos \gamma$ (fig. C-3(b)), the aircraft follows a helical path whose radius is given by

$$R_{HELIX} = (V \cos \gamma)^2 / g \sqrt{(n^2 - 1)}$$

The radius of the helix is minimized by climbing as steeply as possible (maximum γ), which requires maximum thrust. It is assumed that the aircraft is at light weight, and the thrust loading near sea level is taken as a maximum value of T/W = 0.5.

For a steady climbing turn, the flightpath acceleration dV/dt vanishes, and the streamwise force equation (C-7d) becomes

$$\sin \gamma = T/W - D/W = T/W\ (D/L)\ (L/W) = T/W - n/(L/D) \qquad \text{(C-10a)}$$

At the maximum lift coefficient of 1.3 (app. B), the lift/drag ratio for the generic transport model using parameter values from table B-1 (app. B) is found to be 12.36. With T/W = 0.5 and $n_{MAX} = 2.5$, the climb flightpath angle is found from equation (C-l0a) to be $\gamma_{MAX} = 17.33$ deg, and the maximum roll angle is found from equation (C-10) to be $\phi' = 67.55$ deg.

If the pitch angle θ were known, the corresponding bank angle ϕ could be found from equation (C-9b). Conversely, if the bank angle were known, the pitch angle could be found numerically from equation (C-9d). By using an iterative procedure involving both these equations, the solution $\theta = 22.46$ deg, $\phi = 72.69$ deg is found numerically for $\gamma = 17.33$ deg and $\alpha = 15$ deg, which can be verified by direct substitution in equations (C-9b) and (C-9d). These exact values can now be compared with those obtained from the approximate equations (C-9f) and (C-9g).

Approximation Validity

For $\phi' = 67.55$ deg, the approximate value of ϕ obtained from equation (C-9g) is also 67.55 deg. The exact value of ϕ is 72.69 deg, so that the roll error is 67.55 – 72.69 = –5.14 deg. For the values $\gamma = 17.33$ deg, $\alpha = 15$ deg, and $\phi = 67.55$ deg, the approximate value of θ obtained from equation (C-9f) is 23.05 deg. The exact value of θ is 22.46 deg, so that the θ error is +0.59 deg. If the approximate value for ϕ of 67.55 deg is replaced by the exact value of 72.69 deg, the value of θ obtained from equation (C-9f) is then 21.79 deg, so that the θ error becomes –0.67 deg.

These θ errors seem rather insignificant, especially after considering the extreme severity of the assumed flight conditions, and they would be even smaller for operating conditions normally encountered in airline service. Therefore, the kinematic approximation (C-9f) can be considered valid over the whole range of conditions encountered by transport aircraft during coordinated flight. On the other hand, the error in the lift equation (C-7c) resulting from use of the kinematic approximation (C-9g) for roll angle is more significant.

For the minimum-radius climbing turn, if the exact value for the roll angle ϕ' of 67.55 deg is replaced by the exact value for the bank angle ϕ of 72.69 deg, the load factor obtained from equation (C-l0) is 3.21 g. Since the exact value of the load factor is 2.50 g, the normal acceleration error is 0.71 g, an overestimate which amounts to 28% of the lift.

However, if the load factor is limited to 1.1 g (perhaps by proximity to stall), which corresponds to a less extreme bank angle of 39.3 deg in the climbing turn, the normal acceleration error is reduced to 0.078 g, an overestimate of 7.1% of the lift. Furthermore, the lift error decreases rapidly with further decrease of bank angle. Therefore, the approximation (C-9g) can be considered valid for bank angles smaller than about 40 deg; that is, for the range of bank angles normally encountered in airline service.

REFERENCES

Etkin, B.: Dynamics of Flight: Stability and Control. John Wiley (New York), 1959.

McRuer, D.; Ashkenas, I.; and Graham, D.: Aircraft Dynamics and Automatic Control. Princeton University Press (New Jersey), 1973.

Shevell, Richard S.: Fundamentals of Flight, 2nd ed. Prentice Hall (New Jersey), 1989.

Wills, A. P.: Vector Analysis with an Introduction to Tensor Analysis. Dover Publications, Inc. (New York), 1958.

APPENDIX D
ELEMENTS OF PROPOSITIONAL LOGIC

This appendix presents a concise review of elementary propositional logic that is needed to support developments in Volume I of this report. Formal logic is a classical discipline; Greek propositional logic was recast by Boole (Boole, 1854) into algebraic form. The two forms are logically equivalent. Both forms are treated in this appendix, because they illuminate the subject material from different perspectives. However, the logical form is used in the main report.

After a brief review of logical operations and truth tables, several elementary theorems are proved by the method of perfect induction, and a list of theorems is provided for reference. Logical simplification of composite propositions is illustrated by deriving several results needed for the main report, and the appendix concludes with a discussion of condition-action decision tables, which must be characterized by logical consistency and completeness.

ELEMENTARY LOGICAL PROPOSITIONS

Elementary logical propositions are simple declarative statements like "The grass is green" or "It is raining." Logically, it is taken as axiomatic that such elementary statements must be either true or false. In the logical form termed *symbolic logic*, elementary propositions are represented by letter symbols like p and q; in the algebraic form, they are represented by algebraic variables (termed Boolean variables) like X and Y, which are restricted to take on only the binary values zero or one. In Boolean algebra, the symbol 0 represents FALSE, and the symbol 1 represents TRUE.

Truth Tables

Elementary propositions can be combined to form compound statements like "It is raining, *and* the grass is green." Such a compound proposition is itself a single logical entity that must be either true or false, which is termed its *truth value*. The truth value of a compound statement depends on the truth or falsity (abbreviated as T and F) of the elementary propositions from which it is formed; it can be determined by construction of a *truth table* as follows:

TRUTH TABLE FOR CONJUNCTION

p	q	p AND q
F	F	F
F	T	F
T	F	F
T	T	T

The first row of this truth table shows that if both p and q are false, then the compound statement p AND q (which is termed their *conjunction*) is false. The second and third rows show that if p is false and q true, or if p is true and q is false, then in both cases p AND q is false. The fourth row shows that if both p and q are true, then p AND q is true.

In algebraic form, the same truth table has quite a different appearance. Denoting the operation of logical conjunction by the symbol x, the truth table becomes

TRUTH TABLE FOR CONJUNCTION

p	q	p x q
0	0	0
0	1	0
1	0	0
1	1	1

It is obvious from inspection of this table that, from an algebraic viewpoint, the operation of logical conjunction can be regarded as *logical multiplication* acting on the Boolean variables 0 and 1, with its multiplication table defined as follows:

TRUTH TABLE FOR CONJUNCTION

0 x 0 = 0
0 x 1 = 0
1 x 0 = 0
1 x 1 = 1

Proceeding in the same way, the truth value of the compound statement p OR g, which is termed the *logical disjunction* of p and q, can be regarded as *logical addition* (denoted by the symbol +), with truth tables defined as follows:

TRUTH TABLES FOR DISJUNCTION

p	q	p OR q	
F	F	F	0 + 0 = 0
F	T	T	0 + 1 = 1
T	F	T	1 + 0 = 0
T	T	T	1 + 1 = 1

It can be seen from the fourth row of the addition table on the right that logical addition does not follow the same rule as ordinary algebraic addition. Nevertheless, Boolean algebra forms a mathematically consistent system.

Logical Operations

At this point of the discussion, the notions just presented can be generalized to include the other commonly used ways of combining elementary propositions to form compound propositions, which are *negation*, *implication*, and *equivalence*; in Boolean algebra, negation is termed *complementation*, equivalence becomes equality, and implication is not defined. The complete set of operations is therefore conjunction, disjunction, negation, implication, and equivalence; with the exception of negation, these are termed *logical connectives*, since they connect elementary propositions to form compound propositions.

Each of these operations is defined by a truth table similar to those already presented for conjunction and disjunction. The truth tables for negation (denoted by the symbol $\neg$), implication (denoted by the symbol $\Rightarrow$), and equivalence (denoted by the symbol $\equiv$) are as follows:

TRUTH TABLES FOR NEGATION

p	$\neg$p
F	T
T	F

$\neg 0 = 1$
$\neg 1 = 0$

TRUTH TABLE FOR IMPLICATION

p	q	p $\Rightarrow$ q
F	F	T
F	T	T
T	F	F
T	T	T

It should be noted that the first and second rows of the truth table for implication express the rule that "anything follows from a false antecedent," the third and fourth rows agree with the notion of implication in the everyday use of natural language, and also with the mathematical statement "if p, then q."

TRUTH TABLE FOR EQUIVALENCE

p	q	p $\equiv$ q
F	F	T
F	T	F
T	F	F
T	T	T

Equivalence can be regarded as reversible implication: if p implies q and q implies p, then p and q are equivalent.

Elementary Logical Theorems

Consider the compound logical proposition p OR TRUE. Since it has the same form as the proposition p OR q where q is equivalent to TRUE, its truth value can be found by forming the truth table for p OR TRUE, and evaluating the result by referring to the truth table for disjunction:

TRUTH TABLES FOR p OR TRUE

p	T	p OR T	
F	T	T	0 + 1 = 1
F	T	T	0 + 1 = 1
T	T	T	1 + 1 = 1
T	T	T	1 + 1 = 1

The coincidence of the second and third columns shows that p OR TRUE is equivalent to TRUE. (The second and fourth rows are redundant, and can be dropped.) In symbols,

$$p \text{ OR } T \equiv T \qquad p + 1 = 1 \tag{A}$$

Statement (A) is a *theorem* in symbolic logic, which we have proved by the method of *perfect induction* (that is, by comparison of truth table columns—two propositions are logically equivalent if and only if their truth table columns coincide).

By proceeding in a similar manner, we can prove that p AND TRUE is equivalent to p. The truth table is as follows:

TRUTH TABLES FOR p AND TRUE

p	T	p AND T	
F	T	F	0 x 1 = 0
T	T	T	1 x 1 = 1

The third column is obtained by referring to the truth table for conjunction. The coincidence of the first and third columns proves the second theorem:

$$p \text{ AND } T \equiv p \qquad p \times 1 = p \tag{B}$$

Statement (B) is also a theorem in symbolic logic.

As a third example, the truth table for the proposition p OR $\neg$p is as follows:

TRUTH TABLES FOR p OR ¬p

p	¬p	p OR ¬p	
F	T	T	0 + 1 = 1
T	F	T	1 + 0 = 1

The second column is obtained from the first by referring to the truth table for negation, and the third column is obtained from the first two by referring to the truth table for disjunction. The third column shows that the proposition p OR ¬p always holds, without regard to the truth value of p. In symbols,

$$p \text{ OR } \neg p \equiv T \qquad p + \neg p \equiv 1 \tag{C}$$

Statement (C) is another theorem in symbolic logic. (Theorem (C) is the well-known *law of the excluded middle*; all these theorems were known to the Greeks.)

The proposition p OR ¬p is one example of a *tautology*, which is defined as a compound proposition that holds because of its form, independent of the truth values of its component elementary propositions. The proposition p OR TRUE is another example, as shown by Theorem (A).

Other theorems involving more complicated combinations of elementary propositions can also be proved by the method of perfect induction, which is demonstrated next.

COMPOSITE LOGICAL PROPOSITIONS

Since each compound expression is itself a logical proposition, as already noted, it follows that compound propositions can be combined by means of logical connectives to form more complicated propositions; indeed, an elementary proposition is sometimes defined as one that does not contain any connectives. To avoid ambiguity, composite propositions formed by combining three or more elementary propositions must include parentheses to indicate the sequence in which evaluation is to be carried out, just as in ordinary algebra. The commutative, associative, and distributive laws hold axiomatically, just as in ordinary algebra.

For example, consider the composite proposition p OR (p AND q). The parentheses show that the conjunction p AND q is to be evaluated first, by means of the truth table for conjunction. Let the result be denoted by r, so that the equivalence r ≡ (p AND q) holds. The disjunction p OR r is then to be evaluated by means of the truth table for disjunction.

The truth table for the composite proposition p OR (p AND q) is constructed as follows. The first three columns of the combined table are the same as those for the truth table for conjunction, with r replacing p AND q:

TRUTH TABLE FOR p OR (p AND q)

p	q	r	p	p OR r
F	F	F	F	F
F	T	F	F	F
T	F	F	T	T
T	T	T	T	T

To form the disjunction p OR r, the fourth column is added to the table by repeating the first column, and the last column is obtained by evaluating each row of the third and fourth columns according to the truth table for disjunction. It will be seen that the last column coincides with the first; therefore, the truth table proves that the composite proposition p OR (p AND q) is equivalent to p. In symbols,

$$\mathbf{p \text{ OR } (p \text{ AND } q) \equiv p} \qquad \mathbf{p + (p \times q) = p} \qquad \textbf{(D)}$$

Statement (D) is another theorem in symbolic logic.

Theorem (D) can be verified algebraically as follows. Apply the distributive law to factor out p on the left-hand side:

$$\mathbf{p \times (1 + q) = p}$$

Now simplify the parenthesis by applying Theorem (A) to obtain

$$\mathbf{p \times (1) = p,}$$

and simplify the left-hand side by applying Theorem (B) to obtain

$$\mathbf{p = p,}$$

which verifies Theorem (D).

ELEMENTARY THEOREMS IN SYMBOLIC LOGIC

As this example (Theorem (D)) shows, proof of a new theorem is often facilitated by using other theorems already established, instead of proceeding from first principles by the method of perfect induction. Nevertheless, truth tables are regarded as the "gold standard" for logical proof. By combining the two proof methods, other elementary theorems can be established (Dromey, 1989; Bartee, 1985). A reference list of 23 such theorems, which follows the format of Dromey, can be found in the List of Theorems.

LOGICAL SIMPLIFICATION OF COMPOSITE PROPOSITIONS

The process of simplifying composite logical propositions by application of elementary theorems is illustrated by deriving several results needed for the main report.

Simplification of Definition for PE (V)

The partial effectiveness of the V Command mode is defined as follows (Volume I (Effectiveness Requirements)):

$$PE\ (V) \equiv \text{NOT}\ [P\ \text{AND}\ (\gamma_{POT\ TGT} \neq \gamma_{POT\ MAX})]\ \text{AND NOT}\ [Q\ \text{AND}\ (\gamma_{POT\ TGT} \neq \gamma_{POT\ MIN})]$$

Expressing negation symbolically, this of the form

$$PE\ (V) \equiv \neg[P\ \text{AND}\ M]\ \text{AND}\ \neg[Q\ \text{AND}\ N]$$

where M and N are given by the equivalences

$$M \equiv (\gamma_{POT\ TGT} \neq \gamma_{POT\ MAX}) \qquad N \equiv (\gamma_{POT\ TGT} \neq \gamma_{POT\ MIN})]$$

Simplification of PE (V) is needed for the following three cases:

(a) $(\gamma_{POT\ TGT} = \gamma_{POT\ MAX})$ holds;

(b) $(\gamma_{POT\ TGT} = \gamma_{POT\ MIN})$ holds; and

(c) $(\gamma_{POT\ MIN} < \gamma_{POT\ TGT} < \gamma_{POT\ MAX})$ holds.

In case (a), M is false and N is true, so that PE (V) becomes

$$PE\ (V) \equiv \neg[P\ \text{AND}\ F]\ \text{AND}\ \neg[Q\ \text{AND}\ T]$$

By applying Theorem 13, the first bracketed proposition reduces to F, and the second reduces to Q. Removing the brackets by taking negations results in PE (V) = T AND $\neg$Q, which simplifies to $\neg$Q by a second application of Theorem 13. Expressing case (a) in the form of an implication gives

(a) $(\gamma_{POT\ TGT} = \gamma_{POT\ MAX}) \Rightarrow (PE\ (V) \equiv \neg Q)$

In case (b), M is true and N is false, so that PE (V) becomes

$$PE\ (V) \equiv \neg[P\ \text{AND}\ T]\ \text{AND}\ \neg[Q\ \text{AND}\ F]$$

By applying Theorem 13, the first bracketed proposition reduces to P, and the second reduces to F. Removing the brackets by taking negations results in PE (V) $\equiv \neg$P AND T, which simplifies to $\neg$P by a second application of Theorem 13. Expressing case (b) in the form of an implication gives

(b) $(\gamma_{POT\ TGT} = \gamma_{POT\ MIN}) \Rightarrow (PE\ (V) \equiv \neg P)$

In case (c), both M and N are true, so that PE (V) becomes

$$PE\ (V) \equiv \neg[P\ \text{AND}\ T]\ \text{AND}\ \neg[Q\ \text{AND}\ T]$$

By applying Theorem 13, the first bracketed proposition reduces to P, and the second reduces to Q. Removing the brackets by taking negations results in PE (V) ≡ ¬P AND ¬Q. Expressing case (c) in the form of an implication gives

(c) $(\gamma_{POT\ MIN} < \gamma_{POT\ TGT} < \gamma_{POT\ MAX}) \Rightarrow [PE\ (V) \equiv (\neg P\ \text{AND}\ \neg Q)]$

Collecting results, the required simplification of PE (V) is

(a) $(\gamma_{POT\ TGT} = \gamma_{POT\ MAX}) \Rightarrow (PE\ (V) \equiv \neg Q)$

(b) $(\gamma_{POT\ TGT} = \gamma_{POT\ MIN}) \Rightarrow (PE\ (V) \equiv \neg P)$

(c) $(\gamma_{POT\ MIN} < \gamma_{POT\ TGT} < \gamma_{POT\ MAX}) \Rightarrow [PE\ (V) \equiv (\neg P\ \text{AND}\ \neg Q)]$

This completes the first example.

Simplification of Definition for PE (γ)

The partial effectiveness of the γ Command mode is defined as follows (Volume I (Effectiveness Requirements)):

$$PE\ (\gamma) \equiv (\gamma_{TGT} < \gamma_{POT\ MAX})\ \text{OR}\ [(\gamma_{TGT} \geq \gamma_{POT\ MAX})\ \text{AND}\ (V > V_{MIN\ DRAG})]$$

This is of the form

$$PE\ (\gamma) \equiv M\ \text{OR}\ [\neg M\ \text{AND}\ N]$$

where M and N are given by the equivalences

$$M \equiv (\gamma_{TGT} < \gamma_{POT\ MAX}) \qquad N \equiv (V > V_{MIN\ DRAG})$$

By applying the distributive law given by the first statement of Theorem 9, PE (γ) becomes

$$PE\ (\gamma) \equiv (M\ \text{OR}\ \neg M)\ \text{AND}\ (M\ \text{OR}\ N)$$

Because the first bracketed expression is tautologically true (Theorem 4), PE (γ) becomes

$$PE\ (\gamma) \equiv T\ \text{AND}\ (M\ \text{OR}\ N)$$

Applying Theorem 13 reduces this to PE (γ) ≡ (M OR N), and replacing M and N with their equivalent expressions gives the final result:

$$PE\ (\gamma) \equiv (\gamma_{TGT} < \gamma_{POT\ MAX})\ \text{OR}\ (V > V_{MIN\ DRAG}).$$

This result could also have been obtained directly by application of Theorem (D).

CONDITION-ACTION DECISION TABLES

Another logical tool needed for the main report is used to specify actions to be taken by an automated system if and only if certain logical conditions hold. Such actions can be specified in compact form by tables that are termed *condition-action decision tables.* This section describes the arrangement and interpretation of such tables, including conventions for the solid or broken lines that separate the elements of the table and form an essential part of the specification (Sherry, Youssefi, and Hynes, 1995). There are two kinds of decision tables, a simple table that specifies condition-action pairs, and a more complex table that also specifies mode selection. The simple table is treated first.

Simple Condition-Action Tables

A simple condition-action decision table has the following form:

TABLE D-1

Condition	p	q	r
Action	1	2	3

It can be seen that the upper row of table D-1 specifies logical conditions p, q, and r, and the lower row specifies actions 1, 2, and 3. Each column of the table specifies a condition-action pair; the first column specifies the pair (p, 1), the second column specifies the pair (q, 2), and the third column specifies the pair (r, 3). Other columns could be added as desired.

Table D-1 is interpreted as follows. If condition p holds, then the first column shows that action 1 is to be taken; the other columns are interpreted in the same way. Condition p could represent any logical proposition, either simple or compound, and action 1 could represent any action or set of actions that are to be specified.

To avoid ambiguity, it is essential that the conditions be mutually exclusive, so that whatever the truth values of the conditions p, q, and r may be, in any particular situation one and only one action is specified. This property is termed *logical consistency.* If logical consistency does not hold, the table is said to be logically inconsistent. For example, if p and q could both hold, logical consistency would be violated; in that case, more than one action would be specified, so that the specification would fail to be unique.

A second essential property of table D-1 is that disjunction of the conditions (that is, the compound proposition (p OR q OR r)) must be tautologically true, whatever the truth values of p, q, and r. This property is termed *logical completeness.* If logical completeness does not hold, the table is said to be logically incomplete; in that case, other logical conditions or combinations of conditions could exist for which no action is specified.

Mode Selection Tables

For the automated system described in Volume I of this report, a mode is defined as a characteristic set of actions that the system can take; that is, a physical behavior (Volume I (Flight Control System)). Therefore, decision tables involving mode selection must specify the three-way relationship between the logical conditions that govern mode selection, the modes available for selection, and the set of actions associated with each mode. Such tables have the form illustrated by the following example:

TABLE D-2

Mode	**Mode A**	**Mode B**	**Mode C**	
Scenario			**Normal**	**Abnormal**
Condition				
m	T			
¬m		T	T	
n		T		
¬n	T			
p	T			T
q	T	T		
r			T	
Action	Action 1	Action 2	Action 3	

It can be seen that the upper row of table D-2 specifies three modes A, B, and C. The second row specifies an entity termed a scenario, which is explained later and should be ignored for the present. The legend Condition in the left column identifies seven logical conditions m, ¬m, n, ¬n, p, q, and r, which are arranged in the next seven rows below the Condition legend. The significance of the broken horizontal lines in table D-2 will be explained shortly; for the present, all the horizontal lines should be regarded as solid. The lowest row of table D-2 specifies three actions 1, 2, and 3. Other columns could be added to the table as desired.

In each column, the entries in the body of table D-2 show the logical conditions that must hold for selection of the mode corresponding to that column, and also the action that is to be taken when that mode is selected. For example, in the first column the conditions required to hold for selection of mode A are indicated by the various entries of the symbol T, which denotes TRUE; it can be seen that conditions m, ¬n, p, and q are required to hold for selection of mode A. If mode A is selected, the lowest row of the left column shows that action 1 is to be taken. The entries in the other columns are interpreted in the same way. Blank spaces in each column of the table indicate conditions whose truth values are not relevant for mode selection in that column.

The two columns on the right both correspond to mode C, which is to be selected if the conditions in the third column (the normal scenario) hold, or alternatively, if the conditions in the fourth column (the abnormal scenario) hold. In both cases, action 3 is to be taken; each action is uniquely associated with its corresponding mode, without regard to the scenario (column) by which mode selection is determined.

Line codes– It can be seen that the rows of table D-2 are separated by horizontal lines of two kinds, either solid or broken. The interpretation of this line code is as follows. Broken horizontal lines indicate disjunction of the conditions in the rows they separate, while solid lines indicate conjunction. For example, in the column for mode A, it may be seen that the T entries in the rows for conditions p and q are separated by a broken horizontal line. This shows that the disjunction (p OR q) is required for selection of mode A. The solid lines separating the T entries in the m row, the $\neg$n row, and the p row show that the conjunction of m and $\neg$n with the compound condition (p OR q) is required for selection of mode A. That is, the compound condition that must hold for selection of mode A as specified by table D-2 can be stated in implication form as follows:

$$[\text{m AND } \neg\text{n AND (p OR q)}] \Rightarrow \text{(Selection of mode A)}$$

The compound conditions in the columns for mode B and mode C are specified by the line code in the same way.

Logical consistency and completeness– For logical completeness, the logical disjunction of the conditions in rows separated by broken lines must hold tautologically. For example, because the rows for conditions p, q, and r are separated by broken lines (table D-2), their logical disjunction (p OR q OR r) must hold tautologically; otherwise, table D-2 would be logically incomplete.

Logical completeness requires careful attention to the definition of logical conditions that depend on physical variables. For example, suppose that p represents the condition ($X \leq U$), q represents the condition ($U < X < V$), and r represents the condition ($X \geq V$), where X is a continuous physical variable and U and V are constants. The requirement for logical completeness is satisfied by these definitions, because physical continuity ensures that no value for X exists for which none of the three conditions p, q, or r holds. On the other hand, if p were defined as the condition ($X < U$) instead of ($X \leq U$), then logical completeness would be violated, because if X took the value ($X = U$), none of the three conditions would hold. In this example, a parsimonious use of symbols could be achieved by using the logical simplification $q \equiv \neg p\, \neg r$ to eliminate q. The conditions appearing in table D-2 would then be p, $\neg p\, \neg r$, and r; their disjunction can be seen by inspection to hold tautologically. It is clear that the line code in table D-2 facilitates checking the table for logical completeness.

Logical consistency is a more delicate matter. For logical consistency, the selection logic for each column must be mutually exclusive; that is, the pattern of T entries must be different in each column. If any two columns had the same pattern, then either or both of the corresponding modes could be selected, depending on the exact details of the implementation code. Therefore mode selection would fail to be mutually exclusive (unique) as required. For large decision tables with many columns, checking logical consistency by inspection can become quite tedious, but the task can be automated by means of utility programs developed for that purpose.

Hierarchical decision tables– For a large automated system like that described in the main report, it is often convenient to combine several decision tables into a hierarchical relationship. This can be achieved without changing the structure already described for table D-2 by specifying additional actions, such as "Enter Table E." Table E could then contain an action "Enter Table F" and so on. The hierarchical structure can be built up recursively in this way to whatever extent is desired.

REFERENCES

Bartee, Thomas C.: Digital Computer Fundamentals, 6th edition, McGraw-Hill (New York), 1985.

Boole, George: An Investigation of the Laws of Thought, on Which are Founded the Mathematical Theories of Logic and Probabilities. Macmillan (London), 1854; reprint, Dover Publications (New York), 1958.

Dromey, R. G.: Program Derivation, Addison-Wesley (Menlo Park, Calif.), 1989.

Sherry, Lance; Youssefi, David; and Hynes, Charles S.: A Formalism for the Specification of Operationally Embedded Reactive Avionic Systems. Honeywell Publication C69-5370-001, Honeywell Air Transport System Division (System Engineering Technology), Phoenix, Ariz., 1995.

LIST OF THEOREMS (after Dromey)

Symbols

Conjunction	x	Disjunction	+	Negation	¬
Equivalence	≡	Implication	⇒		

Theorems

(1)	$p \equiv p$	Law of identity
(2)	$p + p \equiv p$ $p \times p \equiv p$	Idempotent laws
(3)	$\neg(\neg p) \equiv p$	Law of double negation
(4)	$p + \neg p \equiv T$	Law of the excluded middle
(5)	$\neg(p \times \neg p) \equiv T$	Law of contradiction (also used as $p \times \neg p \equiv F$)
(6)	$(p \Rightarrow \neg p) \equiv \neg p$	*Reductio ad absurdum*
(7)	$p + q \equiv q + p$ $p \times q \equiv q \times p$ $(p \equiv q) \equiv (q \equiv p)$	Commutative laws
(8)	$(p + q) + r \equiv p + (q + r)$ $(p \times q) \times r \equiv p \times (q \times r)$	Associative laws
(9)	$p + (q \times r) \equiv (p + q) \times (p + r)$ $p \times (q + r) \equiv (p \times q) + (p \times r)$	Distributive laws
(10)	$(p \Rightarrow q) \times (q \Rightarrow r) \Rightarrow (p \Rightarrow r)$ $(p \equiv q) \times (q \equiv r) \Rightarrow (p \equiv r)$	Transitive laws
(11)	$\neg(p + q) \equiv \neg p \times \neg q$ $\neg(p \times q) \equiv \neg p + \neg q$ $\neg(p \Rightarrow q) \equiv p \times \neg q$ $\neg(p \equiv q) \equiv (p \equiv \neg q)$	De Morgan's laws

(12)	$p + T \equiv T$ $p + p \equiv p$ $p + (p \times q) \equiv p$	OR simplification (note: $p + F \equiv p$ $T + T \equiv T$ $T + F \equiv T$)
(13)	$p \times T \equiv p$ $p \times p \equiv p$ $p \times (p + q) \equiv p$	AND simplification (note: $p \times F \equiv F$ $T \times F \equiv F$ $T \times T \equiv T$)
(14)	$(p \Rightarrow q) \times (q \Rightarrow r) \equiv (p \Rightarrow q \times r)$ $(p \Rightarrow r) \times (q \Rightarrow r) \equiv (p + q \Rightarrow r)$ $(p \Rightarrow q) + (p \Rightarrow r) \equiv (p \Rightarrow q + r)$ $(p \Rightarrow r) + (q \Rightarrow r) \equiv (p \times q \Rightarrow r)$	Implication simiplification
(15)	$(p \Rightarrow q) \equiv (\neg q \Rightarrow \neg p)$ $(p \equiv q) \equiv (\neg p \equiv \neg q)$	Contraposition
(16)	$p \Rightarrow p + q$ $(p \Rightarrow q) \Rightarrow (p \Rightarrow q + r)$ $(p \Rightarrow q) \Rightarrow (p \times r \Rightarrow q)$ $(p \Rightarrow q) \Rightarrow (p \Rightarrow (p \times q))$	Law of addition Law of absorption
(17)	$p \times q \Rightarrow p$	Law of simplification
(18)	$(p \times q \Rightarrow r) \Rightarrow (p \Rightarrow (q \Rightarrow r))$ $(p + q \Rightarrow r) \Rightarrow (p \Rightarrow r)$	Law of exportation
(19)	$(p \Rightarrow (q \Rightarrow r)) \Rightarrow (p \times q \Rightarrow r)$ $(p \Rightarrow (q \times r)) \Rightarrow (p \Rightarrow q)$	Law of importation
(20)	$(p \Rightarrow (q \times \neg q)) \Rightarrow \neg p$	Law of absurdity
(21)	$p \times (p \Rightarrow q) \Rightarrow q$	Law of detachment
(22)	$\neg q \times (p \Rightarrow q) \Rightarrow \neg p$	
(23)	$\neg p \times (p + q) \Rightarrow q$	

APPENDIX E
STATECHART SEMANTICS

Statecharts provide a graphical representation of discrete logical systems, which are termed state machines. In this report, statecharts represent the discrete elements of hybrid systems such as flight control systems. The continuous elements of these hybrid systems are represented by block diagrams containing input/output transfer functions, such as those illustrated by figure 11 in Volume I. This appendix summarizes statechart interpretation conventions (termed semantics), which enable statechart diagrams to serve as rigorous specifications for the operation of discrete state machines.

Such state machines could be implemented directly in hardware by means of relays, or in concurrent (parallel) digital computers. However, for reasons that will become clear in the discussion to follow, within the aircraft industry it is considered desirable to implement both the discrete and continuous elements of hybrid systems within a single clock-based sequential processor. Several changes to conventional statechart semantics are needed to facilitate implementation within a single sequential machine. These issues are discussed in detail, and suitable semantic modifications proposed. It is shown by a simplified example that these modifications enable implementation code for a sequential machine to be prepared directly from statechart diagrams.

In particular, it is required by conventional statechart semantics that changes in the logical conditions governing mode transitions be propagated instantaneously throughout the system. This convention, termed broadcast synchronization, can be violated in a sequential machine. Such violations are analyzed in detail, and their implications for formal validation are assessed; it is shown that, under certain conditions, unacceptable delay in the identification of safety-critical failures could result from an improperly chosen sequence of computation.

CONVENTIONAL STATECHART SEMANTICS

State Transition Diagrams

A state transition diagram for a simple state machine is illustrated by figure E-1. In figure E-1, the three circles represent states designated A, B, and C, and the arrows represent transitions between states. For example, these states could be identified with the modes of a flight control system. Each transition is governed by a condition indicated on the diagram by legends labeling each transition arrow. For example, condition 1 must hold for the transition from state A to state B to occur, condition 2 must hold for the transition from state B to state C to occur, condition 3 must hold for the transition from state C to state A to occur, and condition 4 must hold for the transition from state A to state C to occur. The unlabeled arrow pointing to state A indicates that the system is to be initialized in state A before operation commences. The rectangles in the diagram represent actions that must be taken at the time a transition occurs; for example, action (a) must be executed whenever the system transitions from state A to state B.

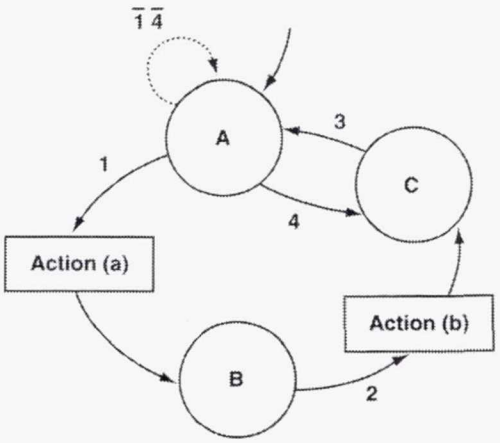

Figure E-1. State transition diagram.

For the deterministic state machines considered in this report, logical consistency requires that operation be specified uniquely, so that state transitions must be mutually exclusive. For example, in state A, condition 1 and condition 4 must not both hold at the same time; otherwise, machine operation is nondeterministic. Logical completeness requires that operation be specified for all possible combinations of the conditions governing transitions; otherwise, a combination of conditions could be presented for which operation of the machine would be undefined.

Null transitions can be represented explicitly if desired. For example, if the system is in state A and conditions 1 and 4 are both false, the system remains in state A, as indicated by the broken arrow. For logical completeness, the broken arrow must be labeled by the concatenation of the negations of each condition that would cause transition out of state A, as shown on the diagram. Explicit representation of null transitions enables verification of logical completeness. However, such arrows clutter the diagram, and the concatenation of all transitions out of state A can become logically complex in large systems. Alternatively, null transitions can be suppressed to simplify the diagram after logical completeness has been verified by some other means.

It is clear that state transitions depend only on the current state and the current conditions, and not on the past history of the state evolution, so that the process is Markovian. It is assumed that changes in the logical conditions are propagated instantaneously throughout the system, a convention termed broadcast synchronization.

Hierarchical Statecharts

An elaboration of conventional state transition diagrams that provides a more natural representation of aircraft systems and possesses several other advantages (Harel, 1987) is illustrated by figure E-2. In figure E-2, two state machines have been combined to form a higher-level entity termed a supermode in the diagram, with system hierarchy indicated by enclosing the two lower-level machines within an outer boundary. Thus figure E-2 is to be regarded as the projection of a three-dimensional structure onto the two-dimensional plane. In figure E-2, the states are represented by rectangles with rounded comers instead of circles as in figure E-1. Concurrent (parallel) operation of the two lower-level machines is indicated by the broken vertical line in the diagram, which shows

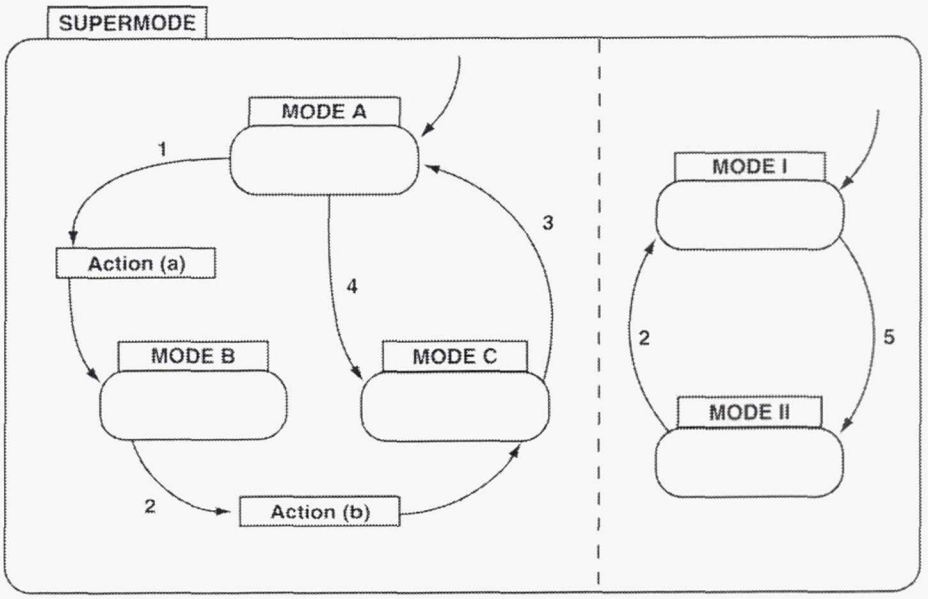

Figure E-2. Hierarchical statechart.

that the supermode consists of the Cartesian product of the two lower-level systems. It should be noted that, in the diagram, condition 2 governs transitions in both lower-level machines.

To express the operation of the system of figure E-2 as a conventional state transition diagram like Figure E-l, six states are required to form the Cartesian product, since the machine on the left of figure E-2 has three states, and the machine on the right has two. Thus representation of the combined system in the hierarchical form of figure E-2 has saved one state. This economy should not be regarded as trivial. If each of the lower-level machines contained 100 states, 10,000 states would be required to represent the system as a conventional "flat" state transition diagram, while representation in the three-dimensional hierarchical form would require only 200 states. Corresponding economies are also realized in the effort required to analyze the operation of such complex systems, which increases rapidly with the number of states involved.

Furthermore, if each of the lower-level machines represents an aircraft subsystem (such as a hydraulic system and an electrical system), the hierarchical representation enables designers to deal with them in a natural way, avoiding the need to form their Cartesian product. Finally, in preparing system documentation for use by groups representing different design disciplines, the hierarchical representation enables low-level detail to be suppressed to whatever extent is considered desirable, since the internal details of figure E-2 could be omitted without destroying the usefulness of the diagram at still higher levels.

It should be noted that hierarchical decision tables can serve as an alternative method for specifying state machine operation that is logically equivalent to statecharts (Sherry, Youssefi, and Hynes, 1995). The statecharts discussed in this report could be translated into such decision tables, for which automatic generation of implementation code is available (King et al., 1994).

Aircraft Implementation

Several fundamental issues discussed later can be clarified by considering some simple physical models. In principle, the continuous elements of the hybrid control system could be implemented in analog hardware, and their discrete elements implemented by relays controlled directly by analog signals, as they were in aircraft autopilots designed before the mid-1970s. Alternatively, the state machine illustrated by figure E-l could be implemented within a parallel computer, with three processors synchronized by the exchange of interrupts.

In current aircraft, the continuous elements are implemented by digital computation using short clock-based time steps. A real-time operating system representative of current aircraft is illustrated in statechart form by figure E-3. It can be seen that when power is applied, the system first initializes computer memory and then enters the operating mode. In the operating mode, the processor continuously executes various background tasks not requiring precise timing, until it is interrupted by the clock. The clock interrupt transfers execution to foreground tasks, such as flight control, that require precise timing.

In figure E-4, a state machine for flight control mode selection is shown embedded in this flight computer system as one of many foreground tasks, together with other tasks that implement the continuous system elements that are controlled by mode selection. Since there is only a single processor, the various foreground tasks must be executed sequentially instead of concurrently. In figure E-4, the broken vertical lines now represent sequential operation, with time increasing to the right, in contrast to the concurrent operation represented by the broken vertical line in figure E-2. All foreground tasks must be completed before the next clock interrupt starts foreground execution again. Whatever time remains after foreground execution is complete is applied to the background task, which resumes at the point at which it was previously interrupted.

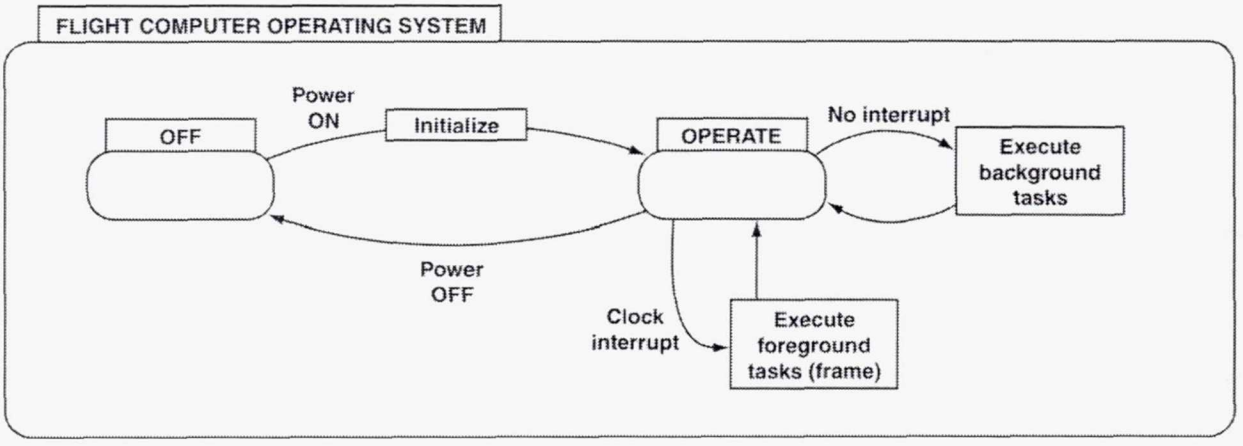

Figure E-3. Real-time operating system.

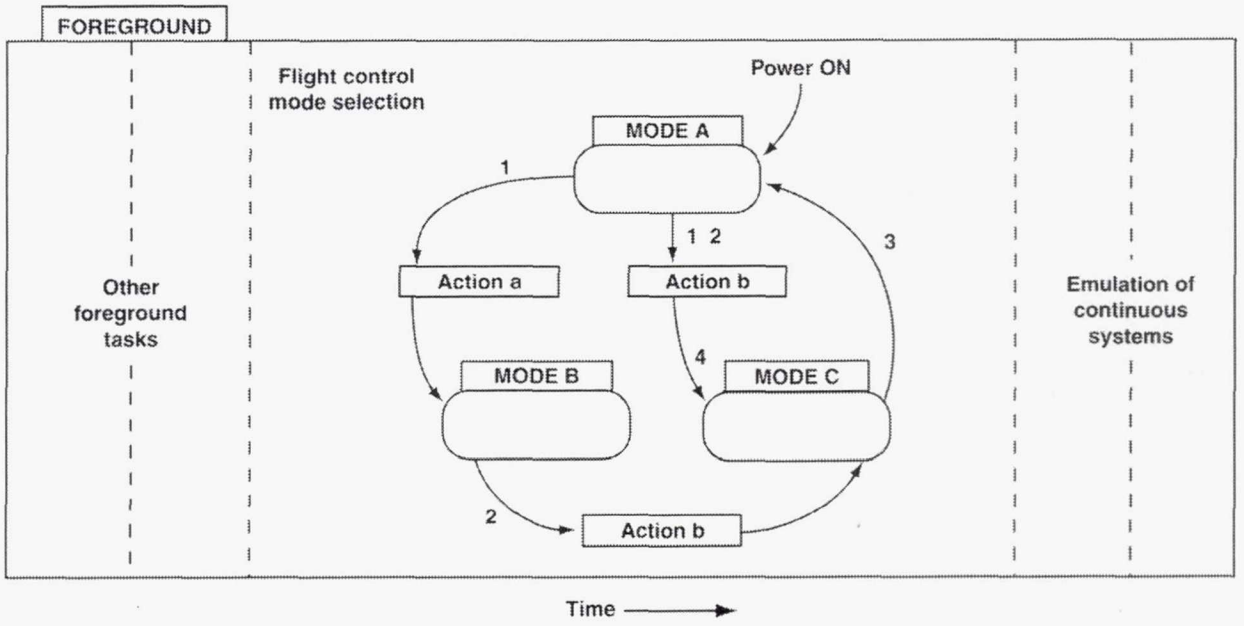

Figure E-4. Flight control mode selection example.

Because sequential computation can only approximate concurrent processing instead of implementing it exactly, it is clear that implementation in a sequential, clock-based machine instead of a concurrent, interrupt-driven machine may require some modifications to conventional statechart semantics. These modifications are discussed in detail in the next section. The discussion begins by considering emulation of the continuous system elements.

MODIFICATIONS FOR SEQUENTIAL PROCESSING

Emulation of Continuous System Elements

Continuous functions of time are approximated in digital computation by discrete staircase functions that coincide with the continuous function only at the instant of update (fig. E-5). The duration of these time steps must be short relative to the time scale of the continuous process being approximated, in order to achieve sufficient computational accuracy and avoid numerical instability. In current aircraft, the duration of each time step, which is termed the computation frame, ranges from 10 milliseconds in high-performance aircraft to 50 milliseconds in older transports.

In the emulation of a continuous dynamical process, the computations should be carried out in a well-defined sequence that is determined by functional dependency. For example, state estimates such as altitude should be updated before they are used as inputs to the control laws. Otherwise, excess delay is introduced by out-of-sequence computations that degrades both dynamic accuracy and closed-loop stability. Because the requirement that the calculations be carried out in correct sequence severely restricts the possibilities for parallel computation, the discrete emulation of a continuous dynamical process can be regarded as inherently clock-based and sequential.

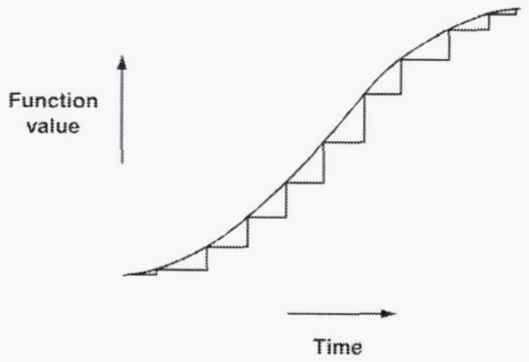

Figure E-5. Discrete emulation of continuous function.

Emulation of Discrete System Elements

The question can now be raised: how should the emulation of the concurrent, interrupt-driven system represented by conventional statecharts be related to the sequential, clock-based emulation of the underlying continuous process that is being controlled by mode selection? Since mode transitions are initiated by changes in the conditions, which are evaluated continuously in conventional statechart semantics, it is logical to ask first how these conditions should be discretized.

Within each computation frame, the natural time reference is the instant at the beginning of the frame, which is the time at which the emulation of the continuous system is most accurate. It follows that the conditions should be updated to the beginning of each frame before they are used in the emulation of the state machine to determine mode transitions. This policy emulates the broadcast synchronization convention at the instant of update.

Definition of Time Step

In the concurrent system illustrated by figure E-6(a), suppose that the system is in state A, and that condition 1 is FALSE and condition 2 is TRUE. The system remains in state A. If now some external stimulus makes condition 1 TRUE, the system transitions first to state B and then to state C (fig. E-6(a)). Generalizing, it is clear that, in a complex system, a single external stimulus can produce a flurry of transitions before a new steady state is reached. Observation of such equilibrium states has been proposed as the basis for definition of a time step in concurrent systems (Harel, 1987; Leveson et al., 1992).

It is difficult to emulate this process within a sequential processor in real time. To illustrate the difficulty, consider a naive attempt to emulate the state machine of figure E-6(a) by embedding the following pseudocode within the foreground tasks of figure E-4.

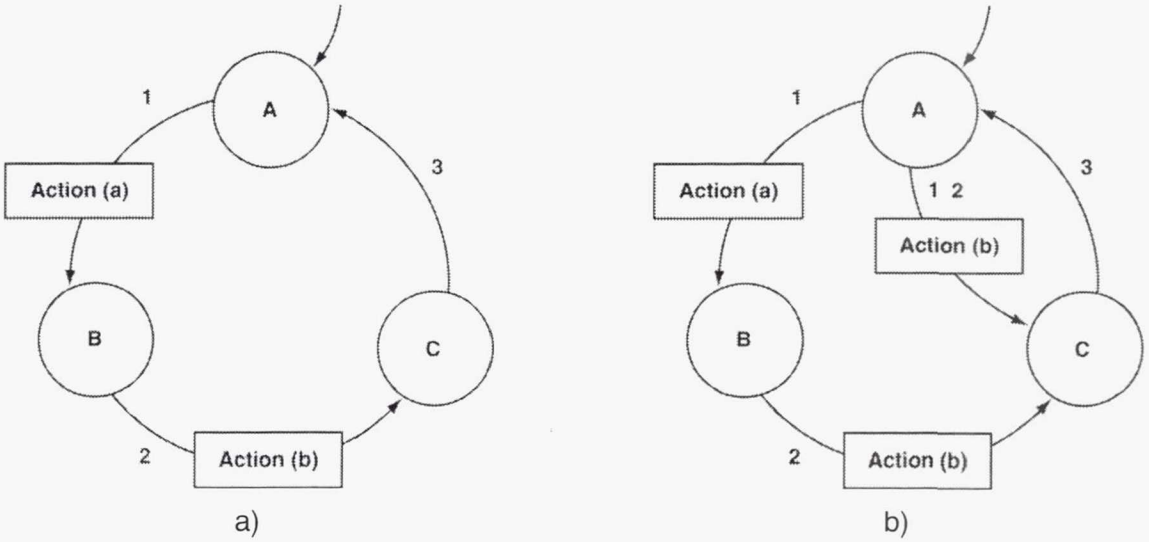

Figure E-6. Modification of state machine for sequential implementation.

```
IF (State A) THEN
        IF (Condition 1) THEN
                Transition to State B
        ELSE
                Remain in State A
        END IF

ELSE IF (State B) THEN
        IF (Condition 2) THEN
                Transition to State C
        ELSE
        Remain in State B
        END IF

ELSE IF (State C) THEN
        IF (Condition 3) THEN
                Transition to State A
        ELSE
                Remain in State C
        END IF

END IF
```

According to the IF...ELSE IF syntax, whenever a TRUE condition is found the processor executes a single mode transition and then skips to the following END IF. Furthermore, the entire routine is executed only once during each frame (figs. E-3 and E-4). Therefore, it is clear that this pseudocode allows only one mode transition per time step. If the system is initially in state A and condition 1 and condition 2 both hold, the machine specified by this pseudocode transitions to state B and remains there during the first time step (frame). At the next time step, the system transitions to state C. Thus

the semantics of the pseudocode differ from those of the conventional statechart (fig. E-6(a)), for which the transition from state A to state C would be instantaneous.

This difference is not trivial. For example, suppose that the falsity of condition 2 is required for validity of the mode corresponding to state B, and that the truth of condition 2 represents a sensor failure that requires the system to transition to state C. If the underlying continuous system emulated in state B involves state estimation by recursive filtering, a single frame of computation in the mode corresponding to state B with an invalid input could fatally corrupt the recursive estimates.

Possibly the pseudocode implementation could be modified so as to match the statechart semantics by executing the pseudocode repeatedly until a steady state is observed. However, such iteration is undesirable in real-time code because it contributes an unknown variation in execution time. Furthermore, if external stimuli continue to be presented, causing changes in the conditions governing transition, the system may never reach a well-defined, observable equilibrium state.

Alternatively, the statechart semantics can be modified to incorporate a convention that allows only a single mode transition per frame. This definition of time step for the state machine seems to be the natural one for a clock-based sequential system. The function of the original statechart can be restored by adding a transition path directly from state A to state C that is traversed if both condition 1 and condition 2 hold (fig. E-6(b)). The pseudocode for the modified system is then as follows.

```
IF (State A) THEN
        IF (Condition 1) THEN
                Transition to State B
        ELSE IF (Condition 1 and Condition 2) THEN          ! Modification
                Transition to State C
        ELSE
                Remain in State A
        END IF

ELSE IF (State B) THEN
        IF (Condition 2) THEN
                Transition to State C
        ELSE
                Remain in State B
        END IF

ELSE IF (State C) THEN
        IF (Condition 3) THEN
                Transition to State A
        ELSE
                Remain in State C
        END IF

END IF
```

This modification method can be generalized. Provided that the desired function of the state machine can be specified by adding appropriate transition paths to the conventional statechart while retaining the modified semantic convention that allows only a single mode transition per frame, then implementation of the modified state machine within a sequential processor is straightforward. If null transitions are represented explicitly on the diagram, the modified statechart has the appealing interpretation that, at the beginning of each frame ("tick of the clock"), the system is required to execute one and only one of the state transitions indicated explicitly on the statechart by the transition arrows.

Violation of Broadcast Synchronization Convention

In emulation of statecharts within a sequential processor, another problem can be encountered that involves violation of the broadcast synchronization convention. As mentioned previously, this convention requires that all changes to the conditions governing transition be propagated instantaneously throughout the system. For emulation, the logical conditions that govern transition should be updated to the beginning of the frame, as discussed previously. This updating process is straightforward for transition conditions that depend only on quantities external to the flight control system, such as sensor measurements and their associated Boolean valids (that is, auxiliary quantities that report the results of external sensor validity tests).

However, some transition conditions may depend on internally computed quantities like commanded flightpath angle and airspeed. These computed quantities are, in general, mode-dependent, and therefore cannot be updated until after the flight control modes have been selected for the current frame. Before update, these quantities are referred to the beginning of the previous frame, and so also are the transition conditions dependent upon them. It follows that propagation of these transition conditions is effectively delayed by one frame at the time of mode selection, violating the broadcast synchronization convention.

Implications for Formal Validation

In assessing the consequences of such violations, it seems useful to distinguish between cases for which not a single frame of delay in mode transition can be permitted, which is termed hard violation, and those in which one or more frames of delay can be tolerated, which is termed soft violation. For example, consider a sensor failure that requires an immediate mode reversion without a single frame of delay. If detection of this failure depended on testing computed, mode-dependent quantities, the mode reversion would occur one frame too late to avoid the execution of servo commands to the aircraft control surfaces that were dependent on the failed sensor, constituting a hard violation. Such a design should be considered unacceptable for flight safety.

Formal validation of systems subject to such failures lies outside the scope of this report. However, the dynamical process of mode evolution tends to proceed at a slower pace than the evolution of the underlying continuous states—typically, each mode transition is separated from the preceding one by several hundred frames. Therefore, most violations of the broadcast synchronization convention encountered in flight control systems are found to be soft. It is clear that formal validation of the flight control system by the methods developed in this report requires verification of the softness of each such violation.

A DETAILED IMPLEMENTATION EXAMPLE

With the modifications to conventional statechart semantics just developed, the statechart diagram forms a complete specification from which implementation code can be prepared. To illustrate this process, a simplified example is presented in this section, and the resulting pseudocode is compared with pseudocode generated by the well-established Jackson program design method (Jackson, 1975). It is shown that the two specification methods are equivalent for the example to be discussed.

Statechart Example

To illustrate the implementation procedure, it is assumed that the discrete mode control system illustrated by figures E-4 and E-6(b) is to be embedded in the clock-based sequential machine illustrated by figure E-3. The mode control task is to be accomplished by a subroutine (procedure) called from foreground, which selects the mode for the current frame and makes it available for use by the emulation of continuous system elements that follows mode selection (fig. E-4).

It can be seen that the system is to be initialized in MODE A when power is first applied (fig. E-4). Thereafter, transitions between the three states MODE A, MODE B, and MODE C are governed by conditions 1, 2, and 3. According to the modified semantic convention developed in the previous section, only one mode transition is allowed at each time step, and the statechart of figure E-4 has been modified accordingly, as previously discussed. It is assumed that conditions 1, 2, and 3 have been updated to the beginning of the frame by one of the other foreground tasks (fig. E-4) executed before mode control processing begins.

Since the system is to be initialized in MODE A on the first frame of operation, but not subsequently (fig. E-4), it is logical to set a flag (to be called the Init_DONE flag) to indicate that initialization should be skipped during all subsequent frames. It is assumed that the Init_DONE flag is initialized FALSE by the operating system when power to the flight computer is first applied (fig. E-3).

After initialization, the mode selection depends on conditions 1, 2, and 3 as well as upon the mode selected during the previous frame. A nested IF structure could test conditions first, or previous mode first, or alternatively a case structure could avoid nesting entirely by combining condition and previous mode into a single compound condition. The choice among these alternatives must be based on psychological criteria relating to ease of use by humans, since considerations of computational efficiency are trivial in this simple example.

For this example it has been decided to test first for previous mode, based on our opinion that this choice leads to pseudocode that is easier to understand than that resulting from either of the other choices. Making use of standard structural forms for sequence and for choice among mutually exclusive alternatives, the pseudocode is then as follows (table E-1). (The numbers in parentheses following each action to be performed relate to the Jackson program design example to be discussed next, and should be ignored for the present.)

TABLE E-1

Operating System Initialization

```
Set Init_DONE flag FALSE (1)
```

Subroutine Flight Control Mode Selection ! Called from Foreground

```
IF (not Init_DONE) THEN                          ! First frame
        Select MODE A (3)
        Set Init_DONE flag TRUE (2)
ELSE                                             ! All subsequent frames

        IF (MODE A) THEN                         ! Process MODE A

                IF (not Condition 1) THEN
                        Select MODE A (3)
                ELSE IF (Condition 1 and not Condition 2) THEN
                        Perform Action (a) (6)
                        Select MODE B (4)
                ELSE IF (Condition 1 and Condition 2) THEN
                        Perform Action (b) (7)
                        Select MODE C (5)
                END IF

        ELSE IF (MODE B) THEN                    ! Process MODE B

                IF (not Condition 2) THEN
                        Select MODE B (4)
                ELSE IF (Condition 2) THEN
                        Perform Action (b) (7)
                        Select MODE C (5)
                END IF

        ELSE IF (MODE C) THEN                    ! Process MODE C
                IF (not Condition 3) THEN
                        Select MODE C (5)
                ELSE IF (Condition 3) THEN
                        Select MODE A (3)
                END IF

        END IF

END IF

RETURN (8)
```

Jackson Program Design Example

The Jackson program design method (Jackson, 1975) begins with the preparation of a diagram representing the structure of the input and output data streams hierarchically (fig. E-7). In figure E-7, the vertical dimension indicates hierarchy, and the horizontal dimension indicates time sequence, with time increasing from left to right. An asterisk placed at the upper right within a block indicates iteration, while a small circle indicates one among several mutually exclusive alternatives.

Correspondences are then established between input and output data elements that occur in the same sequence (broken lines in figure E-7), and the corresponding data elements are combined to create a processing structure (fig. E-8). Specific operations (see Notes, figure E-8) necessary to achieve the required output are enumerated, and then added to the processing structure in the appropriate locations determined by the required sequence of operations (fig. E-8). Finally, pseudocode is prepared directly from the program structure chart (fig. E-8). The Jackson method results in a unique program structure that guarantees correct sequential operation. Readers unfamiliar with the Jackson method who desire a more detailed discussion can consult Michael Jackson's 1975 textbook (Jackson, 1975).

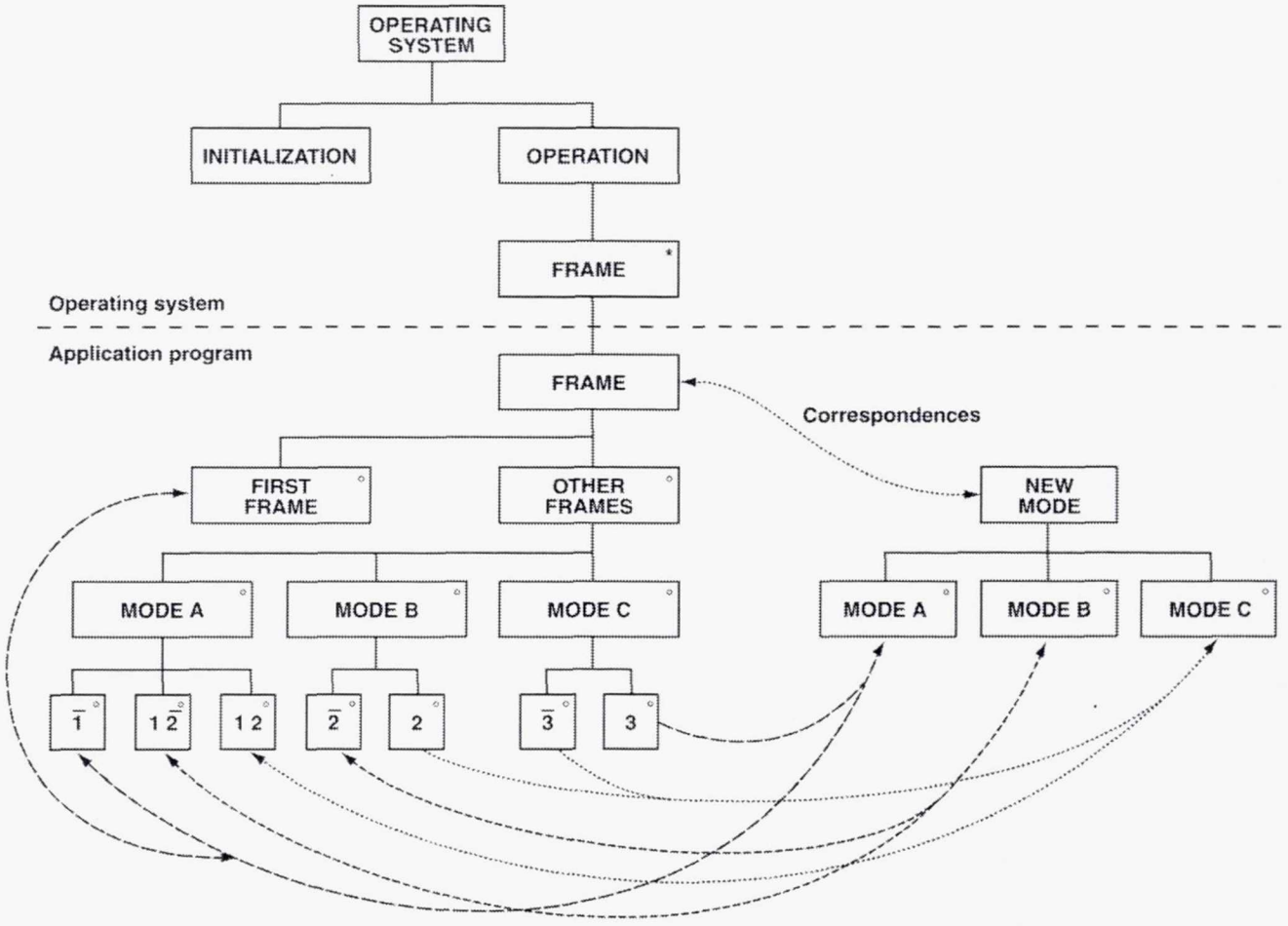

Figure E-7. Jackson Data Structure Chart for mode control example.

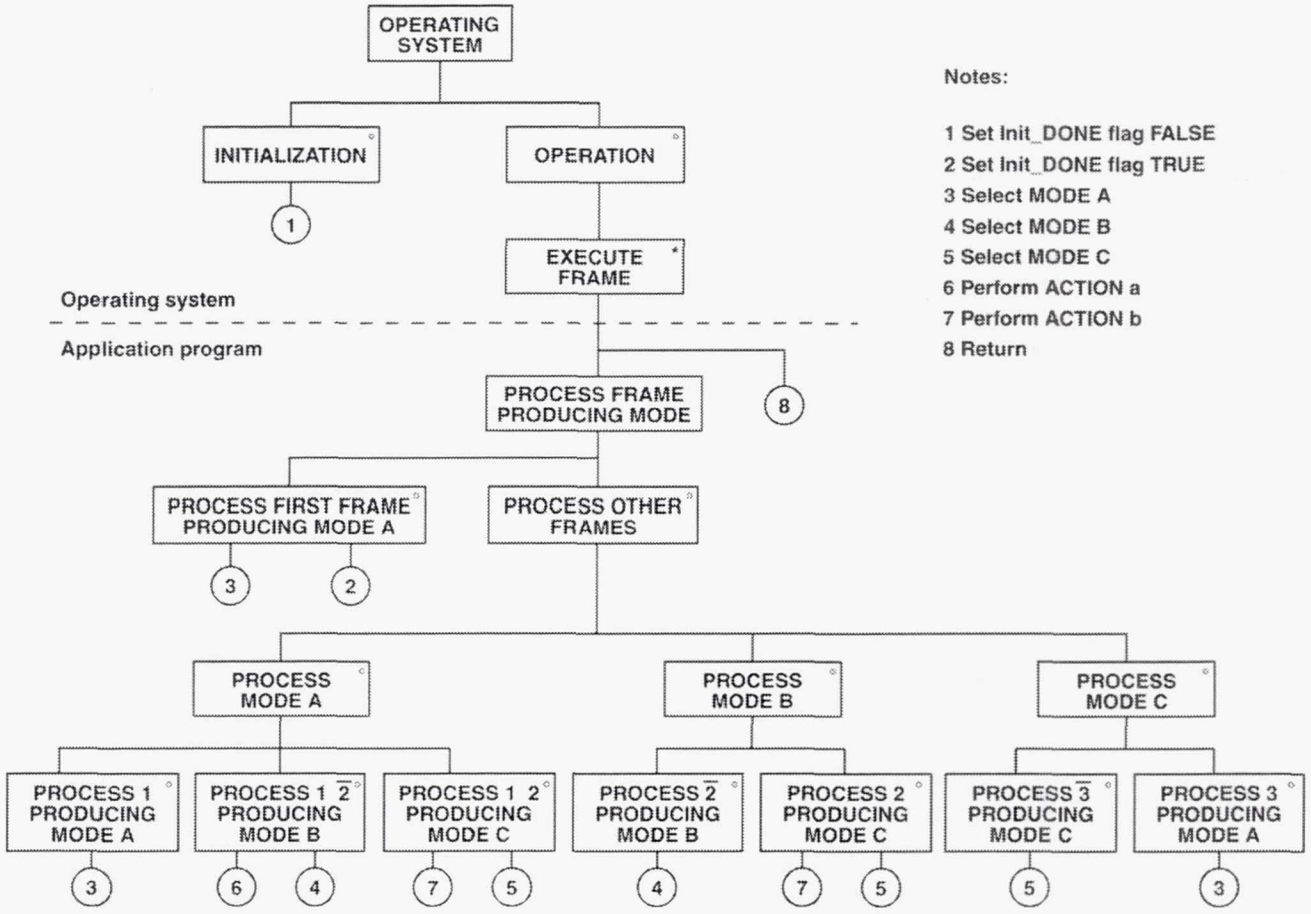

Figure E-8. Jackson Program Structure Chart for mode control example.

To prepare pseudocode from the program structure chart of figure E-8, the chart is read as follows. Starting at the top and working downward, each row is read from left to right. The first operation encountered is setting the Init_DONE flag FALSE, which must be taken care of by the operating system (compare Operating System Initialization, table E-1). Working downward and to the left into the application program (compare Subroutine Flight Control Mode Selection, table E-1), the second row consists of two mutually exclusive alternatives (note the small circles at the upper right in each block), of which the first is "Process the first frame producing MODE A." The two alternatives are distinguished by testing the Init_DONE flag. On the first frame, two operations must be carried out (see the two large circles below the first-frame block referring to Note 3 and Note 2). Reading from left to right, first the system must be initialized by selecting MODE A, and then the Init_DONE flag must be set TRUE, causing the initialization to be skipped on all subsequent frames. The pseudocode specified by the diagram of figure E-8 is as follows, from the top down to and including the second row of the application program. The numbers in parentheses following each action to be performed refer to the Notes on the Jackson chart (fig. E-8).

Operating System Initialization

Set Init_DONE flag FALSE (1)

Subroutine Flight Control Mode Selection ! Called from Foreground

```
    IF (not Init_DONE) THEN                    ! First frame
            Select MODE A (3)
            Set Init_DONE flag TRUE (2)

    ELSE                                       ! All subsequent frames
            Process other frames

    END IF

    RETURN
```

The processing required during subsequent frames is specified by the lower two rows of the application program structure chart. Continuing to work downward and to the left, the third row consists of three mutually exclusive alternatives, which are distinguished by testing the mode selected during the previous frame, beginning with MODE A. If MODE A was selected, the bottom row requires testing the conditions to distinguish among the three mutually exclusive alternatives shown. The block at the extreme left of the bottom row specifies that, if condition 1 is FALSE, then MODE A must be selected again for the current frame (Note 3). The next block to the right specifies that, if condition 1 is TRUE and condition 2 is FALSE, first action (a) must be performed (Note 6), and then MODE B selected (Note 4). The third block specifies that, if both condition 1 and condition 2 are TRUE, first action (b) must be performed (Note 7), and then MODE C selected (Note 5).

Since there are no other blocks to the right in the last row under the block "Process MODE A" in the third row, this completes the MODE A processing. Now moving up to the third row, it can be seen that the next block to the right specifies the processing for MODE B, and the last block specifies the processing for MODE C. At this point, the pseudocode is as shown in table E-2.

It will be seen that the mutually exclusive alternatives in the program structure chart are translated directly into the standard IF...ELSE IF structures in the pseudocode. This direct structural correspondence between chart and pseudocode, which is made possible by the use of standard structural forms, is fundamental to the Jackson method.

In table E-2, the stubs for processing MODE B and MODE C are completed in the same manner as that just explained for MODE A. The processing for MODE B and MODE C completes the processing for the third row (fig. E-8). Moving up to the second row, it can be seen that processing is now complete for the block "Process other frames" at the right of the second row, and also for the block "Process frame producing mode" in the first row. Moving to the right in the first row, the last operation is specified by Note 8, RETURN.

TABLE E-2

Operating System Initialization

```
Set Init_DONE flag FALSE (1)

Subroutine Flight Control Mode Selection          ! Called from Foreground

IF (not Init_DONE) THEN                           ! First frame
        Select MODE A (3)
        Set Init_DONE flag TRUE (2)

ELSE                                              ! All subsequent frames
        IF (MODE A) THEN                          ! Process MODE A

                IF (not Condition 1) THEN
                        Select MODE A (3)
                ELSE IF (Condition 1 and not Condition 2) THEN
                        Perform Action (a) (6)
                        Select MODE B (4)
                ELSE IF (Condition 1 and Condition 2) THEN
                        Perform Action (b) (7)
                        Select MODE C (5)
                END IF

        ELSE IF (MODE B) THEN                     ! Process MODE B
                Process MODE B

        ELSE IF (MODE C) THEN                     ! Process MODE C
                Process MODE C

        END IF

END IF

RETURN (8)
```

The program is now complete. The complete pseudocode (table E-2) is found to correspond exactly to that prepared directly from the modified statechart (table E-1), showing that, for this example, the method based on the proposed statechart modification is equivalent to the well-established Jackson program design method.

REFERENCES

Harel, David: Statecharts: A Visual Formalism for Complex Systems. Science of Computer Programming, vol. 8, no. 3, June 1987, pp. 231–274. See also Harel, D.; Pneuli, A.; Schmidt, J. P.; and Sherman, R.: On the Formal Semantics of Statecharts. In Proceedings of the 2nd IEEE Symposium on Logic in Computer Science, Ithaca, N.Y, June 22–24, 1987. IEEE Press (New York), pp. 54–64.

Jackson, M. A.: Principles of Program Design. Academic Press (London), 1975.

King, Tim; Krueger, Jon; Ward, Jon; Hughes, Banni; Michaels, Matt; and Sherry, Lance: Generating Software from a Hierarchy of Operational Procedure Tables. Honeywell Technical Report SST-R94-009, Honeywell Technology Center, Minneapolis, Minn., 1994.

Leveson, Nancy G.; Heimdahl, Mats P. E.; Hildreth, Holly; and Reese, Jon D.: Requirements Specification for Process-Control Systems. Technical Report 92-106, Information and Computer Science Dept., University of California, Irvine, Calif., 1992.

Sherry, Lance; Youssefi, David; and Hynes, Charles S.: A Formalism for the Specification of Operationally Embedded Reactive Avionic Systems. Honeywell Publication C69-5370-001, Honeywell Air Transport System Division (System Engineering Technology), Phoenix, Ariz., 1995.

APPENDIX F
THEOREMS ON SYSTEM BEHAVIORAL PROPERTIES

Volume I presents a new method for synthesizing hybrid systems from design requirements, and applies it to the design of a system for longitudinal control of transport aircraft. The resulting system satisfies general requirements for safety and effectiveness specified a priori. This appendix presents theorems that summarize the behavioral properties of the hybrid system (Volume I, (Synthesis of Altitude Command Supermode)), and provides methodology for generating formal proofs. These theorems enable theoretical assessment of system dynamical behavior and verification of system safety and effectiveness independent of the synthesis method. By this means, formal validation of the complete system can be achieved.

The discussion begins with some considerations of proof methodology, followed by the theorems themselves and their proofs. For clarity, an informal proof outline is presented immediately before each formal proof. A short discussion shows by example how a rather subtle design error committed during the synthesis process was revealed by attempted formal proof and subsequently corrected.

Finally, it is shown that currently available codes for automated hypothesis testing can provide the basis for a theorem-proving tool. By this means, any hypothesis could in principle be tested to determine whether it is a theorem of the formal system. In future system development making use of the synthesis methods described in this report, such hypothesis testing could play a role similar to that of simulation in today's development process, but unlike simulation it would lead to results that would be rigorous and logically complete.

PROOF METHODOLOGY

Objectives

Several of the theorems to be discussed describe system dynamical behavior, such as capture of altitude and airspeed targets, that is inherently time-dependent. The time required for capture of a new target depends on the initial conditions prevailing at mode engagement, and ranges from a few seconds for a small change of airspeed to more than 30 minutes required for the aircraft to climb and capture the cruising altitude following system engagement just after takeoff (appendix B). Therefore, any attempt to characterize such time variations precisely would lead to an extremely complicated analysis, with correspondingly complex theorems and formal proofs.

Fortunately, that effort is unnecessary. In our opinion, variations in the time required for target capture are unimportant for formal assessment of system behavior, for two reasons: first, the human flight crew will know roughly what variations to expect based on simulator training and flight experience; and second, this rough knowledge is adequate for supervision of the automated system, just as it is for supervision of a human crewmember during manual flight. What is essential for supervision

is assurance that the system cannot fail to capture a selected target without generating an appropriate warning. Therefore, the theorems to be discussed can be regarded as guarantees of system behavior offered to the flight crew by the system designers.

Approach

This viewpoint suggests a simplified approach to the formal description of system behavior. By ignoring time-dependent detail, the essential behavior can be stated formally by logical propositions of the form (A B C $\Rightarrow$ D), where A denotes selection of a primitive mode, B denotes selection of a valid target, C denotes satisfaction of a guarding condition, and D denotes capture of the selected target in the long term after some unspecified time has elapsed. For example, let A denote selection of the primitive γ-V Command mode described in Volume I, B denote selection of valid flightpath and airspeed targets, C denote absence of thrust saturation (table 3, Volume I), and D denote (eventual) capture of the selected flightpath and airspeed targets. The proposition (A B C $\Rightarrow$ D) then has the semantic interpretation that continuous engagement of the γ-V Command mode AND continuous selection of the (fixed) flightpath and airspeed targets AND continuous absence of thrust saturation IMPLY eventual capture (and hold) of the selected flightpath and airspeed targets.

It should be noted that the truth value of the proposition (A B C $\Rightarrow$ D) depends only on the stability properties of the flightpath and airspeed regulators, which are continuous elements of the hybrid system. Their stability properties characterize the closed-loop dynamical behavior of the aircraft with the γ-V Command mode engaged, as discussed in detail in Volume I. Regulator stability, which is governed by continuous differential equations, can be verified by well-known control-theoretic methods independent of the discrete mode selection logic. In this example, the mode selection logic determines the truth values of the conditions A, B, and C, but *not* the truth value of the implication (A B C $\Rightarrow$ D), which depends only on regulator stability.

It follows that, after independent verification, the proposition (A B C $\Rightarrow$ D) can be taken as an axiom of the formal system that describes the essential dynamical behavior of the γ-V Command mode. Other axioms similar in form can describe the essential dynamical behavior of the other primitive modes (that is, the γ Command mode and the V Command mode). Ordinary propositional logic (appendix D), which is inherently static in nature because it deals with propositions whose truth values are independent of time, can then be applied to these axioms (together with other system properties to be defined in the next section) in order to establish formally the dynamical behavior of the complete system.

Framework of Analysis

The mode structure of the complete system is organized hierarchically on three levels, as explained in detail in Volume I. On the first level, the three primitive modes (whose dynamical behavior is summarized by the axioms just discussed) are combined to form the lowest-level supermode, which is termed Path/Speed Command. The mode selection logic for the Path/Speed Command supermode determines which one of the three primitive modes is engaged at any time, and must provide an appropriate strategy for switching between them as flight conditions change. On the second level of the mode hierarchy, higher-level supermodes accept altitude and airspeed targets entered manually into the aircraft mode control panel by the flight crew, generate appropriate flightpath and airspeed

targets, and select the first-level Path/Speed Command supermode, which becomes an internal element of the higher-level supermode that invokes it. (The third level of the hierarchy, which is not treated in detail by this report, enables aircraft trajectories to be optimized to conserve time and fuel by appropriate automated selection of altitude and airspeed targets.) The dynamical evolution of all the modes in this hierarchy constitutes the system behavior that must be summarized by the theorems to be presented.

For analysis, this dynamical mode evolution is considered to be composed of piecewise-continuous segments, each of which is characterized by a set of modes and supermodes on different levels of the hierarchy that remain selected throughout the (unspecified) time duration of that segment. The segments are separated by well-defined mode transitions, which occur instantaneously in accordance with the convention of broadcast synchronization (appendix E).

At each mode transition, mode selection for the next segment depends only on (1) the set of modes, supermodes, and targets selected for the current segment, and on (2) currently prevailing flight conditions (specifically, flightpath angle, airspeed, and thrust). Mode selection is independent of the past history of mode selection previous to current selections, and of flight conditions previous to prevailing conditions (the Markovian property). The continuous variables representing prevailing flight conditions are discretized for mode selection by separating the flightpath-airspeed plane into 7 regions (termed geometric stability regions) with mathematically sharp boundaries. These boundaries correspond to minimum airspeed, maximum airspeed, minimum thrust, maximum thrust, and speed for minimum drag, which are estimated on board the aircraft based on real-time sensor measurements and on stored aircraft performance data. Detailed discussion of this mode selection logic can be found in Volume I.

The following discussion shows that the system behavior theorems to be presented can be established formally by applying propositional logic to this structural framework.

DEFINITIONS

Logical Symbols

Logical symbols are defined as follows (List of Symbols, Volume I):

Equivalence	$\equiv$	Negation	$\neg$	Implication	$\Rightarrow$
Logical OR	$\cup$	Logical AND will be omitted			

Elementary Theorems

A reference list of theorems in symbolic logic can be found in appendix D (Dromey, 1989; Bartee, 1985). For example, Theorem 17 is referenced as follows:

$$(17)\quad p\,q \Rightarrow p$$

Symbolic Logical Propositions

For reference, the following definitions are taken from Volume I:

$V1 \equiv (V \leq V_{MIN\ DRAG})$ $\quad$ $VT3 \equiv (V_{TGT} \leq V_{MIN\ DRAG})$

$V3 \equiv (V = V_{TGT})$ $\quad$ $V4 \equiv (V > V_{TGT})$

$G1 \equiv (\gamma = 0)$ $\quad$ $GT6 \equiv (\gamma_{TGT} \geq \gamma_{POT\ MAX})$

$P \equiv (\gamma_{TGT} \geq \gamma_{SPEED\ MAX})$ $\quad$ $Q \equiv (\gamma_{TGT} \leq \gamma_{SPEED\ MIN})$

$DC1 \equiv (\gamma_{POT\ MIN} < 0)$ $\quad$ $PF1 \equiv (\gamma_{POT\ MAX} = \gamma_{POT\ MIN})$

$TC1 \equiv (\gamma_{POT\ MAX} < 0)$ $\quad$ $TC2 \equiv (\gamma_{POT\ MAX} = 0)$

$TS1 \equiv (\gamma \leq \gamma_{SPEED\ MIN})$ $\quad$ $TS2 \equiv (\gamma \geq \gamma_{SPEED\ MAX})$

$TT1 \equiv (\gamma_{POT\ TGT} = \gamma_{POT\ MIN})$ $\quad$ $TT2 \equiv (\gamma_{POT\ TGT} = \gamma_{POT\ MAX})$

$\neg PE\ (\gamma) \equiv (GT6 \ \ V1 \ \ TS2)$ $\quad$ $\neg PE\ (V) \equiv (P \ \ TT1) \cup (Q \ \ TT2)$

$\neg PP \equiv (PRIORITY \equiv SPEED)$ $\quad$ $PP \equiv (PRIORITY \equiv PATH)$

Mode Selection Strategy

Denote mode selection by the following symbols:

AC ≡ Altitude Command supermode

CH ≡ Altitude Capture / Hold supermode $\quad$ CD ≡ Climb / Descend supermode

CM ≡ Climb supermode $\quad$ DM ≡ Descend supermode

PS ≡ Path / Speed Command supermode

VC ≡ V Command mode $\quad$ GC ≡ γ Command mode

Path/Speed Command Supermode Selection

The primitive mode selection logic for the Path/Speed Command supermode can be summarized as follows (table 7, Volume I):

$$PS \neg PP \Rightarrow VC \qquad PS\ PP \Rightarrow GC$$

Altitude Command Supermode Selection

The supermode selection logic for the Altitude Command supermode can be summarized as follows for the abnormal cases (table 12, Volume I):

$$AC \neg PE(\gamma) \Rightarrow CD \qquad AC\ PE(\gamma) \neg PE(V) \Rightarrow CH$$

The supermode selection logic for the Altitude Capture/Hold supermode and the Climb/Descend supermode within the Altitude Command supermode can be summarized as follows (table 10, Volume I). (Note that $(\Delta H < 0) \equiv (H > H_{TGT})$ and $(\Delta H \geq 0) \equiv (H \leq H_{TGT})$.)

$$CD\ (H > H_{TGT}) \Rightarrow DM \neg PP\ PS \qquad CD\ (H \leq H_{TGT}) \Rightarrow CM \neg PP\ PS$$

$$CH \Rightarrow PP\ PS$$

Combining the selection logic for the supermodes within the Altitude Command supermode with that for the Altitude Command supermode itself results in the following combined selection logic:

$$AC \neg PE(\gamma) \Rightarrow CD \neg PP\ PS \qquad AC\ PE(\gamma) \neg PE(V) \Rightarrow CH\ PP\ PS$$

Drag Condition

The following property holds for all transport aircraft (Volume I (Flight Control System)):

$$DC1 \equiv (\gamma_{POT\ MIN} < 0)$$

Thrust Condition

During total propulsion failure, the following properties hold (Volume I (Flight Control System)):

$$T_{MAX} = T_{MIN} \qquad \gamma_{POT\ MAX} = \gamma_{POT\ MIN} \qquad \gamma_{SPEED\ MAX} = \gamma_{SPEED\ MIN}$$

Therefore, from the definitions of PFl, TCl, and DCl, the following property holds:

$$PF1 \Rightarrow (TC1 \equiv DC1)$$

In the absence of total propulsion failure, the following properties hold (Volume I (Flight Control System)):

$$T_{MAX} > T_{MIN} \qquad \gamma_{POT\ MAX} > \gamma_{POT\ MIN} \qquad \gamma_{SPEED\ MAX} > \gamma_{SPEED\ MIN}$$

Therefore, from the definitions of PF1, TSl, TS2, TT1, and TT2 the following properties hold:

$$\neg PF1 \Rightarrow (\gamma_{POT\ MAX} > \gamma_{POT\ MIN})(\gamma_{SPEED\ MAX} > \gamma_{SPEED\ MIN})$$

$$\neg PF1 \Rightarrow (TS2 \equiv \neg TS1)(TT2 \equiv \neg TT1)$$

Strategy for Setting Target Thrust

When thrust is saturated, the strategy for setting target thrust can be summarized as follows (table 5, Volume I):

$$PF1 \Rightarrow TT1\ \neg TT2 \qquad \neg PF1\ TS1 \Rightarrow TT1\ \neg TT2 \qquad \neg PF1\ TS2 \Rightarrow TT2\ \neg TT1$$

From the definitions already stated, these implications are equivalent to the following propositions:

$$(\gamma \leq \gamma_{SPEED\ MIN}) \Rightarrow (\gamma_{POT\ TGT} = \gamma_{POT\ MIN})$$

$$(\gamma \geq \gamma_{SPEED\ MAX}) \Rightarrow (\gamma_{POT\ TGT} = \gamma_{POT\ MAX})$$

Speed Regulator

The parameter γ_{SPEED} is defined as follows (Volume I (Flight Control System)):

$$[TT2 \equiv (\gamma_{POT\ TGT} = \gamma_{POT\ MAX})] \Rightarrow (\gamma_{SPEED} = \gamma_{SPEED\ MAX})$$

$$[TT1 \equiv (\gamma_{POT\ TGT} = \gamma_{POT\ MIN})] \Rightarrow (\gamma_{SPEED} = \gamma_{SPEED\ MIN})$$

Because the acceleration command $(dV/dt)_{CMD}$ is assumed proportional to airspeed error (Volume I (Flight Control System)), $(dV/dt)_{CMD}$ vanishes when $V = V_{TGT}$.

The speed regulator has the following properties (Volume I (Flight Control System) and figure 11(c)):

$$(\gamma_{SPEED\ MAX} = \gamma_{POT\ MAX}) \Rightarrow [V3 \equiv (V = V_{TGT})]$$

$$[V3 \equiv (V = V_{TGT})] \Rightarrow (\gamma_{SPEED\ MAX} = \gamma_{POT\ MAX})$$

$$(\gamma_{SPEED\ MAX} > \gamma_{POT\ MAX}) \Rightarrow [V4 \equiv (V > V_{TGT})]$$

$$[V4 \equiv (V > V_{TGT})] \Rightarrow (\gamma_{SPEED\ MAX} > \gamma_{POT\ MAX})$$

Longitudinal Acceleration Limiter

The longitudinal acceleration limiter has the following property (Volume I (Flight Control System)):

$$(\gamma_{\text{SPEED MIN}} < 0)$$

Height Regulator

The height regulator has the following property (Volume I (Synthesis of Altitude Command Supermode) and figure 11(b)):

$$(\gamma_{\text{TGT}} < 0) \Rightarrow (H > H_{\text{TGT}})$$

Definition of H_{MAX}

By definition of the maximum altitude H_{MAX}, the following property holds (Volume I, (Synthesis of Altitude Command Supermode)):

$$(H \leq H_{\text{MAX}}) \Rightarrow (\gamma_{\text{TGT}} \geq 0.3 \text{ deg})$$

Subscripts

Subscripts denote conditions prevailing at different times, as follows:

0 Initial conditions

C Conditions at capture of V_{TGT}

Logical propositions without subscripts hold at all times. Specialization of such unrestricted propositions to particular conditions is indicated by the properties

$$(\bullet) \Rightarrow (\bullet)_0 \qquad (\bullet) \Rightarrow (\bullet)_C$$

which follow from the subscript definitions because any proposition which holds in general must hold at any particular time.

Fixed Speed and Altitude Targets

The properties

$$VT \equiv (V_{\text{TGT}} = V_{\text{TGT}\,0}) \qquad HT \equiv (H_{\text{TGT}} = H_{\text{TGT}\,0})$$

hold if and only if the speed target V_{TGT} and the altitude target H_{TGT} remain fixed at their initial values.

V Command Capture Axiom

The eventual capture of flightpath and airspeed targets after some unspecified time has elapsed following engagement of the primitive V Command mode can be expressed by the axiom

$$VC\ HT\ VT \Rightarrow (\gamma_C = \gamma_{SPEED\ C})\ V3_C$$

which follows from the stability of the flightpath and airspeed regulators (Volume I, figs. 11(e) and 11(c)). (Regulator stability can be verified independently by well-known control-theoretic methods.)

V Command Hold Axiom

Following capture, continuous engagement of the V Command mode ensures that the conditions $(\gamma = \gamma_{SPEED})$ and $(V = V_{TGT})$ continue to hold indefinitely. This property can be expressed by the axiom

$$VC\ HT\ VT\ (\gamma_C = \gamma_{SPEED\ C})\ V3_C \Rightarrow (\gamma = \gamma_{SPEED})\ V3$$

which follows from the stability of the flightpath and airspeed regulators (Volume I, figs. 11 (e) and 11 (c)). (Regulator stability can be verified independently by well-known control-theoretic methods.)

PERFORMANCE DEGRADATION

The first theorem to be presented (Theorem 1) shows that the abnormal condition $\neg PE\ (\gamma)\ \neg PE\ (V)$ can occur only if performance has become so degraded that maximum thrust is insufficient for steady level flight. (This condition could be encountered following engine failure at cruising altitude.) Lemma A treats the case of total propulsion failure, and Lemma B treats its absence.

Lemma A

$$PF1 \Rightarrow TC1$$

Informal Proof Outline

By definition of total propulsion failure, the property

$$PF1 \equiv (\gamma_{POT\ MAX} = \gamma_{POT\ MIN})$$

holds following total propulsion failure. By hypothesis, PF1 holds. Since $\gamma_{POT\ MAX}$ then coincides with $\gamma_{POT\ MIN}$, it follows from their definitions that the equivalence

$$TC1 \equiv (\gamma_{POT\ MAX} < 0) \equiv (\gamma_{POT\ MIN} < 0) \equiv DC1$$

holds. But the property $DC1 \equiv (\gamma_{POT\ MIN} < 0)$ holds for all transport aircraft (Volume I (Flight Control System)). Therefore, the property $TC1 \equiv (\gamma_{POT\ MAX} < 0)$ holds following total propulsion failure, and the lemma is established.

Formal Proof

1.	$PF1 \Rightarrow (TC1 \equiv DC1)$	Thrust condition property during total propulsion failure.
2.	PF1	Hypothesis.
3.	$TC1 \equiv DC1$	Lines 1 and 2.
4.	DC1	Drag condition.
5.	TC1	Lines 3 and 4. QED

Lemma B

$$\neg PF1\ \neg PE(\gamma)\ \neg PE(V) \Rightarrow TC1$$

Informal Proof Outline

By definition, $\neg PE(\gamma) \equiv (GT6\ V1\ TS2)$. Since $\neg PE(\gamma)$ holds by hypothesis, in particular the property $TS2 \equiv (\gamma \geq \gamma_{SPEED\ MAX})$ must hold. By definition of total propulsion failure, the condition $(TS2 \equiv \neg TS1)(TT2 \equiv \neg TT1)$ holds in its absence, as required by the hypothesis. Therefore, since TS2 holds, ¬TS1 must hold. According to the strategy for setting target thrust, the property TT2 holds after thrust is set, and TT1 cannot hold.

From the definition of $\neg PE(V)\ \neg PE(V) \equiv (P\ TT1) \cup (Q\ TT2)$, which holds by hypothesis, and from the conditions ¬TT1 and TT2 just established, it follows that the condition $Q \equiv (\gamma_{TGT} \leq \gamma_{SPEED\ MIN})$ must hold. Combining this condition with the property of the longitudinal acceleration limiter $(\gamma_{SPEED\ MIN} < 0)$ shows that the condition $(\gamma_{TGT} \leq \gamma_{SPEED\ MIN} < 0)$ must hold.

Since the condition $\neg PE(\gamma) \equiv (GT6\ V1\ TS2)$ holds by hypothesis, in particular the property $GT6 \equiv (\gamma_{TGT} \geq \gamma_{POT\ MAX})$ must hold. Now, combining this condition with the condition $(\gamma_{TGT} \leq \gamma_{SPEED\ MIN} < 0)$ just established shows that the condition

$$(\gamma_{POT\ MAX} \leq \gamma_{TGT} \leq \gamma_{SPEED\ MIN} < 0)$$

must hold. But then in particular the property $TC1 \equiv (\gamma_{POT\ MAX} < 0)$ must hold, and the lemma is established.

Formal proof

1. $\neg$PE (γ) $\equiv$ (GT6 V1 TS2)	Definition of $\neg$PE (γ).
2. $\neg$PF1 $\neg$PE (γ)	Hypothesis.
3. $\neg$PF1 TS2	Lines 1 and 2.
4. $\neg$PF1 TS2 $\Rightarrow$ TT2 $\neg$TT1	Thrust setting strategy.
5. TT2 $\neg$TT1	Lines 3 and 4.
6. $\neg$PE (V) $\equiv$ (P TT1) $\cup$ (Q TT2)	Definition of $\neg$PE (V).
7. $\neg$PE (V)	Hypothesis.
8. (P TT1) $\cup$ (Q TT2)	Lines 6 and 7.
9. Q	Lines 5 and 8.
10. Q $\equiv$ ($\gamma_{TGT} \leq \gamma_{SPEED\ MIN}$)	Definition of Q.
11. ($\gamma_{TGT} \leq \gamma_{SPEED\ MIN}$)	Lines 9 and 10.
12. ($\gamma_{SPEED\ MIN} < 0$)	Property of longitudinal acceleration limiter.
13. ($\gamma_{TGT} \leq \gamma_{SPEED\ MIN} < 0$)	Lines 11 and 12.
14. GT6	Lines 1 and 2.
15. GT6 $\equiv$ ($\gamma_{TGT} \geq \gamma_{POT\ MAX}$)	Definition of GT6.
16. ($\gamma_{TGT} \geq \gamma_{POT\ MAX}$)	Lines 14 and 15.
17. ($\gamma_{POT\ MAX} \leq \gamma_{TGT} \leq \gamma_{SPEED\ MIN} < 0$)	Lines 13 and 16.
18. ($\gamma_{POT\ MAX} < 0$)	(17) p q $\Rightarrow$ p and Line 17.
19. TC1 $\equiv$ ($\gamma_{POT\ MAX} < 0$)	Definition of TC1.
20. TC1	Lines 18 and 19. QED

Theorem 1 (Performance Degradation Theorem)

Statement

$\neg$PE (γ) $\neg$PE (V) $\Rightarrow$ TC1

Informal Proof Outline

There are two cases: (a) total propulsion failure present, or (b) total propulsion failure absent.

Case (a)– Assume that total propulsion failure is present. In that case, according to Lemma A, the condition TC1 $\equiv$ ($\gamma_{POT\ MAX} < 0$) holds, and the theorem is established for case (a).

Case (b)– Assume that total propulsion failure is absent. In that case, according to Lemma B, if both PE (γ) and PE (V) are violated, then the condition TC1 $\equiv$ ($\gamma_{POT\ MAX} < 0$) holds. Since by hypothesis both PE (γ) and PE (V) are violated, the condition TC1 $\equiv$ ($\gamma_{POT\ MAX} < 0$) must hold, and the theorem is established for case (b).

Therefore, the condition TC1 $\equiv$ ($\gamma_{POT\ MAX} < 0$) holds whether or not total propulsion failure occurs, and the theorem is established in general.

Formal Proof

1.	PF1 $\Rightarrow$ TC1	Lemma A.
2.	$\neg$PF1 $\neg$PE (γ) $\neg$PE (V) $\Rightarrow$ TC1	Lemma B.
3.	$\neg$PE (γ) $\neg$PE (V)	Hypothesis.
4.	$\neg$PF1 $\Rightarrow$ TC1	(13) p T $\equiv$ p and Lines 2 and 3.
5.	(PF1 $\cup$ $\neg$PF1) $\Rightarrow$ TC1	Lines 1 and 4.
6.	(PF1 $\cup$ $\neg$PF1)	(4) (p $\cup$ $\neg$p) $\equiv$ T.
7.	TC1	Lines 5 and 6. QED

RECOVERY FROM ABNORMAL CONDITIONS

The next three theorems (Theorem 2, Theorem 3, and Theorem 4) to be presented are concerned with recovery from the three abnormal conditions for the Altitude Command supermode. As discussed in Volume I (table 11), these abnormal conditions are $\neg$PE (γ) $\neg$PE (V) $\neg$PE (γ) PE (V), and PE (γ) $\neg$PE (V); the normal condition is PE (γ) PE (V). The point of the three recovery theorems is to show that, starting from any of the three abnormal conditions, the system recovers to the normal condition without crew intervention. If recovery to the normal condition should be precluded by performance limitations, then it is demonstrated that the aircraft stabilizes in a desirable flight condition and that no potentially unsafe behavior results.

Because all three recovery theorems involve dynamical behavior, their proofs are more complex and difficult than the proof of the static theorem (Theorem 1) already presented. The discussion begins with a (static) lemma that specifies initial conditions for the ¬PE (γ) ¬PE (V) Recovery Theorem (Theorem 2) that hold in the absence of total propulsion failure.

Lemma C

$\neg PF1\ \neg PE(\gamma)\ \neg PE(V) \Rightarrow$

(a) $(\gamma_{POT\ MAX} \leq \gamma_{TGT} \leq \gamma_{SPEED\ MIN} < 0)$

(b) $(\gamma_{SPEED\ MIN} < \gamma_{SPEED\ MAX} \leq \gamma)$

(c) $(V_{TGT} < V \leq V_{MIN\ DRAG})$

(d) $(H > H_{TGT})$

Informal Proof Outline

Part (a)– The hypothesis coincides with that of Lemma B. The first claim is established by Line 17, Lemma B.

Part (b)– By hypothesis, the condition ¬PE (γ) ≡ (GT6 VI TS2) holds. In particular, the condition TS2 ≡ $(\gamma \geq \gamma_{SPEED\ MAX})$ holds. Since ¬PF1 ⇒ $(\gamma_{SPEED\ MAX} > \gamma_{SPEED\ MIN})$ holds by the thrust condition property, and since ¬PF1 holds by hypothesis, $(\gamma_{SPEED\ MAX} > \gamma_{SPEED\ MIN})$ must hold. Combining this with TS2 shows that $(\gamma_{SPEED\ MIN} < \gamma_{SPEED\ MAX} \leq \gamma)$ must hold, establishing the second claim.

Part (c)– The condition $(\gamma_{POT\ MAX} \leq \gamma_{TGT} \leq \gamma_{SPEED\ MIN} < 0)$ holds by Part (a) and the condition $(\gamma_{SPEED\ MIN} < \gamma_{SPEED\ MAX} \leq \gamma)$ holds by Part (b). Combining these conditions shows that the condition $(\gamma_{SPEED\ MAX} > \gamma_{POT\ MAX})$ must hold. By the property of the speed regulator, the implication $(\gamma_{SPEED\ MAX} > \gamma_{POT\ MAX}) \Rightarrow (V > V_{TGT})$ holds. Therefore, the condition $(V > V_{TGT})$ holds. By hypothesis, ¬PE (γ) ≡ (GT6 V1 TS2) holds. In particular, V1 ≡ $(V \leq V_{MIN\ DRAG})$ holds. Combining the conditions $(V > V_{TGT})$ and $(V \leq V_{MIN\ DRAG})$ shows that the condition $(V_{TGT} < V \leq V_{MIN\ DRAG})$ holds, establishing the third claim.

Part (d)– The implication $(\gamma_{TGT} < 0) \Rightarrow (H > H_{TGT})$ holds by the height regulator property, and the condition $(\gamma_{TGT} < 0)$ holds by part (a). Therefore, the condition $(H > H_{TGT})$ must hold, establishing the fourth claim.

Therefore, the lemma is established.

Formal Proof

Part (a)

1.	$\neg PF1\ \neg PE(\gamma)\ \neg PE(V) \Rightarrow (\gamma_{POT\ MAX} \leq \gamma_{TGT} \leq \gamma_{SPEED\ MIN} < 0)$	Line 17, Lemma B.
2.	$\neg PF1\ \ \neg PE(\gamma)\ \ \neg PE(V)$	Hypothesis.
3.	$(\gamma_{POT\ MAX} \leq \gamma_{TGT} \leq \gamma_{SPEED\ MIN} < 0)$	Lines 1 and 2.

Part (b)

4. $\neg PE(\gamma) \equiv (GT6\ V1\ TS2)$ — Definition of $\neg PE(\gamma)$
5. TS2 — lines 2 and 4.
6. $TS2 \equiv (\gamma \geq \gamma_{SPEED\ MAX})$ — Definition of TS2.
7. $(\gamma \geq \gamma_{SPEED\ MAX})$ — Lines 5 and 6.
8. $\neg PF1 \Rightarrow (\gamma_{SPEED\ MAX} > \gamma_{SPEED\ MIN})$ — Thrust condition property.
9. $(\gamma_{SPEED\ MAX} > \gamma_{SPEED\ MIN})$ — Lines 2 and 8.
10. $(\gamma_{SPEED\ MIN} < \gamma_{SPEED\ MAX} \leq \gamma)$ — Lines 7 and 9.

Part (c)

11. $(\gamma_{SPEED\ MAX} > \gamma_{POT\ MAX}) \Rightarrow (V > V_{TGT})$ — Speed regulator property.
12. $(\gamma_{POT\ MAX} \leq \gamma_{SPEED\ MIN})$ — Line 3
13. $(\gamma_{POT\ MAX} < \gamma_{SPEED\ MAX})$ — Lines 9 and 10.
14. $(V > V_{TGT})$ — Lines 11 and 13.
15. V1 — Lines 2 and 4.
16. $V1 \equiv (V \leq V_{MIN\ DRAG})$ — Definition of V1.
17. $(V \leq V_{MIN\ DRAG})$ — Lines 15 and 16.
18. $(V_{TGT} < V \leq V_{MIN\ DRAG})$ — Lines 14 and 17.

Part (d)

19. $(\gamma_{TGT} < 0) \Rightarrow (H > H_{TGT})$ — Height regulator property.
20. $(H > H_{TGT})$ — Lines 3 and 19. QED

The next lemma establishes initial mode selection for the initial conditions of Lemma C.

Lemma D

(a) AC $\neg$PE(γ) $\Rightarrow$ CD $\neg$PP PS VC

(b) AC $\neg$PF1 $\neg$PE(γ) $\neg$PE(V) $\Rightarrow$ CD DM $\neg$PP PS VC

Informal Proof Outline

Part (a)– The implication AC $\neg$PE (γ) $\Rightarrow$ CD $\neg$PP PS holds by the property of the Altitude Command supermode selection logic. Since AC $\neg$PE (γ) holds by hypothesis, the condition CD $\neg$PP PS must hold. The implication $\neg$PP PS $\Rightarrow$ VC holds by the property of the Path/Speed Command supermode selection logic. Since $\neg$PP PS holds, VC must hold. Combining these results shows that CD $\neg$PP PS VC must hold, establishing the first claim.

Part (b)– The implication $\neg$PF1 $\neg$PE (γ) $\neg$PE (V) $\Rightarrow$ (H > H_{TGT}) holds by Lemma C, and the condition AC $\neg$PF1 $\neg$PE (γ) $\neg$PE (V) holds by the hypothesis of part (b). Therefore, the condition (H > H_{TGT}) must hold. But the implication CD (H > H_{TGT}) $\Rightarrow$ DM holds by the property of the supermode selection logic within the Altitude Command supermode, and AC CD (H > H_{TGT}) holds. Therefore DM holds (the Descend supermode is selected). Combining this result with that of part (a) shows that the condition CD DM $\neg$PP PS VC holds, establishing the second claim.

Therefore, the lemma is established.

Formal Proof

Part (a)

1.	AC $\neg$PE(γ) $\Rightarrow$ CD $\neg$PP PS	Altitude Command supermode selection property.
2.	AC $\neg$PE(γ)	Hypothesis.
3.	CD $\neg$PP PS	Lines 1 and 2.
4.	$\neg$PP PS $\Rightarrow$ VC	Path/Speed Command supermode selection property.
5.	CD $\neg$PP PS VC	Lines 3 and 4.

Part (b)

6.	AC $\neg$PF1 $\neg$PE(γ) $\Rightarrow$ CD $\neg$PP PS VC	Part (a).
7.	AC $\neg$PF1 $\neg$PE(γ) $\neg$PE(V)	Hypothesis of Part (b).
8.	CD $\neg$PP PS VC	Lines 6 and 7.
9.	$\neg$PF1 $\neg$PE(γ) $\neg$PE(V) $\Rightarrow$ (H > H_{TGT})	Lemma C, part (d).

10. $(H > H_{TGT})$	Lines 7 and 9.	
11. CD $(H > H_{TGT}) \Rightarrow$ DM	Altitude Command supermode selection property.	
12. CD DM ¬PP PS VC	Lines 8, 10, and 11.	QED

Initial Conditions for ¬PE (γ) ¬PE (V) Recovery

To summarize the initial conditions implied when ¬PE (γ) ¬PE (V) holds, the conditions on γ_{TGT}, V, and V_{TGT} specified by Lemma C severely constrain the location of the initial (V, γ_{TGT}) point within the (V, γ_{TGT}) plane. The situation is illustrated qualitatively by figure F-l, which can be constructed from the specification of Lemma C together with the definitions of ¬PE (γ) and ¬PE (V). The initial point must be located within the shaded area (fig. F-l). Furthermore, upon engagement of the Altitude Command supermode the primitive V Command mode is selected, as required by Lemma D. During the first segment of the subsequent mode evolution, the (V, γ_{TGT}) point follows a trajectory in the (V, γ_{TGT}) plane (fig. F-l) that is determined by the initial (V, γ) operating point and by the V Command regulator law, as discussed in Volume I. The resulting dynamical behavior of the system can be analyzed informally as follows.

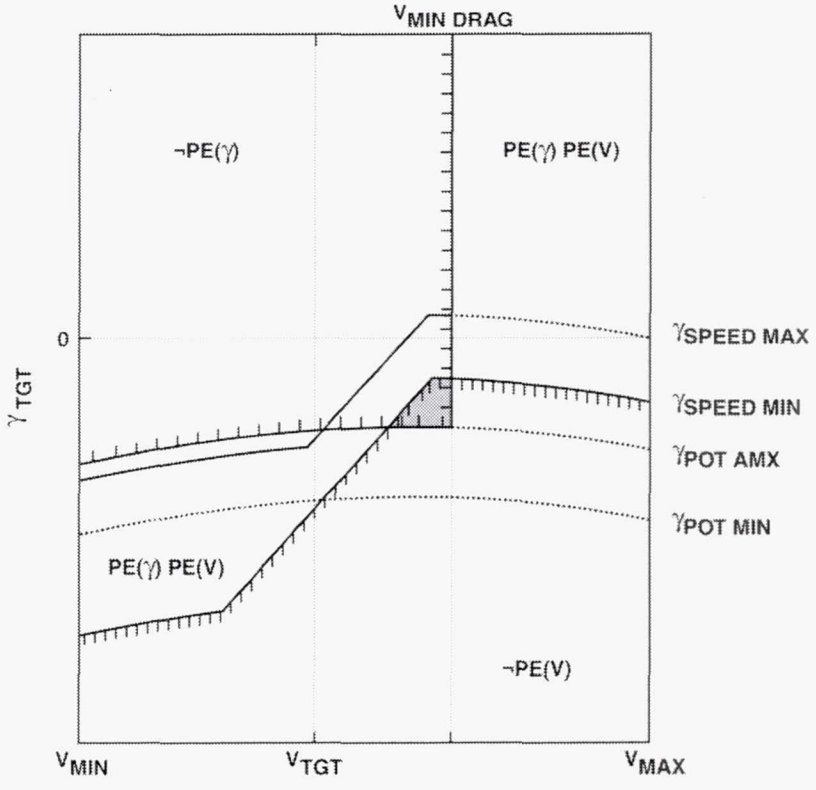

Figure F-1. Conditions for ¬PE (γ) ¬PE (V) recovery.

Dynamical Analysis

The system attempts to capture $\gamma_{SPEED\ MAX}$ and then to capture V_{TGT} by decelerating along the $\gamma_{SPEED\ MAX}$ contour. Consider first the $\gamma_{SPEED\ MAX}$ capture maneuver. According to Lemma C, the condition ($\gamma \geq \gamma_{SPEED\ MAX}$) holds initially, but since $\gamma_{SPEED\ MAX}$ is not specified it could take either positive or negative values. Therefore, the aircraft could either climb or descend initially. According to Lemma C, the condition ($H > H_{TGT}$) holds initially. If the aircraft climbs away from the target altitude, it follows from the height regulator law (Volume I, fig. 11 (b)) that γ_{TGT} must decrease. If the aircraft descends, then γ_{TGT} must increase. Since the condition ($\gamma > \gamma_{POT\ MAX}$) holds initially (Lemma C, parts (a) and (b)), it follows from the longitudinal equation of motion (equation (1c), Volume I (Aircraft Model)) that the longitudinal acceleration is initially negative, so that the speed must decrease. Since V must decrease initially, but γ_{TGT} could either increase or decrease, it can be seen from figure F-l that transitions are possible from the shaded region where the condition $\neg$PE (γ) $\neg$PE (V) holds to regions where either the condition $\neg$PE (γ) PE (V), the condition PE (γ) $\neg$PE (V), or the normal condition PE (γ) PE (V) holds. There are therefore three possible recovery cases.

Furthermore, both figure F-l and Lemma C, part (c), also show that the initial condition $\neg$PF1 $\neg$PE (γ) $\neg$PE (V) cannot continue to hold at $V = V_{TGT}$. Therefore, one of the three possible recoveries must occur before V_{TGT} is captured. If either the PE (γ) $\neg$PE (V) or the PE (γ) PE (V) recovery occurs, then the Altitude Command supermode selection logic (table 12, Volume I) shows that the Altitude Capture/Hold supermode is selected. In that case, either the γ Command mode or the γ-V Command mode is selected, ending the first segment of the mode evolution. On the other hand, if the $\neg$PE (γ) PE (V) recovery occurs, the primitive V Command mode remains selected, and the first segment continues. We shall continue the analysis of dynamical behavior for this latter case of $\neg$PE (γ) PE (V) recovery.

Since the condition $\neg$PE (γ) $\equiv$ (GT6 V1 TS2) continues to hold by assumption, the condition $TS2 \equiv (\gamma \geq \gamma_{SPEED\ MAX})$ must hold, in particular along the $\gamma_{SPEED\ MAX}$ contour where the condition ($\gamma = \gamma_{SPEED\ MAX}$) holds. Therefore, $TT2 \equiv (\gamma_{POT\ TGT} = \gamma_{SPEED\ MAX})$ remains selected. The definition $\neg PE\ (V) \equiv (P\ TT1) \cup (Q\ TT2)$ shows that, since PE (V) holds by assumption and TT2 continues to hold, $Q \equiv (\gamma_{TGT} \leq \gamma_{SPEED\ MIN})$ cannot hold. Therefore, the condition $\neg Q \equiv (\gamma_{TGT} > \gamma_{SPEED\ MIN})$ must hold. Since this condition can hold at $V = V_{TGT}$ (fig. F-l), the V Command mode can remain selected, and the V Command capture property then ensures capture of V_{TGT}. At $V = V_{TGT}$, the condition ($\gamma_{SPEED\ MAX} = \gamma_{POT\ MAX}$) holds by the property of the speed regulator. The condition $TC1 \equiv (\gamma_{POT\ MAX} < 0)$ holds initially by Theorem 1 (Thrust Degradation Theorem).

If TC1 continues to hold at $V = V_{TGT}$ the aircraft descends steadily in the V Command mode, passing through the target altitude without attempting to capture it, although the Climb mode is then selected at all lower altitudes. During descent, γ_{TGT} increases monotonically by the height regulator property. At $V = V_{TGT}$, γ_{TGT} is unbounded above (fig. F-l). Therefore, the descent of the aircraft can continue indefinitely in the V Command mode. But maximum thrust increases as altitude decreases (appendix B). If a lower altitude is reached where ($\gamma_{POT\ MAX} = 0$) holds, then the condition ($\gamma = \gamma_{SPEED\ MAX} = \gamma_{POT\ MAX} = 0$) holds in the long term, so that the aircraft stabilizes in level flight at $V = V_{TGT}$ without crew intervention. The Climb mode remains selected. (The crew would then be expected to select a lower target altitude within the performance capability of the aircraft, which would enable the system to recover to the normal condition PE (γ) PE (V).)

Notice that the diagram of figure F-l plays a role in the foregoing dynamical analysis somewhat similar to that of diagrams in Euclidean geometry—such diagrams can aid in discovering a rigorous proof, but cannot themselves be used to prove anything directly. Therefore, the kind of informal dynamical analysis just presented is suggestive, but not decisive. Nevertheless, the outline of a theorem for ¬PE (γ) ¬PE (V) recovery can be seen emerging from the discussion, which can be stated informally as follows.

Theorem 2 (¬PE (γ) ¬PE (V) Recovery Theorem)

Informal Statement

If both PE (γ) and PE (V) are violated initially, and if the Altitude Command supermode is selected and the target altitude H_{TGT} and the target airspeed V_{TGT} remain fixed, then in the absence of total propulsion failure

(a) the condition ($V_{TGT} < V \leq V_{MIN\ DRAG}$) must hold initially;

(b) recovery from the condition ¬PE (γ) ¬PE (V) occurs before V_{TGT} is captured;

(c) if the conditions ¬PE (γ) PE (V) and TC1 ≡ ($\gamma_{POT\ MAX} < 0$) hold at capture of V_{TGT} and continue to hold thereafter, then the aircraft stabilizes in descent at $V = V_{TGT}$, and the V Command mode remains selected; and

(d) if a lower altitude is reached where the condition ($\gamma_{POT\ MAX} = 0$) holds in the long term, the aircraft stabilizes in level flight at $V = V_{TGT}$.

Approach to Formal Proof

To establish this theorem formally, we shall first construct an informal proof outline based on the initial conditions and on the dynamical analysis just presented. The cases corresponding to total propulsion failure, to recovery to the condition PE (γ) ¬PE (V) or PE (γ) PE (V), and to the condition ($\gamma_{POT\ MAX} \geq 0$) at $V = V_{TGT}$, which are ruled out by the hypothesis of the present theorem, can be treated by the same method. In constructing the informal proof outline, logical gaps resulting from missing definitions of system properties can be ignored temporarily, because they can be filled in later by formalizing material from Volume I as necessary.

Informal Proof Outline

Part (a)– In the absence of total propulsion failure, the condition ¬PF1 holds. The implication

$$\neg PF1\ \neg PE(\gamma)\ \neg PE(V) \Rightarrow \quad (\gamma_{POT\ MAX} \leq \gamma_{TGT} \leq \gamma_{SPEED\ MIN} < 0)$$

$$(\gamma_{SPEED\ MIN} < \gamma_{SPEED\ MAX} \leq \gamma)\ \text{AND}$$

$$(V_{TGT} < V \leq V_{MIN\ DRAG})\ (H > H_{TGT})$$

holds by Lemma C, and the condition ¬PF1 ¬PE (γ) ¬PE (V) holds by hypothesis. Therefore, the condition

$$(\gamma_{\text{POT MAX}} \leq \gamma_{\text{TGT}} \leq \gamma_{\text{SPEED MIN}} < 0)$$

$$(\gamma_{\text{SPEED MIN}} < \gamma_{\text{SPEED MAX}} \leq \gamma) \text{ AND}$$

$$(V_{\text{TGT}} < V \leq V_{\text{MIN DRAG}})\,(H > H_{\text{TGT}})$$

must hold. In particular, the condition ($V_{TGT} < V \leq V_{MIN\ DRAG}$) must hold, establishing the first claim.

Part (b)– The second claim can be established by means of contradiction. The implication AC ¬PE (γ) $\Rightarrow$ CD ¬PP PS VC holds by Lemma D, part (a). Assume that the condition AC ¬PF1 ¬PE (γ) ¬PE (V) continues to hold. Therefore, VC holds, so that the primitive V Command mode is selected and continues to hold. Since the implication VC $\Rightarrow$ $V3_C$ holds by the V Command capture axiom and VC holds, $V3_C$ must eventually hold when V_{TGT} is captured. Because the condition ¬PF1 ¬PE (γ) ¬PE (V) holds by assumption, the condition ($\gamma_{POT\ MAX} \leq \gamma_{TGT} \leq \gamma_{SPEED\ MIN} < 0$) must hold by Lemma C, part (a), and the condition ($\gamma_{SPEED\ MIN} < \gamma_{SPEED\ MAX} \leq \gamma$) must hold by Lemma C, part (b). Combining these conditions, the condition ($\gamma_{SPEED\ MAX} > \gamma_{POT\ MAX}$) holds in general. In particular, the condition ($\gamma_{SPEED\ MAX\ C} > \gamma_{POT\ MAX\ C}$) must hold when V_{TGT} is captured. But since the implication V3 $\Rightarrow$ ($\gamma_{SPEED\ MAX} = \gamma_{POT\ MAX}$) holds by the property of the speed regulator, and since $V3_C$ eventually holds, the condition ($\gamma_{SPEED\ MAX\ C} = \gamma_{POT\ MAX\ C}$) must hold, contradicting the condition ($\gamma_{SPEED\ MAX\ C} > \gamma_{POT\ MAX\ C}$) just established. It follows that the assumption that the condition AC ¬PF1 ¬PE (γ) ¬PE (V) continues to hold until V_{TGT} is captured is false, establishing the second claim.

Part (c)– Since the condition AC ¬PF1 ¬PE (γ) PE (V) HT VT TC1 holds at V_{TGT} capture by the hypothesis of part (c), and the implication AC ¬PE (γ) $\Rightarrow$ CD ¬PP PS VC holds by Lemma D, part (a), the condition VC must hold, so that the V Command mode remains selected at V_{TGT} capture. By hypothesis, the condition ¬PE (γ) $\equiv$ (GT6 V1 TS2) holds. In particular, the condition TS2 $\equiv$ ($\gamma \geq \gamma_{SPEED\ MAX}$) holds. In the absence of total propulsion failure, ¬PF1 holds, as required by the hypothesis. Therefore, the condition ¬PF1 TS2 holds. According to the strategy for setting target thrust, the condition TT2 $\equiv$ ($\gamma_{POT\ TGT} = \gamma_{POT\ MAX}$) then holds after thrust is set. Therefore, the condition ($\gamma_{SPEED} = \gamma_{SPEED\ MAX}$) holds by definition of γ_{SPEED}. Since the implication VC $\Rightarrow$ ($\gamma_C = \gamma_{SPEED\ C}$) $V3_C$ holds by the V Command capture axiom, and since VC holds, γ_{SPEED} and V_{TGT} are captured. Since ($\gamma_{SPEED} = \gamma_{SPEED\ MAX}$) holds, the conditions ($\gamma = \gamma_{SPEED\ MAX}$) and V3 $\equiv$ ($V = V_{TGT}$) hold at V_{TGT} capture. Since $V3_C$ holds, and since the implication V3 $\Rightarrow$ ($\gamma_{SPEED\ MAX} = \gamma_{POT\ MAX}$) holds as a property of the speed regulator, the condition ($\gamma_{SPEED\ MAX\ C} = \gamma_{POT\ MAX\ C}$) holds. Combining these conditions shows that the condition $V3_C$ ($\gamma_C = \gamma_{SPEED\ MAX\ C} = \gamma_{POT\ MAX\ C}$) holds at V_{TGT} capture. Furthermore, the condition TC1 $\equiv$ ($\gamma_{POT\ MAX} < 0$) holds by the hypothesis of part (c). Therefore, the condition $V3_C$ ($\gamma_C < 0$) holds at $V = V_{TGT}$. This shows that the aircraft descends initially at $V = V_{TGT}$ after V_{TGT} capture.

Since the implication VC ($\gamma_C = \gamma_{SPEED\,C}$) $V3_C \Rightarrow$ ($\gamma = \gamma_{SPEED}$) V3 holds by the V Command hold axiom, and since the condition VC ($\gamma_C = \gamma_{SPEED\,C}$) $V3_C$ holds, it follows that the condition ($\gamma = \gamma_{SPEED}$) V3 must hold in general after V_{TGT} capture. Since ($\gamma_{SPEED} = \gamma_{SPEED\,MAX}$) also holds, the condition VC ($\gamma = \gamma_{SPEED\,MAX}$) V3 must hold. Furthermore, since the implication V3 $\Rightarrow$ ($\gamma_{SPEED\,MAX} = \gamma_{POT\,MAX}$) holds as a property of the speed regulator and V3 holds, the condition ($\gamma_{SPEED\,MAX} = \gamma_{POT\,MAX}$) holds. Combining these conditions shows that the condition VC ($\gamma = \gamma_{POT\,MAX}$) V3 holds. Finally, since the condition TC1 $\equiv$ ($\gamma_{POT\,MAX} < 0$) holds by the hypothesis of part (c), the condition ($\gamma < 0$) VC V3 holds in general after V_{TGT} capture, establishing the third claim.

Part (d)– By the hypothesis of part (d), the condition ($\gamma_{POT\,MAX} = 0$) holds in the long term. Since the condition ($\gamma = \gamma_{SPEED\,MAX} = \gamma_{POT\,MAX}$) was established by part (c), it follows that the condition ($\gamma = \gamma_{POT\,MAX} = 0$) holds in the long term. Furthermore, V3 $\equiv$ ($V = V_{TGT}$) continues to hold by the V Command hold axiom. Therefore, the condition ($\gamma = 0$) ($V = V_{TGT}$) holds in the long term. This shows that the aircraft eventually stabilizes in level flight at $V = V_{TGT}$, establishing the fourth claim.

Therefore, the theorem is established.

Formal Statement of ¬PE (γ) ¬PE (V) Recovery Theorem

AC ¬PF1 $\neg PE(\gamma)_0$ $\neg PE(V)_0$ HT VT $\Rightarrow$

(a) ($V_{TGT\,0} < V_0 \leq V_{MIN\,DRAG}$) AND

(b) ¬[AC ¬PF1 ¬PE(γ) ¬PE(V) HT VT] $V3_C$

(c) AC ¬PF1 ¬PE(γ) PE(V) HT VT TC1 $\Rightarrow$ ($\gamma < 0$) VC V3

(d) AC ¬PF1 ¬PE(γ) PE(V) HT VT TC2 $\Rightarrow$ ($\gamma = 0$) VC V3

Formal Proof

Part (a)

1. ¬PF1 ¬PE(γ) ¬PE(V) $\Rightarrow$ — Lemma C.
   - (a) ($\gamma_{POT\,MAX} \leq \gamma_{TGT} \leq \gamma_{SPEED\,MIN} < 0$)
   - (b) ($\gamma_{SPEED\,MIN} < \gamma_{SPEED\,MAX} \leq \gamma$)
   - (c) ($V_{TGT} < V \leq V_{MIN\,DRAG}$)
   - (d) ($H > H_{TGT}$)
2. $\neg PF1\ \neg PE(\gamma)_0\ \neg PE(V)_0$ — Hypothesis

3. $(\gamma_{\text{POT MAX }0} \leq \gamma_{\text{TGT }0} \leq \gamma_{\text{SPEED MIN }0} < 0)$	Lines 1 and 2 and subscript.
AND $(\gamma_{\text{SPEED MIN }0} < \gamma_{\text{SPEED MAX }0} \leq \gamma_0)$	specialization property
AND $(V_{\text{TGT }0} < V_0 \leq V_{\text{MIN DRAG}})\,(H_0 > H_{\text{TGT }0})$	$(\bullet) \Rightarrow (\bullet)_0$

Remark– In particular, the condition $(V_{\text{TGT }0} < V_0 \leq V_{\text{MIN DRAG}})$ holds, establishing the first claim.

Part (b)

4. AC $\neg$PE(γ) $\Rightarrow$ CD $\neg$PP PS VC	Lemma D, part (a).
5. AC $\neg$PF1 $\neg$PE(γ) $\neg$PE(V)$_0$ HT VT	Assumption.
6. VC	Lines 4 and 5.
7. VC HT VT $\Rightarrow$ V3$_C$	V Command capture axiom.
8. V3$_C$	Lines 6 and 7.
9. $(\gamma_{\text{POT MAX}} \leq \gamma_{\text{TGT}} \leq \gamma_{\text{SPEED MIN}} < 0)$ AND $(\gamma_{\text{SPEED MIN}} < \gamma_{\text{SPEED MAX}} \leq \gamma)$	Lines 1 and 5.
10. $(\gamma_{\text{SPEED MAX C}} > \gamma_{\text{POT MAX C}})$	Line 9 and subscript specialization property $(\bullet) \Rightarrow (\bullet)_C$.
11. V3 $\Rightarrow$ $(\gamma_{\text{SPEED MAX}} = \gamma_{\text{POT MAX}})$	Speed regulator property.
12. $(\gamma_{\text{SPEED MAX C}} = \gamma_{\text{POT MAX C}})$	Lines 8 and 11.
13. $\neg$[AC $\neg$PF1 $\neg$PE(γ) $\neg$PE(V) HT VT]	Lines 5, 10, and 12.
14. $\neg$[AC $\neg$PF1 $\neg$PE(γ) $\neg$PE(V) HT VT] V3$_C$	Lines 8 and 13.

Remark– The contradiction of Lines 10 and 12 shows that the assumption of Line 5 is false. The second claim is established by Line 14.

Part (c)

15. AC $\neg$PF1 $\neg$PE(γ) PE(V) HT VT TC1	Hypothesis of part (c).
16. VC HT VT	Line 15 and Lemma D, part (a).
17. $\neg$PE(γ) $\equiv$ (GT6 V1 TS2)	Definition of $\neg$PE(γ).
18. TS2	Lines 15 and 17.
19. $\neg$PF1 TS2	Lines 15 and 18.
20. $\neg$PF1 TS2 $\Rightarrow$ TT2 $\neg$TT1	Thrust setting strategy.

21. TT2	Lines 19 and 20.
22. TT2 $\Rightarrow$ ($\gamma_{SPEED} = \gamma_{SPEED\ MAX}$)	Definition of γ_{SPEED}.
23. ($\gamma_{SPEED} = \gamma_{SPEED\ MAX}$)	Lines 21 and 22.
24. VC HT VT $\Rightarrow$ ($\gamma_C = \gamma_{SPEED\ C}$) $V3_C$	V Command capture axiom.
25. ($\gamma_C = \gamma_{SPEED\ MAX\ C}$) $V3_C$	Lines 16, 23 and 24.
26. ($\gamma_C = \gamma_{POT\ MAX\ C}$) $V3_C$	Lines 11 and 25.
27. TC1 $\equiv$ ($\gamma_{POT\ MAX} < 0$)	Definition of TC1.
28. ($\gamma_{POT\ MAX} < 0$)	Lines 15 and 27.
29. ($\gamma_C < 0$) $V3_C$	Lines 26 and 28.

Remark– This result shows that the aircraft initially descends at $V = V_{TGT}$ (that is, at V_{TGT} capture and immediately afterward).

30. VC HT VT $\Rightarrow$ ($\gamma_C = \gamma_{SPEED\ C}$) $V3_C \Rightarrow$ ($\gamma_=$ γSPEED) V3	V Command hold axiom.
31. ($\gamma = \gamma_{SPEED\ MAX}$) VC V3	Lines 16, 23, and 30.
32. ($\gamma_{SPEED\ MAX} = \gamma_{POT\ MAX}$)	Lines 11 and 31.
33. ($\gamma = \gamma_{POT\ MAX}$) VC V3	Lines 31 and 32.
34. ($\gamma < 0$) VC V3	Lines 16, 28, and 33.

Remark– This result shows that the aircraft continues to descend at $V = V_{TGT}$, establishing the third claim.

Part (d)

35. AC $\neg$PF1 $\neg$PE(γ) PE(V) HT VT TC2	Hypothesis of part (a).
36. VC HT VT	Line 35 and Lemma D, part (a).
37. $\neg$PE(γ) $\equiv$ (GT6 V1 TS2)	Definition of $\neg$PE(γ).
38. TS2	Lines 35 and 37.
39. $\neg$PF1 TS2	Lines 35 and 38.
40. $\neg$PF1 TS2 $\Rightarrow$ TT2 $\neg$TT1	Thrust setting strategy.
41. TT2	Lines 39 and 40.
42. TT2 $\Rightarrow$ ($\gamma_{SPEED} = \gamma_{SPEED\ MAX}$)	Definition of γ_{SPEED}.
43. ($\gamma_{SPEED} = \gamma_{SPEED\ MAX}$)	Lines 41 and 42.

44. VC HT VT $\Rightarrow$ ($\gamma_C = \gamma_{SPEED\ C}$) $V3_C$	V Command capture axiom.
45. ($\gamma_C = \gamma_{SPEED\ MAX\ C}$) $V3_C$	Lines 36, 43 and 44.
46. ($\gamma_C = \gamma_{POT\ MAX\ C}$) $V3_C$	Lines 11 and 45.
47. VC HT VT ($\gamma_C = \gamma_{SPEED\ C}$) $V3_C \Rightarrow$ ($\gamma = \gamma_{SPEED}$) V3	V Command hold axiom.
48. ($\gamma = \gamma_{SPEED\ MAX}$) V3	Lines 36, 45, and 47.
49. ($\gamma_{SPEED\ MAX} = \gamma_{POT\ MAX}$)	Lines 11 and 48.
50. ($\gamma = \gamma_{POT\ MAX}$) V3	Lines 48 and 49.
51. ($\gamma_{POT\ MAX} = 0$)	Line 35 and definition of TC2.
52. ($\gamma = 0$) VC V3	Lines 36, 50, and 57. QED

Remark– This result shows that, if the condition ($\gamma_{POT\ MAX} = 0$) holds in the long term, the aircraft eventually stabilizes in level flight at $V = V_{TGT}$, establishing the fourth claim.

Therefore, the theorem is established.

Proof Automation

Formal proof of the ¬PE (γ) ¬PE (V) Recovery Theorem (Theorem 2) is long and complex even though the theorem has been stated in a weak form: the total propulsion failure case has been excluded, and likewise the cases of recovery to the conditions PE (γ) ¬PE (V) and PE (γ) PE (V), as shown by the dynamical analysis presented previously. Despite these simplifications, formal proof of the ¬PE (γ) ¬PE (V) Recovery Theorem, together with its auxiliaries Lemma C and Lemma D, require a total of 84 steps. Formal proof of the Performance Degradation Theorem (Theorem 1) together with Lemma A and Lemma B previously required 36 steps, making a total of 120 steps for the formal proofs of the theorems presented thus far. Furthermore, three theorems involving complicated dynamical behavior remain to be proved.

In our opinion, the development of formal proofs such as that just presented for the ¬PE (γ) ¬PE (V) Recovery Theorem (Theorem 2) by means of manual pencil-and-paper methods would be too complex and laborious for routine use by the aircraft industry. On the other hand, informal proofs of the kind outlined may not be sufficiently rigorous to provide an independent check of the integrity of the synthesis process, as indicated by failure to reveal omission through oversight of a total propulsion failure case to be discussed later. A potential resolution of this dilemma might be achieved by using currently available theorem-proving software (Rushby, 1999; Schumann, 2001) to generate formal proofs. To enable such machine-generated formal proofs to be checked manually if desired, a sequential listing of the detailed steps (together with their justifications) should be provided for each proof by the theorem-proving software.

The development of practical working methods for formalizing informal proof outlines is currently being investigated. The first step is to formalize the definitions of system properties suggested by

the informal proof outline, as already illustrated for the ¬PE (γ) ¬PE (V) Recovery Theorem (Theorem 2). Some iteration of this first step may be required during attempts at formal proof (Lakatos, 1976). Development of methods for automating formal proofs remains incomplete, and only informal proof outlines will be offered for the three theorems to be presented next. In the meantime, these informal proof outlines, while not rigorous, can be regarded as making the existence of rigorous formal proofs plausible.

Theorem 3 (PE (γ) ¬PE (V) Recovery Theorem)

Informal Statement

If PE (V) is violated initially, but PE (γ) holds, and if the Altitude Command supermode is selected and the target altitude H_{TGT} remains fixed with $H_{TGT} \leq H_{MAX}$, then in the absence of total propulsion failure PE (γ) PE (V) must eventually hold.

Informal Proof Outline

By hypothesis, the condition PE (γ) ¬P (V) holds, where

$$\neg PE\ (\gamma) \equiv (\gamma_{TGT} \geq \gamma_{POT\ MAX})\ AND\ (V \leq V_{MIN\ DRAG})\ AND\ (\gamma \geq \gamma_{SPEED\ MAX})$$

$$\neg PE\ (V) \equiv [P\ AND\ (\gamma_{POT\ TGT} = \gamma_{POT\ MIN})]\ OR\ [Q\ AND\ (\gamma_{POT\ TGT} = \gamma_{POT\ MAX})]$$

and

$$P \equiv (\gamma_{TGT} \geq \gamma_{SPEED\ MAX}) \qquad Q \equiv (\gamma_{TGT} \leq \gamma_{SPEED\ MIN}).$$

By definition of ¬PE (V), there are two possible cases for evaluation: (i) the conditions P and $(\gamma_{POT\ TGT} = \gamma_{POT\ MIN})$ hold; or else (ii) the conditions Q and $(\gamma_{POT\ TGT} = \gamma_{POT\ MAX})$ hold. Since the Altitude Command supermode is selected and PE (γ) ¬PE (V) holds by hypothesis, according to the Altitude Command supermode selection strategy the Altitude Capture/Hold supermode is selected in both cases.

Case (i)– Assume that the conditions P and $(\gamma_{POT\ TGT} = \gamma_{POT\ MIN})$ hold. According to the strategy for setting the target thrust, there are three subcases that correspond to the resulting condition $(\gamma_{POT\ TGT} = \gamma_{POT\ MIN})$. Either (a) the thrust saturation condition $(\gamma \leq \gamma_{SPEED\ MIN})$ holds; or else (b) thrust is unsaturated and Q holds; or else (c) thrust is unsaturated and ¬P ¬Q holds, in which case $\gamma_{POT\ TGT}$ is not updated, but could previously have been set to $\gamma_{POT\ MIN}$.

(a) Assume that the condition $(\gamma \leq \gamma_{SPEED\ MIN})$ holds. Since the Altitude Capture/Hold supermode is selected, the flightpath angle γ is driven toward the flightpath target γ_{TGT} by the stability property of the path regulator. Since $P \equiv (\gamma_{TGT} \geq \gamma_{SPEED\ MAX})$ holds by assumption, if the Altitude Capture/Hold supermode were to remain selected until path capture were complete, the condition $(\gamma \geq \gamma_{SPEED\ MAX})$ would hold. In that case, the initial condition $(\gamma \leq \gamma_{SPEED\ MIN})$ would change to the final condition $(\gamma \geq \gamma_{SPEED\ MAX})$ during path capture. As a consequence of the physical condition $(\gamma_{POT\ MIN} < \gamma_{POT\ MAX})$, the condition $(\gamma_{SPEED\ MIN} < \gamma_{SPEED\ MAX})$ holds by definition. Therefore, provided that the Altitude Capture/Hold supermode remains selected, the intermediate condition $(\gamma_{SPEED\ MIN} < \gamma < \gamma_{SPEED\ MAX})$ must hold at some time during path capture because of the physical continuity of the flightpath angle γ. In that case, thrust is unsaturated. Since P also holds by

assumption, $\gamma_{POT\ TGT}$ is reset to $\gamma_{POT\ MAX}$ according to the strategy for setting target thrust. Then PE (V) holds by definition. Therefore, PE (γ) PE (V) holds, demonstrating the theorem for subcase (a).

(b) Assume that thrust is unsaturated and Q holds. Since P also holds by the assumption of case (i), PQ must hold. But since the condition ($\gamma_{SPEED\ MIN} < \gamma_{SPEED\ MAX}$) holds by definition, the condition PQ is impossible. Therefore, subcase (b) is impossible.

(c) Assume that thrust is unsaturated and $\neg P\ \neg Q$ holds. Since the assumption that $\neg P$ holds contradicts the assumption of case (i) that P holds, subcase (c) is impossible.

Since the theorem holds for subcase (a), and since both subcase (b) and subcase (c) were shown to be impossible, the theorem holds for case (i).

Case (ii)– Assume that the conditions Q and ($\gamma_{POT\ TGT} = \gamma_{POT\ MAX}$) hold. According to the strategy for setting the target thrust, there are three subcases that correspond to the resulting condition ($\gamma_{POT\ TGT} = \gamma_{POT\ MAX}$). Either (a) the thrust saturation condition ($\gamma \geq \gamma_{SPEED\ MAX}$) holds; or else (b) thrust is unsaturated and P holds; or else (c) thrust is unsaturated and $\neg P\ \neg Q$ holds, in which case $\gamma_{POT\ TGT}$ is not updated, but could previously have been set to $\gamma_{POT\ MAX}$.

(a) Assume that the condition ($\gamma \geq \gamma_{SPEED\ MAX}$) holds. Since the Altitude Capture/Hold supermode is selected, the flightpath angle γ is driven toward the flightpath target γ_{TGT} by the stability property of the path regulator. Since $Q \equiv (\gamma_{TGT} \leq \gamma_{SPEED\ MIN})$ holds by assumption, if the Altitude Capture/Hold supermode were to remain selected until path capture were complete, the condition ($\gamma \leq \gamma_{SPEED\ MIN}$) would hold. In that case, the initial condition ($\gamma \geq \gamma_{SPEED\ MAX}$) would change to the final condition ($\gamma \leq \gamma_{SPEED\ MIN}$) during path capture. As a consequence of the physical condition ($\gamma_{POT\ MIN} < \gamma_{POT\ MAX}$), the condition ($\gamma_{SPEED\ MIN} < \gamma_{SPEED\ MAX}$) holds by definition. Therefore, provided that the Altitude Capture/Hold supermode remains selected, the intermediate condition ($\gamma_{SPEED\ MIN} < \gamma < \gamma_{SPEED\ MAX}$) must hold at some time during path capture because of the physical continuity of the flightpath angle γ. In that case, thrust is unsaturated. Since Q also holds by assumption, $\gamma_{POT\ TGT}$ is reset to $\gamma_{POT\ MIN}$ according to the strategy for setting target thrust. Then PE (V) holds by definition. Therefore, PE (γ) PE (V) holds, demonstrating the theorem for subcase (a).

(b) Assume that thrust is unsaturated and P holds. Since Q also holds by the assumption of case (ii), PQ must hold. But since the condition ($\gamma_{SPEED\ MIN} < \gamma_{SPEED\ MAX}$) holds by definition, the condition PQ is impossible. Therefore, subcase (b) is impossible.

(c) Assume that thrust is unsaturated and $\neg P\ \neg Q$ holds. Since the assumption that $\neg Q$ holds contradicts the assumption of case (ii) that Q holds, subcase (c) is impossible.

Since the theorem holds for subcase (a), and since both subcase (b) and subcase (c) were shown to be impossible, the theorem holds for case (ii).

Since the theorem holds for both case (i) and case (ii), it is established in general.

Theorem 4 (¬PE (γ) PE (V) Recovery Theorem)

Informal Statement

If PE (γ) is violated initially, but PE (V) holds, and if the Altitude Command supermode is selected and the target altitude H_{TGT} remains fixed with $H_{TGT} \leq H_{MAX}$ and if Climb effectiveness holds while in the Climb mode, then in the absence of total propulsion failure the condition PE (γ) PE (V) must eventually hold.

Informal Proof Outline

By hypothesis, the Altitude Command supermode is selected and the condition ¬PE (γ) PE (V) holds, where

$$\neg PE\ (\gamma) \equiv (\gamma_{TGT} \geq \gamma_{POT\ MAX})\ AND\ (V \leq V_{MIN\ DRAG})\ AND\ (\gamma \geq \gamma_{SPEED\ MAX})$$

$$\neg PE\ (V) \equiv [P\ AND\ (\gamma_{POT\ TGT} = \gamma_{POT\ MIN})]\ OR\ [Q\ AND\ (\gamma_{POT\ TGT} = \gamma_{POT\ MAX})]$$

and

$$P \equiv (\gamma_{TGT} \geq \gamma_{SPEED\ MAX}) \qquad Q \equiv (\gamma_{TGT} \leq \gamma_{SPEED\ MIN}).$$

According to the Altitude Command supermode selection strategy, the Climb/Descend supermode is selected. There are two cases depending on the altitude error ΔH: (i) the descent case $\Delta H < 0$; and (ii) the climb case $\Delta H \geq 0$.

Case (i)– Assume that the condition ($\Delta H < 0$) holds. Therefore, by the height regulator law, the condition ($\gamma_{TGT} < 0$) holds for the flightpath target γ_{TGT}. Since as a consequence of the definition of H_{MAX} the condition ($\gamma_{POTMAX} \geq 0.3$ deg) must hold, and the condition ($\gamma_{TGT} < 0$) also holds, it follows that the condition ($\gamma_{TGT} < 0 < \gamma_{POT\ MAX}$) must hold. Therefore, PE (γ) holds by definition, contradicting the hypothesis that ¬PE (γ) holds. Therefore, case (i) (the descent case) is impossible.

Case (ii)– Assume that the condition ($\Delta H \geq 0$) holds. Since by hypothesis ¬PE (γ) PE (V) holds, according to the Altitude Command mode selection strategy the Climb mode is selected. By hypothesis, the climb effectiveness condition CE holds. Therefore, by the definition of climb effectiveness, the aircraft vertical velocity must remain strictly positive. It follows that, during operation in the Climb mode, the altitude error ΔH decreases monotonically toward zero. By the height regulator law, the target flightpath angle γ_{TGT} is proportional to the altitude error ΔH for $|\Delta H|$ sufficiently small. Therefore, the flightpath target γ_{TGT} also decreases monotonically toward zero for $|\Delta H|$ sufficiently small (that is, when the aircraft approaches the target altitude sufficiently closely from below). Since the condition ($\gamma_{POT\ MAX} \geq 0.3$ deg) holds by definition of H_{MAX}, the condition ($\gamma_{TGT} < \gamma_{POT\ MAX}$) must hold for $|\gamma_{TGT}|$ sufficiently small. In that case, PE (γ) holds by definition. Therefore, since PE (V) holds by hypothesis, the condition PE (γ) PE (V) must hold, and the theorem is demonstrated for case (ii).

Since the theorem holds for case (ii) and since case (i) was shown to be impossible, the theorem is established in general.

EFFECTIVENESS OF ALTITUDE COMMAND SUPERMODE

This section presents a theorem (Theorem 5) concerned with the effectiveness of the Altitude Command Supermode, which requires capture of altitude and airspeed targets (Volume I (Synthesis of Altitude Command Supermode)). In the absence of design error, effectiveness of the Altitude Command Supermode should be guaranteed by the design synthesis process (Volume I). Therefore, the theorem to be presented next (Theorem 5) provides an independent check of the integrity of the system design process described in Volume I.

Theorem 5 (Altitude Command Supermode Effectiveness Theorem)

Informal Statement

If the target altitude H_{TGT} lies at or below H_{MAX} and H_{TGT} remains fixed, and if climb effectiveness holds while in the Climb mode, and if descent effectiveness holds while in the Descend mode, then selection of the Altitude Command supermode ensures that

(a) the target altitude H_{TGT} will be captured; and

(b) if normal effectiveness of the γ Command mode holds while in the Altitude Capture/Hold mode, then the target airspeed V_{TGT} will also be captured.

Informal Proof Outline

By definition of H_{MAX}, the condition ($\gamma_{POT\ MAX} \geq 0.3$ deg) holds at H_{MAX} and at all lower altitudes. Since by hypothesis the condition ($H_{TGT} \leq H_{MAX}$) holds, the condition ($\gamma_{POT\ MAX} \geq 0.3$ deg) must hold in the neighborhood of H_{TGT}.

In general, four cases are possible initially for the Altitude Command supermode:

(i) $\neg$PE (γ) $\neg$PE (V)
(ii) PE (γ) $\neg$PE (V)
(iii) $\neg$PE (γ) PE (V)
(iv) PE (γ) PE (V)

Case (i)– Assume that the condition $\neg$PE (γ) $\neg$PE (V) holds initially. By Theorem 2 ($\neg$PE (γ) $\neg$PE (V) Recovery Theorem), the condition $\neg$PE (γ) $\neg$PE (V) cannot hold except in the short term. According to the recovery theorem, recovery to the condition PE (γ) $\neg$PE (V) (case (ii)), the condition $\neg$PE (γ) PE (V) (case (iii)), or the condition $\neg$PE (γ) $\neg$PE (V) (case (iv)) must occur before the target airspeed V_{TGT} is captured. Therefore, case (i) need not be considered further.

Case (ii)– Assume that the condition PE (γ) $\neg$PE (V) holds. By Theorem 3 (PE (γ) $\neg$PE (V) Recovery Theorem), $\neg$PE (γ) $\neg$PE (V) cannot hold except in the short term, and terminates in the condition PE (γ) PE (V) (that is, in case (iv)). Therefore, case (ii) need not be considered further.

Case (iii)– Assume that the condition $\neg$PE (γ) PE (V) holds. Since by hypothesis the Altitude Command supermode is selected and the target altitude H_{TGT} remains fixed with $H_{TGT} \leq H_{MAX}$, by Theorem 4 ($\neg$PE (γ) PE (V) Recovery Theorem), the condition PE (γ) PE (V) must eventually hold.

Therefore, case (iii) terminates in the condition PE (γ) PE (V) (that is, in case (iv)). Therefore, case (iii) need not be considered further.

Case (iv)– Because it has been demonstrated that the abnormal conditions for case (i), case (ii), and case (iii) terminate in the normal condition PE (γ) PE (V) (that is, case (iv)), the normal condition PE (γ) PE (V) must eventually hold. Therefore, according to the supermode selection strategy for the Altitude Command supermode, there are two cases for supermode selection: either the condition $P \cup Q$ holds, resulting in the selection of the Climb/Descend supermode, or else the condition $\neg P\ \neg Q$ holds, resulting in the selection of the Altitude Capture/Hold supermode. Furthermore, if $P \cup Q$ holds and the condition ($\Delta H \geq 0$) holds for the altitude error ΔH, then the Climb mode is selected, and if $P \cup Q$ holds and the condition ($\Delta H < 0$) holds, then the Descend mode is selected. Therefore, the following three subcases must be considered: (a) $P \cup Q$ and the climb condition ($\Delta H \geq 0$) hold; (b) $P \cup Q$ and the descent condition ($\Delta H < 0$) hold; and (c) the condition $\neg P\ \neg Q$ holds.

(a) Assume that $P \cup Q$ and the climb condition ($\Delta H \geq 0$) hold. In that case, by definition of the altitude error ΔH (Volume I), the target altitude H_{TGT} lies above the initial altitude. By the height regulator law, the flightpath target γ_{TGT} has the same sign as the altitude error ΔH. Therefore, the condition ($\gamma_{TGT} \geq 0$) holds. Since the condition ($\gamma_{SPEED\ MIN} < 0$) holds by the property of the longitudinal acceleration limiter, and since the condition ($\gamma_{TGT} \geq 0$) also holds, the condition $Q \equiv (\gamma_{TGT} \leq \gamma_{SPEED\ MIN})$ cannot hold. Therefore, since $P \cup Q$ holds by assumption, P must hold initially.

Since by assumption PE (γ) PE (V) holds, and since by assumption $P \cup Q$ and the condition ($\Delta H \geq 0$) also hold, according to the Altitude Command mode selection strategy the Climb mode is selected. By hypothesis, the climb effectiveness condition CE holds. Therefore, according to the definition of climb effectiveness (Volume I), the aircraft vertical velocity must remain strictly positive. It follows that, during operation in the Climb mode, the absolute altitude error $|\Delta H|$ decreases monotonically toward zero, provided that H_{TGT} remains fixed as required by the hypothesis. According to the height regulator law, the target flightpath angle γ_{TGT} is proportional to the absolute altitude error $|\Delta H|$ for $|\Delta H|$ sufficiently small. Therefore, the absolute flightpath target $|\gamma_{TGT}|$ also decreases monotonically toward zero for $|\Delta H|$ sufficiently small (that is, when the aircraft approaches the target altitude sufficiently closely from below).

Since the condition ($\gamma_{POT\ MAX} \geq 0.3$ deg) holds by definition of H_{MAX}, the condition ($\gamma_{SPEED\ MAX} > 0.3$ deg) must hold by the property of the speed regulator. Therefore, the condition $\neg P \equiv (\gamma_{TGT} < \gamma_{SPEED\ MAX})$ must hold for $|\gamma_{TGT}|$ sufficiently small, contradicting the assumption of subcase (a) that $P \cup Q$ holds.

Because it was demonstrated that Q cannot hold, the condition $\neg P\ \neg Q$ must hold (subcase (c)) for $|\gamma_{TGT}|$ sufficiently small, which results in selection of the Altitude Capture/Hold supermode according to the Altitude Command supermode selection strategy. Therefore, operation in the Climb mode (that is, subcase (a)) terminates in selection of the Altitude Capture/Hold supermode when the aircraft approaches the target altitude sufficiently closely.

(b) Assume that $P \cup Q$ and the condition ($\Delta H < 0$) hold. In that case, by definition of the altitude error ΔH (Volume I), the target altitude H_{TGT} lies below the initial altitude. By the height regulator law, the flightpath target γ_{TGT} has the same sign as the altitude error ΔH. Therefore, the condition ($\gamma_{TGT} < 0$) holds. Since the condition ($\gamma_{POT\ MAX} \geq 0.3$ deg) holds by definition of H_{MAX}, the condition ($\gamma_{SPEED\ MAX} > 0.3$ deg) must hold by the property of the speed regulator. Therefore, since the condition ($\gamma_{TGT} < 0$) also holds, the condition $P \equiv (\gamma_{TGT} \geq \gamma_{SPEED\ MAX})$ cannot hold. Therefore, since $P \cup Q$ holds by assumption, Q must hold initially.

Since by assumption PE (γ) PE (V) holds, and since by assumption $P \cup Q$ and the condition ($\Delta H < 0$) also hold, according to the Altitude Command mode selection strategy the Descend mode is selected. By hypothesis, the descent effectiveness condition DE holds. Therefore, according to the definition of descent effectiveness (Volume I), the aircraft vertical velocity must remain strictly negative. It follows that, during operation in the Descend mode, the absolute altitude error $|\Delta H|$ decreases monotonically toward zero, provided that H_{TGT} remains fixed as required by the hypothesis. According to the height regulator law, the target flightpath angle γ_{TGT} is proportional to the altitude error ΔH for $|\Delta H|$ sufficiently small. Therefore, the flightpath target $|\gamma_{TGT}|$ also decreases monotonically toward zero for $|\Delta H|$ sufficiently small (that is, when the aircraft approaches the target altitude sufficiently closely from above).

Since the condition ($\gamma_{SPEED\ MIN} < 0$) holds by the property of the longitudinal acceleration limiter, the condition $\neg Q \equiv (\gamma_{TGT} > \gamma_{SPEED\ MIN})$ must hold for $|\gamma_{TGT}|$ sufficiently small, contradicting the assumption of subcase (b) that $P \cup Q$ holds.

Because it was demonstrated that P cannot hold, the condition $\neg P\ \neg Q$ must hold (subcase (c)) for $|\gamma_{TGT}|$ sufficiently small, which results in selection of the Altitude Capture/Hold supermode according to the Altitude Command supermode selection strategy. Therefore, operation in the Descend mode (that is, subcase (b)) terminates in selection of the Altitude Capture/Hold supermode when the aircraft approaches the target altitude sufficiently closely.

(c) Because it was demonstrated that both subcase (a) and subcase (b) terminate in the condition $\neg P\ \neg Q$ (that is, in subcase (c)) when the aircraft approaches the target altitude sufficiently closely, $\neg P\ \neg Q$ must eventually hold. Because it was demonstrated that PE (γ) PE (V) must also hold eventually, the condition PE (γ) PE (V) $\neg P\ \neg Q$ must hold eventually. Therefore, according to the Altitude Command mode selection strategy, the Altitude Capture/Hold supermode is then selected. Since PE (γ) holds, by definition of PE (γ) capture of the flightpath target γ_{TGT} is assured. Therefore, capture of the target altitude H_{TGT} is assured by the stability property of the height regulator, establishing the first claim.

Since PE (γ) holds, by definition of PE (γ) an acceptable point of airspeed equilibrium is captured, although in general this equilibrium airspeed differs from the target airspeed. By definition, normal effectiveness of the γ Command mode (Volume I) requires that the longitudinal acceleration have the correct sign leading to capture of the target airspeed V_{TGT}. By hypothesis, normal effectiveness of the γ Command mode holds while the Altitude Capture/Hold supermode is selected. It follows that the airspeed target V_{TGT} must be captured, establishing the second claim.

Therefore, the theorem is established.

CORRECTION OF A DESIGN OVERSIGHT

During the synthesis process, a design oversight was committed by assuming tacitly that maximum thrust would always be computationally distinct from minimum thrust, ignoring the possibility of total propulsion failure. For multiengine transport aircraft, the probability of such a failure is small, but not negligible. Since all engines depend on the aircraft fuel system, fuel contamination could cause simultaneous failure. Furthermore, incidents have occurred in which fuel mismanagement by the human flight crew resulted in an attempt to feed all engines from empty fuel tanks while other tanks contained fuel, leading to total propulsion failure that was soon corrected.

In our opinion, such emergency situations should not be complicated by anomalous actions of the flight control system that result from failure to account for the possibility of total propulsion failure at the design level. Therefore, total propulsion failure should be considered in control system design.

Error Identification

The logic error resulting from this oversight was revealed during attempted formal proof of the Performance Degradation Theorem (Theorem 1). It can be seen that step 5 of Lemma B establishes the condition TT2 $\neg$TT1, but since by definition

$$TT1 \equiv (\gamma_{POT\ TGT} = \gamma_{POT\ MIN}) \quad \text{and} \quad TT2 \equiv (\gamma_{POT\ TGT} = \gamma_{POT\ MAX}),$$

the required condition TT2 $\neg$TT1 does not hold during total propulsion failure, because in that case the condition PF1 $\equiv (\gamma_{POTMAX} = \gamma_{POTMIN})$ holds.

Strategy for Setting Target Thrust

Further consideration of the strategy for setting target thrust (table 5, Volume I) then showed that the original table was logically incomplete because the case in which both the conditions TS1 $\equiv (\gamma \leq \gamma_{SPEED\ MIN})$ and TS2 $\equiv (\gamma \geq \gamma_{SPEED\ MAX})$ hold simultaneously had erroneously been considered logically impossible. Therefore, the original thrust setting strategy (table F-l) was logically indeterminate in the event of total propulsion failure.

TABLE F-1. ORIGINAL STRATEGY FOR SETTING TARGET THRUST

TS1	**TS2**		**$\neg$TS1 $\neg$TS2**	
		Q	**P**	**$\neg$P $\neg$Q**
Set TT1 TRUE	Set TT2 TRUE	Set TT1 TRUE	Set TT2 TRUE	$\gamma_{POT\ TGT}$ not updated

In that case, several possible actions could result, depending on the exact details of the implementation code. Target thrust might be set to minimum thrust (TT1), or to maximum thrust (TT2), or not be set at all (in that case, the previous setting would prevail), or a thrust setting error might be annunciated, or the autothrottle might be disconnected (with unpredictable consequences for the subsequent motion of the aircraft if normal engine operation should be restored). In our opinion, such behavioral uncertainties should be considered unacceptable in a safety-critical system.

Correction of Error

After the design error was identified, case analysis was applied to the logically complete set of cases

$$TS1\ \neg TS2 \quad TS1\ TS2 \quad \neg TS1\ TS2 \quad \neg TS1\ \neg TS2$$

to determine the best thrust setting strategy. This analysis resulted in the revised strategy as follows (table F-2).

TABLE F-2. REVISED STRATEGY FOR SETTING TARGET THRUST

PF1			**¬PF1**		
	TS1	**TS2**		**¬TS1 ¬TS2**	
			Q	**P**	**¬P ¬Q**
Set TT1 TRUE	Set TT1 TRUE	Set TT2 TRUE	Set TT1 TRUE	Set TT2 TRUE	$\gamma_{POT\ TGT}$ not updated

It can be seen that in case of total propulsion failure, the target thrust is set to minimum thrust (TT1) in order to minimize the thrust transient if normal engine operation is restored.

Discussion

This case history shows by example how formal proofs of system properties can provide an independent check of system design integrity. It should be noted that omission of the total propulsion failure case was not revealed by informal proof. It seems likely that, in most cases in which attempted formal proof of a theorem reveals that some case has been omitted through oversight, the situation could be dealt with by a trivial strengthening of the hypothesis of the theorem so as to rule out the omitted case. In the exceptional case just described, it was decided that design iteration was necessary to remedy the logic error, instead of ruling out the total propulsion failure case because of its low probability.

CONCLUDING REMARKS

Several theorems have been presented that summarize the behavioral properties of the hybrid system for transport aircraft longitudinal control, which is the subject of Volume I. These theorems enable theoretical assessment of system dynamical behavior and verification of system safety and effectiveness independent of the design method. They can therefore provide an independent check of system design integrity, enabling formal validation of the complete system to be achieved.

Methods have been demonstrated for generating formal proofs of these behavioral theorems based on informal dynamical analysis. However, formal proof of such behavioral theorems by manual pencil-and-paper methods may be too complex and laborious for routine use by the aircraft industry. On the other hand, informal proof is not sufficiently rigorous to provide a check of system design integrity, as shown by a case study involving omission through oversight of a total propulsion failure case.

Resolution of this dilemma can be achieved by using currently available theorem-proving software to generate formal proofs. To enable such machine-generated formal proofs to be checked manually if desired, a sequential listing of the detailed steps should be provided for each proof. Practical working methods for achieving partial automation of formal proofs by means of theorem-proving software are under current investigation.

By means of automated hypothesis testing, any hypothesis could in principle be tested to determine whether it is a theorem of the formal system. In future system development making use of the synthesis methods described in this report, such hypothesis testing could play a role similar to that of simulation in today's development process, but unlike simulation it would lead to results that would be rigorous and logically complete.

REFERENCES

Lakatos, Imre: Proofs and Refutations: The Logic of Mathematical Discovery. Cambridge University Press (New York), 1976. (Reprinted 1987.)

Rushby, John: Mechanized Formal Methods: Where Next? Invited paper presented at The World Congress on Formal Methods: PM 99, Toulouse, France, September 1999. Springer-Verlag Lecture Notes in Computer Science, vol. 1708, 1999.

Schumann, Johann: Automated Theorem Proving in Software Engineering. Springer-Verlag (Heidelberg, New York), 2001.

APPENDIX G
SELECTED TRANSPORT AIRCRAFT ACCIDENTS AND INCIDENTS

The following statements briefly summarize the aspects of four selected transport aircraft accidents and incidents that are considered relevant to issues of system design. Available references should be consulted for more complete accounts of these occurrences.

L-1011, EVERGLADES, 1972

After encountering an indication of unsafe nose landing gear extension during a night approach to the Miami airport, the aircraft requested and received radar vectors from Miami Approach Control to a nearby area where troubleshooting of the landing gear problem could be conducted with minimal conflict with other traffic. The assigned altitude was 2000 ft above ground level, and the assigned airspace was over the Everglades swamp in an area without lights on the ground. The autopilot was operating in its barometric altitude hold mode. At one point in the troubleshooting procedure, the first officer was required to enter the nose tunnel in order to make a visual inspection of the position of the nose gear strut. It is believed that in leaving his seat, the first officer may have bumped the control column, which would have caused the autopilot to change modes. Alternatively, the mode reversion may have resulted from some other cause.

Whatever the cause, the autopilot reverted from the barometric hold mode, in which it was engaged, to the pitch attitude hold mode, which held the pitch attitude at which the aircraft had last been trimmed. The annunciation of this mode reversion was cautionary in nature, in contrast to the warning provided for complete disconnect of the autopilot, and failed to claim the attention of the crew. The target pitch attitude held by the autopilot then allowed the aircraft to descend slowly below the assigned altitude. The crew failed to monitor the system performance adequately because they were distracted from their normal duties by the elaborate procedure required for troubleshooting the landing gear problem. The absence of lights on the ground also contributed to their lack of altitude awareness. The aircraft struck the surface of the swamp and was totally destroyed, with heavy loss of life. (NTSB, 1972).

B-767, SAN FRANCISCO, LATE 1980s

Several altitude violations on departure from San Francisco led to an investigation. Within the autoflight system of the aircraft, it was found that the conditional branching that governed the transition from the climb mode to the altitude capture mode contained a test for validity of the vertical velocity, a common programming strategy intended to defend the altitude capture routine against invalid input data. If the vertical velocity were invalid, execution would be transferred to the exit from the climb routine, skipping the test for transition to the altitude capture mode. Validity of the vertical velocity was determined by a reasonableness test that examined whether the vertical velocity lay within the expected range specified a priori.

But at light aircraft weight and lower-than-standard atmospheric temperature, and for northeast departures not requiring noise abatement procedures using partial thrust, the vertical velocity during climb could reach values that lay outside the tolerance limit imposed by the reasonableness test. Under these seldom-encountered conditions, the reasonableness test generated false indications of invalid vertical velocity that caused the test for transition to the altitude capture mode to be skipped, so that the system remained by default in the climb mode. The result was that the aircraft failed to level off at the assigned altitude. No annunciation was provided to the crew. These altitude overshoots violated the traffic separation required by Air Traffic Control (ATC), and could have resulted in a catastrophic midair collision. (Lauber, J. K., Member, National Transportation Safety Board, personal communication, 1994.)

B-737, DENVER, EARLY 1990s

In airline training simulations, failure of the glideslope receiver during instrument landing system (ILS) approach is often simulated. The autoflight system reverts from ILS approach mode to the vertical velocity hold mode. This mode reversion is annunciated by the vanishing of a small symbol on the primary flight display, a cautionary annunciation that is frequently overlooked by the crew. The system then holds the vertical velocity that prevailed at the instant of failure, a situation that could cause the aircraft to fly into the ground short of the runway. Identical system behavior in the aircraft has been verified. (Irving, Capt. James, United Airlines, personal communication, 1996.)

A-330, TOULOUSE, JUNE 1994

This accident occurred during a test flight commanded by the manufacturer's chief pilot. Immediately following takeoff at light weight and with center of gravity far aft, the flight test card required the pilot to engage the autoflight system and then simulate engine failure by cutting one engine. (The A-330 is a twin-engine aircraft.) The purpose of the test, which had been carried out successfully with engines of a different type, was to verify that safe airspeed margins were preserved following the simulated engine failure.

Other demonstrations had been conducted earlier in the flight, and a target altitude of 2000 ft above ground level remained in the system from a previous entry. With this target altitude and the unusually high rate of climb achieved shortly after takeoff under the test conditions, the system transitioned from the climb mode to the altitude capture mode immediately after engagement. In the altitude capture mode, the flightpath was commanded to follow the specified altitude capture trajectory. Path error was fed back to pitch control, and with thrust fixed at maximum thrust there was no closed-loop control of airspeed. Furthermore, an automatic de-clutter mode would remove mode annunciations from the primary flight display at nose-high pitch attitudes exceeding 25 deg.

The crew may not have appreciated the significance of the reversion to the altitude capture mode, or alternatively they may not have been aware of it. They cut the engine as required by the flight test card at an airspeed of about 150 kt. The thrust available with one engine out was inadequate for steady climb at the commanded path angle, so the airspeed decayed rapidly and the aircraft settled

below the commanded altitude capture trajectory. The system responded by increasing pitch attitude to excessive nose-high angles that reached 32 deg, which increased the rate of decay of airspeed. The airspeed decayed below the minimum-control speed of 118 kt, and the aircraft began an uncontrollable roll into the dead engine. According to the Director General of Armaments' report (1994), the crew was slow in deciding to take over manually, although their decision may have been delayed by the automatic de-cluttering of the primary display, which removed mode annunciations. The pilot attempted to recover roll control by cutting the remaining engine, which also disabled the envelope protection based on angle of attack (the "alpha floor"). But sufficient altitude for recovery was not available, and the aircraft stalled and crashed, reaching airspeeds as low as 77 kt before the impact. The aircraft was totally destroyed, with fatal injuries to all those on board.

REFERENCES

Director General of Armaments (France): Investigation Committee report on A330 Accident in Toulouse on 30 June 1994. Unpublished report. See also Sparaco, Pierre: Autopilot a factor in A330 accident. Aviation Week and Space Technology, vol. 141, no. 2, July 11, 1994; and A330 crash to spur changes at Airbus. Aviation Week and Space Technology, vol. 141, no. 6, August 8, 1994, pg. 20.

NTSB: Eastern Air Lines L-1011, Miami, FL, December 29, 1972. NTSB Report no. AAR-73-14, Washington, D.C., National Transportation Safety Board, 1972.

REPORT DOCUMENTATION PAGE

Form Approved
OMB No. 0704-0188

The public reporting burden for this collection of information is estimated to average 1 hour per response, including the time for reviewing instructions, searching existing data sources, gathering and maintaining the data needed, and completing and reviewing the collection of information. Send comments regarding this burden estimate or any other aspect of this collection of information, including suggestions for reducing this burden, to Department of Defense, Washington Headquarters Services, Directorate for information Operations and Reports (0704-0188), 1215 Jefferson Davis Highway, Suite 1204, Arlington, VA 22202-4302. Respondents should be aware that notwithstanding any other provision of law, no person shall be subject to any penalty for failing to comply with a collection of information if it does not display a currently valid OMB control number.
PLEASE DO NOT RETURN YOUR FORM TO THE ABOVE ADDRESS.

1. REPORT DATE *(DD-MM-YYYY)*	2. REPORT TYPE	3. DATES COVERED *(From - To)*
21-12-2007	Technical Publication	

4. TITLE AND SUBTITLE

Synthesis from Design Requirements of a Hybrid System for Transport Aircraft Longitudinal Control
Volumes I and II

5a. CONTRACT NUMBER

5b. GRANT NUMBER

5c. PROGRAM ELEMENT NUMBER

6. AUTHOR(S)
Charles S. Hynes[1], Gordon H. Hardy[1], and Lance Sherry[2]

5d. PROJECT NUMBER

5e. TASK NUMBER

5f. WORK UNIT NUMBER
411931

7. PERFORMING ORGANIZATION NAME(S) AND ADDRESS(ES)
[1]Ames Research Center, Moffett Field, CA 94035
[2]Honeywell International Inc., Flight Control Systems Design, Phoenix, AZ

8. PERFORMING ORGANIZATION REPORT NUMBER
A-070008

9. SPONSORING/MONITORING AGENCY NAME(S) AND ADDRESS(ES)
National Aeronautics and Space Administration
Washington, D.C. 20546-0001

10. SPONSORING/MONITOR'S ACRONYM(S)
NASA

11. SPONSORING/MONITORING REPORT NUMBER
NASA/TP–2007-213475

12. DISTRIBUTION/AVAILABILITY STATEMENT
Unclassified — Unlimited Distribution: Standard
Subject Category: 03, 06, 08, 54, 66
Availability: NASA CASI (301) 621-0390

13. SUPPLEMENTARY NOTES
Point of Contact: Jeffery A. Schroeder, Ames Research Center, MS 210-4, Moffett Field, CA 94035-0001
(650) 604-4037

14. ABSTRACT

Volume I of this report presents a new method for synthesizing hybrid systems directly from design requirements, and applies the method to design of a hybrid system for longitudinal control of transport aircraft. The resulting system satisfies general requirement for safety and effectiveness specified a priori, enabling formal validation to be achieved. Volume II contains seven appendices intended to make the report accessible to readers with backgrounds in human factors, flight dynamics and control, and formal logic.

Major design goals are (1) system design integrity based on proof of correctness at the design level, (2) significant simplification and cost reduction in system development and certification, and (3) improved operational efficiency, with significant alleviation of human-factors problems encountered by pilots in current transport aircraft.

This report provides for the first time a firm technical basis for criteria governing design and certification of avionic systems for transport aircraft. It should be of primary interest to designers of next-generation avionic systems.

15. SUBJECT TERMS
Air transportation and safety, Avionics, Aircraft stability and control, Flight controls and autopilots, Man/machine systems, Systems analysis

16. SECURITY CLASSIFICATION OF:			17. LIMITATION OF ABSTRACT	18. NUMBER OF PAGES	19a. NAME OF RESPONSIBLE PERSON
a. REPORT	b. ABSTRACT	c. THIS PAGE			Jeffery A. Schroeder
Unclassified	Unclassified	Unclassified	Unclassified	168	19b. TELEPHONE *(Include area code)* (650) 604-4037